In Silico Modeling of Cation Homeostasis in *Saccharomyces cerevisiae*

D i s s e r t a t i o n

zur Erlangung des akademischen Grades

doctor rerum naturalium
(Dr. rer. nat.)
im Fach Biophysik

eingereicht an der
Mathematisch-Naturwissenschaftlichen Fakultät I
Humboldt-Universität zu Berlin

von
M.Sc. Susanne Gerber

Präsident der Humboldt-Universität zu Berlin:
Prof. Dr. Jan-Hendrik Olbertz

Dekan der Mathematisch-Naturwissenschaftlichen Fakultät I:
Prof. Dr. Andreas Herrmann

Gutachter:
1. Prof. Dr. Dr. h.c. Edda Klipp
2. Ph.D. Hella Lichtenberg-Fraté
3. Prof. Dr. Christof Schütte

eingereicht am: 24.03.2011
Tag der mündlichen Prüfung: 27.07.2011

Ich widme diese Arbeit meinen Eltern
für Ihre bedingungslose Unterstützung
zu jeder Zeit und in jeder Lebenslage
auf dem Weg bis hierher.

Danksagung

An erster Stelle möchte ich mich bei Prof. Dr. Dr. h.c. Edda Klipp bedanken, für die Überlassung des hochinteressanten Themas, die wissenschaftliche Betreuung und die wertvollen Ratschlägen die sehr zum Gelingen dieser Arbeit beigetragen haben. Die gleichzeitig große Freiheit, die ich während der gesamten Zeit hatte, ermöglichte es mir auch weitere interessante Fragestellungen die sich im Rahmen des Forschungsprojektes aufgetan haben zu verfolgen und dabei neue Interessen und Fertigkeiten zu gewinnen.

Genau so sehr möchte ich auch meiner Zweit-Betreuerin, PD Dr. Hella Lichtenberg-Fraté danken, die mich seit meinem Start im Translucent-Projekt in vielerlei Hinsicht unterstützt und gefördert hat. Sie war jederzeit bereit wissenschaftliche Diskussionen zu führen und von ihren kritischen und gleichzeitig äußerst konstruktiven Ratschlägen durfte ich viel lernen.

Allen Kolleginnen und Kollegen im Projekt TRANSLUCENT möchte ich auch meinen Dank aussprechen, da mit ihnen sowohl auf Tagungen und während der Projekttreffen als auch elektronisch immer ein offener, freundlicher und in der Sache weiterführender Austausch möglich war.

Bei meiner Freundin und Kollegin Martina Fröhlich möchte ich mich in vielerlei Hinsicht bedanken: die wissenschaftliche Zusammenarbeit, ihre Hilfe bei der Parameterschätzung und die unzähligen zusammen verbrachten Stunden.

Ich möchte mich bei der gesamten Arbeitsgruppe Theoretische Biophysik für die angenehme und kollegiale Atmosphäre bedanken. Insbesondere bei Szymon Stoma und Christian Diener für Zusammenarbeit, Hilfe und gute Ideen, sowie Christian Waltermann, der mir fast 3 Jahre lang direkt gegenüber saß, und zu jedem Zeitpunkt ein humorvoller und gerne gesehener Zimmergenosse war.

Einen besonders wichtigen Dank möchte ich an dieser Stelle meinen Eltern aussprechen, die mir in jeglicher Hinsicht im Studium und während der Zeit der Doktorarbeit Rückhalt geboten haben und ohne die beides nicht möglich gewesen wäre.

Zum Schluss möchte ich mich noch bei meinem Freund Illia bedanken, für Rückhalt, Zuversicht und Unterstützung.

Abstract

The present thesis was conducted in frame of the European TRANSLUCENT project entitled *Gene interaction networks and models of cation homeostasis in Saccharomyces cerevisiae* at the Theoretical Biophysics group at Humboldt University of Berlin under the supervision of Professor Dr. E. Klipp.
Cationic toxicity is relevant for a number of qualitatively different biological and medical phenomena such as cationic surfactants, salt and heavy metal stress in plants and a number of pathological conditions which share similar critical metabolic processes (i.e. protein aggregation and oxidative stress). In line with the overall project goals the scientific work contributed to i) the analysis, graphical presentation and the respective assessment of specific genomic promoter-regions, ii) the conversion, evaluation and genome wide analysis of micro-array experiments on the effects of exposition of *S. cerevisiae* to heavy metals, iii) a simulation environment comprising modules for digitalization, presentation, analysis and mathematical modeling of the spatio-temporal distribution of biologically relevant molecules, and iv) a cation homeostasis modeling approach based on the non-linear thermodynamics theory.
The bioinformatical work focused on an iterative process in which available experimental results were transferred into meaningful models or applications and results of modeling or prediction into corresponding new experimental designs. The software for the promoter-analysis and the simulation environment for integration of spatio-temporal distribution of biologically relevant molecules like labeled signal molecules have already been published and successfully implemented. The results of the genome-wide analysis - based on experiments of a project partner - provide insights in the individual mechanisms and strategies of the yeast cell upon exposition to various (heavy) metals in toxic concentrations. The theoretical biophysical-thermodynamic approach provides a fundamental model of cation homeostasis in *S.cerevisiae* of the major cations: potassium, sodium and protons. The model - confronted with experimental data - is capable to reproduce the observed uptake rates to a reasonable degree. Perspectives for further development of the model are discussed.

Zusammenfassung

Die vorliegende Dissertation wurde zum Thema *Gene interaction networks and models of cation homeostasis in* Saccharomyces cerevisiae im Rahmen des europäischen TRANSLUCENT Projekts in der Arbeitsgruppe Theoretische Biophysik an der Humboldt Universität zu Berlin unter Anleitung von Professor Dr. Dr. h.c. Edda Klipp angefertigt.
Die toxische Wirkung von Kationen ist verantwortlich für eine Reihe biologischer und pathologischer Erscheinungen. Zu den übergreifenden Zielen des Gesamtvorhabens wurden als wissenschaftliche Arbeiten i) die Analyse, graphische Darstellung und darauf basierende Gewichtung spezifischer genomischer Promotor-Regionen, ii) die Verarbeitung, Auswertung und genomweite Analyse von Mikro-Array Experimenten über die Auswirkung verschiedener Schwermetalle auf *S. cerevisiae*, iii) Mitarbeit an einer Simulations-Umgebung mit Modulen zur Digitalisierung, Präsentation, Analyse und mathematischer Modellierung der räumlichen Verteilung biologisch relevanter Moleküle sowie iv) ein Ansatz zur Modellierung der Kationen-Homöostase unter Verwendung der Theorie der Nichtgleichgewichts Thermodynamik beigetragen. Im Vordergrund der bioinformatorischen Arbeiten stand dabei der iterative Prozess, in dem verfügbare experimentelle Ergebnisse in aussagefähige Modelle oder Anwendungen übertragen wurden und die Resultate der Modellierung oder Vorhersage wiederum in neue entsprechende Experimente umgesetzt wurden. Die Anwendungsumgebung zur Promotoranalyse sowie die Simulationsumgebung zur räumlichen Verteilung biologisch relevanter Moleküle wie zum Beispiel markierte Signalmoleküle wurde bereits veröffentlicht und erfolgreich eingesetzt. Die Ergebnisse der genomweiten Analyse liefern Erkenntnisse über die individuellen Mechanismen und Strategien der Hefe auf verschiedene Metallionen in toxischer Konzentration zu reagieren.
Der theoretische biophysikalisch-thermodynamische Ansatz liefert ein fundamentales Modell der Kationen-Homöostase der zahlenmäßig bedeutendsten Kationen: Kalium, Natrium und Protonen. Das Modell wurde an experimentellen Daten getest und konnte diese reproduzieren. Entsprechende Perspektiven für die Weiterentwicklung des Modells werden diskutiert.

List of Symbols

A	Affinity of a chemical reaction
c_i	Molar concentration of component i
d_m	Thickness of the membrane
D	Diffusion coefficient $u_i RT$
$\mathfrak{F}$	Faraday constant, $9.6485 \cdot 10^4$ coulombs/mol
G	Gibbs free energy
J_i	Absolute flow of component i in moles per unit area per unit time
$J_{i,eq}$	Flow of component i under equilibrium conditions (X=0)
J_q	Flow of heat
J_S	Flow of entropy
J_{ch}	Rate of chemical reaction per unit flow
K	Equilibrium constant for a chemical reaction
k	Boltzmann constant, $1.380\,650\,4 \cdot 10^{-23} J/K$
L_{ij}	Phenomenological coefficient relating the ith flow to the jth force
n_i	Number of moles of component i
P_i	Permeability coefficient of component i
p	Pressure
Q	Heat
q_v	Heat in a small subvolume
$\mathcal{R}$	Gas constant, $8.314472\ \frac{J}{mol \cdot K}$
S	Entropy
$d_i S$	Entropy produced within a system
$d_e S$	Entropy exchanged with the environment of a system
s	Entropy of a small subvolume
s_v	Local entropy per unit volume
T	Absolute temperature
t	Time
U	Internal energy

u	Energy of a small subvolume
u_v	Local internal energy per unit volume
u_i	Mobility of an ion i
V	Volume
v	Subvolume
v_i	Reaction velocity
z_i	Valence of a charges ions i
W	Work
X_i	Thermodynamic force acting on component i
α_i	Deviation of the ith parameter of a system from its equilibrium value
β_i	Partition coefficient
η_i	Electrochemical potential of component i
μ_i	Chemical potential of component i
μ_0	Standard chemical potential of component i
φ	Electric potential
σ	Entropy production density
Φ	Local dissipation function
ψ	Local electric potential
ω_i	Mobility of component i

Abbreviations and acronyms

ATP	Adenosin triphosphate
pbc	Proton buffer capacity
FCS	Fluorescence Correlation Spectroscopy
FLIM	Fluorescence lifetime imaging microscopy
FP	Fluorescent protein
GFP	Green fluorescent protein
GUI	Graphical user interface
MIC	Minimal inhibitory concentration
MIFE	Microelectrode ion flux measuring
PM	Polygonal mesh
TF	Transcription factor
TFbs	Transcription factor binding site
STSE	Spatio Temporal Simulation Environment
WT	Wild Type

In order to discriminate consistently between gene names and the associated gene-products the following notation will be used:

- **Gene names** (e.g. TRK1,2, ENA1, BMH1,2, TOK, ENA1 ...) are written in capital letters.
- **Protein names** (e.g. Trk1,2, Ena1, Bmh1,2, Tok, Ena1,....) start with a capital letter.
- **Mutant names** (e.g. Δ*trk1,2*, Δ*ena1*, Δ*bmh1,2*, Δ*tok*, Δ*ena1*) are written small type.

Contents

1 Introduction

1.1 Overview

Why cation induced stress?

System responses to cation induced stress (toxicity) play a pivotal role in a wide range of essential cellular processes. Cationic toxicity is relevant for a number of qualitatively different biological and medical phenomena, i.e. cationic surfactants (alkyl ester ammonium salts that are used in fabric softeners), salt and heavy metal stress in plants and, not least, a number of pathological conditions which share similar critical metabolic processes such as protein aggregation and oxidative stress, both of which are associated with the involvement of metal ions. Cationic pollutants can exhibit their hazardous potential in several different manners, e.g. specific inhibition of enzymes like it is the case for cytochromoxidase by cyanide or on a more general cellular level by causing oxidative stress as for heavy metals (see chapter 3).
Among the heavy metals the transition metals such as copper, zinc, nickel, and iron are involved in redox processes of respiratory activity; others, such as magnesium, nickel, and cobalt, are part of complex molecules, stabilize protein structures, and serve in maintaining the osmotic balance, like potassium, or stabilize various enzymes (Zn^{2+} fingers) and DNA through electrostatic forces, like magnesium and zinc [JLLF09]. Although considered as essential co-factors for a variety of enzymatic reactions and for important structural and functional roles in cell metabolism, (alkali) metals at high concentrations are potent toxic pollutants [Eid00, Eid01]. Toxic effects can include blocking of functional groups on important bio-molecules as well as denaturation of enzymes [BTA98] and DNA damage as for copper, chromium, zinc, and nickel. Another mechanism of metal toxicity (copper, nickel, cadmium) involves the transition-metal-catalyzed generation of reactive oxygen species in the Fenton reactions and subsequent lipid peroxidation [SB95]. Furthermore, metal toxicity (cadmium, cobalt) may be also caused by depletion of glutathione, considered as a major antioxidant in eukaryotic cells [FZBB96].
Therefore the ability of organisms - from single cells to complex structures like plants - to tolerate - or adapt to - a range of environmental stress conditions like e.g. aridity, very high or almost nil concentrations of salt, pollutants and even xenobiotica (chemicals that are foreign to biological systems and include industrial chemicals, pesticides, herbicides, and fungicides) received already significant scientific attention for decades. Such investigations were particularly enhanced since advanced genomic and proteomic technologies provide a wealth of data and information.
One of the most sensitive challenges of a cell in this context is its capacity to maintain an optimum cytoplasmic concentration of several cations even under rapidly changing external disturbances like salt- osmotic- or alkaline pH stress. Since cationic and heavy metal toxicity is involved in a substantial number of diseases in mammals as well as it aggravates the growth capacities of crop plants in inhospitable areas of salted soils the understanding of tightly regulated transporter activities and the interplay of regulatory mechanisms is of substantial interest.
Commonly known as baker‘s, brewer‘s or budding yeast, the unicellular eukaryote *Saccharomyces cerevisiae* has been used as a standard laboratory microorganism since 1950. The cellular structure is similar to that of mammals with internal organelles and similar chromosome structure and DNA repair and metabolic processes. Yeast has proved to be a remarkably versatile model

system. Its applications range from the study of cellular mechanisms of cancer to neurological diseases and, particularly within the post genomics era, as biological tool from gene expression profiling to protein-protein interaction mapping. Such opportunities accrue from the already known functional annotation of the majority of genes, the cultivation in defined laboratory conditions, the relative ease of genetic modifications and a very reasonable background of microbiological and biochemical data. Genomic, transcriptomic and metabolomic data are accessible via a number of public available databases (SGD, MIPS, GIMS, KEGG) and literature reports. Since the yeast *S. cerevisiae* belongs to the best-studied and characterized eukaryotic organisms [Smu01] it has also been recognized as an excellent organism to study the transport properties and physiological function of alkali-metal-transporters [Syc04]. Yeast - among other model organisms - is a most promising model for such assays since it is amenable to genetic studies and because of the vast amount of genomics knowledge, resources, and manipulative tools associated with this unicellular fungus.
Recently, due to the increasing amount of genetic and physiological data an integrated experimental and theoretical approach explored *S. cerevisiae* as model organism for system biology purposes[Kli07].
In *S. cerevisiae* most of the proteins responsible for transport of sodium, potassium, protons and diverse heavy metals across the cellular membrane have been identified and some single transport mechanisms are well described. However, despite considerable experimental work, much less is known concerning the molecular basis for **integration of activities of the transport systems** into more general aspects of cation homeostasis like the interplay between particular ion transport proteins, respective regulatory elements and factors controlling the rate of transport.
It was anticipated that a systems approach including predictive mathematical models may provide a deeper understanding of the principle rationale of homeostasis employed by nature. For example, comparison of yeast and e.g. human transcription programs already showed that conservation across species involves basic functional units. A better understanding of sensing, signaling and responding mechanisms offers the potential to identify in the long run cation related toxic stressors and thresholds more quickly and thus lead to optimized in silico models enabling the provision of a more scientific basis for extrapolation to higher eukaryotic systems.

1.1.1 TRANSLUCENT a SysMo ERA-NET project

The present thesis was conducted within the SysMO framework project TRANSLUCENT. SysMO is a European transnational funding and research initiative on "Systems Biology of Microorganisms" with the objective to record and describe dynamic molecular processes in unicellular microorganisms. Obtained (comprehensive) data collections serve to present such processes in the form of computerized mathematical models.
The TRANSLUCENT network comprises six partners plus an associate partner, assembling a team of nine independent laboratories from five different countries (Austria, Czech Rep., Germany, Spain and The Netherlands). In Figure 1.1 the approaches and experimental techniques in TRANSLUCENT are illustrated.
The sequenced genome of *S. cerevisiae* and, despite complexity, the identification and functional characterization of components of the innate cation transporter/channel systems that play a critical role in front-line maintenance of cellular cation homeostasis or defense against cationic stressors laid the basis for this systems biology approach. Based on transcription modules, metabolic profiling and biochemical transport protein characteristics this project aims to infer an *in silico* model of cation homeostasis.
Cation homeostasis related gene expression profiles, selective functional changes and related

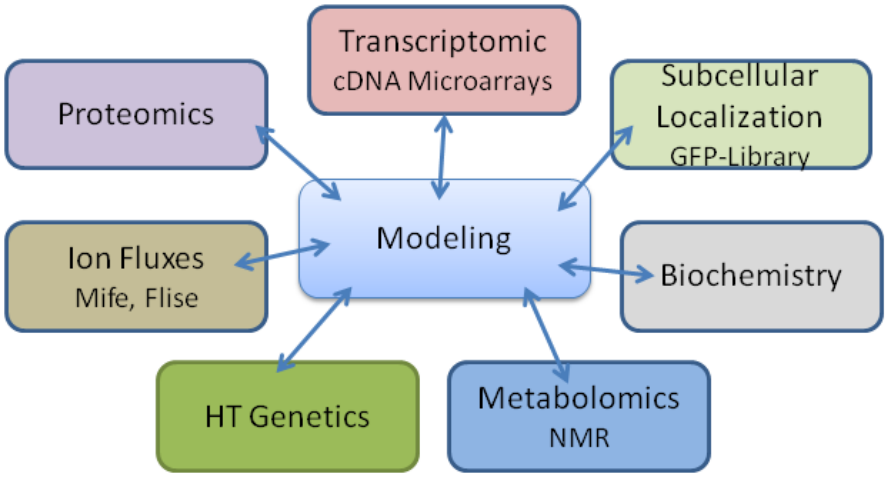

Figure 1.1: Experimental approaches in TRANSLUCENT

protein accumulation data of specifically targeted yeast mutants enable analysis of the complex system responses to cation stress and finally lead to the identification of involved genetic networks and better understanding of sensing, transport, signaling and response/detoxification mechanisms in the yeast *S. cerevisiae*. Within the network experimental data produced by transcriptomic, proteomic and metabolomic techniques and physiological methods are evaluated by bioinformatics, statistical and biophysical analysis.
The analysis is expected to provide an outline of the *S. cerevisiae* gene clusters involved in system responses to cationic stress as a network of protein complexes with a level of organization beyond binary interactions. Developed higher-order genetic maps contain fundamental biological information to guide the identification of specific gene regulatory and metabolic mechanisms and thus offer the context for a more reasoned and informed approach to model and predict specific target candidate toxicity profiles.

1.1.2 Conceptual formulation: Bioinformatics data analysis and *in silico* modeling

The range of experiments performed within the TRANSLUCENT research project include but are not limited to determination of transcriptional levels of known and possible new genes, metabolic and proteomic profiles, transport properties of individual transporters by construction of targeted yeast knock-out mutants and functional analysis of proteins.
All these qualitatively different data (biochemical, genetic, biophysical) must be adequately analyzed and evaluated to provide input for the consecutive step within an iterative experimental/modeling process (Figure 1.2). Therefore, prior to the actual modeling process a number of preparatory and enabling tasks were addressed.

These centered on different bioinformatic questions:

- The analysis of gene promotor regions
- microarray data analysis and

- the development of a spatio-temporal modeling environment (aimed to provide an application environment for protein localization and accumulation data).

The corresponding work flows are described in the following chapters.
The thermodynamical description of transport processes across the membrane should finally contribute to a systemic view of cationic homeostasis. This *in silico* model can support an understanding of the global interplay between active and passive transport systems as well as involved regulatory mechanism. Consequently, the current thesis focused on the interplay of the transport proteins and regulatory elements responsible for the homeostasis of the three most important cations: potassium (K^+), sodium (Na^+) and protons (H^+) in the yeast *S. cerevisiae*. The presentation of the work is organized along the above mentioned tasks preceded by a paragraph "Biological Background". This overview should provide an introduction to the model organism, known mechanisms employed by yeast cells in the adaption-to-stress process and membrane physiology parameters and is necessary for the understanding of the function of the various components involved in cellular cation-homeostasis.

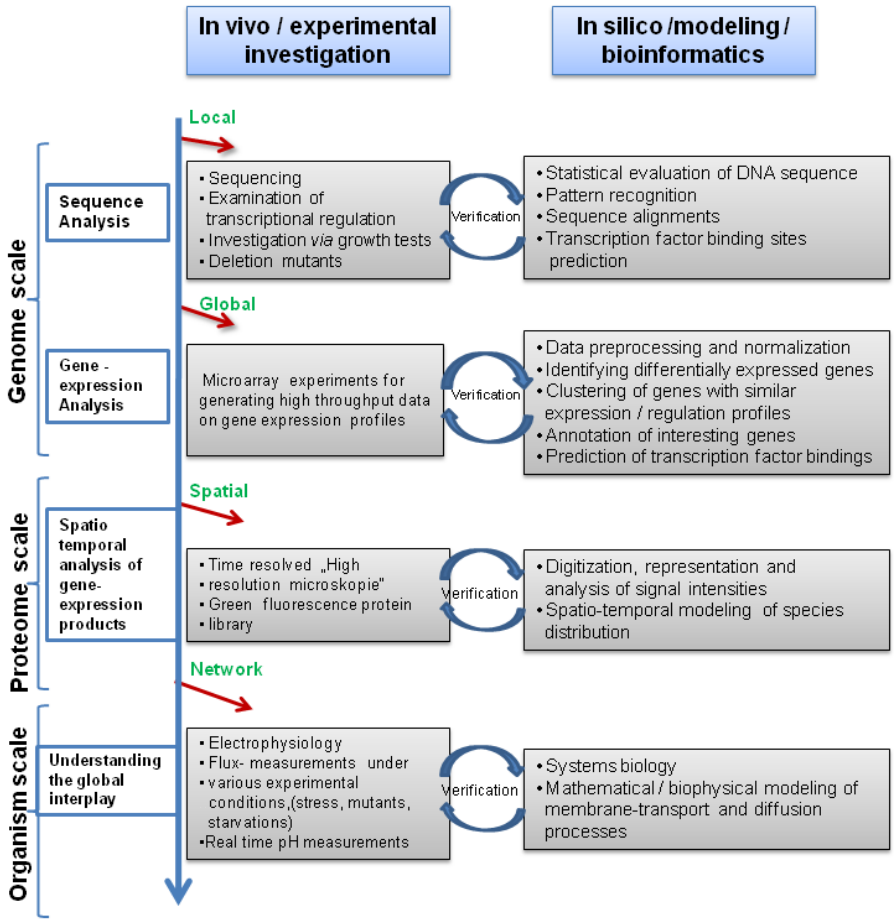

Figure 1.2: Pipeline and strategies of the present thesis to understand the complex system of cation homeostasis in *S.cerevisiae*

1.1.3 Organization of the Thesis

Chapter 2 (Promotor Analysis): A basic task in understanding processes of biological systems is addressed: sequence analysis. Within this chapter the analysis of promoter regions of genes encoding relevant plasma-membrane cation transporters and global regulators is presented. The aim of this work was a tool to analyze genetic elements upstream of coding regions to identify potential transcription factors that may regulate the expression.

Chapter 3 (Evaluation of microarray data:) The genome wide analysis and evaluation of yeast stress-response due to various toxic heavy metal perturbations is described. The raw data of several microarray experiments were normalized, analyzed and evaluated to provide an outline of the *S. cerevisiae* gene clusters involved in system responses to cationic stress as a network of protein complexes.

Chapter 4 (Spatio-Temporal-Modeling Environment - STSE:) An integrated modeling environment suitable for linking together cellular spatial and temporal independent processes at a granular level is presented. Such environment may be used for analysis and interpretation of time resolved protein localization and accumulation data upon definite stress challenges.

Chapter 5 (Thermodynamic Model:) A systematic thermodynamic formulation for cation regulation in *S.cerevisiae* is presented. The model is based on the theory of non-equilibrium thermodynamics and considers fluxes of the major cations K^+, Na^+ H^+, the utilization of ATP as an active driving force and the consideration of the membrane potential.

Chapter 6 (Summary and Global Discussion:) The different studies in this thesis are summarized and discussed in the context of the global project goal.

1.2 Biological Background

As the most simple eukaryotic organism yeast is broadly accepted as a laboratory model organism because it is easily propagated and manipulated in the laboratory and shares a common life cycle and cellular architecture with higher eukaryotes. The high degree of homology of essential cellular organization and metabolism has already enabled study of aspects of cellular stress and phenomena of relevance to human biology at the molecular level [RMR+97, CO04, RC00].
Such research has offered many insights into the complex mechanisms underlying the sensing and response to a variety of stressors [GdBDC03, GS00]. The degree to which gene expression profiles are conserved upon environmental stress and the regulation of key pathway elements enabled the identification of human signal transduction homologues [BIB04, GHM+01]. Due to the highly conserved nature of the cell-cycle machinery between yeast and humans, budding yeast is also an eligible model to study cell- cycle regulation, which is defective in cancer cells [YLA+08, Har02]. Consequently, as such well characterized unicellular eukaryotic organism [Smu01] *S. cerevisiae* was also subjected to in depth analysis of membrane transport properties [BF88] and physiological function of membrane bound alkali-metal-transporters [Syc04].
The complete genome [GBB+96] as well as large-scale experimental -omics data together with a number of methodological tools provide suitable research conditions. Yeast is classified as a GRAS (generally recognized as safe) microorganism and since 1997 [HDR+97] the complete set of the 6275 genes (of which about 5,800 are believed to be true functional genes) is available as open-source database information.

1.2.1 Yeast as a model organism

The application of yeast for genome-wide studies of nutrient homeostasis has significantly increased with completion of the *S. cerevisiae* Genome Deletion Project [WSA+99, ECN+05]. This large-scale project resulted in a comprehensive collection of deletion mutants disrupted in almost each gene in the yeast genome that does not negatively interfere with the viability of the cell. Since 1996, when the *S. cerevisiae* genome was completely sequenced [GBB+96] regular updates have been collected at the Saccharomyces Genome Database (SGD) [CAB+98, DHD+02], a highly annotated and cross-referenced database for yeast researchers.
An analysis performed in 1997 reported that about one-third of yeast proteins had significant homology to mammalian sequences [BCC97]. Powerful methods in classical yeast genetics including homologous recombination, generation of knock-outs strains and homologous or heterologous expression tools have been amended by tools increasingly oriented toward high-throughput and highly parallel systematic methodologies.
The two-hybrid system continues to advance and expand; yeast microarrays are by now relatively cheap and easy to manufacture and yeast continues to be at the forefront of technology development in genomics and proteomics [Hug02].

1.2.2 Regulation of intracellular cation content

The homeostasis of intracellular ion concentrations and the dynamic regulation of ion trans-port is an essential property of every living cell. In comparison to the relatively controlled environment of most animal cells (within the tissue context), the cells of plants, algae and fungi must tolerate a wider range of sometimes rapidly changing environmental conditions like osmotic pressures, pH, and salt concentrations in their natural habitats.

In yeast potassium is accumulated from relatively dilute solutions to sustain a cytosolic K^+ concentration within the range of approximately 175-300 mM which counterbalances the intracellular high negative charge. Proteins, inorganic and organic negatively charged polyanions (the latter originated mainly from carboxylic acids and mono- or diester phosphates) account for a bulk of negative charges in the cytosol and organelles. To sustain overall electro-neutrality high concentrations of cations are accumulated within the cellular compartments [RN00].

Besides a stable and balanced intracellular cation content monovalent cation transport is also required for other important physiological parameters such as maintenance of the cell volume and internal pH, the membrane potential, protein synthesis and enzyme activation [Jen95, Rot64, Tos64]. These fundamental physiological functions are highly dependent on the regulation of uptake- and extrusion systems for the major monovalent cations sodium and potassium. Although sodium (Na^+) is the most abundant naturally occurring cation potassium (K^+) is the crucial physiological cation and sufficient intracellular concentrations are an absolute requirement for many cellular functions such as osmotic regulation, protein synthesis and enzyme activation [EW71]. In *S. cerevisiae* Na^+ is not necessary when K^+ is not limited [CRRN81].
Even though Na^+ can replace potassium in K^+ depleted environments [RHRN90, Syc04] and serve to temporarily assist to adjust intracellular pH and cell volume [RHRN90], high concentrations of (Na^+) or its biophysical analogue Lithium (Li^+) are generally toxic to yeast cells [Syc04, ZCR06]. High intracellular Na^+-concentrations inhibit most enzyme reactions due to the perturbation of the hydrophobic-electrostatic balance between the forces maintaining protein structure [JP83, MBS95, AYGM$^+$00]. As a consequence, many metabolic reactions and membrane functions appear to be negatively affected by higher salt concentrations [GdLVS92, GTG$^+$93] due to such structural changes in membrane proteins [Ser96]. In addition to these relatively nonspecific salt effects, individual enzymes may vary widely in their sensitivity to Na^+ or Cl^- at much lower concentrations upon specific interactions of the ions with inhibitory binding sites. However, fungal and also plant cells are not completely impermeable to Na^+. Even if a high Na^+/K^+ - ratio is detrimental an increased concentration of internal Na^+ is, in comparison, less toxic than an intracellular acidic pH.
To ensure viability even under adverse external environmental conditions yeast cells have evolved several response systems to saline, osmotic and alkaline pH stress [ARS10, RN00, SRN01, GS00]. The intracellular concentrations providing optimal growth conditions are approximately 175 - 300 mM potassium and less than 100 mM sodium with a ratio of $K^+/Na^+ > 1$. To maintain an optimum cytoplasmic pH of approx 6.5 and a stable balanced intracellular Sodium/Potassium ratio yeast cells invest high amounts of biological energy (ATP) and employ three distinct strategies [Syc04]:

- The strict discrimination among alkali metal cations at the level of influx (higher affinity of transporters for potassium than for sodium)
- A proper disposal of toxic cations
- A selective sequestration of cations in organelles

1.2.3 The plasma-membrane of *S. cerevisiae*

The outermost layer of *S. cerevisiae* envelope is the cell wall. This mechanical barrier maintains the structure and the rigidity of the cell but is freely permeable for solutes smaller than 600 Da [SLG74].
The adjacent plasma-membrane forms a lipid bilayer of approximately 7.5 nm wide and is permeable to small hydrophobic molecules, such as hydrogen, carbon dioxide, water and glycerol

[AJ02] whereas it is highly impermeable to hydrophilic, charged and larger molecules. The plasma membrane serves as the interface between the machinery in the interior of the cell and the extracellular fluid that bathes all cells. The membrane must shield cellular metabolism from changes in the environment to prevent undesirable agents from entering cells and keep required molecules on the inside. The lipids in the plasma membrane are phospholipids like phosphatidyl ethanolamine and cholesterol. Phospholipids are amphiphilic with the hydrocarbon tail of the molecule being hydrophobic; its polar head hydrophilic.
As the plasma membrane faces watery solutions on both sides, its phospholipids accommodate this by forming a phospholipid bilayer with the hydrophobic tails facing each other. Lipid bilayers are impermeable to most essential molecules and ions. The lipid bilayer is permeable to water molecules and a few other small, uncharged, molecules like oxygen (O_2) and carbon dioxide (CO_2). These diffuse freely in and out of the cell. Lipid bilayers are not permeable to:

- cations such as K^+, Na^+, Ca^{2+}
- anions such as Cl^-, HCO^{3-}
- small hydrophilic molecules like glucose
- macromolecules like proteins and RNA

To function effectively, advanced strategies to selectively pass molecules, ions, and signals from one side to the other have been evolved. Transport proteins are the principal constituents of the plasma membrane. Many of the proteins associated with the plasma membrane are tightly bound to it. Some are attached or anchored to lipids in the bilayer. In other transport proteins - the transmembrane proteins - the polypeptide chain actually traverses the lipid bilayer. In all these cases, the portion within the lipid bilayer consists primarily of hydrophobic amino acids. These are usually arranged in an alpha helix so that the polar $-C=O$ and $-NH$ groups at the peptide bonds can interact with each other rather than with their hydrophobic surroundings. Some transmembrane proteins that span the bilayer several times form a hydrophilic channel through which certain ions and molecules can enter (or leave) the cell. Peripheral membrane proteins are more loosely associated with the membrane. They are usually attached noncovalently to the protruding portions of integral membrane proteins.
The plasma membrane of *S. cerevisiae* can contain up to 10^5 to 10^6 transporter molecules, which is roughly 50% of all plasma membrane proteins [Ser91]. The principal plasma membrane ATPase, encoded by the PMA1 gene, by itself, can additionally account for almost 50% of the plasma membrane protein content in growing cells [Ser91]. Other proteins are involved in cell wall synthesis [Fle91] or signal transduction [OC94].
Some of the proteins exposed at the interior face of the plasma membrane are tethered to cytoskeletal elements like actin microfilaments[BDS90]. Some proteins are the exterior face of the plasma membrane and anchored to components of the extracellular matrix like collagen. Cation transport mediated by integral membrane-proteins with different substrate specificities and primary and secondary transport mechanisms (see Figure 1.3)

1.2.4 Transport- mechanisms

Mechanisms by which cells transport ions and small molecules across their membranes involve:

Facilitated diffusion

Facilitated diffusion of ions takes place through proteins, or assemblies of proteins, embedded in the plasma membrane.

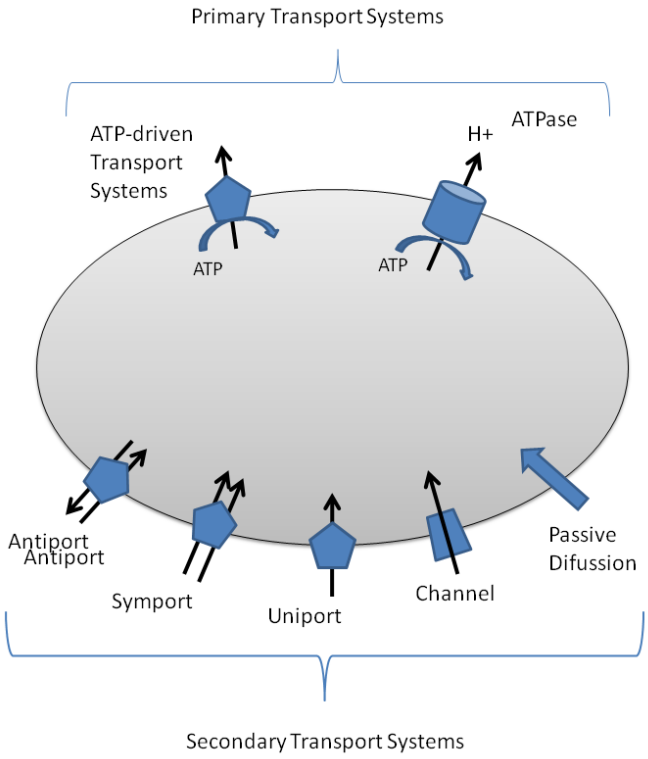

Figure 1.3: Primary and secondary transport systems in *S. cerevisiae* as discussed in [vdRKN+95]

These transmembrane proteins form a water-filled channel through which ions and some small hydrophilic molecules can pass by diffusion down their concentration gradients. The transmembrane channels that permit facilitated diffusion can be opened or closed by different mechanisms and are thus "gated". The gating mechanism indicates the type of ion channel: ligand-gated, mechanically-gated or voltage-gated. In all cases of facilitated diffusion through channels, the channels are selective; that is, the structure of the protein admits only certain types of molecules through. In *S. cerevisiae* two distinct types of ion channels have been identified in the plasma-membrane: voltage dependent K^+-channels (see below) and rather unspecific channels that are activated by stretching the bilayers [GZMK88].

Active transport

The mechanism of active transport is the pumping of molecules or ions through a membrane against their concentration gradient. It requires: a transmembrane protein (usually a complex of them) and energy.
The source of this energy is ATP whereby the energy of ATP may be used directly or indirectly. Within direct or primary active transport transporters bind ATP directly and use the energy of its hydrolysis to drive active transport. Indirect or secondary active transport utilizes the energy already stored in the gradient of a directly-pumped ion.

Primary transport

Primary transport is defined as transport in which light or chemical energy is converted into electrochemical energy (i.e solute or ion concentration gradients). Active transport of the ion establishes a concentration gradient. When this is relieved by facilitated diffusion, the energy released can be harnessed to the transport of some other ion or molecule (secondary). Transmembrane proteins use the hydrolysis of ATP to force ions or small molecules through the membrane against their concentration gradient. For *S. cerevisiae*, only ATP-driven primary transport systems have been described [vdRKN$^+$95]. The plasma-membrane contains a highly active proton exporting ATPase (Pma1) [Ser91, Ser89]. The hydrolysis of ATP by Pma1 results in the generation of an electrochemical gradient of protons. The free energy present in this gradient exerts a force on the protons (proton motive force) which is utilized to drive membrane-associated processes. The transport of nutrients and ions is largely coupled to the proton-gradient, allowing intracellular Na^+ and K^+ to be independently regulated [Ste90a].

Secondary transport

Secondary transport means that the energy for the translocation of solutes is supplied by (electro-) chemical gradients of other solutes/ions. Three general categories of secondary transport systems can be distinguished: uniport, symport and antiport.
Uniporter are carrier proteins facilitating the transport of a single solute without the movement of a coupling solute. When the transport involves the coupled movement of two solutes in the same direction, the transport is referred to as symport. Antiporters refer to the coupled movement of solutes in opposite direction [vdRKN$^+$95]. Since the solutes transported by secondary transport systems can be neutral, negatively or positively charged and since different numbers of solutes may be co- or counter-transported, the driving forces on these processes may vary considerably. For a comprehensive review on secondary transport, see [PK83, FKR$^+$95].

1.2.5 Plasma-membrane transport-proteins in *S. cerevisiae*

S. cerevisiae contains at least ten transport systems mediating efflux and influx of the examined most important cations H^+, K^+ and Na^+ with different substrate specificities and mechanisms [ARS10](Figure 1.4).
These transporters accommodate the following properties [ARS10]:

- Providing the cell with necessary and sufficient amounts of potassium
- Maintaining the potassium homeostasis.
- Elimination of toxic sodium or lithium cations.
- Regulation of the intracellular pH.
- Preservation of the membrane potential.
- Retention of a positive turgor inside.
- adapting with osmotic stress.

Most of them are associated with the plasma membrane others with the membranes and of intra-cellular organelles. Some intracellular transporters have only recently been identified and characterized. These comprise mainly alkali-metal cation/H^+-antiporter, located in the vacuolar membrane (Vnx1), endosomal membrane (Nhx1) and the Golgi apparatus membrane (Kha1).

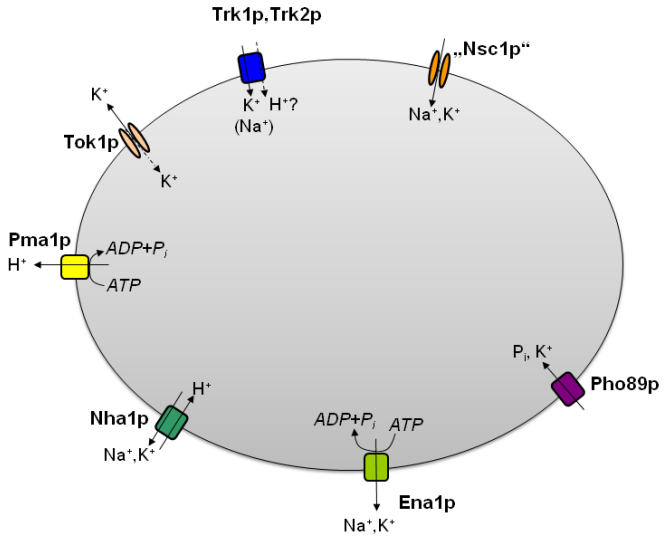

Figure 1.4: The major cation homeostasis relevant plasma-membrane transporters in the yeast *S.cerevisiae*

Name	Type	Substrate specificity	Main function
Trk1	Uniporter	K^+ (Rb^+)	K^+-uptake
Trk2	Uniporter	K^+ (Rb^+)	K^+-uptake
Tok1	Channel	K^+	K^+-extrusion
Nsc1	Channel	unspecific	Function unknown
Ena1	ATPase	Na^+,Li^+ (K^+,Rb^+)	Detoxification
Nha1	Antiporter	Na^+,K^+ (Li^+,Rb^+)	Na^+,K^+-Extrusion
Pma1	ATPase	H^+	H^+-extrusion
Pho89	Symporter	Na^+, P_i	Phosphate-uptake

Table 1.1: Plasma-membrane alkali-metal cation transporter in *S. cerevisiae*

These organellar systems also serve to regulate the intracellular K^+- and pH-homeostasis and may play an important role in detoxification of sodium by sequestration in the vacuole. For these intracellular transport systems almost no time resolved biochemical transport data are currently available and were thus not included in further mathematical models.

The yet eight well-characterized transport proteins relevant to the regulation and maintenance of intracellular alkali-metal cation content (see Table 1.1) are briefly described. Comprehensive reviews detail further details and mechanisms, regulatory elements and the "long-term" regulation processes by transcription [Syc04, ARS10, RN00].

1.2.6 Plasma Membrane ATPase - Pma1

Yeast cells generate a large amount of protons during metabolism. To maintain an stable intracellular pH surplus protons become actively extruded by the as Plasma Membrane ATPase - Pma1 [Ser83, GS81, MSG00]. PMA1 as one of the most prominent housekeeping genes in

S. cerevisiae encodes the major plasma membrane H^++-ATPase [SKBF86] and is essential for viability.
As highly conserved member of the E2 family of P-type ATPases the H^+-ATPase is a single, 100 kDa polypeptide firmly embedded in the lipid bilayer [AMS00]. The electrogenic proton pump, driven by hydrolysis of phosphoanhydride bonds, is the major source for cytosolic proton extrusion and generation of the electrochemical gradient (proton motive force, PMF) across the cellular membrane.
It is estimated that this process consumes at least 20% of all cellular ATP with a stoichiometry of one proton extruded per molecule of ATP hydrolized [GS89, SKBF86, GFF$^+$00]. This electrochemical inward gradient of protons is responsible for secondary active transport mechanisms for a variety of solutes such as sugars, amino acids, nucleosides and is also involved in pH homeostasis [vdRKN$^+$95]. The proton gradient together with the plasma membrane potential can be used as an energy source for nutrient acquisition and to pump out surplus or toxic alkali metal ions [vdRKN$^+$95].
Even in the presence of abundant oxygen *S. cerevisiae* greatly prefers fermentation to oxidative phosphorylation, as long as sugars are readily available for consumption, to maintain the production of ATP (Adenosine triphosphate) by glycolysis. ATP is a nucleotide that performs many essential roles in the cell and is the biological energy currency of the cell, providing the energy for most of the energy-consuming activities of the cell.
In being the major protein component of the plasma membrane (15-20%) of total plasma membrane protein; [AMS00] the activity of this proton pump is precisely regulated according to the metabolic activity and physiological conditions to match its numerous requirements [KG94, FSC03]. Maresova et al. [MMZ$^+$09] showed that Pma1 has minimal activity in the absence of glucose whereas external glucose supply is a powerful stimulus leading to a rapid and strong activation [Ser83]. In order to increase the glucose uptake rate, it has been shown that the activity of Pma1 is up-regulated up to 10 fold [Ser83, GFF$^+$00]. Its activity is also positively regulated in response to decreased intracellular pH or increased potassium uptake [SYP91]. Not surprisingly, ΔPma1 mutants are non-viable.

1.2.7 Potassium exchange with the environment

With K^+ as the most abundant cellular cation, potassium exchange plays a pivotal role in a number of essential processes like electrical activity of excitable cells, enzymatic activities [BSBG$^+$98], cellular K^+ homeostasis and, indirectly, pH regulation. Since Potassium constitutes a large proportion of plasma osmolytes (intra-cellular soluble compounds affecting osmosis) it's intracellular concentration has considerable impact on cell volume and fluid balance [PCH$^+$00, PCA93].
The high potassium content in yeast cells corresponds to the steady state between simultaneous influx and efflux across the plasma membrane This continuous circulation is believed to be necessary for maintenance of potassium homeostasis, constant intracellular pH and regulation of cell volume [ORN85, LK98]. K^+ uptake is a major influx of positive charges that balances the proton extrusion. As a result, potassium transporters are also involved in setting the membrane potential and intracellular pH [MGRRN98]. Therefore, in yeast cells a variety of transporters and complex mechanisms evolved to regulate the uptake of K^+ and extrusion of the toxic - in excess amounts - Na^+ ([RN00, Syc04, ARS10]).

Potassium uptake

In *S. cerevisiae*, the TRK genes are involved in potassium influx. The optimum intracellular potassium content is 175 -300mM [Syc04, RHRN90, FKR$^+$95], whereby the available K^+ con-

centration in natural habitats is in the micromolar range [RNR84, RN00]. For this purpose, *S. cerevisiae* cells have developed specific potassium transport systems. Two active transporters (Trk1p and Trk2p) [KG91, KBG90, BRL$^+$03] and the Nsc1 [BSB98, BSB02] channel for which, however the genetic equivalent has not yet been identified, ensure the uptake of K^+ in yeast cells.

Trk1 and Trk2 are high-affinity potassium carrier located in the plasma membrane. In *S. cerevisiae*, two closely related plasma membrane localized K^+ translocation systems, Trk1 and Trk2 mediate K^+ uptake to maintain a high intracellular potassium concentration to counterbalance the high negative charge on nucleic and amino acids. TRK1 is the most important gene related to potassium uptake and its gene product mediates potassium transport with high affinity and high velocity [BRL$^+$03, HRN02]. TRK2 is highly homologous to TRK1, but it is poorly expressed in wild type cells and mediates potassium uptake with moderate affinity and very low V_{max} [KG91, KBG90, RAHRN94]. Its activity in wild-type strains, if any, would be masked in the presence of Trk1 [ARS10]. While disruption of TRK1 produces cells that are viable in normal media but lack most of the K^+ uptake in the micro molar range and requiring higher potassium concentrations to grow [FKR$^+$95], disruption of TRK2 does not induce any apparent potassium transport defect in TRK1 cells [RCRN85, Gab88, Gab88, RAHRN94]. Cells lacking both genes require relatively high concentrations of potassium to grow ($> 10mM$), show potassium uptake with low V_{max} and low affinity [YMHS05, BRL$^+$03], are sodium sensitive (see [RAHRN94] and references therein) and also show plasma-membrane hyperpolarization [MGRRN98]. The nature of this potassium transport activity has not been definitively established and it has been proposed that it may be related to the activity of several non-specific potassium transporters [KLG93, WRG$^+$97, MGRRN98].
Under non-stress conditions, K^+ becomes accumulated in yeast cells against a large concentration gradient via these carriers [KG91, KBG90, RAHRN94]. The membrane potential might be the energy source for this process [RN00]. The activity of the Trk1,2 system also has a substantial impact on the membrane potential, since the high potassium influx rate is a major return current for the H^+- extrusion by Pma1 [MGRRN98].

The **N**on **S**pecific **C**ation channel **Nsc1**. Using electrophysiological recording techniques, Bihler et al. [BSB98, BSB02] identified a large inward rectifying cation conductance (Nsc1) whose activity is independent of TRK1, TRK2 and the potassium efflux channel gene, TOK1. This non-selective inward rectifying conductance is permeable to K^+,NA^+, Li^+ and NH4$^+$ with similar affinities but is inhibited by extracellular divalent cations, just as growth of the trk1, trk2 double deletion strain under K^+ limiting conditions. Based on kinetic and pharmacological grounds, Bihler et al. [BSB98, BSB02] concluded that this conductance may result from the activity of a single rather than from several different types of transport proteins. However, since the gene for this proposed transport system has not been identified so far, the nature of the TRK-independent potassium uptake system remains unclear. However, this channel appears to be a good candidate to explain the "very low affinity" potassium uptake process in ΔTrk1/ΔTrk2 mutants [ARS10].

Potassium efflux

At least three different transporters, Ena1, Nha1 and, Tok1 contribute to the potassium efflux, depending on the physiological conditions. In response to KCl (excess) stress, potassium can be actively extruded by the Ena1-ATPase [HGRN91, WNS$^+$95] or by the Nha1 antiporter [BSBG$^+$98]. Both were primarily identified as Na^+-extrusion systems but can also mediate K^+-efflux under certain conditions. Tok1 is the only potassium-specific efflux-system in *S. cerevisiae*.

Tok1: Yeast cells contain only one member of the K^+ channel superfamily, Tok1 is a two-pore, voltage-dependent outward rectifying K^+-channel that under certain conditions also mediates inward K^+ uptake [KJS$^+$95, FZK99]. In resting yeast cells this channel shows only minor current. The biophysical properties of this K^+-channel are well described [BSG93, BRL$^+$03] but the physiological role of Tok1 has not yet been fully characterized. Tok1 is activated by plasma-membrane depolarization to release intracellular accumulated K^+ in order to regenerate the membrane potential [BBR$^+$98, MUGS06] the channel is open at positive and very low negative membrane voltage [FZK99, BSG93].
It has been demonstrated that the activity of Tok1 seems to be regulated by external potassium concentrations [LS99]: The gating of the Tok1 channel is specifically controlled by external K^+ concentrations above millimolar inactivate Tok1. The channel catalyzes potassium efflux (outward rectification) when the membrane potential is higher (less negative) than the K^+ equilibrium potential. Apart from mediating K^+ outward rectification, a small inward flux can be observed when the membrane potential is below the potassium equilibrium potential [FZK99]. Deletion of TOK1 gene results in a significant depolarized membrane, whereas strains with a TOK1 overexpression are hyperpolarized and show a lower intracellular K^+ concentration [KZGS06, MUGS06].

1.2.8 Sodium exchange with the environment

In contrast to potassium uptake transporters, yeast cells do not encode transporters for sodium uptake but rather active transporters for efficient Na^+ elimination. Sodium ions carry a single positive charge and the interior of the cell is negatively charged. So the attraction between opposite charges provides a force for bringing Na^+ into the cell. When yeast cells are exposed to salt stress, Na^+ enters the cell unspecifically as a low-affinity substrate through several cation-transporting systems, mainly those involved in potassium uptake, although with much lower affinity [RCRN85]. Since increased cytoplasmic concentration of this toxic cation are unfavorable in *S. cerevisiae*, three mechanisms function cooperatively to prevent a sustained sodium accumulation: restriction of influx, active efflux and compartimentation of Na^+ in the vacuole.The maintenance of the very low intracellular Na^+ concentration is ensured by the capacity of two main extrusion mechanisms: The Na^+/H^+-antiporter, encoded by the NHA1 gene and the P-type ATPase pump, encoded by the ENA system [KZGS06, Syc04].

Nha1 is a plasma membrane Na^+, K^+/H^+ antiporter, first characterized by Prior in 1996 [PPSS96]. As a secondary active transport system Nha1 utilizes the inward gradient of protons as a driving force to eliminate sodium cations. Nha1 also contributes to the cellular homeostasis my mediating the efflux not only of toxic Na^+ and Li^+ cations but also, with however low capacity excessive K^+ and Rb^+ [BSBG$^+$98, KRPS01, KPS01] to maintain the intracellular pH. Nha1 participates thus as a short-term safety valve in the maintenance of a stable membrane potential [KZGS06, MUGS06] and, is involved in the rapid rescue mechanism during the immediate cell response of osmotic or saline shock [KRPS01] by utilizing the K^+-outward gradient as a driving force for proton in-flux [ORN85, BSBG$^+$98]. Deletion-mutants (ΔNha1) show a significantly decreased tolerance to salt stress in acidic and neutral conditions whereas Nha1 overexpression leads to a higher membrane potential [KZGS06] and a higher tolerance to NaCl stress conditions.

ENA is the abbreviation for **E**xitus **NA**tru and appears to be the most efficient sodium detoxification system [WNS$^+$95, HGRN91, RA07, GRQ$^+$93]. The Na^+ transporter gene ENA1/PMR2A is the first repeat in a tandem array of five open reading frames, the PMR2 locus encoding nearly identical proteins. The importance of this efflux system is underlined by the observation that it

is present in all fungi as well as in certain plants and evolutionary conserved.
As P-type ATPase Ena1 couples ATP hydrolysis to pump cations against electrochemical gradients [HGRN91, CdKG97] and extrudes Na^+, Li^+ and also K^+ with different capacities and affinities [RA07, BGRN02]. Under normal growth conditions the Ena1 ATPase is present in very low copy numbers, but the expression can rapidly increased under stress with excess NA^+- Li^+ or alkaline pH-stress [MS96, Syc04, PR06, MRRNP94, PCA95, RNQG94].
Cells lacking ENA1 genes are highly sensitive to high external Na^+ and Li^+ concentrations [WNS$^+$95, GRQ$^+$93, HGRN91] and show a markedly increase of the cytoplasmic content of these cations. Although the primary role of the ENA-system is detoxification of sodium (and to some extend lithium) cations these ATPases are also be involved in potassium homeostasis, e.g at higher-than-neutral pH, when the K^+/H^+ antiporter, Nha1 is not active [RA07].
Construction of a mutant strain with deletions of genes encoding both Na+-ATPase and Na+/H+ antiporter (ΔENA1 and ΔNHA1) confirmed that both transport systems are necessary for cell tolerance to high external concentrations of salts and for the maintenance of intracellular steady-state concentrations of K^+ and Na^+ [Syc04]. The two systems exhibit complementary activity in the maintenance of intracellular steady-state concentrations of K^+ and Na^+: The Nha1 antiporter is responsible for cell growth on high concentrations of KCl and NaCl at acidic external pH values, and the Ena1 ATPase is necessary at higher pH values [BSBG$^+$98].
The dual role is also reflected in the different expression patterns of both systems. Whereas NHA1 expression is constitutive, very low and does not seem to be inducible by salts, pH changes or osmotic shocks, the ENA1 expression is transcriptionally regulated and can be induced by Na^+, Li^+ or high pH values [RYA03, RA07].

Pho89 represents the only Na^+-coupled secondary anion transport system so far identified in *S. cerevisiae* [ARS10] however, detailed studies on the relevance of sodium entry mediated by this transporter are lacking.

1.2.9 Membrane Potential

The separation of ions and thus electrical charges by biological membranes creates an electrical potential difference across the membrane. This total difference commonly called the membrane potential plays a crucial role in many membrane functions [HC98, BS88, Jak80, Sch80, Wil93]. Since the membrane potential defines the electrical energy loss when ions cross the cellular membrane it also determines, at least in part the energy stored in ion concentration gradients. The electric field associated with the membrane potential may regulate the activities of membrane proteins by acting on their dipolar groups. Voltage-dependent channels, for instance, open and close in response to changes in the membrane potential. Despite several decades of investigation and efforts a reliable quantitative experimental determination of the membrane potential in *S. cerevisiae* is still lacking. Direct methods like electrophysiological approaches suffer from the impenetrable cell wall and the small size of yeast cells (3-4 μm). Quantitative membrane potential estimations by direct and indirect methods revealed values of -200 mV (under normal growth conditions) and up to -300 mV (in starved cells) [Ser91, SKS90, RN00]. Indirect techniques by e.g. flow cytometry using fluorescence probes provide qualitative comparative data under defined conditions but no quantitative "real" measurements. Madrid et al. [MGRRN98] showed by this technique that *S. cerevisiae* must have a membrane potential very similar to *N. crassa* which - amenable to electrophysiologicall measurements - could be determined as to be about -300 mV [RNBS86]. Grassmann and Rodriguez-Navarro predict his value to be underestimated by 20 or 40 mV [GWS93, RN00] and assume the membrane potential of K^+ starved cell to be more

negative than -300mV [RN00].
Glucose supply is known to increase the membrane potential toward more negative values by enhancing the H^+ pumping activity of Pma1 [Ser83] but again, no exact determination has been reported yet.

2 Promotor Analysis

2.1 Abstract

One of the first tasks in understanding biological systems is the systematic study of genomic sequences. In the following paragraphs the analysis of specific regions of selected genes involved in cellular potassium homeostasis and regulation is described. To analyze relevant and interesting transcription factors (TF) a simple graphical presentation for the results of a transcription factor pattern matching analysis was designed. The TF analysis algorithm utilized known sequence signature motifs from several databases. The graphical presentation enabled a quick overview of potential TF binding sites, their frequency and spacing on both DNA strands and thus straight forward identification of promising candidates for further experimental investigations. The developed tool was applied on in total four *S. cerevisiae* gene promoter regions.
The selected differentially expressed genes belong to functionally different families and encode duplicated functions, TRK1 and TRK2 as ion transporters and BMH1 and BMH2 as multiple regulators. Output evaluation revealed a number of TFs with intriguing differences. Experimental investigations were performed by using corresponding TF yeast mutants for either phenotypic analysis of potassium transport mediated growth or expression analysis of BMH1,2 genes. Upon the phenotypic testing one TF mutant exhibited severely impaired growth under non-permissive conditions. This TF, Mot3p was identified as of most abundant potential binding sites and distinctive patterns among the TRK promoter regions.
The experiments for evaluating the predictions were prepared and provided by Guido Hasenbrink, University of Bonn and Wouter Hendriksen, University of Leiden within the above mentioned TRANSLUCENT project.
Source code as well as detailed output tables for all 288 tested TF sequence motifs for genes TRK1,2 PMA1, TOK, NSC1, ENA1, PHO89 and for BMH1,2 are accessible on
http://jaguar.biologie.hu-berlin.de/∼sgerber.
The result of this analysis is presented in
S. Gerber, G. Hasenbrink, W. Hendriksen, P. Van Heusden, J. Ludwig, E. Klipp, and H. Lichtenberg-Fraté: Graphical analysis and experimental evaluation of *Saccharomyces cerevisiae* $P_{TRK1|2}$ and $P_{BMH1|2}$ promoter region. Genome Informatics 22, (11-20);(2010).

2.2 Introduction

In the post-genome era the task of regulatory elements prediction and in particular promoter region analysis has received increasing interest and a considerable number of algorithms, tools and analyzing strategies were developed. However, despite many useful approaches signal finding such as pattern discovery in DNA sequences is still a fundamental problem in molecular biology with such important applications as locating regulatory sites and drug target identification. Most signals in DNA sequences are indeed complex or not yet discovered, so that there is a lack of reliable algorithms for their authentic recognition. For instance, some transcription factor binding sequences are injective but the majority shows a rather high degree of unspecificity leading to a bijective behavior. Concerning the model organism *S. cerevisiae* the currently available tools

like AlignACE [HETC00], Consensus [HS99], TESS [SO97], TRANSFAC [WCF+01, WDKK96] or Genomatix [CFG+05] differ from each other basically in the definitions of what constitutes a motif, what constitutes statistical over-representation of a motif and the methods used to identify statistically overrepresented motifs (for a review see [Tom05]). As a result these tools differ significantly in their binding site predictions or recognize motifs that are not even specific for the queried organism, e.g. mammalian TF motifs for promoter regions of *S. cerevisiae*.
In all cases the graphical presentation of positive hits on both strands is a highly condensed and information-wise insufficient image. Since only a few assessments or reviews of some of these motif discovery tools have yet been published there is little guidance in the choice among these tools ([PS00, Tom05]) and it is virtually impossible to decide on objective grounds of whether the results of the tool (A) are better or more plausible than those of tool (B). This lack of a reliable and, in particular "S. cerevisiae" specific tool for promotor analysis and transcription factor binding site prediction rise the challenge to implement a bioinformatical analysis that should reveal first indications of potential TFs for specific genes, or their upstream regulating sequences respectively, involved in cation transport or their possible regulators.
The analysis emphasized on frequency, spacing and accuracy of match and presented the results in a graphical format enabling straight forward visual inspection and decisions on potentially promising candidates for further experimental investigation.
As examples for an explorative approach the promoter regions of the TRK1 and TRK2 and BMH1 and BMH2 were selected. These genes encode duplicated functions in yeast, are differentially expressed and highly regulated and appeared thus as reasonable candidates for a comparative promoter region analysis. TRK1 and TRK2 are components of the potassium transport system [Gab88, KG91, Ko90, YMHS05], and the latter, belonging to the group of 14-3-3 proteins, act as multiple regulators.
14-3-3 proteins are a family of highly conserved proteins and have been identified in all eukaryotic species investigated. *S. cerevisiae* encounters two genes encoding 14-3-3 proteins, BMH1 (major isoform) and BMH2, and these proteins are involved in various cellular processes [vHS06]. Numerous studies revealed that expression of BMH1 and BMH2 is affected by different circumstances (for a review see [vH09]) and might therefore be tightly regulated by transcription factors.

2.3 Material and Methods

2.3.1 Bioinformatic analysis

A data set of all available TFs known to be functional in yeast within the literature documented binding sites was collected. For this purpose the YEASTRACT database (Yeast Search for Transcriptional Regulators And Consensus Tracking) [TMJ+06] that presently contains 30990 regulatory associations between the yeast genes based on more than 1000 bibliographic references was parsed. Each regulation was manually annotated after examination of the relevant references.
Further information about each gene was obtained from the Saccharomyces Genome Database (SGD) [CAB+98, DHD+02], Regulatory Sequence Analysis Tools (RSAT) [vH03] and Gene Ontology (GO) Consortium [Con00]. The assembled dataset for this study contained the description of 288 specific and in the literature documented DNA binding sites for a group of 108 transcription factors.
The analysis was performed by implementing a Matlab program that imports a promoter sequence in FASTA-format and the data set of TFs with their potential DNA-binding sequences. If the TF binding sequence contains IUPAC codes other than one of the four nucleotides the

Transcription Factor	TRK1			TRK2		
matches	forward	reverse	total	forward	reverse	total
Fkh1p	4 ∗	5∗	9	3 ∗	1	4
Fkh2p	4 ∗	5∗	9	3 ∗	1	4
Mot3p	2 ∗	11∗	13	6	1	7
Msn2p		1	1	3		3
Msn4p		1	1	3		3
Stb5p	3	1	4	4	6	10

Table 2.1: Selected transcription factors for experimental analysis. Entries labelled with asterisk ∗ show the total number of hits with more than one possible binding sequence

program will identify all possible matches. For example, the symbol $'R'$ in a sequence represents a Purine at this position (either G or A) and the algorithm would accomplish a pattern search for each sequence on the promoter. For each match the start and stop position on the query promoter sequence is stored as well as the probability of a match of this sequence by just chance. If more than one match of the investigated sequence is identified, the distances between all possible binding sites of this TF are calculated. At the end of the analysis a table with the information of every potential binding sequence is provided. The documentation comprises: the names of the tested TFs and the related sequences; the average likelihood for every sequence to bind on this promoter just by chance; for successful matches the start and stop positions on both strands and, in case that more than one successful match was found, the distances between all these potential binding sites. In addition, a graphical presentation of all potential binding sites on the forward and backward strands for every promoter region is presented.

2.3.2 Yeast strains, media and growth tests

Experiment 1

Haploid *S. cerevisiae* wild type, potassium transporter and TF mutant strains (BY4741; [BDC$^+$98]; Saccharomyces Genome Deletion Project) were used throughout this study as listed in Table 2.1. Growth calculation and statistical analysis was performed by integral determination (approximation of the area under the growth curves) obtained within 17 h incubation according to [HSK$^+$05]. Values for growth were normalized to those of wild type strain values at 50 mM KCl. Details on experimental conditions are provided in the Supplementary Material C.

Experiment 2

In a second experimental scenario the BY4743 wild type and transcription factor mutant cells $MATa/\alpha$ $his3\Delta1/his3\Delta1$ $leu2\Delta0/leu2\Delta0$ $LYS2/lys2\Delta0$ $met15\Delta0/MET15$ $ura3\Delta0/ura3\Delta0$) (*Saccharomyces* Genome Deletion Project [Gia02]) were grown exponentially in YPD. cDNA was produced and ACT1, BMH1, and BMH2 relative gene expression was measured. The oligonucleotide primers used in this study are listed in Table 2.2. BMH1 and BMH2 gene expression ratios were calculated, and these ratios were normalized to ACT1 expression and to wild type BMH1 and BMH2 expression. This procedure was performed for two biological duplicates and expression was measured in triplicate and in duplicate for every sample. Details on experimental conditions are provided in the Supplementary Material C.

Primer name	Sequence 5'-3'	Target
WH11	AGAGTTGCCCCAGAAGAACA	ACT1
WH12	GGCTTGGATGGAAACGTAGA	ACT1
WH29	CGTGCTAGACTCCCACTTAATT	BMH1
WH30	GGCCTTTTCTCTAGCATCG	BMH1
WH15	GTTAGATTCTCATTTAATCCCTTCT	BMH2
WH16	ATAAGCCTCCAAAGAGGAGTTG	BMH2

Table 2.2: Oligonucleotide primers

2.4 Results

The graphical output of the promotor analysis of TRK1, TRK2, BMH1 and BMH2 are given in Figures 2.3 - 2.6. Out of the entire output list promising candidates for experimental investigations were selected along the following criteria:

- Sequence unambiguousness in the pattern matching of TF sequence signature to the DNA.
- The frequency of hits and significant differences in the frequency of hits between the analyzed promoter regions of the gene pairs.
- A rational spacing between the potential TF binding sites (predicted potential binding sites that were at close proximity would constrain each other and were thus devaluated).

Consequently for the TRK1,2 genes 10 potential TFs were selected for further experimental analysis and for the Bmh1,2 genes 7 TFs.
Since in TRANSLUCENT other cation transport systems of *S. cerevisiae* the promoter regions of the *ENA1, TOK1, PHO89, NHA1* and *PMA1* genes are also important these genes were subjected to computational TF sequence signature analysis including graphical presentation. However, these potentially promising transcription factor candidates have not yet been experimentally investigated. Calculations and graphics are provided in the Supplementary Material.

Experiment 1

In *S. cerevisiae* tight control and modulation of the intracellular K^+ concentration (cellular K^+ homeostasis) and corresponding ion fluxes is crucial for cell metabolism, surveillance and growth. Two closely related plasma membrane localized K^+ translocation systems, TRK1p and TRK2p mediate K^+ uptake to maintain a high intracellular potassium concentration. *S. cerevisiae* strains devoid of TRK1 (ΔTRK1) or TRK1 and TRK2 (ΔTRK1,2) are defective in potassium uptake and exhibit impaired growth on limited external potassium concentrations. From the potassium transporters TRK1 and TRK2 promoter region binding site analysis in total 10 potential TFs were obtained. Selection of these TFs or respective mutants as potentially important for further experimental analysis followed the simple rationale of clear frequency and pattern difference within the two promoter regions. Of these, four TF mutant strains are reported as not viable (Saccharomyces Genome Database, SGD).
The methodological approach for the remaining six TF mutants was set accordingly: Will the lack of these TFs influence the TRK-system mediated potassium uptake detectable as growth differences under limited potassium conditions?
The mutant yeast strains Δmot3, Δmsn2, Δmsn4, Δstb5, Δfkh1, Δfkh2 carry disruptions in the respective TF genes. The growth of these strains was compared to that of *S. cerevisiae* wild

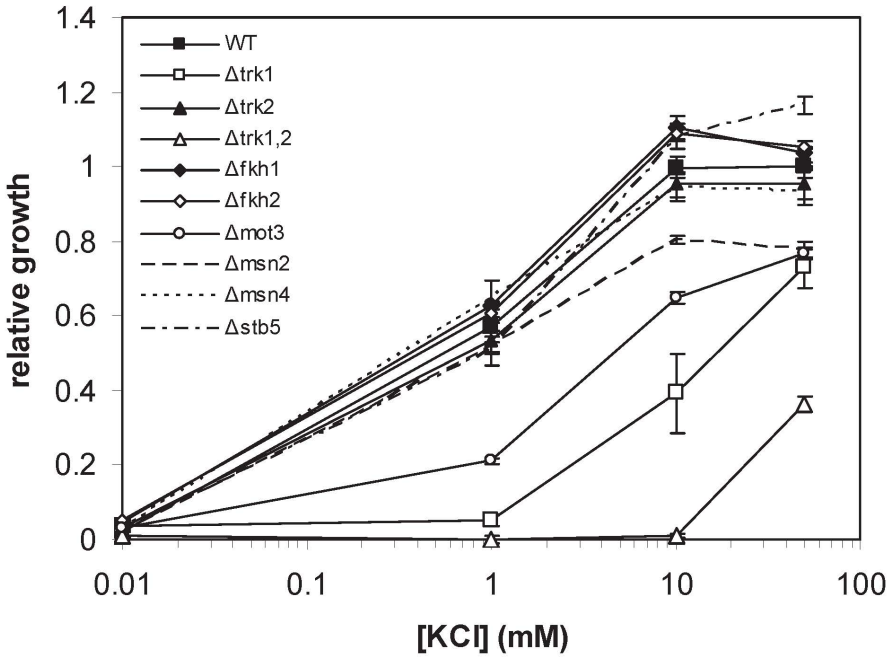

Figure 2.1: Analysis of the survey data from experiment 1

type, ΔTRK1 und ΔTRK1,2 under potassium limited and permissive conditions (Fig. 2.1). At 10 μM KCl_{ext} none of the strains did grow. At 1 mM KCl_{ext} considerable differences between the strains were observed. The ΔTRK1 strain, expressing only the TRK2 transporter grew only marginally above inoculum. In contrast, the ΔTRK2 strain, expressing solely TRK1 grew comparable to the wild type. The double ΔTRK1,2 mutant showed no growth at all. These results were consistent with previously published data [HSK^+05, BRL^+03]. The strains with disruptions in the transcriptions factors FKH1/2, MSN2/4 und STB5 exhibited growth comparable to the wild type.
However, growth of the TF mutant Δmot3 strain was considerably reduced compared to the wild type and the ΔTRK2 strain ($\sim$ 60%). At 10 mM KCl_{ext} the potassium transporter mutant ΔTRK1, ΔTRK1,2 and the Δmot3 strains showed with 51-64% and 20% respectively, reduced growth compared to the wild type. Mutant strains Δfkh1/2 and Δstb5 exhibited slightly enhanced growth ($\sim$ 10%).
At 50 mM KCl_{ext}, ΔTRK1,2, ΔTRK1, Δmot3, Δmsn2 showed impaired growth of 64%, 27%, 24% and 22% compared to the wild type. Strains Δfk1/2 and Δstb5 showed similar growth as the wild type.

Experiment 2

Using mutants for TFs predicted to bind to one or both of the upstream regions of BMH1 and BMH2 (see supplementary material of the bioinformatics output), we tested the effect on expression during exponential growth in YPD medium. The used strains were null mutants of MSN2, RTG1, WAR1, RLM1, ASH1, FKH1, or GSM1. Grown in YPD medium, we did not observe any differences in growth of these strains. Compared to wild-type BY4743, BMH1 expression did not significantly change in the tested mutants and, hence, is probably not be regulated under

the tested condition (Fig. 2.2A). The same was observed for BMH2 expression (Fig. 2.2B). The arbitrary twofold up- or down regulation as cut-off value for differential expression was used. However, subtle regulation by these transcription factors (i.e., fold change not higher than 2 and not lower than 0.5) cannot be excluded. In addition, other TFs may take over the regulatory role of the ones tested in this study. For instance, partial redundancy has been described for several TFs, e.g., MSN2/MSN4 and FKH1/FKH2 [MP96, HBM+00]. In conclusion, it was not possible to show an effect on regulation of BMH1 and BMH2 in the TFs mutants tested in this study.

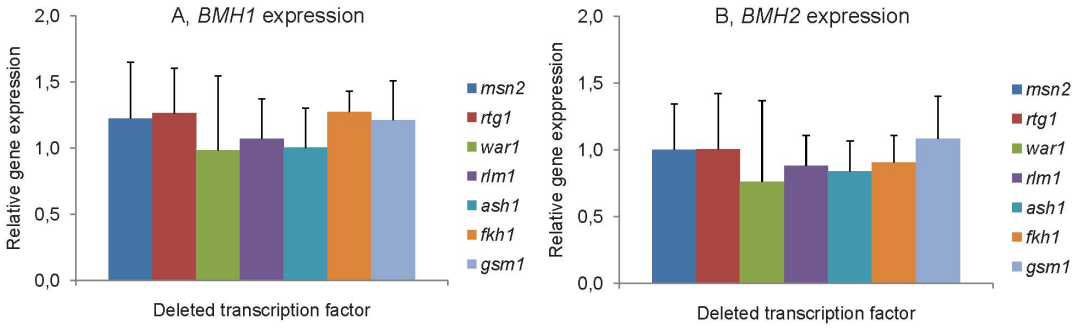

Figure 2.2: Relative gene expression of BMH1 (A) and BMH2 (B) in BY4743 Δ/Δ msn2, Δ/Δrtg1, Δ/Δwar1, Δ/Δrlm1, Δ/Δash1, Δ/Δfkh1, Δ/Δgsm1 measured by real-time PCR. Gene expression was normalized to ACT1 expression and expression of BMH1 and BMH2 in BY4743 wild-type.

2.5 Discussion

Experiment 1

Six potential transcription factors with differential frequency and binding site patterns in the potassium transporters TRK1 and TRK2 promoter regions were subjected to growth tests of respective yeast mutant strains for potassium dependent growth. Disruption of the Fkh1/2 TFs (9 potential binding sites in TRK1 and 4 in TRK2 promoter region) caused at limiting potassium conditions no reduction in mitotic growth.
Both TFs are important in the cell cycle, FKH1 as negative regulator and Fkh2 as positive regulator within the elongation process during transcription. Deletion of the negative regulator caused slight enhancement of growth under permissive conditions.
For the Msn2/4p stress transcription factors (ratio TRK1:TRK2 of 1: 3) on TRK1 region only one potential site on the reverse strand was found whereas on the TRK2 region three potential sites were found on the forward strand. Deletion of these stress TFs had minor consequences on the K^+ growth phenotype. This led to the conclusion that Msn2/4 TFs are inferior for the upregulation of TKR transporters under K^+ stress conditions.

Deletion of Stb5 (4 potential binding sites in TRK1 and 10 in TRK2 promoter region) was, according to the distribution pattern expected to impact mainly on the low affinity TRK2 expression. The Δstb5 mutant did grow slower than a ΔTRK2 disruption (entire K^+ uptake via TRK1), indicating that even a reduced (up) regulation of TRK2 has, with a present TRK1, only a minor impact.

The Δmot3 strain exhibited a growth defect under K^+ limiting conditions of approximately half the effect of disruption of the potassium transporter Trk1p. Mot3p is known as involved in repression of several DAN/TIR genes during aerobic growth, and repression of ergosterol biosynthetic genes. Under the assumption of a direct influence of Mot3p the lack of this TF could be responsible for a reduced expression of TRK1 (13 potential binding sites in TRK1 versus 7 in TRK2). However, alternatively, given the described role of Mot3p in ergosterol biosyntheses pathway, the deletion of this TF might pose an altered - for K^+ uptake transporters unfavorable - lipid composition onto the plasma membrane.
In summary, the results from these initial phenotypic experiments are indeed interesting and hold the potential for extension toward construction and analysis of yeast strains bearing combinations of TF and potassium transporter mutations.

Experiment 2

No significant differences were found for BMH1 and BMH2 gene expression in the tested TFs mutants However, a regulation cannot be excluded. In addition, other TFs may take over regulatory role of the ones tested in this study. Another possibility is that the tested TFs are not active during exponential growth in a rich medium like YPD. In conclusion, it was not possible to show an effect on regulation of BMH1 and BMH2 in the TF mutants tested in this study.

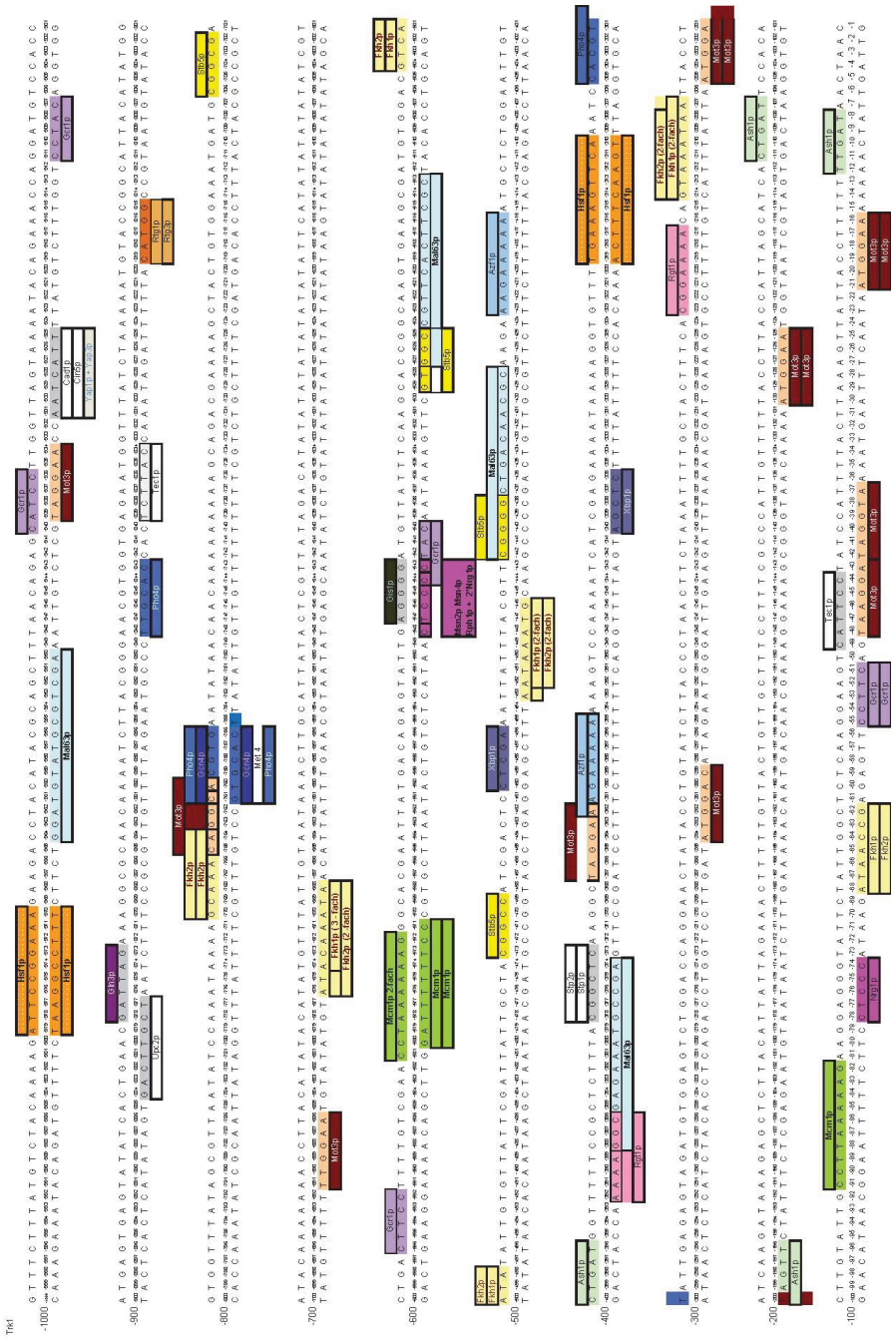

Figure 2.3: Graphical analysis of the TRK1 promotor region

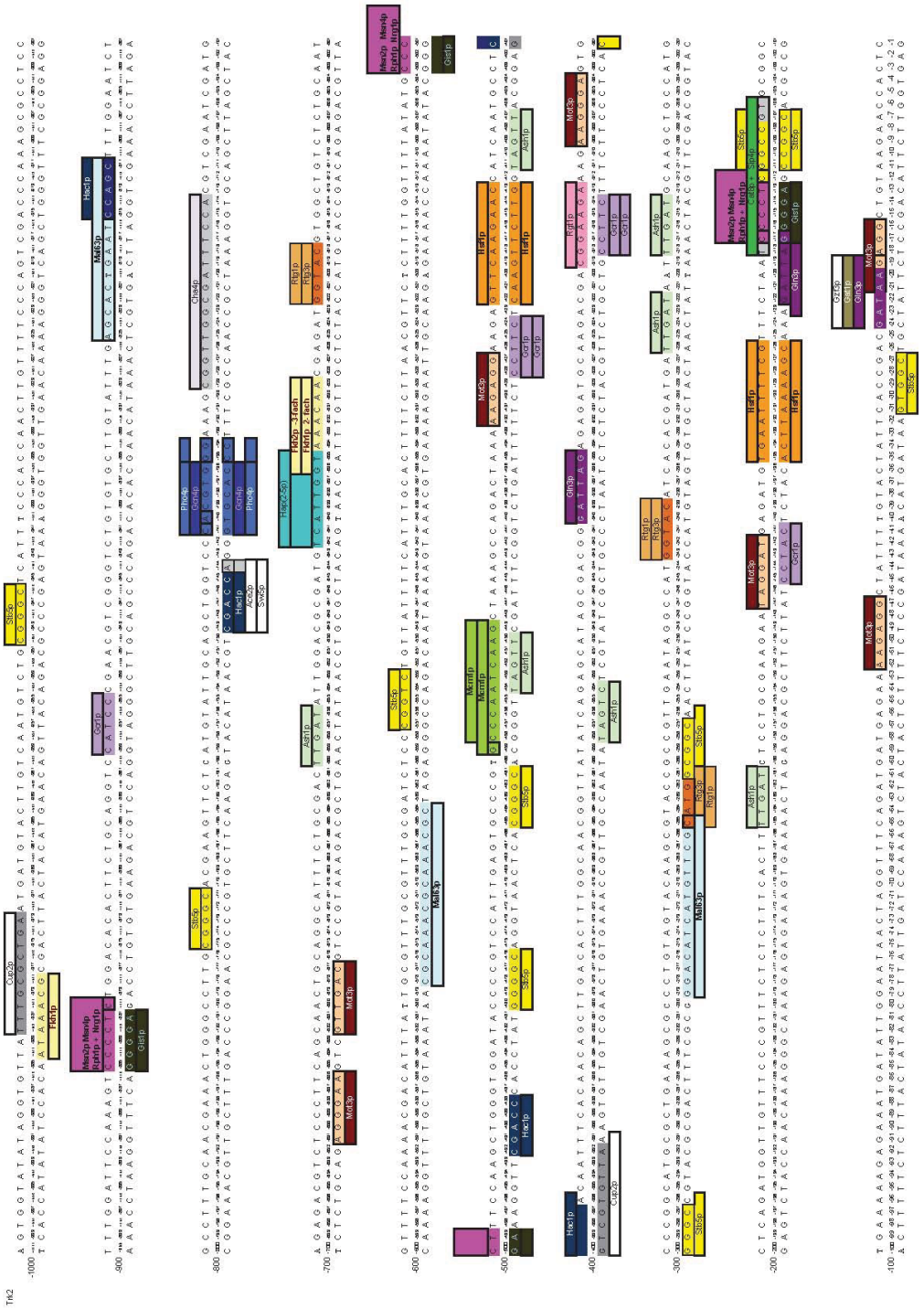

Figure 2.4: Graphical analysis of the TRK2 promotor region

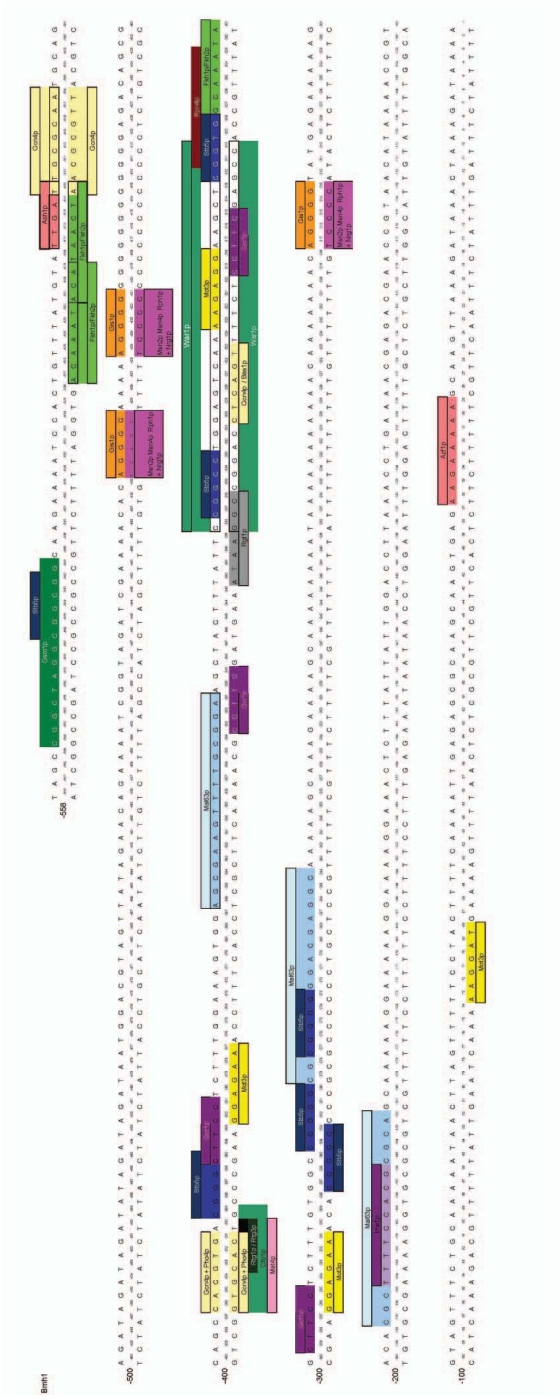

Figure 2.5: Graphical analysis of BMH1 promotor region

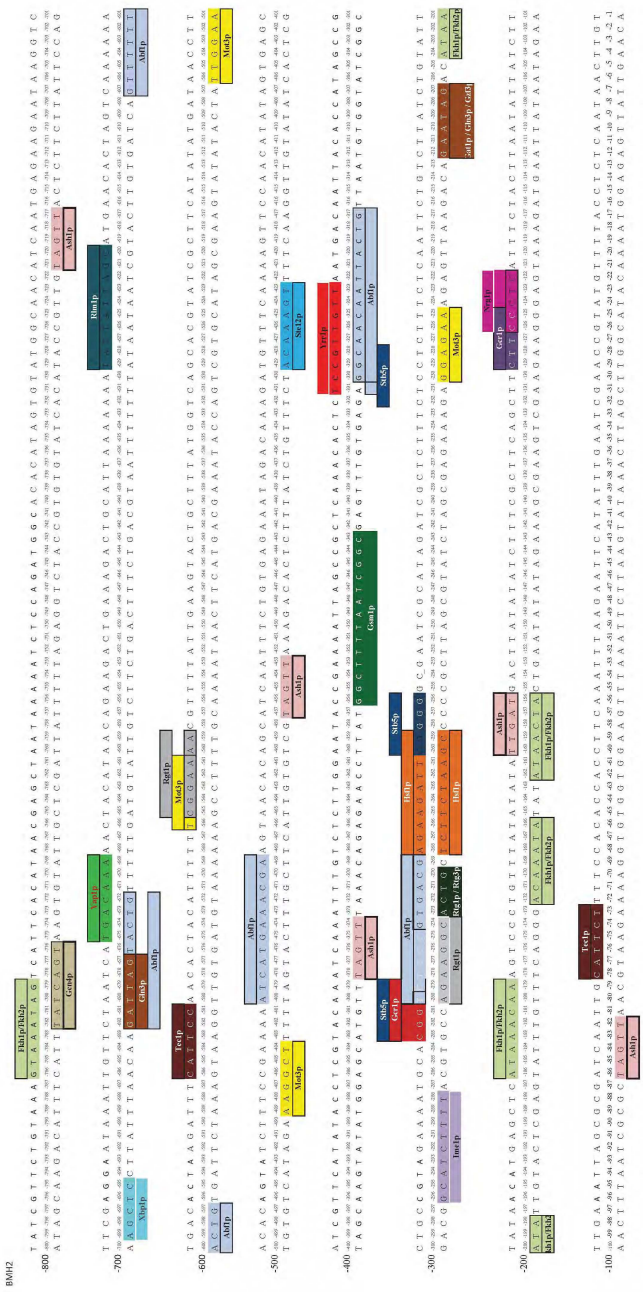

Figure 2.6: Graphical analysis of BMH2 promotor region

3 Investigating Heavy Metal Toxicity with Microarray Experiments

3.1 Abstract

In the present study DNA-microarrays were used to examine the *Saccharomyces cerevisiae* gene expression profile following a variety of cationic stress conditions. Although considered as essential cofactors for a variety of enzymatic reactions and for important structural and functional roles in cell metabolism, metals at high concentrations are potent toxic pollutants. A detailed characterization of global genome expression profiles upon heavy metal toxicity was performed by exposing *S. cerevisiae* to unphysiologically high concentrations of $AgNO_3$, $AlCl_3$, $AsCl_3$, $CdCl_2$, $CoCl_2$, $HgCl_2$, $MnCl_2$, $NiSO_4$, VCl_3 and $ZnCl_3$.
The aim of the experiments and analysis was in particular, to identify possible stressor-caused common transcriptional regulatory networks including the uptake, cytoplasmic trafficking, potential metabolism in intracellular organelles and detoxification that take part in the cellular defense against heavy metal stress.
The results of the study revealed that the common mechanism in yeast in response to heavy metal stress is first an energy saving program. Among the vital functions those with high energy consumption such as protein synthesis are descended. Individual metal defense mechanisms or cellular programs with regard to sequestration, detoxification and regulation of these systems by up- or down regulation of specific genes were not identified.
However, among groups of metals some gene clusters were differentially regulated. It is concluded that yeast cells may differentiate between groups of metal ions by whether these - in concentrations as for essential cofactors - exert physiological functions.
The experiments were prepared and provided by Dagmar Hosiner, University of Wien within the above mentioned TRANSLUCENT project. Raw data are available under the ArrayExpress accession numbers E-MEXP-2985 and E-MEXP-2991. Most of the statistical and computational methods are based on **R** programming by incorporating packages from the BioConductor project. Clustering was performed using the Matlab-Bioinformatics Toolbox. The SGD Database, in particular the GO-Term finder was used to identify genetic pathways or families of genes that are co-regulated. The developed code is open source and can be downloaded at http://jaguar.biologie.hu-berlin.de/∼sgerber.

3.2 Introduction

Metals are an integral part of our environment and all living organisms are exposed to metals in either the natural habitat or through anthropogenic sources. Some metals are intrinsically toxic like cadmium, arsenic, antimony, and mercury others serve in very low concentrations essential cellular functions like copper, and cobalt but become toxic in excess quantities.
Since metal ions cannot be degraded or modified like toxic organic compounds, they form unspecific complex compounds in the cells that by themselves cause toxic effects.

It is broadly accepted that organisms possess systems to evade toxicity and acquire tolerance. For instance, studies in yeast have revealed a number of important tolerance systems encompassing metal uptake and export pathways, metal binding and sequestration systems as well as the regulatory mechanisms that the yeast utilizes to control these systems.

In order to understand the genetic details of the function of these systems, e. g. expression of genes, the model eukaryote *S. cerevisiae* was exposed to a number of transition and heavy metals.
An efficient way to measure and analyze gene expression is by enumerating the abundance of mRNA species present in a cell type for a particular physiological state (transcriptome) [DTW05]. Since it is well-known that significant gene expression control is exerted at the transcriptional level transcriptome analysis is widely employed because measurements can be made using parallel and in at least in part automated approaches. Spotted DNA- or oligonucleotide microarrays are the most common tools currently used for such gene expression studies.
The experimental rationale focused thus on genome expression profiles upon cellular metal exposition. Yeast cells were treated with 10 different metals, and the global mRNA abundance was measured to detect genes being over-expressed or repressed under these conditions. Alterations in expression patterns of normal cells and those treated with the respective metal should guide cluster and pathway analysis to assess common and potentially specific metal binding and sequestration, and detoxification programs in the cellular defense. The work flow of this study is illustrated in Figure 3.1

3.2.1 Biological relevance and toxicity of metals and metalloids

Living organisms have always been exposed to metals, either in food, potable water, soil, air, or industrial applications. Hence, metals and metalloids with biological as well as toxic relevance are widespread in nature and can locally - following for instance metal pollution or extensive use of some metals and metal compounds as fungicides and disinfectants - reach fairly high concentrations. The impact of metals and metalloids on biological systems, from prokaryotes to humans ranges from essential, through beneficial, to nonessential and (highly) toxic when present in excessive amounts [WT10].
In low quantities, many metals (e.g. iron, cobalt, copper, manganese, molybdenum, and zinc) serve as essential nutrients, and are also often used as therapeutic agents [TO03, TM05, BH08]. In fact a very large number of proteins evolved that require metals for catalytic activity and/or for maintaining protein structure [WRFR09].
However, at higher concentrations in particular heavy metals such as mercury, plutonium, and lead exert a threatening influence on living organisms, and their accumulation over time in the bodies of animals and humans can cause serious illness.
The term "heavy metal" comprises however a loosely-defined subset of elements that exhibit metallic properties. It mainly includes the transition metals, some metalloids, lanthanides, and actinides. Biologically relevant metals are mostly the so called "transition metals/elements" including groups 3 to 12 on the periodic table.
For transition elements their valence electrons, that are those that may combine with other elements, are present in more than one shell. The inner *d*-orbital has more energy than the valence-shell *s*-orbital what is the reason why these elements often exhibit several common oxidation states like it is the case for iron. In the *d*-block on the periodic table the atoms of the elements have between 1 and 10 *d* electrons and such incompletely filled *d*-orbitals enable the formation of complex compounds which play structurally and functionally roles in biochemical and physiological reactions [Hos05, Gad93, Nie99, Fra05].
Zinc, cadmium, and mercury are not classified as transition metals since these have in the oxi-

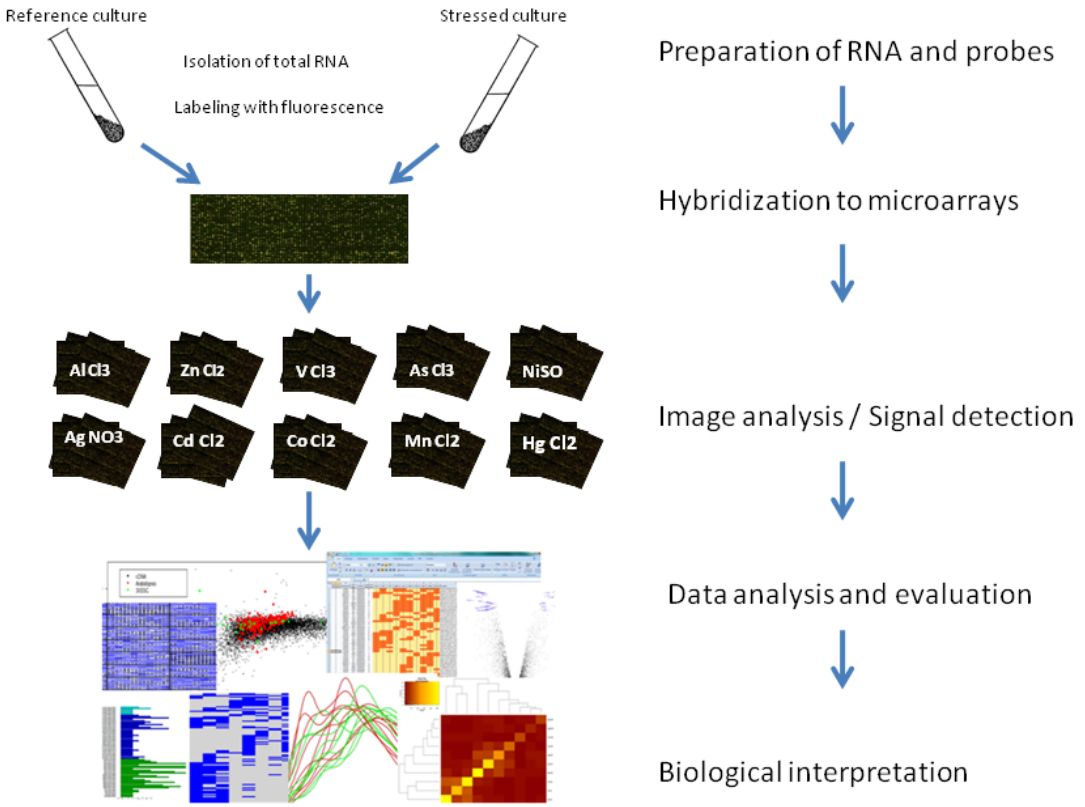

Figure 3.1: Workflow of the process of generating high-throughput gene expression data on metal stress using microarrays. Biological samples were prepared by isolating, labeling and hybridizing RNA from yeast cell cultures following the exposition to metal-salts and the reference strain, respectively. The images were scanned and signal intensities were detected. Raw data - containing fluorescence intensities for each spot - were normalized, analyzed and clustered to identify differentially expressed and co-regulated genes. Analysis results were evaluated and annotated for biological interpretation..

dation state +2 the electronic configuration $d10$, with no incomplete d shell.
Metal toxicity may be caused by oxidative stress, impaired DNA repair, inhibition of enzyme function and by disturbing the function of proteins that regulate proliferation, cell cycle progression, apoptosis or differentiation [WT10, SB95, EGOAB01, CS02, HS03, BH08].
Several studies have shown that metal toxicity may directly cause oxidative stress [VMC05]. Oxyanions, for instance, interfere with the metabolism of structurally related non metals (chromate and molybdate with sulphate, arsenate and vanadate with phosphate). As a consequence, reduction of metal oxyanions leads to the production of extremely reactive hydroxyl radicals, which cause cellular damage such as cleavage of DNA and RNA molecules, lipid peroxidation or membrane damage [Bal02].
Other metal ions, like copper or cobalt, can participate in Fenton-like reactions that generate hydroxyl radicals as well [HG84, LGR$^+$98, EGOAB01]. Since metal ions cannot be degraded

or modified like toxic organic compounds, they form unspecific complex compounds in the cells, which lead to toxic effects. Metal cations (e.g. As, Cd, Hg, and Ni) tend to bind to sulfhydryl groups of proteins, thus altering their enzymatic activity or causing depletion of the antioxidant glutathione, which leads to indirect oxidative stress [WMDJ02, Bal02, VMC05].
Other metal ions may interact with physiologically relevant ions or factors controlling their homeostasis, e.g. Cd^{2+} with Zn^{2+} or Ca^{2+}, Ni^{2+} and Co^{2+} with Fe^{2+}, Zn^{2+} with Mg^{2+}, thereby inhibiting the function of the respective physiological cation [PEZ$^+$98, RB05, QZSH06, BMRT05]. In the presence of excess concentrations even essential cofactors exhibit toxic potential by blocking of functional groups on biomolecules as well as denaturation of enzymes, and DNA damage as for copper, zinc, and nickel.
In mammals, heavy metals, particularly at higher concentrations, but also at low concentrations, become toxic when they are not sequestered by the body and accumulate in the soft tissue. Malfunctions of metal homeostasis or detoxification systems may cause a damaged or reduced mental and central nervous function, lower energy levels, as well as damage to blood composition, lungs, kidneys, liver, and other vital organs [SOIS93, HSC87]. Long-term exposure may result in slowly progressing physical, muscular, and neurological degenerative processes [WEM90, BFWW91, CME98, FPYC98, EAW$^+$98]. Allergies are increasing and repeated long-term contact with some metals or their compounds may cause even cancer [Nie99, CSM00]. In particular arsenic, lead, cadmium and mercury are very toxic and probably also carcinogenic at very low concentrations [CSM00].
To preserve the delicate balance between essential and toxic levels of metal ions, and to cope with sudden stressful environmental changes organisms developed sophisticated mechanisms of uptake, sequestration to the appropriate sub-cellular compartments, as well as detoxification when the ion is in excess. Cells utilize thus a wide array of homeostasis and tolerance mechanisms that regulate the availability of essential metals and limit the damaging effects of toxic elements [WT10].
For this purpose they have to rapidly respond with alterations in global gene expression, thereby adapting to new conditions [MDK95, GS00]. The importance of metals for humans as well as their impact on the environment has greatly promoted research on metal biology and led to a significant progress in understanding metal response and tolerance acquisition mechanisms in many prokaryotic and eukaryotic organisms [WT10].
In recent years a considerable amount of information about how *S. cerevisiae* detects and responses to toxic metals and metalloids accumulated [WT10]. Despite this, relatively little is known about toxicity mechanism at a molecular level. For instance, insights into the molecular mechanisms concerned with specific aspects of metal uptake, sequestration and detoxification are still lacking. In particular, questions like whether and how metals can activate transcription factors and signaling proteins, the post-translational regulation of transporters involved in metal sequestration and the complex cellular "system" response are increasingly being addressed.
In this regard *S. cerevisiae* is a most suitable model organism to unravel the molecular details of metal action and detoxification strategies since many mechanisms involved in metal toxicity and detoxification appear to be conserved in various eukaryotic organisms [WT10].
The research questions addressed by the current approach were to ascertain a potential common mechanism in yeast cells to (heavy) metal stress and to detect disparities in the way of the response compared to stress caused by sodium and/or potassium. Specific aim of this work was to identify some factors, genes, key elements that have a significant role in this regulatory pathway. Does disturbance of ion homeostasis induce specific stress or a general response? The comprehensive data on regulatory associations available in databases such as YEASTRACT [TMJ$^+$06] enable the identification of documented and potential regulatory associations between transcription factors.

The generation of transcriptional regulatory networks enables the analysis of regulatory mechanisms and will support the inference of mechanisms underlying gene regulatory networks since many mechanisms involved in metal toxicity and detoxification appear to be conserved in various eukaryotic organisms [WT10].

3.2.2 Microarray Technology

"Microarrays" have emerged as a powerful technique to simultaneously evaluate quantitative measurements for the expression of thousands of genes [Pev09]. Various variants evolved since this method was first reported in 1995 for gene expression profiling [SSDB95]. In 1997 this technique was first applied for the genome wide expression analysis of the complete genome of *S. cerevisiae* [LDM$^+$97]. Since then the most commonly applied method - that was also utilized for the following study - the so called "Two-color cDNA microarrays" [CMA$^+$99] where the expression profiles of two differently labeled samples are measured and directly compared.
For this purpose, a grid of microscopic spots of known genetic material (probes) is systematically arranged on a glass microscope slide. One array has a capacity of thousands of spots that each holds a droplet representing a different cDNA sequence. In order to quantify the gene expression profile fluorescently labeled cDNA (samples) extracted from the specimen of interest and a reference specimen are mixed and hybridized together to the microarray. To discriminate between both samples different dye colors - cyanine 3 (cy3) and cyanine 5 (cy5), respectively - are used [Sch99, BJ00].
During the hybridization procedure the sample-cDNA binds to their complementary sequence fragments on the array. In a subsequent procedure of purification all non-specific (unbound) samples are washed off. Thus only strongly paired strands will remain hybridized and generate a fluorescent signal that in its strength depends upon the amount of sample-cDNA binding to the probes on the specific spot.
For every spot the intensity of this signal is detected by light-scanning with a high precision microarray scanner. Since the fluorescence probes have different excitation and emission wavelengths the scanning is correspondingly performed at both wavelengths for cy3 and cy5 to visualize the specific fluorescence for each of the two fluorophores. For quality assurance purposes a so called "dye-swap" step is usually included. In this experimental design all conditions remain the same except for the labeling of the treated and untreated cells which is switched. By that possible false data can be identified. The ratio of the fluorescent light emission between the two different wavelengths (corresponding to the different dyes used to label both samples) is the direct measure of the relative gene transcript expression level [MDA05]. Since a single hybridization provides genome wide quantitative expression data such microarray experiments enable a parallel analysis of whole genome samples to identify up- or down-regulated genes under varying conditions or in time-series experiments.
However, these images are subject to considerable uncertainty because of large- and small-scale intensity fluctuations within spots, non-additive background, and fabrication artifacts [BGS01], contributing to sometimes poor-quality images. Other sources of systematic variation, internal or external to the sample, include fluctuations in the physical properties of the dyes, efficiency of dye incorporation, probe coupling and processing procedures, target array preparation in the hybridization process, background effects, and scanner settings among others [MDA05].
Such experimental variation of results in two different computational issues associated with the analysis of microarrays. The first task is the preprocessing of the experimental raw data to produce a result that accurately reflects either absolute amounts of transcripts in cells or, more commonly, the ratio of these amounts under two different experimental conditions. The result of these corrections is a gene expression matrix, one form of which is composed of n rows, each

corresponding to a gene or feature on a microarray, and m columns, each of which corresponds to a condition or a time-point for which expression levels were measured. The content of each element of the matrix is a ratio of two fluorescence intensities.
The second computational task is the analysis and statistical interpretation of the intensity data in the gene expression matrix to identify differentially expressed genes and to enable meaningful interpretation of the data by annotating and clustering procedures of obtained results. Already a vast amount of literature has accumulated, addressing individual problems in data-(pre)processing and analysis including the process of normalization as a subtle challenge. Extended reviews of existing methods can be found, e.g. [SS03, Smy04b, YT03, BR02].
The following section on "Materials and Methods" describes the methods used for the present study.

3.3 Materials and Methods

3.3.1 Metal toxicity assays in Saccharomyces cerevisiae

In order to perform gene expression analysis upon heavy metal stress in S. cerevisiae, the effect of 16 biologically relevant metal ions ($AgNO_3$, $Al_2(SO_4)_3$, $AsCl_3$, $CaCl_2$, $CdCl_2$, $CrCl_2$, $HgCl_2$, KCl, $LiCl_2$, $MnCl_2$, $MoCl_5$, $NiCl_2$, $NiSO_4$, $SnCl_2$, $SrCl_2$, and VCl_3) on yeast growth in liquid cultures or on solid agarplates was examined in preliminary work [Hos05]. Exponentially growing yeast cultures were exposed to increasing concentrations of the metals and incubated at 30°C. The cellular growth was monitored by determining the optical density (OD600nm) of the liquid cultures or by visual evaluation of the spotted yeast cells on solid agar-plates. The results of this work provided the minimal inhibitory concentrations (MICs) of the metal ions as well as the metal concentrations, inducing 50 percent growth inhibition of the *S. cerevisiae* cultures.

3.3.2 Preparation of yeast RNA

To identify those genes most specific for metal stress, microarray experiments were performed with ten of the most toxic metal ions, namely silver (Ag), aluminum (Al), arsenic (As), cadmium (Cd), cobalt (Co), mercury (Hg), manganese (Mn), nickel (Ni), vanadium (V) and zinc (Zn). All these metals cause cellular growth inhibition at concentrations lower than 1mM [Hos05]. In order to avoid the yeast general stress response program [GSK+00] but identify those genes being most sensitive and specific to metal stress, the applied metal concentrations were on average of 2-3-fold higher than the previously specified respective MIC.
Over-night cultures were grown in fresh YPD and stressed with either the indicated concentrations of metal ions (listed in Table 3.1) or, as control were grown untreated. After 30 min incubation with AlC_l, $AgNO_3$, $AsCl_3$, $CdCl_2$, $CoCl_2$, $HgCl_2$, $MnCl_2$, $NiSO_4$, VCl_3 or $ZnCl_2$, respectively total RNA was extracted from both untreated and treated cells. The total mRNAs of both, the stressed cells and the control culture were prepared, labeled with fluorescence-dyes (cy3-CTP, cy5-CTP), and simultaneously hybridized to cDNA microarrays. The experiments were repeated three times for each condition, using independently grown yeast cultures. The microarrays were scanned and image data were quantified using the GenePix Pro 4.1 software (Molecular Devices) that returns quantitative intensities for each spot. Details in experimental conditions are provided in the Supplementary Material C.

Treatment	Cy3	Cy5	Group	Time	Replications
1.5 mM $MnCl_2$	WT	WT+Mn	1	30 min.	2
	WT+Mn	WT	1	30 min.	1
1.5 mM $NiSO_4$	WT	WT+Ni	1	60 min.	1
	WT+Ni	WT	1	60 min.	2
100μM $CoCl_2$	WT	WT+Co	1	30 min.	1
	WT+Co	WT	1	30 min.	2
2μM $CdCl_2$	WT	WT+Cd	1	30 min.	1
	WT+Cd	WT	1	30 min.	2
200μM $AsCl_3$	WT	WT+As	1	30 min.	1
	WT+As	WT	1	30 min.	2
30μM $HgCl_2$	WT	WT+Hg	1	30 min.	1
	WT+Hg	WT	1	30 min.	2
40μM $AgNO_3$	WT	WT+Ag	1	30 min.	2
	WT+Ag	WT	1	30 min.	2
500μM VCl_3	WT	WT+V	2	30 min.	2
	WT+V	WT	2	30 min.	1
1.5 mM $ZnCl_2$	WT	WT+Zn	2	30 min.	2
	WT+Zn	WT	2	30 min.	1
500μM $AlCl_3$	WT	WT+Al	2	30 min.	2
	WT+Al	WT	2	30 min.	1

Table 3.1: Treatment assigned to each slide. WT stand for Wild Type (the untreated sample) whereas WT+X means "stressed with heavy metal from type X".

3.3.3 Computational processing and data analysis

The critical first steps in computational analysis of gene expression data include an attempt to clean the data by procedures that can improve image quality, by separating signal from noise, by handling missing values and by performing appropriate normalization procedures. The data preprocessing as well as the tests for differential expression have been performed by using the **R** computing environment and several software packages from the Bioconductor project (http://www.bioconductor.org), particular the Limma package [Smy04a]. For further data evaluation, clustering algorithms using the Matlab Bioinformatics toolbox were applied to identify groups of genes with similar expression profiles for the time point "30 minutes" following the metal-salt exposition.
In total 31 images of slides were analyzed (Table 3.1).
In the following the individual steps of data processing are presented along the example of $AlCl_3$-stress.

3.3.4 Quality assessment and background correction

Quality assessment is an essential and critical first step for any subsequent data analysis. Data variability introduced in each step of microarray data generation is undesirable because it might

Experiment	**File name** (replicates)	**Cy3**	**Cy5**
Stress with	13737744.gpr	WT (untreated)	WT + stress (treated)
$500\mu M AlCl_3$	13737745.gpr	WT + stress	WT
for 30 Minutes	13737755.gpr	WT	WT + stress

Table 3.2: Experimental design for investigating aluminum-induced stress in *S. cerevisiae*. The experiment was undertaken three times using independently grown yeast cultures and a dye-swap.

affect the entire data quality and mask the effect of interesting biological factors on the gene expression profile. Once detected, less reliable arrays can be excluded from further analysis or lower weights can be assigned to less reproducible replicates to avoid misleading results [RDN+06].
The observed foreground signal is a combination of the true spot intensity (the specific hybridization of interest) and the ambivalent background signal resulting from non-specific binding of labeled samples to the array surface and contamination such as spatial heterogeneity across the array due to dregs left after washing or optical noise during the scanning process.
The most simple way to inspect the experimental outcome at a first stage is a simple reprint of the intensities as shown in Figure 3.2 where in rows 2 and 4 the ambient background signal is visualized for the cy3 (green) and the cy5 (red) channel, respectively.
A range of background correction approaches exist with the aim to improve accuracy and reducing bias by adjusting the data for the ambient fluorescence surrounding each spot (for reviews see [RSO+07, SRS09]). The standard approach is simply to subtract the background estimate directly from the spot intensity. However, this can result in corrected intensities with undesirable statistical properties such as negative intensities whenever the ambient signal is stronger than the foreground intensity [SBM09]. This problem arises in particular when arrays are as noisy as it was the case in the present study.
Therefore, the background correction method developed by Ritchie et al. [RSO+07] was chosen for the current evaluations. By this method a convolution of normal and exponential distributions is fitted to the foreground intensities by using the ambient signal as a covariate. The expected signal given by the observed foreground becomes the corrected intensity. An offset-value (numeric value to add to intensities) of 50 was chosen as is recommended on the basis of previous experience with cDNA microarray experiments [RSO+07, SRS09]. This approach results in a smooth monotonic transformation of the background subtracted intensities. Typical problems such as negative corrected intensities and high variability of low intensity log-ratios [RSO+07, SRS09] were thus avoided.
All spots with missing values as well as "bad"-spots with illegal shape were given zero weight for all further normalization and analysis steps. The corrected intensities were used to form the log-ratio, M, and the average log-intensity, A, for each spot

$$M = log_2\left(\frac{R}{G}\right) \tag{3.1}$$

$$A = \frac{1}{2} log_2(R * G) \tag{3.2}$$

where R and G are the background corrected red and green intensities.
On this scale, $M = 0$ represents equal expression intensities of experimental and control sample, positive M-values correspond to up-regulation (e.g. M=1 represents a 2-fold change between the

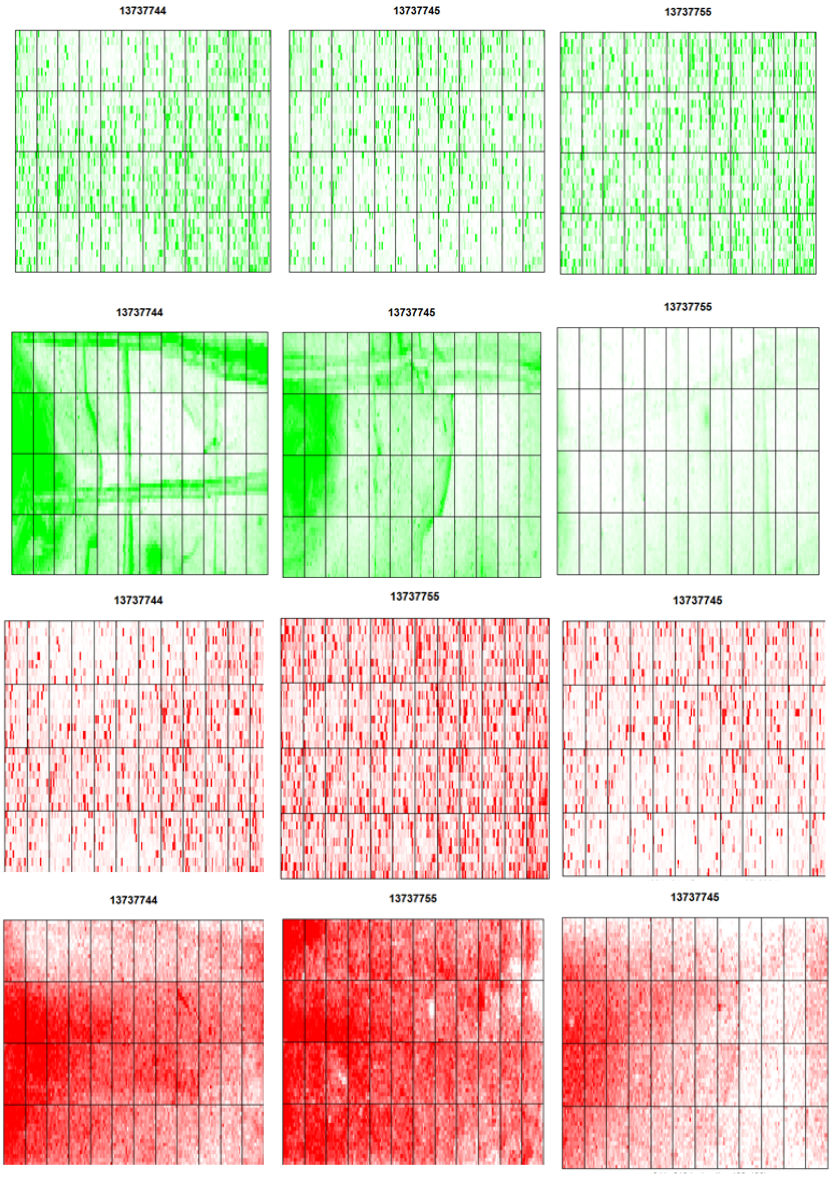

Figure 3.2: Reprint of the foreground and background fluorescence intensities of the three replicates from the experiment with 500 $\mu M\, AlCl_3$-stress. The first row shows the overall intensities of the green channel, the second row the non-specific background effects of the corresponding arrays and rows three and four illustrate the same for the red channel, respectively.

samples) and negative M-values correspond to down-regulation (repression) of the considered gene.

3.3.5 Normalization

Normalization of corrected data intends to remove systematic trends from the expression values which arise from variation in the application of the microarray technique rather than from actual biological differences between the probes or the target samples hybridized to the arrays [SS03]. The need for normalization of the M values within each array results from the fact that the process of printing DNA-spots on the microarrays may take several days. Spots are printed in parallel using a print head containing several print-tips that proceed from top to bottom and right to left in each print tip group. This procedure results in print-order effects that affect the foreground intensity of the spots due to variations between the print-tips (i.e. defective print-tips) or fainting of the signal in large regions of the array. Furthermore, imbalances between the red and the green dye may arise from differences between the efficiencies of labeling or scanning properties [SBM09] which affect one color more than the other.
The standard normalization method is a locally weighted linear regression (Loess) normalization, an intensity-dependent method to account for dye biases [YT03]. This iterative normalization method is carried out based on the assumption that only a small proportion of genes will be differentially expressed among thousands of genes present in the array. In a first step the methods performs a print-tip-group normalization and afterwards a global normalization. However, due to a large amount of "bad" spots and missing data in the print-tip groups of some of the arrays the print-tip Loess is unreliable. Therefore normalization was performed using the a robust spline normalization [SS03] which is an empirical Bayes compromise between Print-tip and Global Loess normalization with 5-parameter regression splines used in place of the Loess curves. Afterwards, a quantile normalization [BIsS03] between all arrays ensured that the average intensities have the same empirical distribution across arrays and across channels. The quantile normalization approach first ranks data on each array and substitutes data of the same rank across all arrays by the mean of the data.
The effects of normalization are demonstrated in Figure 3.3 where MA-plots (log intensity ration versus the mean log intensity) for the three replicates of the $AlCl_3$-stress experiment before and after normalization are shown with Loess fits for individual print-tip-groups.
This plot type is widely used to visualize microarray data because it directly displays the red-to-green ratios. Furthermore, MA-plots enable identification of intensity-dependent biases in the data.
The plots before normalization (first column in Figure 3.3 exhibit obvious curvature deviating from the horizontal line at zero that needs to be normalized in order to achieve consistency in the intensities. The second column shows the same arrays after internal normalization and the third column after global normalization, respectively. The tight clustering of data points around the line $M = 0$ are the majority of genes that do not alter their expression levels significantly under the two conditions compared. Interesting spots with a strong signal and a correspondingly great variation in expression level are unambiguously detected after global normalization (spots marked with lavender color) in the third column in Figure 3.3. Figure 3.4 shows the progress of preprocessing by displaying the smoothed empirical densities for the individual green and red channels. Without background correction there is a considerable variation between both channels as well as negative intensities arising from "bad"-spots (Figure 3.4a). Background correction leads to exclusive positive intensities and the distribution curves close ranks (Figure 3.4b). However, there is still considerable variation between the channels of each array. By internal normalization of the M-values for each array the red and green distribution becomes essentially equal for each array, although there is still variation between the arrays (Figure 3.4c). The application of quantile normalization to the A-values ensures that the distribution is comparable across arrays as well as across channels (Figure 3.4d).

3.3.6 Tests for differential expression

In formal statistical terms, a gene is classified as being differentially expressed if its expression level changes systematically between two treatment conditions even if this difference might be very small. However, on the biological point of view, a gene is assumed to be differentially expressed only if its expression level changes by a worthwhile amount [MS09]. Such amount or threshold must be defined. Therefore, a new generation of statistical tests for significance analysis in microarrays data has been developed. To aid with inference about each individual gene, information from the ensemble of genes is borrowed using an empirical Bayes method to moderate the standard errors of the estimated log-fold changes across genes [Smy04a, Smy04a]. These moderated t-statistics lead to p-values with increased degrees of freedom, reflecting the greater reliability associated with the smoothed standard errors. In order to exclude genes with arbitrarily small fold change it has been commonly accepted to request that differentially expressed genes satisfy both p-values and fold-change criteria simultaneously [PLFS$^+$06, PSvL$^+$05, RZT$^+$08]. The results have been consistently shown to outperform traditional gene-wise statistical tests, and to give results more in line with fold-change rankings [JHC06, KAC$^+$05, STF$^+$05, XJP$^+$04]. Smyth et al. [Smy04a] generalized the moderate t-statistic to a multidimensional case and implemented this approach in the Bioconductor package Limma [SGC$^+$05] that was used to detect differentially expressed genes as follows.
For each gene six data point were available arising from the three performed experimental replicates (independent arrays) where each of the replicates contained two spots with the same probe. A linear model was fitted to the expression of each probe [SGC$^+$05, Smy04a]. Replications of the same treatment were merged in the calculation due to the consideration of dye-swaps. Duplicated spots within a single array were evaluated using a pooled correlation method to make full use of the information [SMS05]. The p-value adjustment method from Benjamini and Hochberg [BH95] was chosen to control the false discovery rate, which is the expected proportion of false discoveries amongst the rejected hypotheses. Genes were ranked in order of evidence for differential expression of the stressed samples in comparison to the reference sample in each experiment. The top-50 genes being most likely differentially expressed in the running $AlCl_3$-example are visualized by a Volcano-plot in Figure 3.5.

3.3.7 Identifying commonly expressed genes

All genes that appeared significantly differentially expressed following the normalization process were taken into account for further analysis and a descriptive statistic approach. Table 3.3 provides the number of shared genes after pairwise comparisons of all experiments. The diagonal line gives the total amount of genes being significantly differently expressed for each experimental condition.
The result is plotted as a heat map with two identical dendrogramms representing the outcome of hierarchical clustering in Figure 3.6. The latter was performed using the similarities in Table 3.3 directly for clustering after transforming the intersect counts into Jaccard (Tanimoto) similarity indices [Gir10, Jac12] which is a correlation coefficient for determining the similarity between two bit-vectors. The size of the intersection becomes divided by the size of the union of the sample sets. This transformation provides better and more reasonable results than simple Euclidean distance and complete linkage since the sample sets show clearly a large size difference (see diagonal in Table 3.3). Furthermore, all possible intersects among more than two sample were computed, as given in Table 3.4.

	$AgNO_3$	$AsCl_3$	$CdCl_2$	$CoCl_2$	$HgCl_2$	$MnCl_2$	$NiSO_4$	$AlCl_3$	VCl_3	$ZnCl_2$
$AgNO_3$	18	5	4	1	5	8	5	1	3	1
$AsCl_3$	5	56	11	1	10	4	5	1	1	1
$CdCl_2$	4	11	42	1	14	6	4	1	1	2
$CoCl_2$	1	1	1	19	1	6	5	2	4	5
$HgCl_2$	5	10	14	1	44	16	5	1	1	1
$MnCl_2$	8	4	6	6	16	145	4	0	1	3
$NiSO_4$	5	5	4	5	5	4	22	2	2	3
$AlCl_3$	1	1	1	2	1	0	2	44	2	3
VCl_3	3	1	1	4	1	1	2	2	33	2
$ZnCl_2$	1	1	2	5	1	3	3	3	2	29

Table 3.3: Pairwise comparison of each experiment to detect shared genes

Counts	**ORF**	**Gene Name**	**SGD ID**	**Condition when differentially expressed**
5	YLR303W	MET17	S000004294	$AgNO_3$ $AsCl_3$ $CdCl_2$ $HgCl_2$ $MnCl_2$
5	YDL124W	NA	S000002282	$AgNO_3$ $AsCl_3$ $CdCl_2$ $HgCl_2$ NiSO4
5	YCL040W	GLK1	S000000545	$AgNO_3$ $AsCl_3$ $CdCl_2$ $HgCl_2$ NiSO4
4	YOR382W	FIT2	S000005909	$CoCl_2$ $MnCl_2$ $NiSO_4$ $ZnCl_2$
4	YHL040C	ARN1	S000001032	$CoCl_2$ $MnCl_2$ VCl_3 $ZnCl_2$
4	YNL160W	YGP1	S000005104	$AsCl_3$ $CdCl_2$ $HgCl_2$ NiSO4
4	YMR173W-A	NA	S000004785	$AsCl_3$ $CdCl_2$ $HgCl_2$ $MnCl_2$
4	YNL208W	NA	S000005152	$AgNO_3$ $HgCl_2$ $MnCl_2$ $NiSO_4$
3	YMR058W	FET3	S000004662	$CoCl_2$ $NiSO_4$ VCl_3
3	YHL047C	ARN2	S000001039	$CoCl_2$ $MnCl_2$ $NiSO_4$
3	YDR534C	FIT1	S000002942	$CoCl_2$ $NiSO_4$ $ZnCl_2$
3	YMR173W	DDR48	S000004784	$CdCl_2$ $HgCl_2$ $MnCl_2$
3	YOL151W	GRE2	S000005511	$AsCl_3$ $CdCl_2$ $HgCl_2$
3	YNL134C	NA	S000005078	$AsCl_3$ $CdCl_2$ $HgCl_2$
3	YLR109W	AHP1	S000004099	$AsCl_3$ $CdCl_2$ $HgCl_2$
3	YPL154C	PEP4	S000006075	$AgNO_3$ $MnCl_2$ $NiSO_4$

Table 3.4: All possible intersections

3.3.8 Determination of genetic network architecture

An important step in order to reduce the amount of data and to achieve biological interpretations is to build subsets of genes with similar expression patterns. The underlying principle is the assumption that genes with similar expression patterns across the experimental setup are likely to be functionally related.
They might be co-regulated in biological processes, function in the same biochemical pathways, share regulatory sequence motives, or correspond to the same regulatory control mechanisms [MDA05, THC+99]. The clustering of these genes may therefore lead to broader and thus potentially new insights into genetic networks and the analysis for transcription factor binding sites might help to identify and/or understand mechanisms of regulation and response.

Clustering

A wide variety of clustering methods such as K-means [MQ67], hierarchical clustering [ESBB98, CBE01, dHINM04, NS02] or self-organizing maps (SOMs; [LKB+04]) can be employed with microarray data to group genes or conditions that lead to similar global expression patterns. All

algorithms depend on the definition of a measure of similarity between expression profiles, and each measure can reveal different features in the data.
The best method depends highly on the question to be solved by the experiment as well as on the characteristics and the quality of the dataset and can - in general - not be anticipated. In order to maintain a general overview on potential genetic groups the selected genes were clustered without prior assumptions with a non-supervised hierarchical approach [PS00, ESBB98, JG06] (Figure 3.7 and *via* using Euclidean distance metric and average linkage to generate the hierarchical tree. Clusters were generated first along the columns (producing row-clustered data), and subsequently, along the rows.
Even though the constructed dendrogramm is indeed helpful to depict the relationships between the genes grouped on the common branch, the tree exhibits ambiguous cluster and it is difficult to define a final amount of clusters.
Therefore, in a second evaluation step, data were clustered using K-means. This method uses a two-phase iterative algorithm to minimize the sum of point-to-centroid distances, summed over a predetermined amount of clusters. Best results were maintained with K=20 cluster by using squared Euclidean distances and is shown in Figure 3.8.

3.3.9 Gene-set enrichment

In order to enable the meaningful biological interpretation of the detected subgroups, the clusters were annotated with available metadata by parsing the "Saccharomyces Genome Database" (SGD)[CAB$^+$98], the Munich Information Center for Protein Sequences (MIPS) [MFG$^+$00], the Kyoto Encyclopedia of Genes and Genomes (KEGG) [KGF$^+$10, KG00] and Gene Ontology (GO) [Con00].
These databases provide interfaces or web-services to enrich lists of genes with biological information available for the corresponding genes or gene-cluster. Most important for the present study were the services of GO and the SGD databases.
The GO project provides a systematic vocabulary of terms for the description of gene characteristics and gene product annotation data and can be used to annotate whole genomes and detect enriched functional categories in groups of genes. This approach compares the number of genes in each GO-category with the number of expected genes in the same category by chance.
Significant associations for the genes of the 20 clusters to GO terms were obtained by the GO Term Finder provided by SGD. The results of this gene set enrichment is given in Table 1 in the Supplementary Material B.
The final outcome of this analysis provided - following manual inspection - is visualized in Figure 3.9. The results of the manually enriched data after K-means clustering were visualized using Java TreeView [Sal04].

3.3.10 Transcription factor analysis

In order to group genes along their regulatory associations with documented transcription factors (TFs) a data set of all available TFs known to be functional in *S. cerevisiae* was collected. For this purpose, the YEASTRACT repository [TMJ$^+$06](Yeast Search for Transcriptional Regulators And Consensus Tracking) was parsed. The repository maintains 48333 regulatory associations between transcription factors and genes based on more than 1200 bibliographic references [AMT$^+$11]. The assembled dataset for the present study contained the description of 298 specific and in the literature documented DNA binding sites for a group of 110 transcription factors. The assignment of TFs to each cluster was carried out following two different search strategies:

1. Associations may base on direct or indirect evidences. Direct evidence was considered to be provided through experiments that prove the direct binding of the TF to the target gene's promoter region, or such as the analysis of the effect on target-gene expression of the site-directed mutation of the TF binding site in its promoter region. Such association strongly suggests that the TF interacts with that specific target promoter [TMJ+06]. Indirect evidences were attributed to experiments such as the comparative analysis of gene expression changes occurring in response to the deletion, mutation or over-expression of a given TF.
2. Pattern matching of already documented transcription factor binding site (TFBS motives within the promoter region of the selected genes. This information for promotor regions and TFBS were also collected from the YEASTRACT database. The query was performed with the tool developed in the previous chapter [GHH+10] to search for potential TFBS on promotor regions in *S. cerevisiae*. Given a group of genes, this pattern discovery program queries forward and reverse strands of the promoter regions for motifs of the interesting transcription factors and returns those whose consensus binding site matches at least one subsequence of the promoter region of the investigated genes. This may give information on potential associations and is particularly useful for the prediction of regulatory motifs from clusters of co-expressed genes.

3.3.11 Biochemical Pathways

As a final step, all genes being significant differentially expressed under at least two experimental conditions were mapped to *S. cerevisiae* biochemical pathways using the "Pathway Tool" [Kar02, PK06]. The results are visualized in Figure 3.10, and - in higher resolution - in the Supplementary Material B. The pathways with the highest density of up- regulated genes are extracted in Figures 3.11 - 3.13 whereas pathways with the highest density of down- regulated genes are given in Figure 3.14. Details will be discussed in the following section.

3.4 Results and Discussion

The inspection of pathways with a high density of significantly up- regulated genes revealed those that are mainly involved in amino acid metabolism. In particular, the synthesis of the amino acids with charged side chains (arginine, lysine and histidine) (Figure 3.11a-c) as well as the aromatic amino acids tryptophan, phenylalanine and tyrosine (Figure 3.11d), cysteine (Figure 3.12a) and amino acids with hydrophobic side chains (leucine, iso-leucine and methionine) as visualized in Figure 3.12b) and c) is considerably enhanced.
These results are in good agreement with observations made on plants, where Cys-rich metal binding peptides including phytochelatin and metallothioneins are synthesized in response to toxic levels of heavy metals [JNH04, WTDG03].
For *S. cerevisiae*, it has been shown that the accumulation of histidine in the vacuole decreases the toxicity of copper, cobalt and nickel [PS99, FMNM05]. It is assumed that histidine (or histidine-rich proteins) may directly interact with divalent metal ions in order to render them harmless. Even though the exact process of vacuolar sequestration *via* histidine still remains unclear the remarkably increased synthesis of the above mentioned amino acids besides histidine, suggests that these may play similar roles in conferring resistance to metal ions and in attenuating metal toxicity.
A number of up- regulated genes were also involved in sulfur (amino acid) metabolism which leads to glutathione synthesis (Figure 3.12a) and d)). This result is consistent with recent studies in *S. cerevisiae*, documenting the conversion of sulfur assimilates into glutathione in response to exposure of arsenic and cadmium [FLA$^+$02, HKC$^+$04]. Glutathione acts as a first line of defense against several stresses by sequestering and forming complexes with toxic metalloids [Ros02, MI01, VSL$^+$01, TM05, WT10]. In the present study glutathione synthesis in response to arsenic and cadmium could be confirmed once more. In addition, sulphur amino acid biosynthesis/metabolism was also notably induced by silver, mercury and manganese (Figure 3.9 cluster 14).
The third major group of genes that can be extracted when analyzing the activated pathways are those involved in carbohydrate and energy metabolism (Figure 3.13). This might probably base on the intention to obtain additional energy which may be required for tolerating the excess of toxic compounds and for the detoxification processes.
The repressed genes - visualized in Figure 3.14 a) and b) - mainly code for proteins involved in growth-related processes such as RNA metabolism and protein biosynthesis. This repression might serve the purpose as energy saving during the cellular systemic defense. The decrease of *de novo* protein synthesis in response to metal stress allows energy to be diverted to the increased expression of genes involved in stress response and specific detoxification mechanisms.

The results in particular consideration

Aluminum is a metal and belongs to the boron (Nr. 13) group of chemical elements in period 3. Aluminum can achieve three oxidations states, is characterized by a very low density and is too chemically reactive to occur in nature as a free metal. Although highly abundant in natural environment, aluminum salts are not known to be utilized by any form of life. Soluble aluminum salts have some demonstrated toxicity to animals but it's long-term toxicity to humans is still under debate. Applied as soluble chloride salt Al caused in this experiment the up regulation of protein catabolism genes and both, the up- and down-regulation of those involved in transcription and chromosome organization (Figure 3.9; first column).
Silver is a transition metal in group 11 of the periodic table (chemical symbol Ag) in direct

neighborhood to copper and gold. It occurs in two different oxidation states and is stable in pure air and water. Silver ions and silver compounds exhibit toxic effects on bacteria, algae and fungi, and is widely used in topical gels and impregnated into bandages because of its wide-spectrum antimicrobial activity. These properties arise from the ionized form, Ag^+ which forms strong molecular complexes with other substances used by bacteria to gain energy. Applied in this experiment as soluble nitrate-salt, silver induced particularly genes of vacuolar protein catabolism, response to (oxidative) stress and response to oxygen radicals (Figure 3.9: column 2). No strong repression of genes could be assessed.
Arsenic is a metalloid (chemical symbol As), and belongs to the group 15 of chemical elements in period 4. As occurs in many minerals, mainly combined with sulfur and metals, and also naturally in the native (elemental) state. Some rare species of bacteria use arsenic compounds as respiratory metabolites, and are thus arsenic-tolerant. To other biological and multicellular life, arsenic is however very toxic due to the interaction of arsenic ions with protein thiols. Arsenic and its derivatives have been extensively used in the production of pesticides, herbicides and insecticides. Applied in this experiment as soluble chloride-salt, arsenic induced the majority of genes in the response to (oxidative) stress groups and vacuolar protein catabolism (Figure 3.9; column 3). Repression of genes could be assessed as for cysteine and ribosome biosynthesis and translation.
Cadmium is an element (chemical symbol Cd) in group 12 and period 5 of the periodic table and is chemically similar to the two other metals of this group, zinc and mercury. Cd occurs similar to zinc mainly in the oxidation state +2 in most of its compounds. Similar to mercury it shows a low melting point compared to transition metals. Zinc, cadmium, and mercury are not classified as transition metals as they have in the oxidation state +2 the electronic configuration d10, with no incomplete d shell. The group 12 may be classed as post-transition metals. Cadmium compounds were used to stabilize plastic and with the exception of its use in nickel-cadmium batteries and cadmium telluride solar panels, the use of cadmium is generally decreasing. These declines are due to cadmium's toxicity and resulting regulations. Only one enzyme, a carbonic anhydrase with cadmium (usually zinc) as reactive center has been discovered in marine diatoms when zinc is limited. Applied in this experiment as chloride-salt, cadmium induced like arsenic genes in the response to (oxidative) stress groups and vacuolar protein catabolism (Figure 3.9; column 4). Furthermore, genes in the sulfur amino acid metabolism were notably induced by cadmium. Repression of genes could be assessed as for cysteine and ribosome biosynthesis and translation although this was not as prominent as for arsenic.
Mercury is also an element (chemical symbol Hg) in group 12 but period 6 of the periodic table and is, as Cd and Zn known as post-transition metal. Mercury is the only metal that is liquid at standard conditions for temperature, Hg poisoning can thus result from exposure to water soluble forms of mercury (such as mercuric chloride or methylmercury), inhalation of mercury vapor, or eating seafood contaminated with mercury. Medical use is for dental amalgams, preservative in vaccines and one topical antiseptic. Applied in this experiment as chloride-salt, Hg induced like the metals mentioned above genes in the response to (oxidative) stress groups and vacuolar protein catabolism (Figure 3.9; column 6). Repression of genes, though not as prominent as for cadmium, could be assessed as for cysteine and ribosome biosynthesis and translation genes. Interestingly, genes in the nitrogen compound metabolism were only induced by Hg.

All before mentioned metals play no role in biological life. A common cellular "program" when these metals were presented to yeast cells was found to be mainly the induction of genes in the response to (oxidative) stress groups, (vacuolar) protein catabolism and repression of ribosomal biosynthesis and subsequent translation processes.
The first observation is not surprising. Numerous studies have shown that excessive metal ex-

posure directly causes oxidative stress [WT10, VMC05, TM05], leads to the production of extremely reactive hydroxyl radicals [HG84, LGR$^+$98, EGOAB01] and causes cellular damage such as cleavage of DNA and RNA molecules or membrane damage [Bal02]. When all metal specific detoxification systems (sequestration and/or active extrusion) are overloaded and metal concentrations are beyond the storage and detoxification capacities of the cell, oxidative stress defense mechanisms are activated. These are associated with both, macromolecular damage and adaptive changes in gene expression [Hos05].
(Vacuolar) protein catabolism (the degradation of proteins) caused by aluminium, silver, arsenic, cadmium and mercury might be due to the fact that these metal ions compete with other molecules for sulfhydryl groups, which leads to protein inactivation and depletion of glutathione [WMDJ02, Bal02, HKC$^+$04]. The degradation of those inactivated proteins which otherwise would interfere with numerous enzyme systems occurs therefore as a result of indirect oxidative stress.
The repression of ribosomal biosynthesis and subsequent translation processes might be seen in conjunction with enhanced energy saving mechanisms during the cellular systemic defense.

Vanadium (chemical symbol V) belongs to group 5, period 4 of the periodic table and is a transition metal. In nature, the element is found only in chemically compounds but large amounts of vanadium ions have been found in a few bacteria and algae, possibly as a toxin. The oxide and some other salts of vanadium exhibit moderate toxicity. Particularly in the ocean, vanadium is used by some marine life forms (sea squirts, tunicates) as an active center of enzymes, such as the vanadium bromoperoxidase of some ocean algae. Applied in this experiment as chloride-salt, V caused only the induction of genes responding to oxygen radicals but a notable repression of genes in the iron homeostasis and glutamate biosynthesis group though weakly, and significantly in the meiosis/sporulation group (Figure 3.9; column 9). A possible interpretation may be that V is far less poisoning than Ag, As, Cd, and Hg and that the cellular response is focused on sequestration (possibly vacuole) and on inhibition of the propagation program.
Cobalt (chemical symbol Co) belongs to group 9, period 4 of the periodic table and is a transition metal. Cobalt is an essential trace element for mammals, as the active center of co-enzymes called cobalamins (prototype B12). These include vitamin B12 which is essential for mammals but Co is also an micronutrient for bacteria, algae, and fungi. Co deficiency results in anaemia, a lethal disorder. Although less common than other metalloproteins (e.g. those of zinc and iron), cobaltoproteins are known aside from B12. These proteins include methionine aminopeptidase 2 and nitrile hydratase. Applied in this experiment as chloride-salt, Co caused induction of genes in the iron homeostasis and glutamate biosynthesis group, and repression in the sporulation and DNA-repair groups (Figure 3.9; column 5). A possible interpretation may be that upon excess Co the cellular response is focused on sequestration (possibly vacuole) and on inhibition of the propagation program and high energy consuming DNA-repair program.
Nickel (chemical symbol Ni) belongs to group 10, period 4 of the periodic table and is a transition metal. It is one of the four elements that are ferromagnetic around room temperature, the other three being iron, cobalt and gadolinium. Ni plays important roles in the biology of microorganisms and plants. The NiFe-hydrogenases contain nickel in addition to iron-sulfur clusters. Such [NiFe]-hydrogenases characteristically oxidise H2. A nickel-tetrapyrrole coenzyme, F430, is present in the methyl coenzyme M reductase which powers methanogenic archaea. One of the carbon monoxide dehydrogenase enzymes consists of an Fe-Ni-S cluster. Other nickel-containing enzymes include a class of superoxide dismutase and a glyoxalase. Applied in this experiment as sulphate, Ni caused the weakest response of all applied metals. Low induction of genes in the iron homeostasis and glutamate biosynthesis and oxidative stress response group, and some minor repression in protein catabolism was assessed (Figure 3.9; column 8). A possible

interpretation may be that even upon excess Ni the cellular defense is necessary and sufficient by sequestration (possibly vacuole) and some energy saving by inhibition of protein assembly.
Zinc (chemical symbol Zn) belongs to group 12, period 4 of the periodic table and is a transition metal similar to the two other metals of this group, zinc and mercury. Zn occurs mainly in the oxidation state +2 and is, together with cadmium, and mercury not classified as transition metals but as post-transition metals. Zinc is an essential trace element, necessary for micro-organisms, plants, and mammals. Zinc is found in nearly 100 specific enzymes and has a prominent role as structural ion in transcription factors and it is stored and transferred in metallothioneins. Applied in this experiment as chloride-salt, Zn caused the second weakest response of all applied metals. Low induction of genes in the iron homeostasis and glutamate biosynthesis group, though other genes than induced by Ni. Significant repression in protein catabolism group of genes (other genes than induced by Ni) was assessed (Figure 3.9; column 10). A possible interpretation may be that due to the biologically highly relevant role of Zn any poisoning threat might require exceptionally high concentrations. Under the given experimental conditions the cellular defense - if any - addresses sequestration and some energy saving by inhibition of protein assembly.
Manganese (chemical symbol Mn) belongs to group 7, period 4 of the periodic table and is a transition metal. In nature it is found as a free element (metal) but often in combination with iron, and in many minerals. Mn is industrially used in the production of stainless steels. Manganese is an essential trace nutrient in all forms of life, and particularly as cofactor in different classes of enzymes ranging from oxidoreductases, transferases, hydrolases, lyases, isomerases, ligases, lectins, to integrins. The best known manganese-containing polypeptides may be arginase, the diphtheria toxin, and the Mn-containing superoxide dismutase (Mn-SOD) which is present in eukaryotic mitochondria, and also in most bacteria. In humans Mn is bound to manganese metalloproteins most notably glutamine synthetase in astrocytes. Applied in this experiment as chloride-salt, Mn caused the most differentiated response of all applied metals. Induction was assessed for nitrogen compound metabolism, iron homeostasis and glutamate biosynthesis, general response to stress and vacuolar protein catabolism, and amino acid metabolism. Repression was found for ribosome biogenesis/transcription and lipid metabolism, chromosome organization and hexose transport (Figure 3.9; column 7). A possible interpretation may be that in the presence of high Mn concentrations the cellular defense program basically stops all vital functions like sugar uptake (and thus energy production), preparation of the chromosomes for transcription, transcription itself, and amino acid assembly.

3.5 Conclusion

The results can be summarized as follows:

- All differentially expressed genes that are significantly up- or down-regulated in response to metal stress participate in a diverse range of cellular processes. The majority of the up-regulated genes is involved in amino acid and carbohydrate metabolism, energy generation, protein degradation, as well as general stress defense and metal-specific detoxification processes (Figures 3.9 and 3.11-3.13).
- The significantly repressed genes mainly belong to the transcription and protein synthesis category (Figures 3.9 and 3.14) .
- Thus the basic common mechanism in yeast in response to heavy metal stress is first an energy saving program. Among the vital functions those with high energy consumption like protein synthesis are descended.

- All three clustering methods (Intersections, Hierarchical clustering and K-means) revealed that every single used metal ion caused its own specific expression pattern.
- Even though some expression profiles are similar as it is the case for cadmium and mercury, cobalt and nickel), others as for manganese and arsenic exhibit even antagonistic expression patterns.
- It thus appears that common metal defense mechanisms or cellular programs with regard to sequestration, detoxification and regulation of these systems by up- or down regulation of specific genes were not identified. However, since among some groups of metals similar gene clusters were differentially regulated it can be assumed that yeast cells may differentiate between groups of metal ions by whether these - in concentrations as for essential cofactors - exert physiological functions, are part of complex molecules, stabilize protein structures or enzymes and DNA through electrostatic forces or are entirely toxic.
- As the uniqueness of each expression profile illustrates, the precision with which yeast responds to changes of environmental cues, *S. cerevisiae* seems to sense various cellular signals simultaneously, and therefore might be able to differentiate between the particular metal stresses.

Even though several gene cluster appear to be co-regulated upon the different stresses the outcome of this study demonstrated that every single metal causes its own specific expression pattern. This leads to the - surprising - conclusion that yeast is able to differentiate between the tested metal ions. However, the results presented above represent only a small part of the full experimental set. The detailed interpretation of all information that could be extracted from the bioinformatical analysis goes beyond the scope of this thesis and will involve expert-knowledge in molecular biology. This task is currently performed by Translucent project partners.

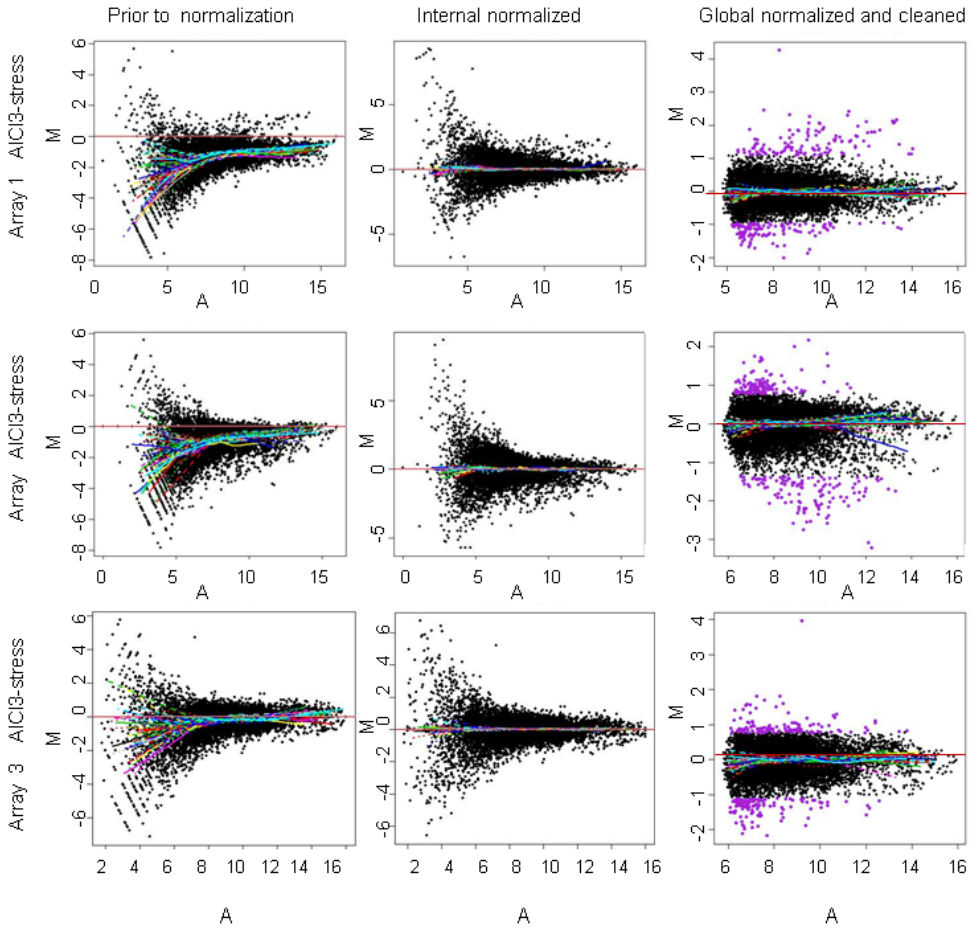

Figure 3.3: MA-plots obtained from the experiment with 500 μM $AlCl_3$-stress where M is the intensity ratio and A the average intensity for a dot in the plot. In each row one of the replicates was plotted and each column shows the progress of normalization with the Loess curve for individual print-tip-groups. First column: The background-corrected MA-values of the three arrays prior to normalization. Second column: Data after internal normalization. Third Column: Data after global normalization and after removal of control-genes as well as low-intensity spots. Spots marked with lavender color are interesting genes reflecting clear divergence from the mean.

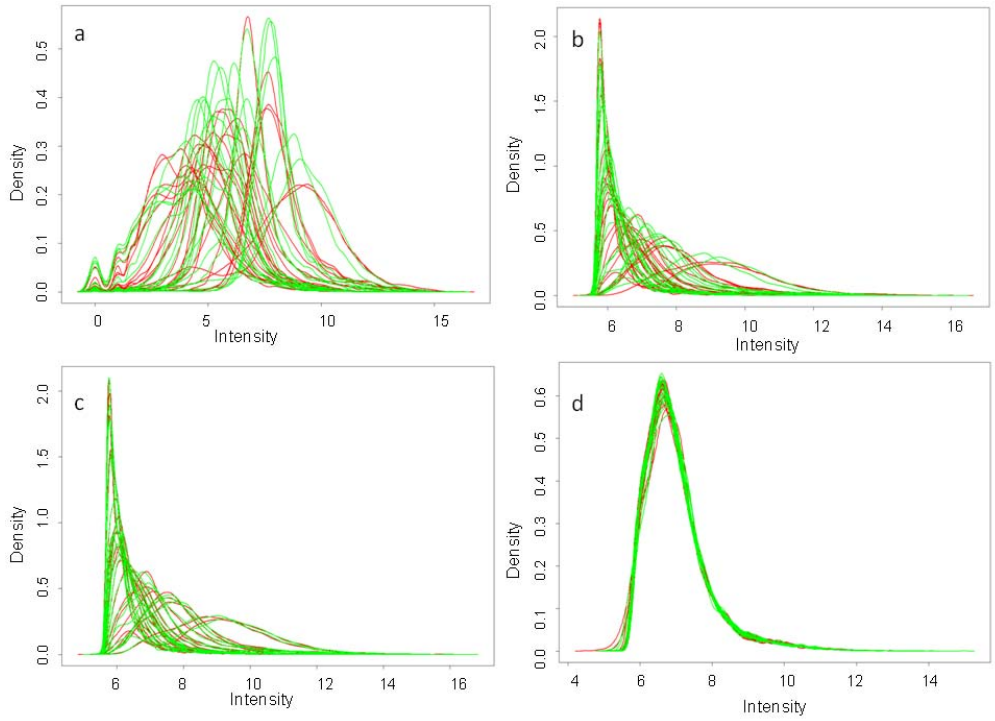

Figure 3.4: Smoothed densities of the green and red channels of all arrays. a: The channels prior to any background correction or normalization. b: After background correction c: After internal normalization d: Corrected channel intensities after global normalization.

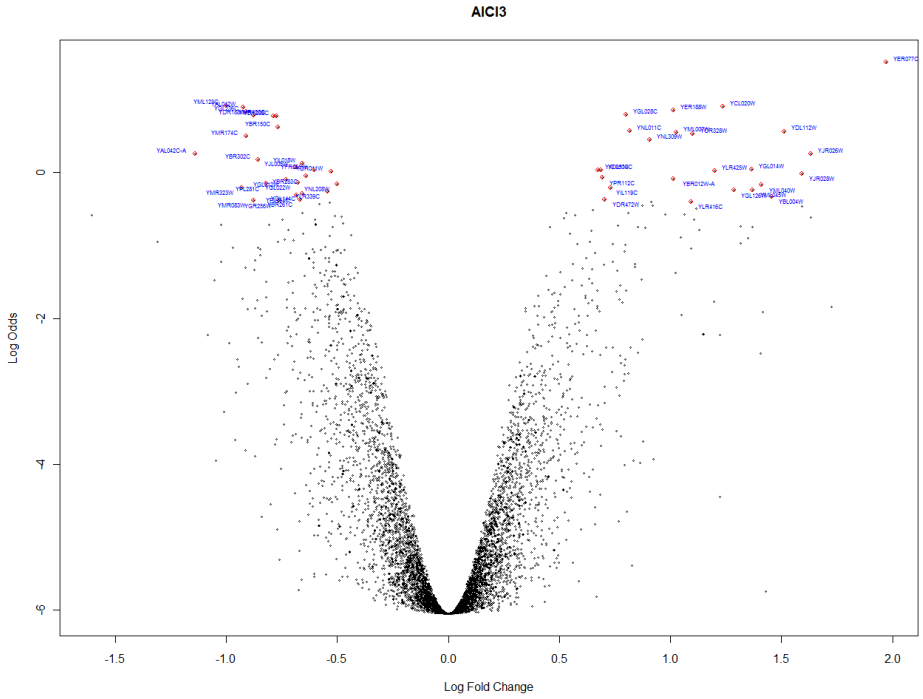

Figure 3.5: Volcano-plot of the top 50 ranked genes in the $AlCl_3$-stress experiment after statistical testing for differential expression. The log fold change is plotted on the x-axis and the significance in form of log odds that the gene is differentially expressed on the y-axis.

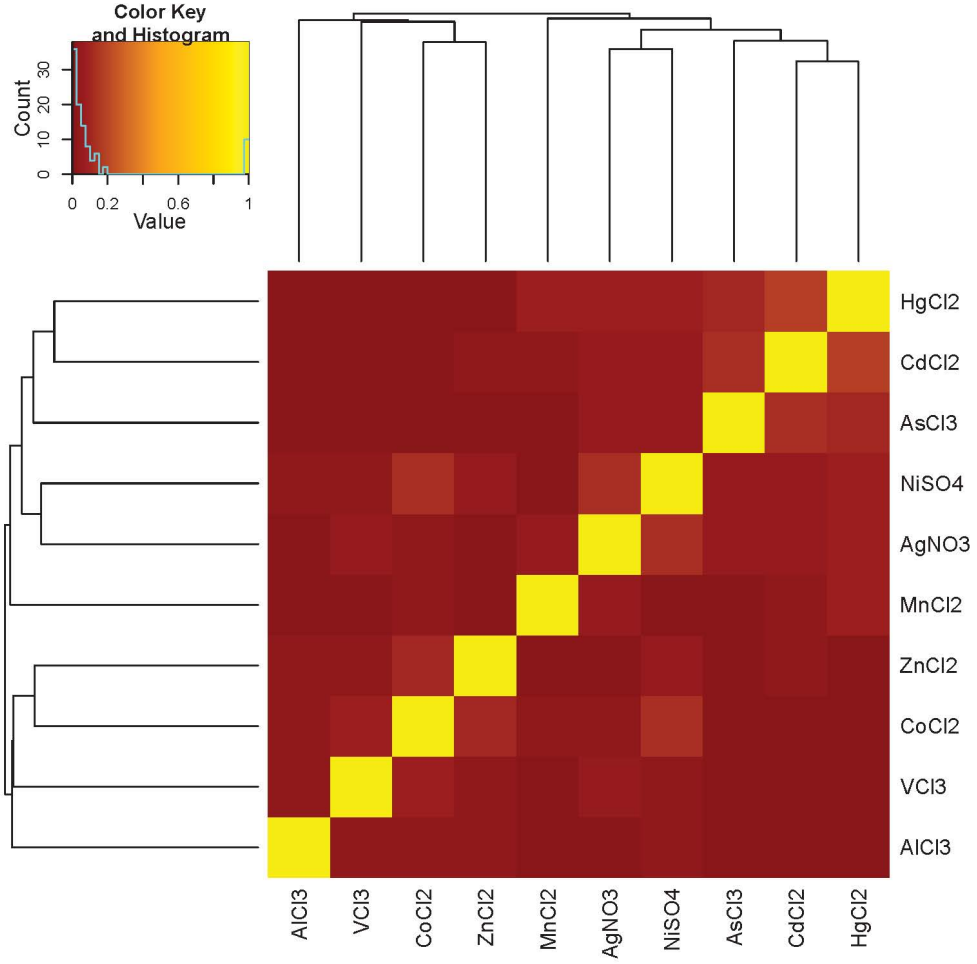

Figure 3.6: Jaccard heat map. Visualizes the degree of pairwise similarity. Conditions are grouped by dendrogramm.

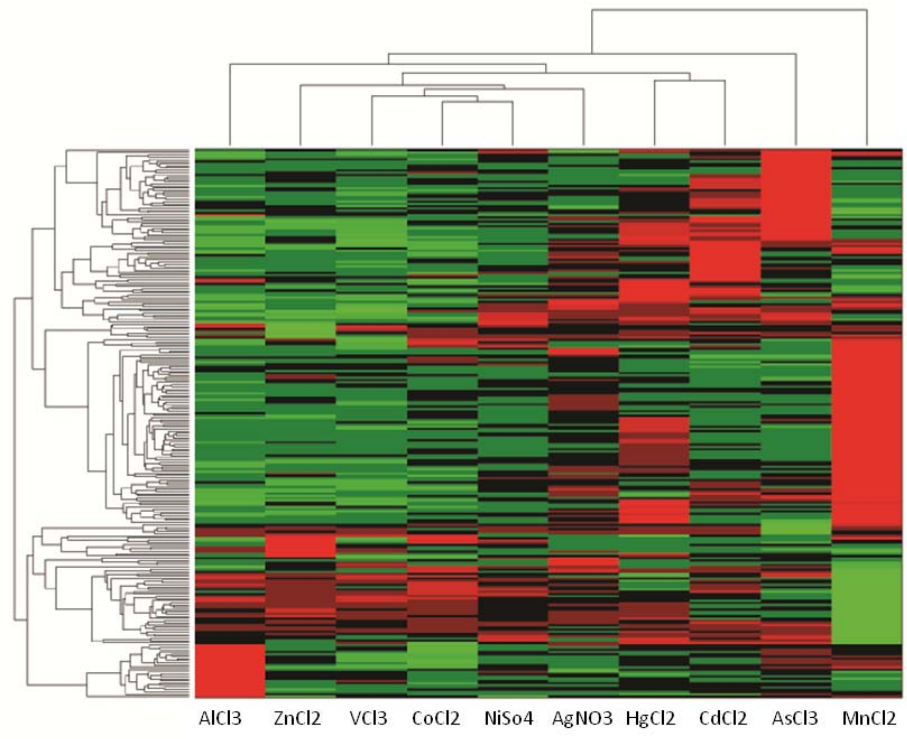

Figure 3.7: Hierarchical clustering analysis applied to the filtered gene expression matrix. The rows correspond to genes and the columns correspond to the ten experimental conditions. Variations in transcript abundance for each gene are depicted by means of color codes, in which shades of red represent increases, and shades of green decreases in mRNA levels, relative to the unstressed culture. Black color indicates undetectable change in transcription level, respectively missing data.

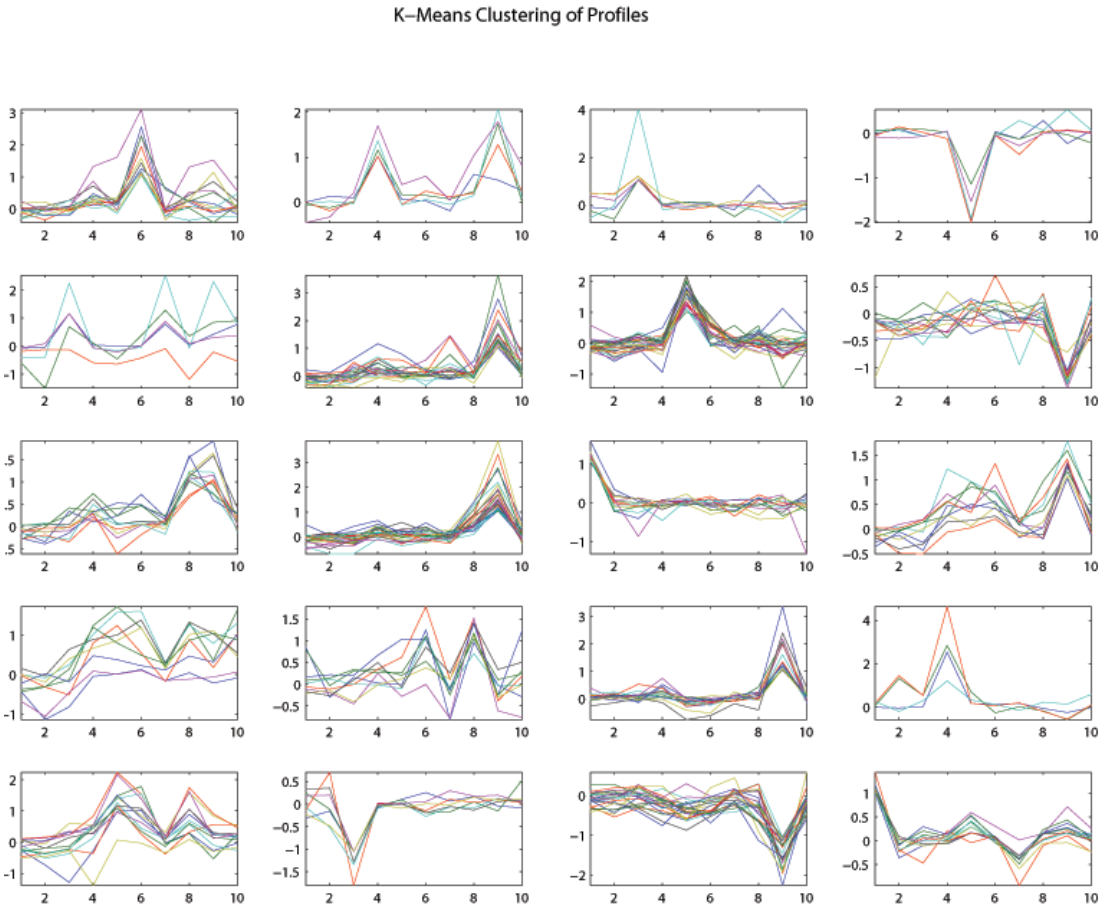

Figure 3.8: Results of K-means clustering of expression patterns for all genes being significantly differentially expressed in at least two of the ten experiments. Best results were achieved with K=20 clusters. The numbers 1-10 on the x-axis stand for the treatments $AlCl_3$, VCl_3, $ZnCl_2$, $AgNO_3$, $AsCl_3$, $CdCl_2$, $CoCl_2$, $HgCl_2$, $MnCl_2$, and $NiSo_4$, respectively. The values on the y-axis are the intensity ratios.

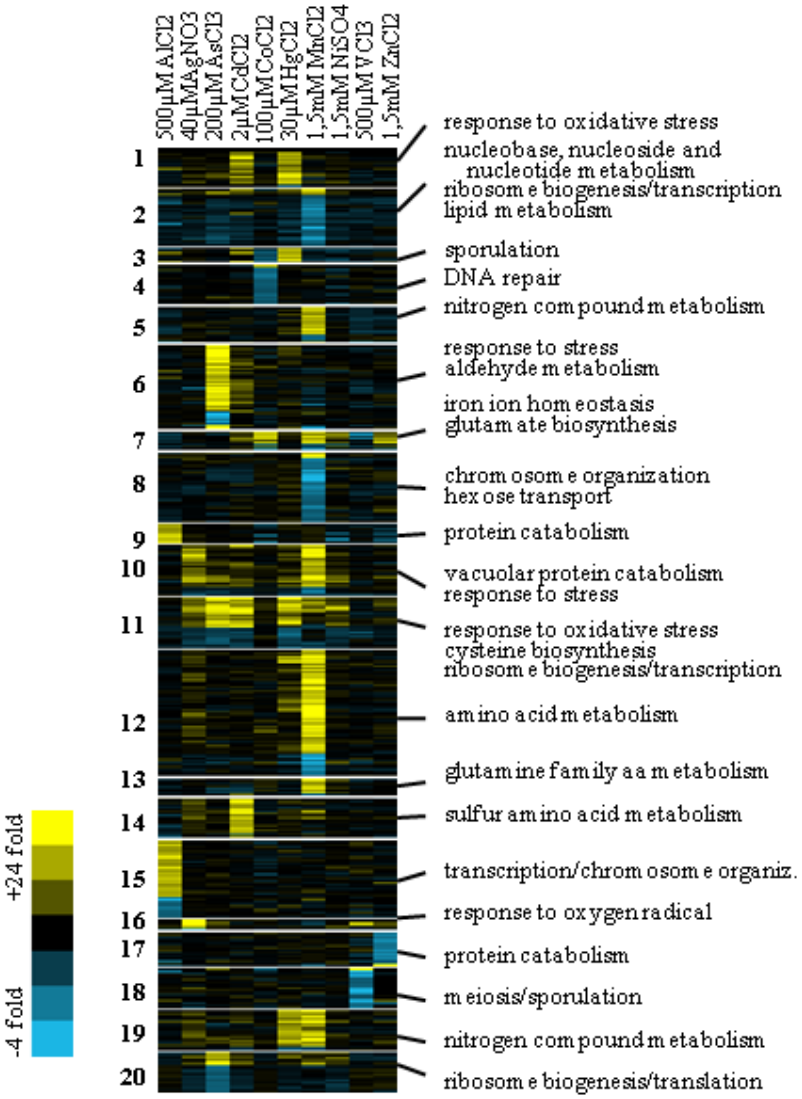

Figure 3.9: Transcript profile of metal stress: K-means clustering of the transcript profile was performed with K = 20 for the genes and the genes in the distinct clusters were closer defined by their corresponding Gene Ontologies. Variations in transcript abundance for each gene are depicted by means of color code, in which shades of yellow represent increases, and shades of blue decreases in mRNA levels, relative to the unstressed culture. Black color indicates an undetectable change in transcript level, respectively missing data.

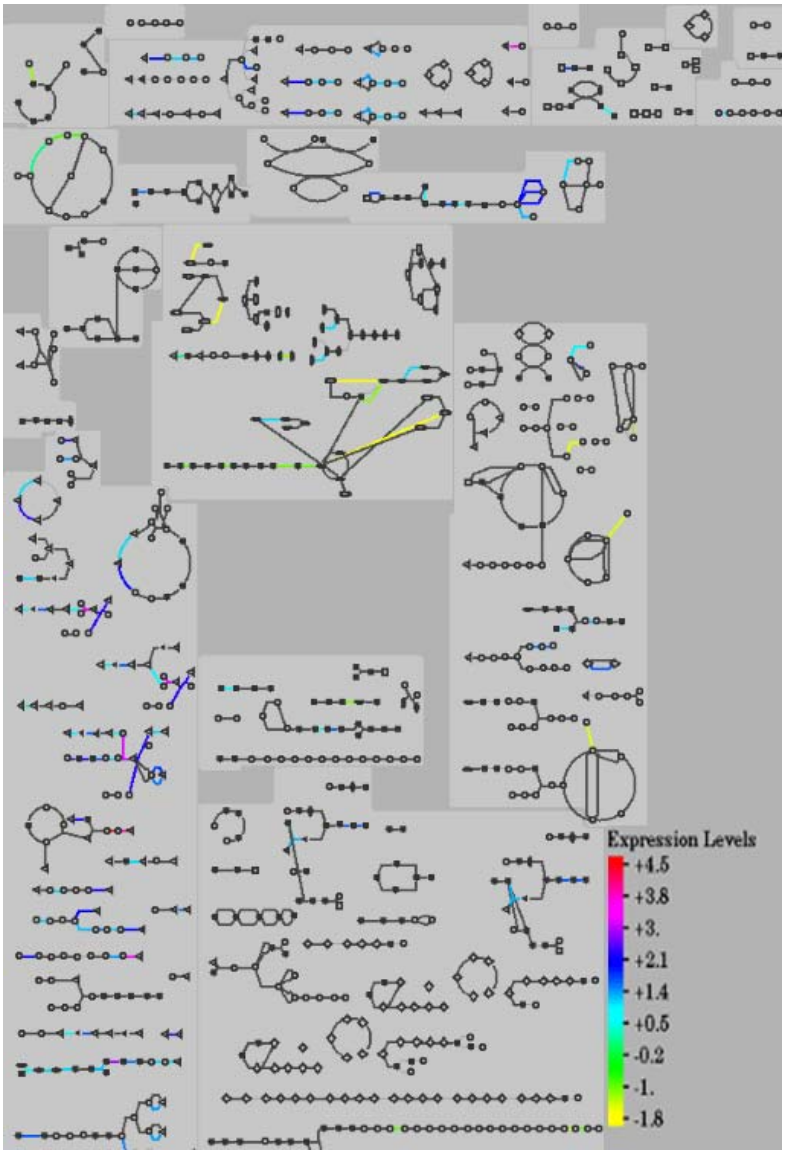

Figure 3.10: Outcome of mapping all significant genes to *S. cerevisiae* pathways using "Pathway Tool". All genes being significantly expressed in more than one experimental condition were mapped to biochemical pathways. Genes being up-regulated are visualized in shades from blue to red whereas shades from green to yellow indicate that the respective genes are repressed.

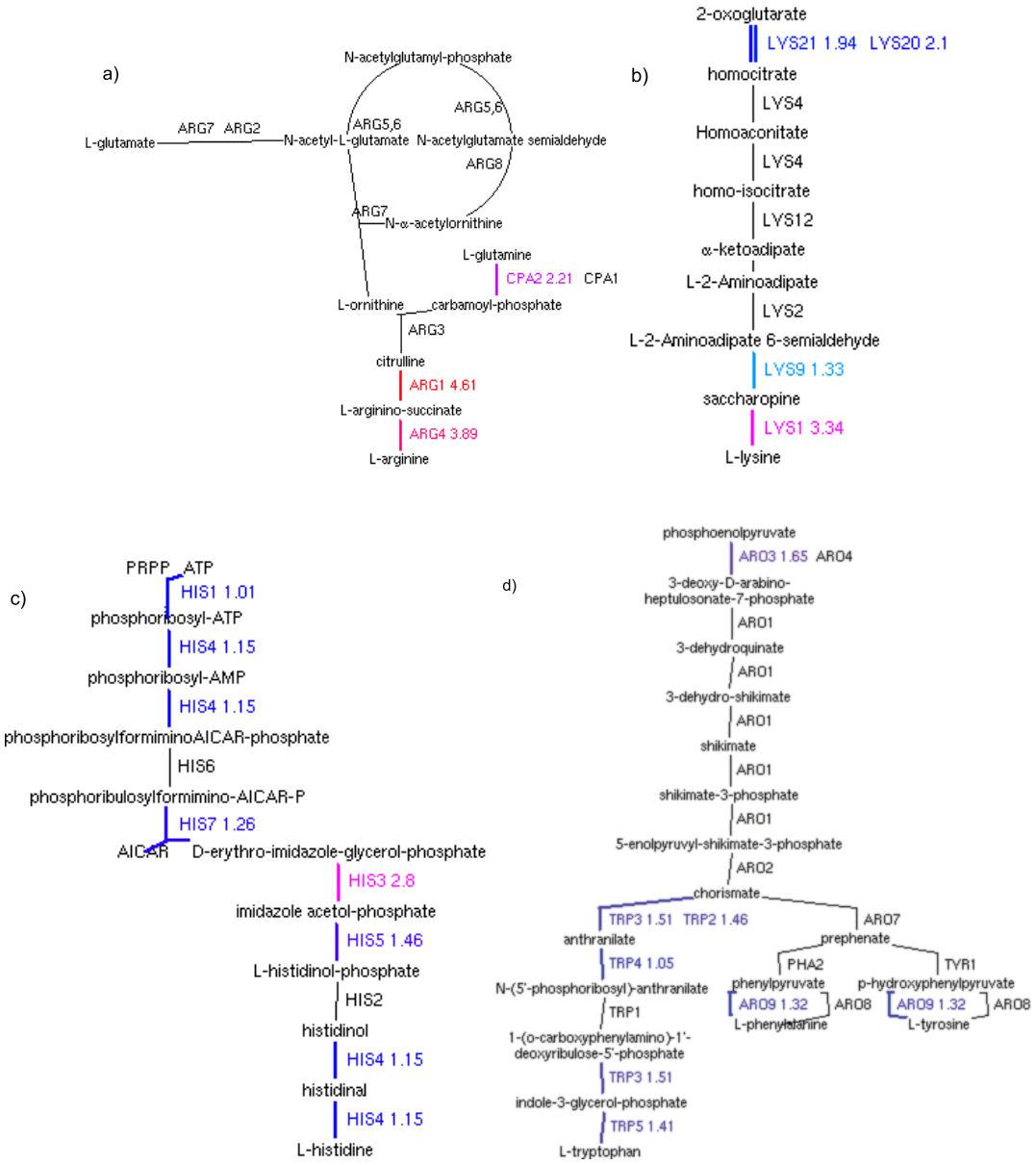

Figure 3.11: Extracted pathways with a high density of up-regulated genes: Synthesis of a) Arginine, b) Lysine, c) Histidine, d) Tryptophan, phenylalanine and tyrosine. Genes are positioned besides the associated reaction within the pathway together with the value of log-fold change. The color-code is adopted from Figure 3.10

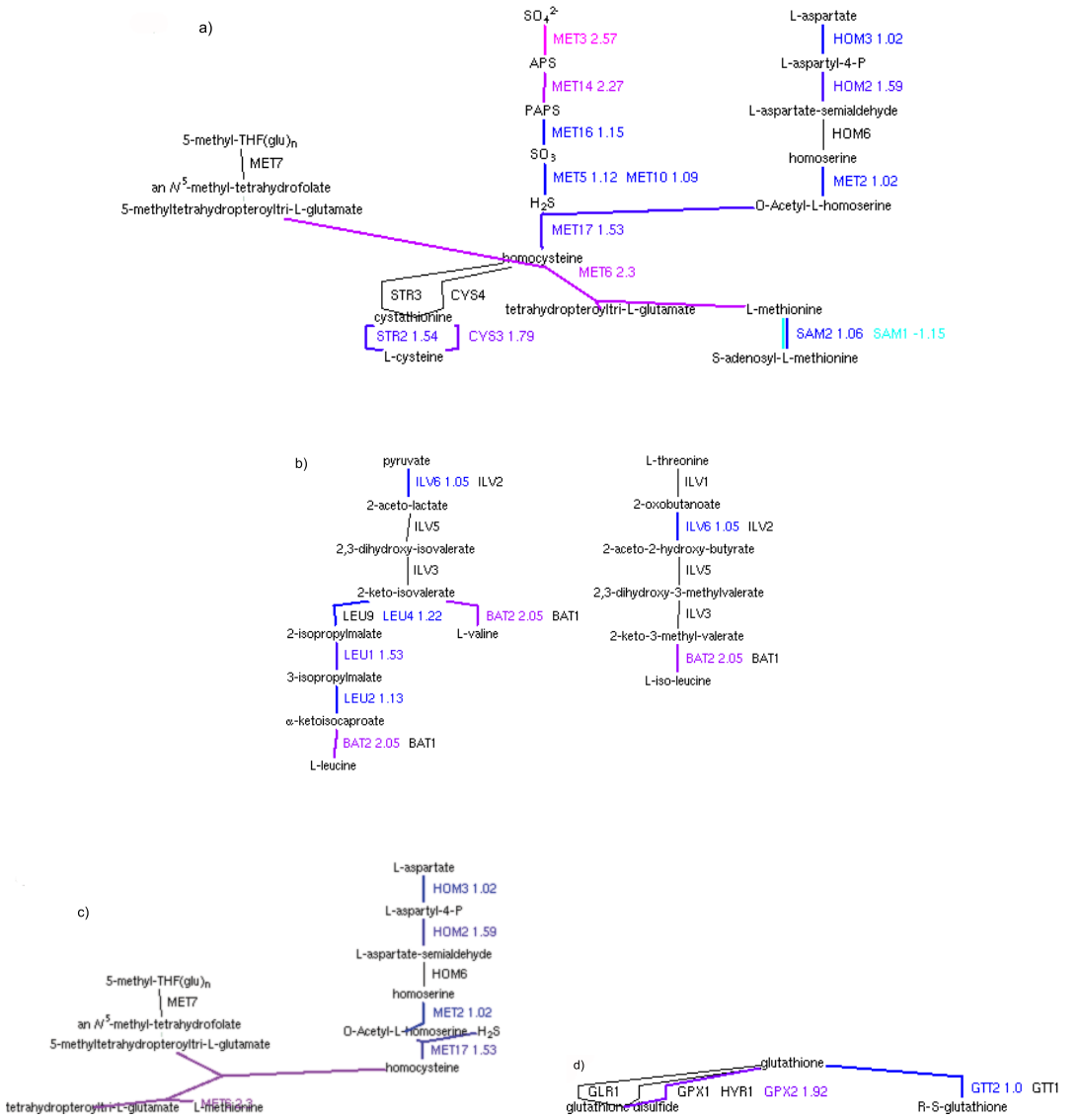

Figure 3.12: Extracted pathways with a high density of up-regulated genes: Synthesis of a) Cysteine, b) Leucine and isoleucine c) Methionine d) Glutathione. Genes are positioned besides the associated reaction within the pathway together with the value of log-fold change. The color-code is adopted from Figure 3.10

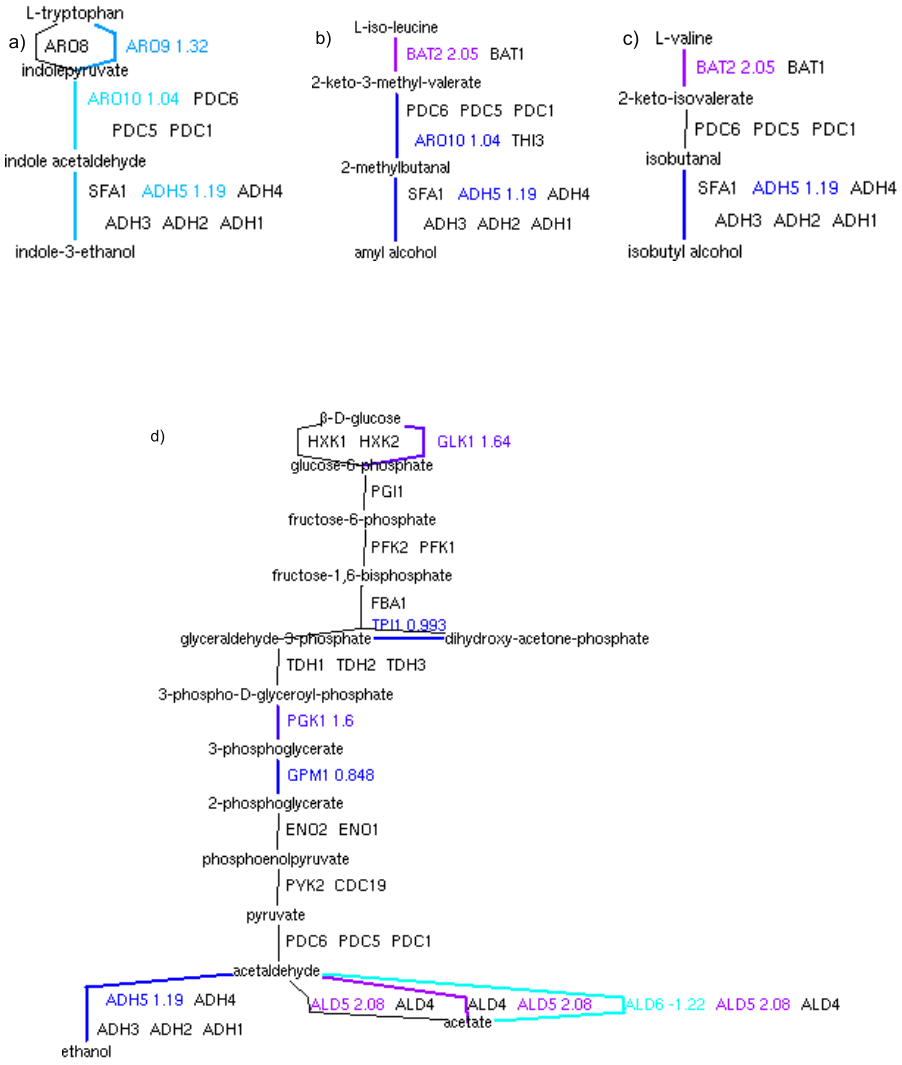

Figure 3.13: Extracted pathways with a high density of up-regulated genes involved in carbohydrate and energy metabolism. Genes are positioned besides the associated reaction within the pathway together with the value of log-fold change. The color-code is adopted from Figure 3.10.

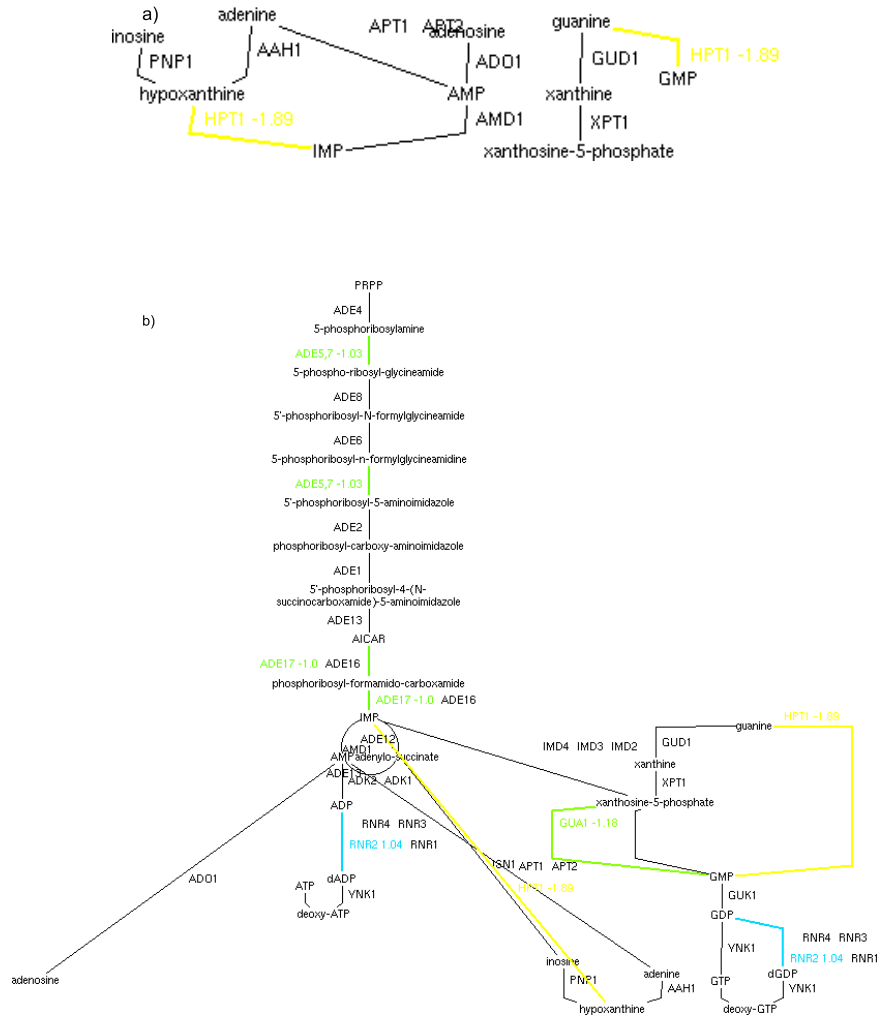

Figure 3.14: Extracted pathways with a high density of down-regulated genes. The repressed genes mainly code for proteins involved in growth-related processes, such as RNA metabolism and protein biosynthesis and are positioned besides the associated reaction within the pathway together with the value of log-fold change. The color-code is adopted from Figure 3.10.

4 Spatio temporal modeling

4.1 Abstract

The availability of high-resolution microscopy together with the advancements in the development of biomarkers as reporters of biomolecular interactions are indicative for the importance of imaging methods in molecular cell biology. These techniques enable the investigation of cellular characteristics like cellular volume and geometry, size, amount, volume and geometry of intracellular compartments, and amount of existing proteins in a spatially resolved manner. Such detailed investigations opened up many new areas of research in the study of spatial, complex and dynamic cellular systems. One of the crucial challenges in this context is the design of a well structured and optimized workflow to provide systematic and efficient hypothesis verification. Computer Science can efficiently address this task by providing software that facilitates handling, analysis, and evaluation of biological data to the benefit of experimenters and modelers.
The Spatio-Temporal Simulation Environment (STSE) is a set of *open-source* tools provided to conduct spatio-temporal simulations in discrete structures based on microscopy images. This environment can be used for the analysis and interpretation of time resolved protein localization and accumulation data like e.g. upon definite stress challenges. The framework contains modules to digitize, represent, analyze, and mathematically model spatial distributions of biochemical species. Graphical user interface (GUI) tools provided with the software enable meshing of the simulation space based on the Voronoi concept. In addition, it supports to automatically acquire spatial information to the mesh from the images based on pixel luminosity (e.g. corresponding to molecular levels from microscopy images).
General concepts of the STSE design and workflow will be discussed with regard to actual application using the example of a signaling cascade that leads to formation of a morphological gradient of the Fus3 protein within the cytoplasm of the mating *S. cerevisiae* cell.
STSE provides the means to relate the simulation to the image data and thus a systematic, image driven model validation or rejection. STSE is freely available either as a stand-alone version or included in the Linux live distribution Systems Biology Operational Software (SB.OS) and can be downloaded from http://www.stse-software.org/. The Python source code as well as a comprehensive user manual and video tutorial are also available to the research community.
Parts of this work have been published as
S. Stoma, M. Fröhlich, S. Gerber and E. Klipp: STSE: Spatio-Temporal Simulation Environment Dedicated to Biology, submitted to BMC Bioinformatics(2010).
Szymon Stoma is the main developer of STSE.

4.2 Introduction and Background

With the availability of high-resolution microscopy and high-throughput technologies in molecular biology the amount of cellular images in very good resolution quality increases significantly. Such amount of available data consecutively demands for image analysis software adapted to utilize the full capacity of these imaging advancements.

The state-of-the-art method of presenting, assessing and evaluating experimental images qualitatively is being increasingly replaced by computational data evaluation. Quantification of e.g. light intensities arising from fluorescent protein (FP) expression in different cellular compartments can be ascertained in a spatially resolved manner. Such quantification may then enable the mathematically verification of the current understanding of biological systems. Unambiguous and reproducible computational extraction increases the quality and exchangeability of information for subsequent automatic processing steps such as digitization, representation, analysis, and modeling.
A variety of image processing-, analysis- or modeling-packages addressing these tasks exist already, either on a commercial basis or as open source software.
Recently, several eminent reviews have been published that outline the most common methods and tools for biological image processing, analysis and modeling (see [LC09, Pen08, MvC07]). One of the key conclusions is that these different tasks are usually separately addressed. Cell segmentation and property extraction, for example, are well established and can be realized by dedicated software such as CellProfiler [LSC07], Cell-ID [GCLC$^+$07] or generic image processing platforms like Labview (National Instruments, Austin, USA) or Imaris (Bitplane, Zurich, Switzerland). A widely used and freely available tool is ImageJ [AMR04], which comprises standard segmentation algorithms as well as surface or profile plots. Also freely available are additional R packages like EBImage [PFS$^+$10], which can be used for the segmentation and analysis steps.
Within spatial modeling and simulation in cell biology following classes of dedicated simulators are distinguished:

- Spatially partitioned ODE systems like "Virtual Cell"
- Spatially partitioned Gillespie systems (e.g. MesoRD [HFE05] or SmartCell [ABDV$^+$04])
- Particle-based simulators (e.g. Smoldyn [AABA10], MCell [SBS$^+$01] or Meredys [TLN10]).

All of these tools offer excellent solutions for the specific problems they were designed to solve. However, it is still difficult or rather time-intensive to perform a contiguous and intuitive workflow, starting with almost raw data images and resulting in a running mathematical model, that enables a directly comparison of the simulation results with biological data.

The STSE platform intends to integrate various tools or software-packages that are in the majority specifically designed for individual steps such as image processing, analysis, modeling and simulation. By providing the workflow guidelines and the access to Python language, the platform offers the advantage of stratifying the interaction with different data-structures and thus minimizes the loss of time and information during the manual export and conversion processes. It should be understood as a set of tools facilitating the intuitive workflow between image analysis tools and simulators. Additionally, within the current implementation the environment provides examples of how to perform such a transition from segmenting tools to simulation engines internally implemented in Python (spatially partitioned ODEs). For these purposes STSE comprises modules for digitizing and representing microscopy data that enable data analysis as well as manipulation, and can be used for mathematical modeling and simulation of spatial distributions of chemical molecules.

4.3 Implementation

The tools are written in Python and have a modular design which allows the modeler to extend their functionality according to custom needs. The default STSE workflow can be summarized

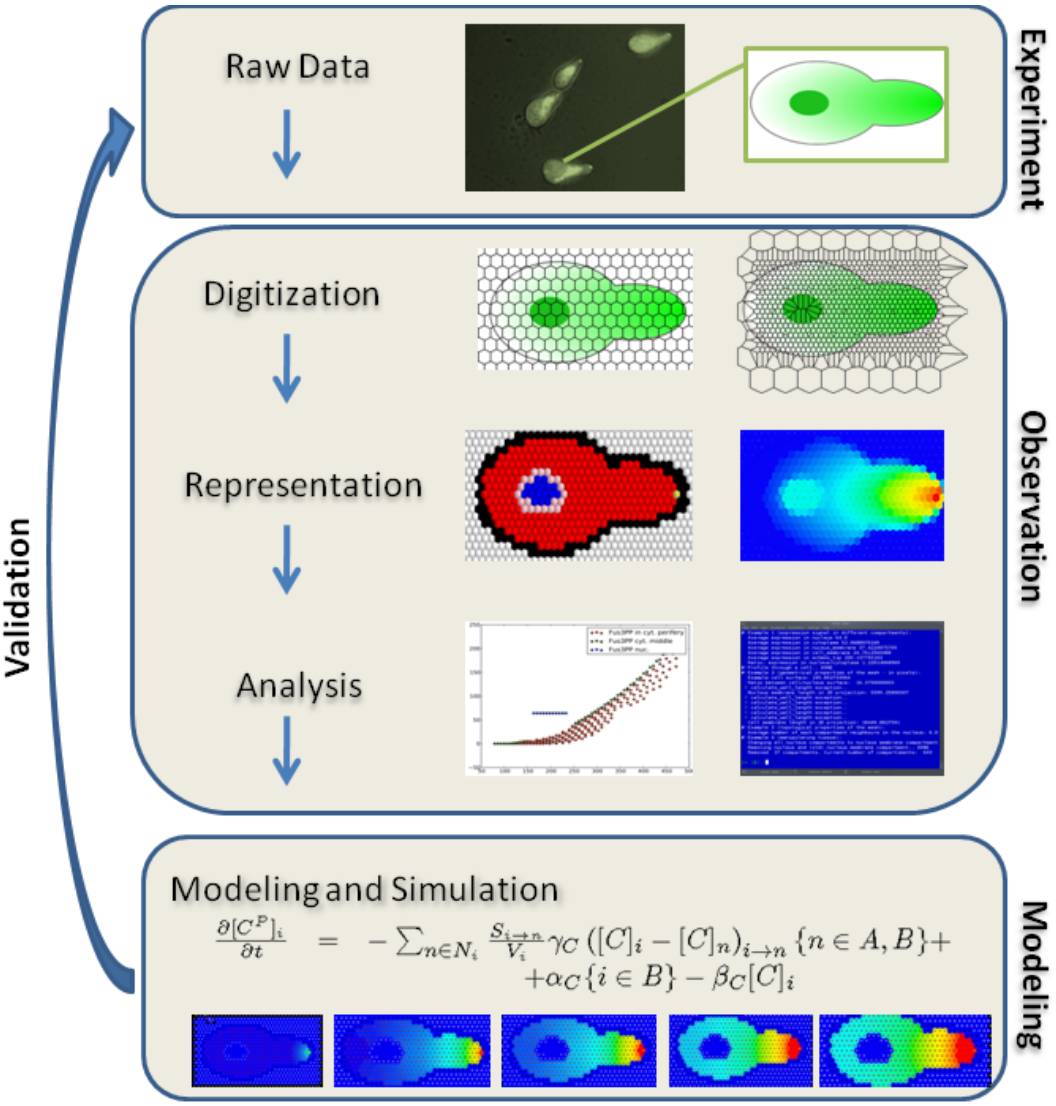

Figure 4.1: Sketch of the structure and the modules combined in STSE that enable an uninterrupted workflow. Starting with microscopy images (raw data) the framework allows to digitize, represent, analyze and mathematically model spatial distributions of species.

as follows (see: Figure 4.1):

1. Preprocessing of microscopic images for the studied object. For optimal use, STSE requires time-series images for the studied object.
2. Definition of a discrete representation of the images. The user starts with a default, hexagonal mesh and is free to modify it.
3. Automatic integration of the information from (time-series) images into the discrete representation.
4. Analysis of the digitized data.
5. Formulation of a model by defining interactions between regions of interest and molecules of interest.
6. Simulations where previously digitized images are used as initial conditions for the evaluation of simulation results.

In the following section a concise overview of the fundamental methods used in STSE will be given.

4.3.1 Spatial segmentation and digitization

The process of digitization first generates a data structure that enables the efficient analysis, representation and modeling. The classical approach is to decompose the microscopy image into physiologically distinguishable compartments (e.g. nucleus, cytoplasm, etc.) which is called image segmentation [Ham09, WS07]. Usually, image segmentation results in a data structure linking the compartments with pixels. STSE differs from this approach by introducing an abstract, intermediate layer composed of so-called sub-compartments. To generate this layer, each compartment is divided into sub-compartments that have the geometry of polygons and are organized in such a way that they fill the entire compartment and do not overlap with each other. The default geometry is automatically composed of equilateral hexagons. The purpose of introducing this abstract layer is to allow for adjusting the digitization precision separately for different compartments, which is useful in later steps of analysis and modeling.
To edit the geometry of sub-compartments a Voronoi 2D tessellation is utilized [Kle89]. By means of the graphical user interface (GUI) editor the user may move sub-compartment centers (corresponding to the vertices in the Voronoi graph) for fine-tuning the individual adjustment. This information implicitly specifies the geometry of each sub-compartment. Since these sub-compartments share edges, the representation resembles a polygonal mesh (PM). Each sub-compartment takes an individual geometry as well as other user-customizable properties such as cellular compartment affiliation, concentrations of specific substances, etc. The GUI enables the user-friendly inspection and editing of these properties. Additionally, due to the software implementation design it is possible to extend the GUI editor by adding custom actions as well as to script the GUI with Python. This reflects one of the main goals of STSE that is to provide the possibility of framework extension and customization to the users. With STSE it is possible to acquire spatial luminosity information from microscopic images, which can correspond e.g. to the inhomogeneous distribution of tagged molecules within the cell. This process is performed on indexed color images (e.g. FP microscopic images). This is an important feature, since it allows for the comparison of simulation results with experimental data.

4.3.2 Representation and analysis

Image representation is performed implicitly by the conversion of the Voronoi-based poligonal mesh to an internal STSE data structure. This design involves less constraints and thus enables more latitude in defining polygonal geometries (e.g. including non-convex ones) as well as physiological information. That is realized by storing the polygon corner coordinates explicitly in the data structure instead of computing them using the Voronoi algorithm. The data structure can easily be modified or inspected *via* Python. This allows for simulating structures changing in time, which has been, for instance, successfully used in the dynamic modeling of meristem growth [SLC+08]. The analysis is conducted *via* the STSE-GUI as well as with Python scripts and enables a comprehensive and differentiated overview of topological, geometrical and physiological information. The routines provided by STSE enables the visualization and inspection of compartment properties and can be used for computing different properties and for further, computational analysis of data from images. All structural information can be exported and saved for persistence and dissemination.

4.3.3 Modeling

The digitized data can be used *directly* to perform spatial modeling (e.g. as initial conditions or evaluation). STSE does not restrict the user with the simulation framework. Instead, a workflow based on the so-called "cell-centered" finite volume method [Mis98] is suggested. According to this scheme, a mechanistic model of a studied process needs to be formalized using a system of ordinary differential equations (ODEs) that describe the interplay of different actors (e.g. chemical molecules) and different cellular compartments with specified kinetic rules on diffusion, chemical reactions, transport, etc. In this case a SciPy library [JOP01] can be integrated to solve the equation system within the STSE framework.

4.4 Results

In the following section it will be demonstrated how to use STSE to analyze and simulate biological systems. A typical STSE workflow including the modules for digitization, representation, analysis and modeling is presented using the running example of a mitogen-activated protein kinase gradient formation (the double-phosphorylated Fus3 ($Fus3^{PP}$) protein in a mating S. cerevisiae yeast cell [MHK+07] (Figure 4.6). Fus3 signaling is part of the yeast mating pheromone pathways: upon stimulation with the pheromone α-factor, an intracellular signaling cascade is activated, which leads to the double phosphorylation of the Fus3 protein. The $Fus3^{PP}$ is released at the shmoo tip and can diffuse within the cell, which results in an observable $Fus3^{PP}$ gradient that can be detected *via* Fluorescence Correlation Spectroscopy (FCS), an experimental technique that monitors the motion of fluorescently labeled molecules in a tiny, optically defined observation volume. When reaching the nucleus, $Fus3^{PP}$ is actively transported across the nuclear membrane and regulates transcription factors that modulate mating-specific gene expression.

In the following section the focus is set rather on the software specifications and the application scenario than on the biological results. To simplify the analysis and to facilitate the usage of examples in a confirmatory way, test data, inspired by the experiments and explanations presented by Maeder et al. [MHK+07] are used.

As a first step the analysis and characterization of the $Fus3^{PP}$ gradient will be demonstrate by:

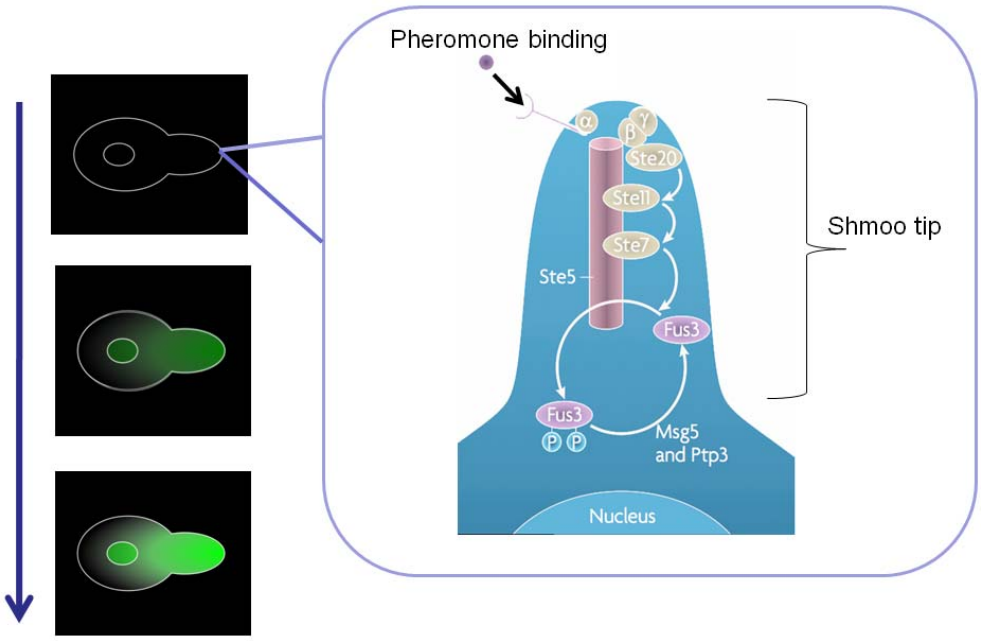

Figure 4.2: Mitogen-activated protein kinase (MAPK) activity gradients in the pheromone response of S.cerevisiae. The Ste5 scaffold protein localizes pheromone-induced phosphorylation of the yeast MAPK Fus3 to the shmoo tip. The homogenously distributed phosphatases Msg5 and Ptp3 dephosphorylate Fus3 globally. Dissociation and diffusion of phosphorylated Fus3 induces the formation of activity gradients, which propagate signals from the shmoo tip and define local cytoplasmic states. α, β and γ are the subunits of trimeric GTP-binding proteins, and Ste20, Ste11 and Ste7 are kinases in a phosphorylation cascade.

- The quantification of the ratio of the average cytoplasm/nucleus expression of $Fus3^{PP}$ based on fluorescence signal intensity acquired from microscopy images.
- The plotting of gradient curves for $Fus3^{PP}$ along the x-axis of the cell data image and around the nucleus, and
- The simulation of the process of $Fus3^{PP}$ diffusion in the cytoplasm to determine the underlying conditions that lead to the qualitative values captured in the image.

The results of the simulations are evaluated and it is discussed of whether the appearance of a $Fus3^{PP}$ gradient throughout the cell can be explained by simple diffusion and how plausible conditions and model parameters allowing to reproduce the experimental observations could be defined.

4.4.1 Digitization

A major issue in this context is the task to adapted the polygonal mesh. If, for instance the focus is on a particular protein like the $Fus3^{PP}$ in this case, the interesting point is the pro-

tein gradient within the cytoplasm but not outside the cell. Thus it is necessary and sufficient to adapt the mesh size according to the area of interest. Here, it is requested to keep a high precision within the cytoplasmic compartment (but not within other compartments) in order to capture and depict the gradient correctly. The analysis accounts the hypothesis that the $Fus3^{PP}$ distribution is neither outside the cell nor in the nucleus. Therefore, varying "sub-compartment densities" in these compartments will be used as presented in Figure 4.3.The default geometry is automatically composed of equilateral hexagons (Figure 4.3*a* and *b*). However, this default geometry of the sub-compartments may after this first step be fine-tuned by using the GUI editor to meet specific analysis and modeling requirements (Figure 4.3c).

Another task within the digitization-package of imaging data is the acquisition of sub-compartment

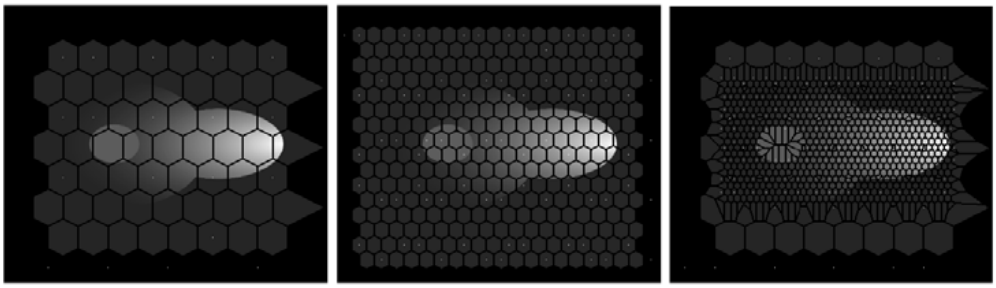

Figure 4.3: Different "sub-compartment density" variants (a) rough regular digitization (b) more refined, regular digitization (c) high density, irregular representation edited with the STSE GUI.

types (i.e. the determination for each abstract sub-compartment the affiliation to a cellular compartment). Each sub-compartment is associated with only one compartment type. In case of a potential conflict occurs (e.g. in the case of overlapping binary masks) the user may alter sub-compartment types manually. This is performed by changing the order of application of the binary masks or by defining sub-compartment types. In this example, binary masks were used for the localization of the following compartment types: the cytoplasm, the nucleus, the cell membrane, the nuclear membrane and the shmoo tip.

The automatic acquisition of the signal from the microscopy image provides the basis for the subsequent analysis and modeling steps. For this purpose indexed color images (e.g. standard light/confocal microscopy images) were used that correspond to the actual concentrations of the molecules of interest. Test data images of the running example were inspired by the experiments described in Maeder et al. [MHK$^+$07], in which the intracellular localization of $Fus3^{PP}$ has been reported by fluorescence lifetime imaging microscopy (FLIM) (see Figure 4.5).

To summarize the previous steps: The necessary inputs for the digitization procedure are i) the binary masks, and ii), the indexed color images. The output of the digitization step is a feasible amount of abstract sub-compartments that cover the microscopic image. Each sub-compartment is allocated with a specific compartment type and the average intensity of the protein(s) of interest is acquired from input data.

4.4.2 Representation and analysis

The analysis in STSE is realized *via* Python scripts. The running example demonstrates common tasks performed with STSE such as inspection of the geometrical, physiological or topo-

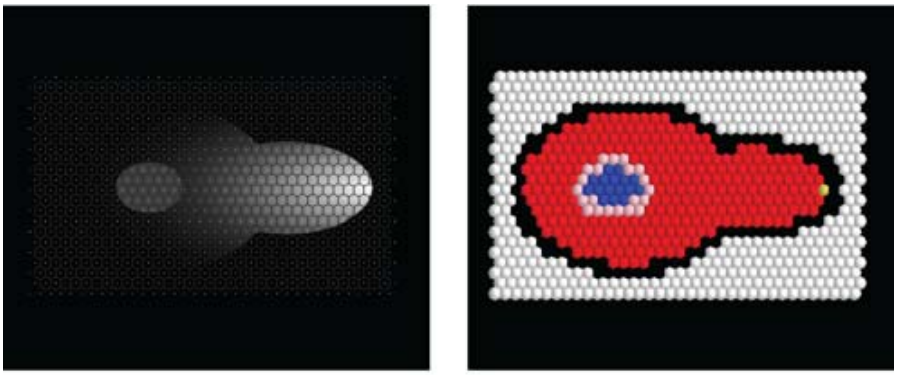

(a) (b)

Figure 4.4: Sub-compartment types assignment (a) mesh showing the geometry of sub-compartments (b) types of sub-compartments acquired from the binary masks. Different sphere colors depict different compartment identities: white - outside, black - the cell membrane, blue - the nucleus, red - the cytoplasm, pink - the nuclear membrane, yellow - the shmoo tip.

logical properties of the sub-compartments/ compartments and removal or resizing the sub-compartments. By this the following information on the $Fus3^{PP}$ gradient can be extracted (Figure 4.6) :

- The distribution of $Fus3^{PP}$ in the cytoplasm along the x-axis in a central part of the analyzed cell is exponential (Figure 4.6c).
- The distribution of $Fus3^{PP}$ around the nucleus reaches its maximum in the point closest to the shmoo tip (Figure 4.6d).
- The average $Fus3^{PP}$ signal in the nucleus is 64.0 (a.u.), which is $\approx 25\%$ of the maximal signal measured in the image.
- The average $Fus3^{PP}$ signal in the cytoplasm is 52.07 (a.u.) (which is $\approx$ 20% of the maximal signal measured in the image).

4.4.3 Modeling

The previously acquired, quantified and structured data can be used to create a dynamic model of the $Fus3^{PP}$ diffusion. According to the STSE data flow paradigm (Figure 4.1), the mechanistic model of the studied process needs to be formalized. By focusing on an specific question like the characteristics of the $Fus3^{PP}$ gradient other processes such as the stimulation mechanisms of Fus3 protein or transport of $Fus3^{PP}$ into the nucleus are not considered. The modeling is therefore focused on a specific feasible part and not confused or unnecessarily bloated. Within the kinetic model the following assumptions of $Fus3^{PP}$ protein distribution are taken:

- $Fus3^{PP}$ appears in the shmoo tip compartment,
- $Fus3^{PP}$ diffuses freely in the cytoplasm compartment,
- $Fus3^{PP}$ is dephosphorylated during the diffusing in the cytoplasm,

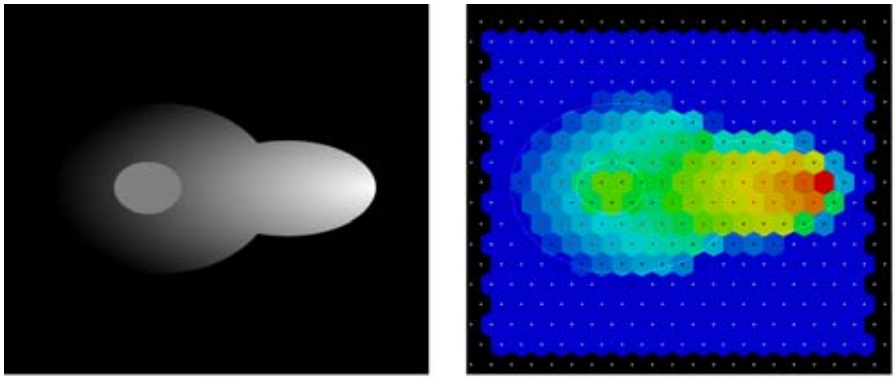

(a) (b)

Figure 4.5: Signal quantification (a) indexed color image of $Fus3^{\mathrm{PP}}$ localization (b) result of $Fus3^{\mathrm{PP}}$ signal quantification based on the indexed color image. Small spheres depict the compartment types.

- $Fus3^{PP}$ is unable to cross the nuclear membrane compartment.

By applying this kinetic model it is next possible to verify whether or not the qualitative properties of the $Fus3^{PP}$ gradient observed in the digitized images can be reproduced. In the example case presented here, for the purpose of simplification a dedicated explicit simulation, written directly in Python was applied. Therefore the model was translated into a system of differential equations and an equation that describes the alterations of the $Fus3^{PP}$ concentration is attributed to each sub-compartment.

$$\frac{\partial FUS3^{PP}{}_i}{\partial t} = -\sum_{n\in N_i} \frac{S_{i\to n}}{V_i}\gamma_{FUS3^{PP}}\left(FUS3^{PP}{}_i - FUS3^{PP}{}_n\right)_{i\to n}[n\in A,B] + \\ +\alpha_{FUS3^{PP}}[i\in B] - \beta_{FUS3^{PP}}FUS3^{PP}{}_i$$

where:

- $FUS3^{PP}{}_i$ is the concentration of $\mathrm{Fus3^{PP}}$ in the subcompartment i,
- $\gamma_{FUS3^{PP}}$ is the diffusion constant for $\mathrm{Fus3^{PP}}$,
- $\alpha_{FUS3^{PP}}$ is the rate of $\mathrm{Fus3^{PP}}$ release in the shmoo tip,
- $\beta_{FUS3^{PP}}$ is the rate constant of $\mathrm{Fus3^{PP}}$ dephosphorylation,
- $S_{i\to n}$ is the area of contact surface between subcompartments i and n,
- V_i is the volume of subcompartment i,
- $i \in A$ / $i \in B$ if i belongs to cytoplasm / shmoo tip compartment,
- N_i is a set of neighbor subcompartments for subcompartment i,
- $[\psi] = \begin{cases} 1 & \text{if } \psi \text{ is True} \\ 0 & \text{otherwise} \end{cases}$, (e.g. $[n \in A \cup B]$ evaluates to 1 when n is element of A or B) [Ive62, Knu92].

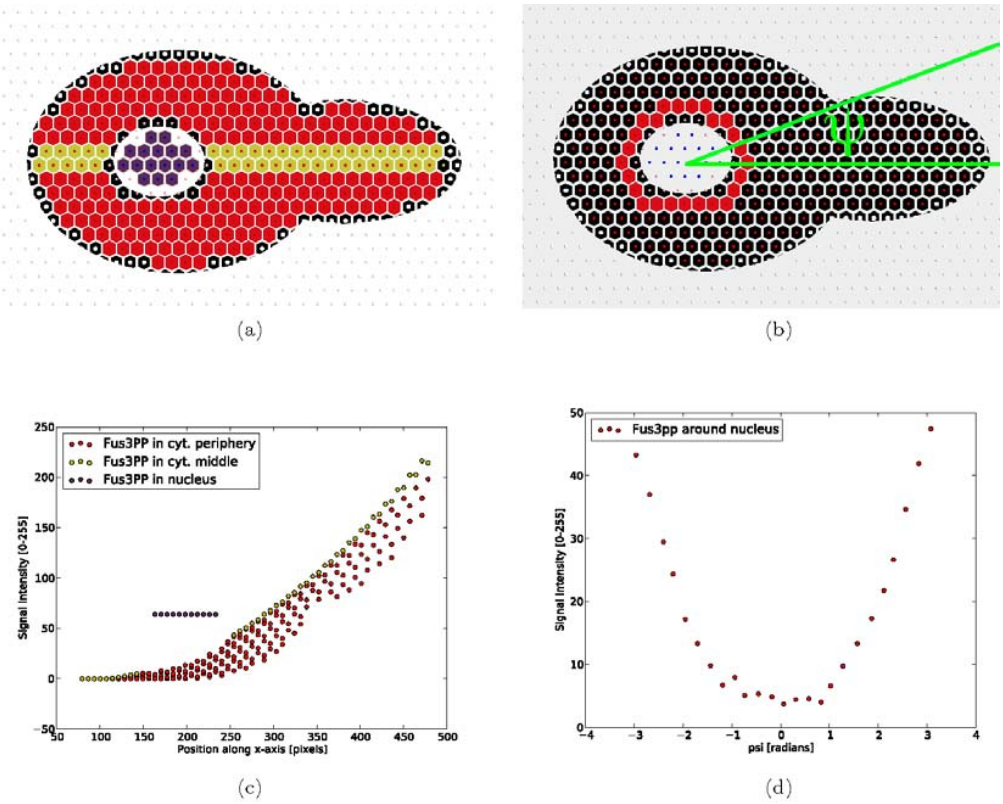

Figure 4.6: $Fus3^{PP}$ profiles along the x-axis and around the nucleus. (a) sub-compartment locations used to distinguish the curves in (c); (b) sub-compartment locations and ψ definition used in (d); (c) $Fus3^{PP}$ profiles along the x-axis; (d) $Fus3^{PP}$ profiles around the nucleus

To complete the model it is necessary to define the rate of $Fus3^{PP}$ release in the shmoo tip ($\alpha_{FUS3^{PP}}$), the rate constant of $Fus3^{PP}$ dephosphorylation $\beta_{FUS3^{PP}}$, the diffusion constant $\gamma_{FUS3^{PP}}$ and the initial parameters that are either derived from literature or - if not available - arbitrarily chosen The initial parameters can also be derived from the digitization step of the image data. As an example, the steady state concentrations for two different simulations are presented in Figure 4.7.
For further illustration of the simulation properties in Figure 4.8 the results of two different initial parameter sets are shown. In this case the protein release rate in the shmoo tip, the rate constant of protein dephosphorylation and the diffusion constant were altered. The shown contrast can be used to discriminate between the different parameter sets and enables to chose the most probable set that reflects the biological observation.

4.5 Discussion

The spatio-temporal simulation environment (STSE) represents a platform that facilitates conduction of spatial simulations of labeled biomolecules based on microscopy images. The software

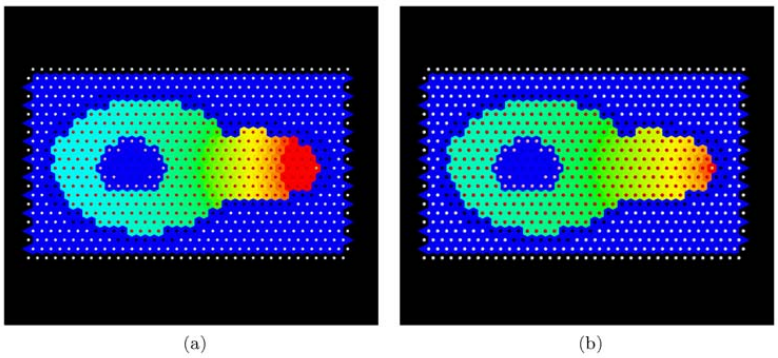

Figure 4.7: Steady state distributions of $Fus3^{\mathrm{PP}}$ for different parameter sets (α_{Fus3},β_{Fus3},γ_{Fus3}): (a) (0.1,0.1,100), (b) (0.1,0.1,50). In the given example it is shown that the gradients obtain different slopes. Such different protein concentration slopes arise from differences in the diffusion constant γ_{Fus3}. To visualize such various $Fus3^{\mathrm{PP}}$ concentrations, a color map is used where the blue color depicts low values and the red color depicts high values.

is a new development and enables an uninterrupted workflow including digitization, representation, analysis, and mathematical modeling. The main benefit of STSE is that it integrates different steps of otherwise time consuming individual computing and visualization steps, allowing the user to tailor the platform to specific needs according to the actual research question. Due to its open modular architecture and integration of the Python language the software also enables full automatization (it applies also to GUI) by utilizing scripts. Such tailoring that however demands individual specific modeling may be seen as clear advantage in comparison to other stand alone applications.
The application of STSE was demonstrated on the example of the yeast pheromone MAP kinase cascade by focusing on the distribution of the double-phosphorylated Fus3 protein. It was demonstrated how to quantify the ratio of the average cytoplasm/nucleus concentration of the $Fus3^{PP}$ protein based on the fluorescence signal intensity that was extracted from the microscopy images. In addition, it was shown how to create gradient curves for $Fus3^{PP}$ along the x-axis of the cell and around the nucleus, and how to simulate the process of $Fus3^{PP}$ diffusion in the cytoplasm The STSE platform provides results on time resolved protein distribution that may guide further hypotheses about possible underlying biological mechanisms.
The result of the simulations confirmed that a set of hypotheses used in the model reproduced the experimental observations. It was also demonstrated how to use the STSE to discriminate between model parameter sets. In view of the Translucent project at least two applications of the simulation can be suggested. If, for instance single transporter or the channel gene(s) could be fused to an individual fluorophore each spatial and temporal distribution could be observed upon specific environmental changes like extremely low or high external potassium or sodium concentrations. In a further design genes that are involved in detoxification or sequestration processes (as discussed in the previous chapter 3 on chapter genomic analysis upon heavy metal stress) like gluthation or the superoxide-dismutase (SOD) could be labeled with a fluorophore. Their expression and subsequent potential protein accumulation could then bes observed in a spatial and temporal manner. Derived from the quantification of protein amounts that for instance may accumulate after a given time in the vacuole further simulations could indicate the

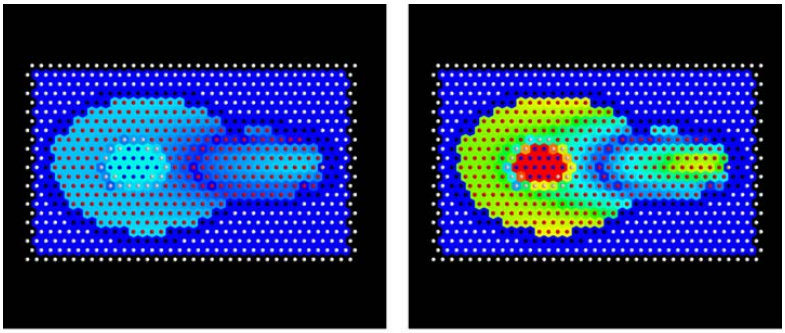

Figure 4.8: Difference of $Fus3^{\mathrm{PP}}$ concentration between $\bar{F}_{(0.01,0.001,50)}$ and $\bar{F}$ (which approximates the error). (a) shows an $E = \left|\bar{F}_{(0.01,0.001,50)} - \bar{F}\right|$ (the overall error did not exceed 20% percent) (b) shows the E/max(E) (when 100% of error was observed in the center; it is important to note, that the model did not allow the $Fus3^{\mathrm{PP}}$ to enter the nucleus compartment). To visualize E, a color map is used where blue depicts low values and red high ones.

- stress dependent - detoxification process. Such simulations could support conclusions derived from the gene expression profile. The fuorescent labeling could be extended for each and any gene thought to be involved in general or specific sensing, transportation, sequestration and detoxification and provide in the long run a more detailed picture of these processes, either cation homeostasis or cellular defense upon heavy metal stress. In any case, the possibility to evaluate in a consistent workflow time resolved protein accumulation and distribution data appear to be a clear advantage for the project.

Further versions of the STSE should provide integration of selected 3rd party simulators, providing other simulation paradigms (e.g. stochastic, agent-based). It would be also crucial to support SBML files, a broadly accepted specification of model format. For the latter, a prior establishment of a standard for spatial modeling would be required.

5 A thermodynamic model of cation homeostasis

5.1 Abstract

This part presents a basic model for the homeostasis of potassium, sodium and protons in the yeast *S. cerevisiae*. The modeling approach is based on the theory of nonequilibrium thermodynamics by assuming that the system is in the vicinity of global equilibrium. A generalized thermodynamical description is developed for the complex interplay of specific cation plasma-membrane transporters, the membrane potential and the consumption of energy for maintaining and restoring specific intracellular cation concentrations.
To account for irreversible processes the system is divided into small subsystems by assuming that each subsystem is in local equilibrium, i.e. can be treated as an individual thermodynamic system characterized by the small number of equilibrium variables. By this assumption the entropy created internally (defined as being the major driving force for physical and chemical changes) by irreversible processes can be calculated. The thermodynamic coupling of the individual fluxes enables that a flow occurs without or against its primary thermodynamic driving force, which may be a gradient of the electrochemical potential or reaction affinity. Due to missing experimental data, a reduced version of the model, excluding sodium fluxes from the consideration was confronted with experimental data to show quantitative simulation results. This model is able to reproduce the experimentally observed potassium and proton fluxes as well as ATP consumption and changes in the internal pH due to an external stimulus with KCl. The estimated phenomenological constants combining kinetic parameters and transport coefficients are in good agreement with the biological understanding of the transporters and provide an informative basis on the control exerted by the coupled fluxes.
Experimental data were prepared and provided by Prof. Sergey Shabala (University of Tasmania). Parameter estimation was performed by Martina Fröhlich using Copasi.

5.2 Introduction

The detailed description of facilitated diffusion and transport mechanisms by ion channels, carriers and pumps through an otherwise impermeable membrane is an important issue in biological studies on the cellular level. Since decades various theories and mathematical descriptions of active and passive transport performed by transmembrane-proteins have been developed. These approaches are as different as complex and have already been extensively published [Cro81, KS98, Din88, Ste90b, Ste86] to mention just a few of them.
Classical studies of nerves and ion fluxes have mainly focused on the measurement and modeling of ion fluxes caused by single transport systems. However, when modeling a living organism, the separated exploration of the individual transport-mechanisms will not lead to an understanding of the biological system. Many other features change simultaneously and should individually be measured and integrated in a global model to obtain a complete picture of the underlying physical processes. This includes - among other parameters - transient pH, enzyme activities, cy-

tosolic buffer capacities, chemical reactions and changes in membrane potential or concentrations of other important ions. This irreducible and concomitant astounding complexity stems from various interactions between the different parts, such cannot be predicted even with complete knowledge of each of the parts within the cell [SH10] but results in the emergent properties and behavior that characterize living systems [WJSK98].
Therefore, in the last decade there has been a shift to a more holistic and systems-level-perspective which led to the emergence of the field of systems biology [KLW+09, Alo06, AW05]. Network models, using kinetic or statistical equations contribute substantially to the understanding and visualization of biological processes and may help to formulate and validate hypotheses of the underlying mechanisms in these complex systems [KO04, Kli07]. However, the most intricate factor in the process of modeling a lifelike transporter-network is the requirement to base on a detailed understanding of structure, function, cooperation and kinetic parameters of all constituent parts of the system.
In order to build up a network model of any considerable size, the following information about the network under study are requested [SH10]:

- All involved system components (proteins, genes, mRNA, metabolites) and their related processes (e.g. transcription, translation, inhibition, and enzymatic transformations);
- The relevant parameters of these components (e.g. transcription rates, binding affinities, dissociation rates, kinetic constants, buffering capacity) that govern their individual behavior;
- The degree of connectivity and the type of interactions between these components (biochemical transformation, activation inhibition, and cooperative effects).

This is considered unfeasible as long as there is still fundamental research underway as it is the case for this cation homeostasis project where the development of an adequate kinetic description of the phenomena requires more detailed information than is currently available or readily obtainable.
It may therefore be advantageous to have a method by which phenomena could be correlated in an alternative, more formal manner independent of specific kinetic or statistical models. This method may offer additional insight into the factors influencing the phenomena in question. A promising step in this direction might be the application of the formalism of "non-equilibrium thermodynamics" to the investigation of the living organism [KC65, Kat70, Lak84].
The real power of classical thermodynamics stems from the fact that only a small number of state variables are required to determine the properties of a uniform equilibrium system. One therefore finds thermodynamics as a basis for physics on all length scales from atomic dimensions up to cosmological scales. Naturally, thermodynamics is also applicable on the level of biological membranes.
However, such equilibrium systems bear little reflection to a living cell which is - at any level - a thermodynamically open nonequilibrium system (exchanges mass and energy with the surrounding environment), and involves heterogeneous and fluctuating intensive variables as well as processes that are mainly irreversible [PNB74].
As such, most of these processes operate far from equilibrium [QB05]. Furthermore they seem to defy the second law of thermodynamics as they generate to its surroundings what Schrödinger termed "negentropy" which he defined as negative entropy or free energy that living systems feed on in order to avoid decay into the inert state of equilibrium [Sch62].
The development of the "thermodynamic theory of irreversible processes" provided the theoretical background to address this issue and study a diversity of biological processes using thermodynamics [PNB74, Lak84, KC65, DM82].

The cornerstone of this theory was laid in 1931 by Lars Onsager [Ons31a, Ons31b], who derived from statistical considerations the law of symmetry of the coefficients in phenomenological equations of flow. It has been experimentally verified for a large number of phenomena [Mil60, Mil66, Mil67, Mil69, MM74, Mil95] and may be regarded as a general statement on macroscopic systems, although of a more limited validity than the first and second law of thermodynamics [KC65].
A coordinated "theory of non-equilibrium thermodynamics" based on the fundamental work of Lars Onsager [Ons31a, Ons31b] has been developed in the early 1950s particularly by Casimir [Cas45], Prigogine [POH48, Pri67, PNB74], de Groot [DM62] and Katchalsky [KS68, KC65]. Non-equilibrium thermodynamics focus on the relationships between driving forces and fluxes, and on irreversible processes that transduce and dissipate energy. These phenomena are the hallmarks of biological systems.
One major advantage of thermodynamics is that it enables the study of the degree of coupling between different processes, as long as the associated forces and fluxes can be measured. Hereby, meaningful insights from these models without a full mechanistic understanding of the underlying mechanisms can be derived [REES80, WHA$^+$81, Rot79, RNKB07]. As a consequence, the theory became popular for modeling and analyzing biophysical problems with experimental uncertainties and/or sparse kinetic knowledge [Hil66, KC65, Kat67, Pri67, EC68, EC81] especially in the treatment of bio-membrane systems [KS68, PNB74, Lak69, Lak84].
Examples of biological systems that could be successfully described by using the theory of non-equilibrium thermodynamics include the coupling between sodium transport and oxygen consumption in frog and toad skin [DV74, CE77], toad bladder [LCE77], and hydrogen-ion transport in turtle urinary bladder [AAMS77, AA77, BAA76].

5.3 Foundations of Non-Equilibrium Thermodynamics

Classical thermodynamics refers to systems in thermodynamic equilibrium and is based on only two fundamental and intuitive laws of physics: the conservation of the internal energy and the maximum entropy principle. Beyond that it is free of any approximations and assumptions. A thermodynamic study of open non-equilibrium systems requires, however, more general concepts than are addressed by equilibrium thermodynamics. Thus basic assumptions of classical thermodynamics, the principles and assumptions of nonequilibrium thermodynamics and their application to the analysis of cation fluxes across the cell-membrane are briefly introduced. Comprehensive treatments and detailed discussions on thermodynamic approaches of modeling the flow of solute and solvents across epithelial tissues and biomembranes can be found elsewhere, e.g. [Sch80, Sch76, Hei07, KC65, Mar87, Lak69, Lak84, Dem08, Ons31a].

5.3.1 Principles and assumptions

The description of a thermodynamic system is based on the specification of a set of *extensive* and *intensive* parameters characterizing its state or condition.
The former include parameters such as mass, charge, heat, volume, etc. being all dependent on the systems size and on the amounts of the various substances present. Intensive parameters, such as pressure and concentrations have definite values at each point in the system and do not depend on its size.

The first law of thermodynamics (the conservation of energy) assumes the form

$$\Delta U = \Delta Q - \Delta W \tag{5.1}$$

stating that the change in the internal energy U of a system is equal to the heat flow (ΔQ) into (or out of) the system and to the work (ΔW) performed on (or by) the system.
The concept of the entropy, S, known as the major driving force for physical and chemical reactions gives a quantitative way to describe the tendency for energy to flow in a particular direction. The Clausius inequality for open systems (second law of thermodynamics)

$$\Delta S \geq \frac{\Delta Q}{T} \tag{5.2}$$

defines the change in entropy ΔS as the flow of energy (or rather heat) divided by the absolute temperature, T, in degrees Kelvin (K).
The physical meaning of this inequality is that in an isothermal open process the entropy of the system increases more than can be accounted for by adsorption of entropy from the surrounding environment. Therefore, a process must take place within the system that creates entropy in the same manner as in a spontaneous adiabatic process.
Prigogine [Pri67] formulated an extended version of the second law of thermodynamics which applies both to isolated and open systems:

$$\frac{dS}{dt} = \frac{d_e S}{dt} + \frac{d_i S}{dt} \qquad \text{with} \qquad \frac{d_i S}{dt} \geq 0 \tag{5.3}$$

stating that the total change in entropy is the sum of the flow of entropy due to exchange with the surroundings, $d_e S$, and the entropy production due to irreversible processes inside the system ("entropy created internally"), $d_i S$.
The internal entropy production is positive-definite; it is greater than zero for all irreversible processes and equal to zero for reversible changes. These equations apply not only for the system as a whole but for all parts of the system. Any element of the system may exchange entropy with its surroundings and $d_e S$ may be either positive or negative, but any entropy change resulting from irreversible processes taking place within the element must be positive-definite.
At equilibrium all macroscopic processes stop and no entropy is created.
The local production of entropy, σ, is related to the rate of increase in entropy within a system as a whole by a volume integral,

$$\int_V \sigma dV = \frac{d_i S}{dt} \geq 0. \tag{5.4}$$

While 5.4 is an over-all indication of the behavior of the system, σ characterizes the local events and their contribution to the total formation of entropy.

5.3.2 Gibbs fundamental equation for local quantities

The calculation of σ is based on a suitable adaption of the second law of thermodynamics to the description of local processes. For this purpose, a small volume, v, in which the entropy, internal energy, and number of moles of a species i are given by s, u, and n_i, respectively, is considered within the total volume V of a system. The volume v is sufficiently small that within it, the intensive properties temperature (T), pressure (p) and the electrochemical potential η_i are virtually equal at all points, but large enough to make the influence of fluctuations negligible. [KC65].

Under this assumption Gibbs equation may be used for the description of changes taking place in v, such as

$$Tds = du + pdv - \sum_{i=i}^{n} \eta_i dn_i. \tag{5.5}$$

The application of equation 5.5 for a system that is not in equilibrium by assuming the existence of a "local" equilibrium is one of the basic assumptions of non-equilibrium thermodynamics. Even if irreversible processes are taking place within the system as a whole, it is assumed that it is possible to isolate a small part of the system that may be considered as being in equilibrium.
By introducing local concentrations of entropy, energy, and matter which are defined by the expressions

$$s_v = \frac{s}{v}, \qquad u_v = \frac{u}{v}, \qquad c_i = \frac{n_i}{v}, \tag{5.6}$$

and integrating equation 5.5 to give

$$Td(vs_v) = d(vu_v) + pdv - \sum_{i=1}^{n} \eta_i d(vc_i) \tag{5.7}$$

Katchalsky and Curran [KC65] derived an additional equation relating the changes in the respective local concentrations by taking the volume as a variable:

$$Tds_v = du_v - \sum_{i=1}^{n} \eta_i dc_i \tag{5.8}$$

$$= dq_v - \sum_{i=1}^{n} \eta_i dc_i. \tag{5.9}$$

While equation 5.5 correlates changes in extensive properties of the volume, v, equation 5.9 relates the local specific properties at any point within the system.
The evaluation of the changes in the local concentrations with time is undertaken by dividing equation 5.9 by dt and requiring that the space coordinates remain constant. Hereby an expression which may be utilized for determination of the local rate of entropy production in a continuous system is given.

$$T\frac{\partial s_v}{\partial t} = \frac{\partial q_v}{\partial t} - \sum_{i=1}^{n} \eta_i \frac{\partial c_i}{\partial t}. \tag{5.10}$$

These differentials are related to divergences of the corresponding flows by the law of conservation and continuity.

$$\frac{\partial s_v}{\partial t} = -\operatorname{div} \mathbf{J}_s + \sigma, \tag{5.11}$$

$$\frac{\partial c_i}{\partial t} = -\operatorname{div} \mathbf{J}_i + v_i J_{ch} \tag{5.12}$$

$$\frac{\partial q_v}{\partial t} = -\operatorname{div} \mathbf{J}_q \tag{5.13}$$

where $\mathbf{J}_s$ is the flow of entropy, $\mathbf{J}_i$ the diffusional flow vector, J_{ch} the rate of chemical change per unit flow and J_q the total flow of heat across the boundaries of the volume element v.

By introducing these expressions into 5.10 such as

$$-\operatorname{div}\mathbf{J}_s + \sigma = -\frac{1}{T}\operatorname{div}\mathbf{J}_q - \sum_{i=1}^{n}\frac{\eta_i}{T}(-\operatorname{div}\mathbf{J}_i + v_i J_{ch}), \tag{5.14}$$

modifying the expression by making use of the relations obtained from differential vector analysis, that

$$\operatorname{div} a\mathbf{b} = a\operatorname{div}\mathbf{b} + \mathbf{b}\cdot\operatorname{grad} a \tag{5.15}$$

gives after rearranging the isolation of the local entropy production σ

$$\sigma = \mathbf{J}_q \cdot \operatorname{grad}\frac{1}{T} + \sum_{i=1}^{n}\mathbf{J}_i \cdot \operatorname{grad}(-\frac{\eta_i}{T}) + \sum_{j=1}^{n_r} J_{ch}\frac{A_j}{T} \tag{5.16}$$

for a multicomponent fluid system under mechanical equilibrium with n species and n_r numbers of chemical reactions. Here $A = -\sum_i v_i\mu_i$ (with v_i is the reaction velocity and μ_i the chemical potential) is the affinity of a chemical reaction considered here.
The rate of entropy production σ due to irreversible processes is always positive, and calculated in terms of conjugated forces X and fluxes J as

$$\sigma = \frac{d_i^2 S}{dV dt} = \sum_{i=1}^{n} J_i X_i \geq 0. \tag{5.17}$$

in which X_i is the force conjugated with the flow J_i. From equation 5.16 the dissipative function Ψ can be obtained.

$$\Psi = T\sigma = \left(-\frac{1}{T}\mathbf{J}_q \cdot \operatorname{grad} T - \sum_{i=1}^{n}\mathbf{J}_i \cdot \operatorname{grad}\eta_i + \sum_{j=1}^{n_r} J_{ch}A_j\right) \geq 0 \tag{5.18}$$

This function identifies a set of conjugated fluxes and forces of the processes under consideration. When the system is in the vicinity of global equilibrium these flows are related to the forces in a linear form with the phenomenological coefficients through phenomenological equations [Dem08, KC65, PVR82, YR89, RH86]. These flows and forces will be considered in more detail in the following section.

5.3.3 Driving forces and the membrane potential

When two different systems are separated by a permeable barrier, flows or displacements of extensive parameters from one system to the other can be observed. The principles of causality demands that for every observable effect there is a cause. Applying this to the flow processes in open systems one finds that a flow (J_i) is always caused by a *conjugated* driving force X_i. If there are no interactions among different flows, the driving force responsible for a given flow is the gradient of its conjugated intensive parameter across the barrier. Since the flow of a charged solute involves a displacement of matter as well as charge, the conjugate driving force for a cation flux is the gradient of the electrochemical potential $\Delta\eta$ (an expression of both the difference in chemical potential and electrical potential).
For systems close to equilibrium (meaning, that the conjugate driving force is very small) it is empirically known that the flow of a species, i is linearly related to its conjugated driving force

so that

$$\begin{aligned} J_i = L_i X_i &= c_i u_i X_i \\ &= c_i u_i \,(\text{- grad}\, \eta_i). \end{aligned} \tag{5.19}$$

The coefficient L_i can be considered as being a product of concentration, c_i and the mobility, u_i. A large number of such phenomenological laws exist that describe irreversible processes in the form of proportionality. Familiar examples are Ohm‘s law for the flow of currents, Fick‘s law relating the flow of a substance and its concentration gradient, Poiseuilles‘s law of volume flow and the mass action law between reaction rate and chemical concentrations or affinities.
If a system is characterized by more than one flow, it is empirically established that each flow may be influenced by other flows and, hence by forces other than it‘s conjugate force. In general, any force can produce any flux and both are complicated non-linear functions of each other.
However, by expanding the non-linear dependence of a flux J_i and the force X_i in Taylor series around the equilibrium such as

$$J_i = J_{i,eq}\,(X_i = 0) + \sum_{j=1}^{n} \left(\frac{\partial J_i}{\partial X_j} \right)_{eq} X_j + \frac{1}{2!} \sum_{j=1}^{n} \left(\frac{\partial^2 J_i}{\partial\, X_j^2} \right)_{eq} X_j^2 + ... \tag{5.20}$$

and neglecting the higher order terms, equation 5.20 becomes a linear relation, resulting in the general type of linear-phenomenological equations for irreversible phenomena [DS02, DM62, Dem07]

$$J_i = \sum_{j=1}^{n} L_{ij} X_j \tag{5.21}$$

Here the L_{ii} are referred to as the "straight coefficients" in as much as they relate the flow of species i, J_i, to it‘s conjugated driving force X_i, by the analogy with either Ohm‘s or Fick‘s laws. The "cross coefficients" L_{ij}, where $j \neq i$ reflect to which extend the flux of species i is affected by the non-conjugated force, X_j, in the system. These so-called "phenomenological -", "Onsager -", or "generalized transport -" coefficients must be determined by experiment [DS02, DS01, Row89]. They are functions of the intensive parameters of the system but are independent of the flows and forces.

In case of electrolyte fluxes, the driving force, X_i, is induced by the negative gradient of the electrochemical potential, η_i, given by

$$\eta_i = \mu_i^0(p,T) + \mathcal{R}T\ln(c_i) + z_i\mathfrak{F}\varphi. \tag{5.22}$$

The electrochemical potential (introduced in 1929 by Guggenheim [Gug29]) is the Gibb‘s free energy per mole of compound i at constant temperature, pressure and composition. μ_i^0 is the standard chemical potential, $\mathcal{R}$ is the universal gas constant, T the absolute temperature, z_i is the valence of ion i, $\mathfrak{F}$ is Faraday‘s constant and φ is the electrical potential at a point x.
For a concentration gradient only in the x-direction and an isobaric as well as isothermic system, instead of the differential operator "grad", the differential quotient can be applied such as

$$\frac{d\eta_i}{dx} = \frac{\mathcal{R}T}{c_i}\frac{dc_i}{dx} + z_i\mathfrak{F}\frac{d\varphi}{dx}. \tag{5.23}$$

Inserting equation 5.23 in 5.19 gives the Nernst-Planck equation

$$J_i = -D_i \left(\frac{dc_i}{dx} + \frac{z_i c_i \mathfrak{F}}{\mathcal{R}T} \frac{d\varphi}{dx} \right) \tag{5.24}$$

where D_i is the diffusion coefficient of i and is given by the relation derived by Einstein, $D_i = u_i RT$. The differential quotients of the concentration $c_i(x)$, and the electrical potential $\varphi(x)$ in equation 5.24 can be integrated only if the corresponding function is known. Several assumptions have been made leading to solutions [Lak69, Hel62, EHHM07, Sch71] but by far the simplest and most useful is the assumption of linear gradients within the membrane according to Fick's "Law of diffusion" for the concentrations and Goldman's "Constant field equation" [Gol43] for the electrical field within the membrane.
Thus, $\frac{\Delta\varphi}{\Delta x}$ and $\frac{\Delta c_i}{\Delta x}$ may be substituted for $\frac{d\varphi}{dx}$ and for $\frac{dc_i}{dx}$ respectively, where Δc is the concentration difference across the membrane and Δx is the thickness of the membrane.
By using these assumptions, Goldman integrated the Nernst-Planck equation

$$J_i = -\frac{P_i z_i \mathfrak{F} \Delta\varphi}{\mathcal{R}T} \cdot \left[\frac{c_i^{in} - c_i^{out} \exp\left(-\frac{z_i \mathfrak{F} \Delta\varphi}{\mathcal{R}T}\right)}{1 - \exp\left(\frac{z_i \mathfrak{F} \Delta\varphi}{\mathcal{R}T}\right.} \right] \qquad \text{with} \quad P_i = \frac{D\beta_i}{\Delta x} \tag{5.25}$$

where c_i^{in} and c_i^{out} are the concentrations in inner and outer aqueous compartments, $\Delta\varphi = \varphi^{in} - \varphi^{out}$, P_i is the permeability coefficient and β_i the partition coefficient (defined as the concentration just within the membrane at the interface divide by that in the outer solution).
Including the postulation of electro-neutrality of the sum of all ion fluxes (cations and anions) and solving the expression for $\Delta\varphi$ gives the Goldman-Hodgkin-Katz equation [Gol43]

$$\Delta\varphi = \frac{\mathcal{R}T}{\mathfrak{F}} ln \frac{\sum_{Anions} P_i c_i^{in} + \sum_{Cations} P_j c_j^{out}}{\sum_{Anions} P_i c_i^{out} + \sum_{Cations} P_j c_j^{in}} \tag{5.26}$$

which will be used in the following to calculate the membrane potential.

5.4 Application to Cation Homeostasis

5.4.1 The model relevant key elements

As illustrated in the chapter "Introduction" the project TRANSLUCENT aims to obtain a complete picture of the mechanisms that ensure correct cation uptake and homeostasis, in particular the regulation of sodium, potassium and intracellular pH in the yeast *S. cerevisiae*. To ensure viability even under adverse external environmental conditions yeast cells have evolved several response- and transport systems for these major cations [ARS10, RN00, SRN01, GS00]. Figure 5.1 shows the system under consideration with the already investigated channels, carriers and pumps.
By applying the theory of non-equilibrium thermodynamics to the study for transport processes across *S. cerevisiaes* plasma membrane the power of this approach as well as it's limitations will be demonstrated and discussed. The fluxes of the cations of interest, H^+, Na^+, K^+ can be

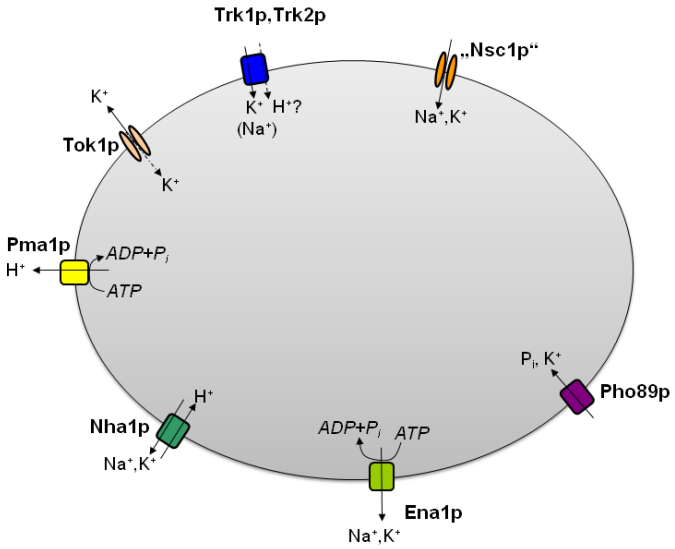

Figure 5.1: Sketch of the model relevant key elements. A detailed description of the individual components is given in the chapter "Introduction".

expressed by the following equation system:

$$\begin{aligned} J_{H^+} &= \frac{d}{dt}\left[H^+\right]_i = J_{Pma1} + J_{Nha1} + J_{Trk12} \\ J_{K^+} &= \frac{d}{dt}\left[K^+\right]_i = J_{Trk12} + J_{Nsc1} + J_{Nha1} + J_{Tok1} + J_{Ena1} \\ J_{Na^+} &= \frac{d}{dt}\left[Na^+\right]_i = J_{Nsc1} + J_{Trk12} + J_{Nha1} + J_{Ena1} \end{aligned} \tag{5.27}$$

According to equation 5.21 any flux can be affected by any force, which leads to an equation system of coupled thermodynamic flows:

$$\begin{aligned} J_{H^+} &= L_{H^+,H^+}\, X_{H^+} + L_{H^+,K^+}\, X_{K^+} + L_{H^+,Na^+}\, X_{Na^+} \\ J_{K^+} &= L_{K^+,H^+}\, X_{H^+} + L_{K^+,K^+}\, X_{K^+} + L_{K^+,Na^+}\, X_{Na^+} \\ J_{Na^+} &= L_{Na^+,H^+}\, X_{H^+} + L_{Na^+,K^+}\, X_{K^+} + L_{Na^+,Na^+}\, X_{Na^+} \end{aligned} \tag{5.28}$$

In the following deduction fluxes are defined to be positive when the intracellular concentration of a species increases (flow goes from outside to inside).
As from now (for visual clarity), the indices $1, 2, 3, 4$ will denote the species H^+, K^+, Na^+ and ATP, respectively.
According to equations 5.19 and 5.23 under the assumption of linear gradients within the membrane, the forces for the cation fluxes can be approximated by the difference of the electrochemical

potential across the membrane

$$\begin{aligned} X_i = -\text{grad}(\eta_i) &\cong \frac{\eta_i^{out}}{\eta_i^{in}} \\ &\cong \frac{\mathcal{R}T}{d_m} \ln \frac{c_i^{out}}{c_i^{in}} + z_i \mathfrak{F} \Delta\varphi \end{aligned}$$

where d_m denotes the thickness of the membrane and the indices ^{in} and ^{out} designate the internal concentrations or concentrations outside the systems boundaries, respectively. The switch in the sign results from the fact that the difference in η_i can be chosen to be positive. The net fluxes of the cations over the membrane can now be expressed in the following way:

$$\begin{aligned} J_{H^+} &= L_{1,1}\left(\frac{\mathcal{R}T}{d_m} \ln \frac{c_1^{out}}{c_1^{in}} + z_1 \mathfrak{F} \Delta\varphi\right) + L_{1,2}\left(\frac{\mathcal{R}T}{d_m} \ln \frac{c_2^{out}}{c_2^{in}} + z_2 \mathfrak{F} \Delta\varphi\right) \\ &\quad + L_{1,3}\left(\frac{\mathcal{R}T}{d_m} \ln \frac{c_3^{out}}{c_3^{in}} + z_3 \mathfrak{F} \Delta\varphi\right) \\ J_{K^+} &= L_{2,1}\left(\frac{\mathcal{R}T}{d_m} \ln \frac{c_1^{out}}{c_1^{in}} + z_1 \mathfrak{F} \Delta\varphi\right) + L_{2,2}\left(\frac{\mathcal{R}T}{d_m} \ln \frac{c_2^{out}}{c_2^{in}} + z_2 \mathfrak{F} \Delta\varphi\right) \\ &\quad + L_{2,3}\left(\frac{\mathcal{R}T}{d_m} \ln \frac{c_3^{out}}{c_3^{in}} + z_3 \mathfrak{F} \Delta\varphi\right) \\ J_{Na^+} &= L_{3,1}\left(\frac{\mathcal{R}T}{d_m} \ln \frac{c_1^{out}}{c_1^{in}} + z_1 \mathfrak{F} \Delta\varphi\right) + L_{3,2}\left(\frac{\mathcal{R}T}{d_m} \ln \frac{c_2^{out}}{c_2^{in}} + z_2 \mathfrak{F} \Delta\varphi\right) \\ &\quad + L_{3,3}\left(\frac{\mathcal{R}T}{d_m} \ln \frac{c_3^{out}}{c_3^{in}} + z_3 \mathfrak{F} \Delta\varphi\right) \end{aligned} \tag{5.29}$$

Another important thermodynamic coupling takes place between the hydrolysis of ATP and the molecular transport of substrates in active transport. The consumption of ATP is given by the following expression:

$$J_{ATP} = \frac{d}{dt} \left[ATP\right]_i . \tag{5.30}$$

The flux of ATP plays a special role in the thermodynamics analysis of the system. According to equation 5.16 the driving force for a chemical reaction is the affinity,

$$\begin{aligned} A &= -\sum_i v_i \mu_i \\ &= \mu_{ATP} - \mu_{ADP} \end{aligned} \tag{5.31}$$

where v_i is the reaction velocity, and μ_i is the chemical potential. Under conditions of equilibrium, A tends to zero so that $\bar{\mu}_{ATP}$=$\bar{\mu}_{ADP}$ in which the bar denotes the equilibrium values of the chemical potentials. Further, the chemical flow should be proportional to the force:

$$J_{ATP} = LA = L(\mu_{ATP} - \mu_{ADP}). \tag{5.32}$$

By introducing the equilibrium concentrations $\bar{c}_{ATP}$ and $\bar{c}_{ADP}$ the deviation α_i, of the concentrations from their equilibrium values can be defined as

$$\begin{aligned} \alpha_{ATP} &= c_{ATP} - \bar{c}_{ATP} \\ \alpha_{ADP} &= c_{ADP} - \bar{c}_{ADP} \end{aligned} \tag{5.33}$$

With the use of expressions 5.33 the chemical potential

$$\mu_i = \mu_i^0 + RT \ln c_i$$

can be inserted into equation 5.31 resulting in

$$\begin{aligned} A = \mu_{ATP}^0 + \mathcal{R}T \ln \bar{c}_{ATP} + \mathcal{R}T \ln \left(1 + \frac{\alpha_{ATP}}{\bar{c}_{ATP}}\right) \\ - \mu_{ADP}^0 + \mathcal{R}T \ln \bar{c}_{ADP} - \mathcal{R}T \ln \left(1 + \frac{\alpha_{ADP}}{\bar{c}_{ADP}}\right) \end{aligned} \tag{5.34}$$

or, in case of "close to equilibrium"-conditions, where $\bar{\mu}_{ATP} \approx \bar{\mu}_{ADP}$,

$$A = \mathcal{R}T \left[ln \left(1 + \frac{\alpha_{ATP}}{\bar{c}_{ATP}}\right) - \ln \left(1 + \frac{\alpha_{ADP}}{\bar{c}_{ADP}}\right)\right]. \tag{5.35}$$

The logarithms may be expanded in series with only the first term being retained so that 5.35 becomes

$$\begin{aligned} A &= \mathcal{R}T \left(\frac{\alpha_{ATP}}{\bar{c}_{ATP}} - \frac{\alpha_{ADP}}{\bar{c}_{ADP}} \right) \\ &= \mathcal{R}T \frac{\alpha_{ATP}}{\bar{c}_{ATP}} (1 + K), \qquad \text{with} \qquad K = \frac{\bar{c}_{ATP}}{\bar{c}_{ADP}} \end{aligned} \tag{5.36}$$

in which K is the equilibrium constant. Further the assumption $\alpha_{ATP} + \alpha_{ADP} = 0$ is used implying that the reaction proceeds without exchange of matter with the surroundings.
Inserting this result into equation 5.32 yields

$$J_{ATP} = L_{44} \cdot \left(\frac{\mathcal{R}T}{\bar{c}_{ATP}} \alpha_{ATP} (1 + K) \right). \tag{5.37}$$

Rearranging equation system 5.29 and integrating the driving force of ATP (index 4) leads to the final model equation system that will be confronted with experimental data in the following section.

$$
\begin{aligned}
J_{H^+} &= \frac{\mathcal{R}T}{d_m}\left[L_{11}\,\ln\frac{c_1^{out}}{c_1^{in}} + L_{12}\,\ln\frac{c_2^{out}}{c_2^{in}} + L_{13}\,\ln\frac{c_3^{out}}{c_3^{in}}\right] + \\
&\quad + z\mathfrak{F}\Delta\varphi\left[L_{11}+L_{12}+L_{13}\right] + L_{14}\left(-\frac{\mathcal{R}T}{\bar{c}_{ATP}}\alpha_{ATP}\left(1+K\right)\right) \\
J_{K^+} &= \frac{\mathcal{R}T}{d_m}\left[L_{21}\,\ln\frac{c_1^{out}}{c_1^{in}} + L_{22}\,\ln\frac{c_2^{out}}{c_2^{in}} + L_{23}\,\ln\frac{c_3^{out}}{c_3^{in}}\right] + \\
&\quad + z\mathfrak{F}\Delta\varphi\left[L_{21}+L_{22}+L_{23}\right] + L_{24}\left(-\frac{\mathcal{R}T}{\bar{c}_{ATP}}\alpha_{ATP}\left(1+K\right)\right) \\
J_{Na^+} &= \frac{\mathcal{R}T}{d_m}\left[L_{31}\,\ln\frac{c_1^{out}}{c_1^{in}} + L_{32}\,\ln\frac{c_2^{out}}{c_2^{in}} + L_{33}\,\ln\frac{c_3^{out}}{c_3^{in}}\right] + \\
&\quad + z\mathfrak{F}\Delta\varphi\left[L_{31}+L_{32}+L_{33}\right] + L_{34}\left(-\frac{\mathcal{R}T}{\bar{c}_{ATP}}\alpha_{ATP}\left(1+K\right)\right) \\
J_{ATP} &= L_{44}\left(\frac{RT}{\bar{c}_{ATP}}\alpha_{ATP}\left(1+K\right)\right)
\end{aligned}
$$

The driving force of ATP affecting the ions has to be negative since fluxes are defined to be positive if the intracellular concentration increases. The developed flux of ATP, however is an expression for the ATP consumption. The higher the reaction affinity the larger is the *efflux* of the coupled cations. Since all cations considered here are monovalent, $z_1 - z_3$ can be omitted.

5.4.2 Phenomenological equations relating flows and forces

From the theory of fluctuations Lars Onsager discovered an underlying symmetry in the thermodynamic description of irreversible processes for which he was awarded in 1968 with the Nobel Prize in chemistry.
Onsager's observations can be summarized as follows:

- Each flow J_i - in isolation - is linearly proportional to its conjugated force X_i.
- Each force X_j will contribute to a flow $J_i\,(i \neq j)$ if the coupling coefficients (cross coefficients) L_{ij} differ from zero (this dependency is also linear).
- The reciprocal relation $L_{ij} = L_{ji}\,(i \neq j)$ states that the matrix of cross coefficients is symmetrical.

Onsager's proof of the reciprocal relation between coefficients is based on statistical and mechanical considerations that hold for processes close to equilibrium [Ons31a, Ons31b].
An impressive amount of experimental material has been critically analyzed and in general the relations have been found to hold to a close approximation. For detailed reviews refer to [Mil60, MM74, Mil69].
However, only for systems "not too far" distant from a state of equilibrium it has been demonstrated *theoretically* that 5.21 will be a valid description of the system and that the phenomenological coefficients L_{ij} obey Onsager's reciprocal relations [Ons31a, PNB74, DM62].
Unfortunately "not too far" is a very vague term, on the other hand it includes very steep gradients of concentration, temperature, and electric potential [Mil95] and the validity of the linear phenomenological relations was demonstrated for a number of coupled flow processes despite significant displacement from equilibrium [Mil60, EC81].

Additional information on the character of the driving forces and the local entropy production can be detected by substituting equation 5.21 in equation 5.17:

$$\frac{d_i S}{dt} = \sum_i \sum_j L_{ij} X_i X_j \geq 0. \tag{5.38}$$

In the case of equilibrium forces and fluxes in equation 5.21 vanish and under this condition equality exists for the latter part of equation 5.38 whereas for nonequilibrium situations the coefficients have to be chosen such that the inequality-condition is fulfilled.
For $j = i$, equation 5.38 yields

$$\frac{d_i S}{dt} = \sum_i L_{ii} X_i^2. \tag{5.39}$$

Since X_i^2 is always positive, the straight coefficients L_{ii} are therefore always positive, too. However, equation 5.38 shows that the coupling coefficients L_{ij} may be positive or negative depending on the direction of the forces X_i and X_j.
With the help of these statements transport processes in biological organisms are now to be conceived thermodynamically:
In non-living systems all transport processes are taken entirely passive (fluxes always have to go in the direction of the conjugated forces), whereas in living systems some transport processes are considered as being "active" in the sense that fluxes are driven against the direction of the conjugated forces (concentration gradient). Separately considered, this clearly violates the second law of thermodynamics by causing a negative entropy production which is conceptually unsound and thermodynamically impossible.
In non-equilibrium thermodynamics theory, however, although inequality 5.38 will always hold as demanded by thermodynamics, the expression does not require all contributions to the entropy production as positive.
A dissipation due to either diffusion or chemical reaction can be negative, as long as the process couples with another one with a comparatively larger positive modulus in an anisotropic medium. The thermodynamic condition of positive entropy production will still be satisfied in this case.
The requirement for the anisotropy of the media stems from the so-called *Curie-Prigogine principle*, which states that in isotropic systems no coupling can exist between phenomena of different tensorial order. As a consequence, the affinity of a chemical reaction which is a scalar force cannot drive transport flows of vectorial order without violating mathematical rules.
However, within anisotropic systems as it is precisely the case of biomembranes the chemical reactions drive vectorial processes. Since the movement of an ion within the pores of the membrane has a defined spatial orientation and is possible only in a predetermined direction its conductivity consequently becomes a vector [Mit79, MHL63, Mar87].

Qualitative implication of the approach

As stated before the phenomenological coefficients L_{ij} (i,j= 1,2,3,4), stating the considered ions H^+, K^+, Na^+ as well as ATP in the equations

$$J_i = \sum_i^4 L_{ij} X_j \tag{5.40}$$

are assumed to satisfy the Onsager reciprocal relations $L_{ij} = L_{ji}$, meaning that the matrix is symmetric. The description of transport processes in a system of n components, therefore, requires the measurement of only $\frac{n(n+1)}{2}$ coefficients not all n^2 coefficients.

This does not only lead to an appreciable reduction in the number of independent coefficients but permits the prediction of correlations between flow phenomena.

5.4.3 The coefficients under the biological point of view

Before actually starting with the estimation of the L_{ii} and all necessary L_{ij} from the experimental data it is actually advantageous to understand their biological meaning. According to Figure 5.1 and to the definition of the relevant involved parties of the cation-fluxes from equation system 5.27 the Ls can be interpreted as an influence of the following cellular components to the different fluxes:

- $\mathbf{L_{1,1}}$: Diffusion of protons through the plasma membrane including facilitated diffusion, e.g. by channels.
- $\mathbf{L_{2,2}}$: Diffusion of potassium through the plasma membrane. The passive flux can be facilitated by the **Trk1/2**-system and the "open-state-probability" in the case of the voltage-gated channels **Tok1p** and **Nsc1**. Perhaps also the channel Pho89 might contribute since there exist scattered information on its ability to let K^+ pass (see chapter "Introduction").
- $\mathbf{L_{3,3}}$: Diffusion of sodium through the plasma membrane. Contributors that facilitate the passive sodium fluxes are **Nsc1** and **Trk1,2** since sodium is able to enter the cell *via* these potassium-specific transporters if the conjugated force, X_3 is strong enough. Also Pho89 is assumed to be penetrable for Na^+.
- $\mathbf{L_{4,4}}$: The straight coefficient for the flux of ATP shall be understood somewhat different to those of the before mentioned cations. Changes in the total amount of free ATP will not lead to an in- or efflux of ATP but to a change in its reaction-affinity to drive energy consuming transport-processes.
- $\mathbf{L_{1,2} = L_{2,1}}$: The activity of the H^+/K^+-antiporter **Nha1p** is clearly the major contributor to the magnitude of the coupling coefficients $L_{1,2} = L_{2,1}$. However, the **Trk1,2-**system is also assumed to play a role as an K^+/H^+-symporter and might therefore contribute, too. Depending on the conditions (amount of free internal potassium and pH) the coefficient might therefore be
  - notably positive (low internal $[K^+]$ and/or high internal pH: Trk1,2 drive potassium in symport with protons in the cell)
  - negative (high internal $[K^+]$ and/or high internal pH: Nha1p extrudes potassium in antiport with H^+ by utilizing the proton gradient)
  - close to zero (fluxes of protons and potassium are uncoupled)
- $\mathbf{L_{1,3} = L_{3,1}}$: Like potassium, sodium, too becomes extruded via the same mechanism of an H^+/Na^+- antiport by **Nha1p**. This coupling coefficient should therefore be negative in this case, reflecting the nature of antiport.
  However, if the H^+-symport mechanism of Trk1,2 exists and if sodium enters the cell using the Trk1,2 system, and if the cell does not extrude Na^+ in the same amount as it enters the cell, then, the coefficient could become positive.
- $\mathbf{L_{1,4}}$: **Pma1p** couples the proton-flux with the ATP-flux by catalyzing H^+ extrusion under ATP consumption.

- $\mathbf{L_{2,3} = L_{3,2}}$: Since K^+ and Na^+ compete against each other by utilizing the same transport-systems, there should exist no coupling under normal conditions (the high affinity for K^+ suppresses efficiently sodium influx and the internal concentration of Na^+ does not impact on the magnitude of the potassium-flux.) However, under potassium-starvation conditions (very small value of X_2) and excess of Na^+ sodium might be utilized as a replacement for K^+ which allows for fluxes of Na^+ *via* the potassium transporters Nsc1 and Trk1,2.
- $\mathbf{L_{2,4}}$: The activity of the **Ena1** detoxification system can be interpreted as defining the degree of coupling between the flux of K^+ with the consumption of ATP.
- $\mathbf{L_{3,4}}$: The degree of coupling between Na^+ and ATP is (in the same way as for potassium) most relevantly affected by the activity of the **Ena1** - ATPase.

.

5.5 Confronting the Model with Experimental Data

In order to estimate the phenomenological coefficients for the equation-system data sets for potassium and proton fluxes from the laboratory of Prof. Sergey Shabala (University of Tasmania) were used. Data aquisition was performed by using monolayers of *S. cerevisiae* cells (starved in water over night) immobilized on Poly-L-Lysin treated glass coverslips. Each cover slip was placed in a total of 3 ml sample buffer volume in a petri dish. After addition of the specific concentration of KCl the cells were energized with glucose to enable generation of ATP and thus the performance of secondary active transport mechanisms. Net fluxes of K^+ and H^+ were measured non-invasively using the microelectrode ion flux measuring (**MIFE**; University of Tasmania, Hobart, Australia) technique as described by Shabala et al. [SNJ97, Sha00, SDS$^+$06]. Details on the preparation of the cells and measurement techniques are provided in the Supplementary Material, Part C.
Figure 5.2 shows the resulting data for independent measurements of potassium 5.2a and proton 5.2b fluxes in wild-type strains after treatment with four different concentrations of KCl.

5.5.1 Reduced model for qualitative simulations

Data of sodium fluxes are still lacking. However, to demonstrate the utility of the above introduced approach a reduced equation system is used in the following section to present some qualitative simulations. Since the cells were starved in water over night, and the external medium contains zero Na^+ in the data considered here, the flux of sodium as well as it's force on the fluxes of potassium and protons were neglected for the time being. The complete set of equations used for the following simulations is listed below. As mentioned earlier, the index "in" stands for *internal* concentrations or volume whereas the index "out" represents the concentrations and volume of the *outer* medium

5.5.2 Initial values and parameters

The initial values and parameters were set as stated in the Tables 5.1 and 5.2.
The surface of all cells and the inner volume, V_{in} were calculated from the detected optical density ($1.2 \cdot 10^7$ cells per ml OD 1) applied to achieve monolayer and by assuming a single cellular surface of $63{,}6\mu m^2$ and a volume of 50 fL according to Sherman, 2002 [She02].
The content of intracellular potassium (K^+_{in}) and chloride (Cl^-_{in}) was determined by Hella Lichtenberg-Frat*é*, partner in the TRANSLUCENT project.

Equation System 1 Reduced model for simulations of H^+ and K^+ fluxes

$$J_{H^+} = \frac{\mathcal{R}T}{d_m}\left[L_{11}\,\ln\frac{[H^+_{out}]}{[H^+_{in}]} + L_{12}\,\ln\frac{[K^+_{out}]}{[K^+_{in}]}\right] + z\mathfrak{F}\Delta\varphi\,[L_{11}+L_{12}] + L_{14}\left(-\frac{\mathcal{R}T}{\bar{c}_{ATP}}\alpha_{ATP}\,(1+K)\right)$$

$$J_{K^+} = \frac{\mathcal{R}T}{d_m}\left[L_{21}\,\ln\frac{[H^+_{out}]}{[H^+_{in}]} + L_{22}\,\ln\frac{[K^+_{out}]}{[K^+_{in}]}\right] + z\mathfrak{F}\Delta\varphi\,[L_{21}+L_{22}] + L_{24}\left(-\frac{\mathcal{R}T}{\bar{c}_{ATP}}\alpha_{ATP}\,(1+K)\right)$$

$$J_{ATP} = L_{44}\,\frac{\mathcal{R}T}{[\bar{c}_{ATP}]}\alpha_{ATP}\,(1+K)$$

$$\Delta\varphi = \frac{\mathcal{R}T}{\mathfrak{F}}\ln\frac{P_{K^+}\cdot[K^+_{out}] + P_{Cl^-}\cdot[Cl^-_{in}] + P_{H^+}\cdot[H^+_{out}]}{P_{K^+}\cdot[K^+_{in}] + P^-_{Cl}\cdot[Cl^-_{out}] + P_{H^+}\cdot[H^+_{in}]}$$

$$\frac{d[H^+_{out}]}{dt} = \frac{-J_{H^+}\cdot Surface}{V_{out}}$$

$$\frac{d\,pH_{in}}{dt} = \frac{-J_{H^+}\cdot \mathrm{Surface}}{V_{in}\cdot pbc}$$

$$[H_{in}] = 10^{-pH_{in}}\cdot cf$$

$$\frac{d[K^+_{out}]}{dt} = \frac{-J_{K^+}\cdot \mathrm{Surface}}{V_{out}}$$

$$\frac{d[K^+_{in}]}{dt} = \frac{J_{K^+}\cdot \mathrm{Surface}}{V_{in}}$$

$$\frac{d[ATP]}{dt} = -J_{ATP}$$

$$\alpha_{ATP} = [ATP]\cdot[\bar{c}ATP]$$

ATP was set to 0 ahead of the glucose addition due to the assumption that in the starved cells no ATP is available for other than basic vital processes and that addition for glucose is necessary to induce secondary and active transport mechanisms [LNS07, LAP+05]. Accordingly, the parameters L_{14}, L_{24} and L_{44} were initially set to 0.
The available ATP after the glucose stimulus was set to 2.5 mM due to Özalp's et al. [zPNO10] observational research.
The proton buffer function of the cytosol (pbc) was calculated due to the experimental observation that an exchange of approximately 200 mM H^+ is necessary to change the internal pH by 1. A conversion factor between units (cf = 1000 mmol/mol) was used for the calculation of the internal proton concentration from the internal pH.

5.5.3 Time course simulation and parameter estimation

Time course simulation and parameter estimation were performed with COPASI [HSG+06] by running the particle swarm algorithm [KE95] 1000 times with iteration limit 400, swarm size 40,

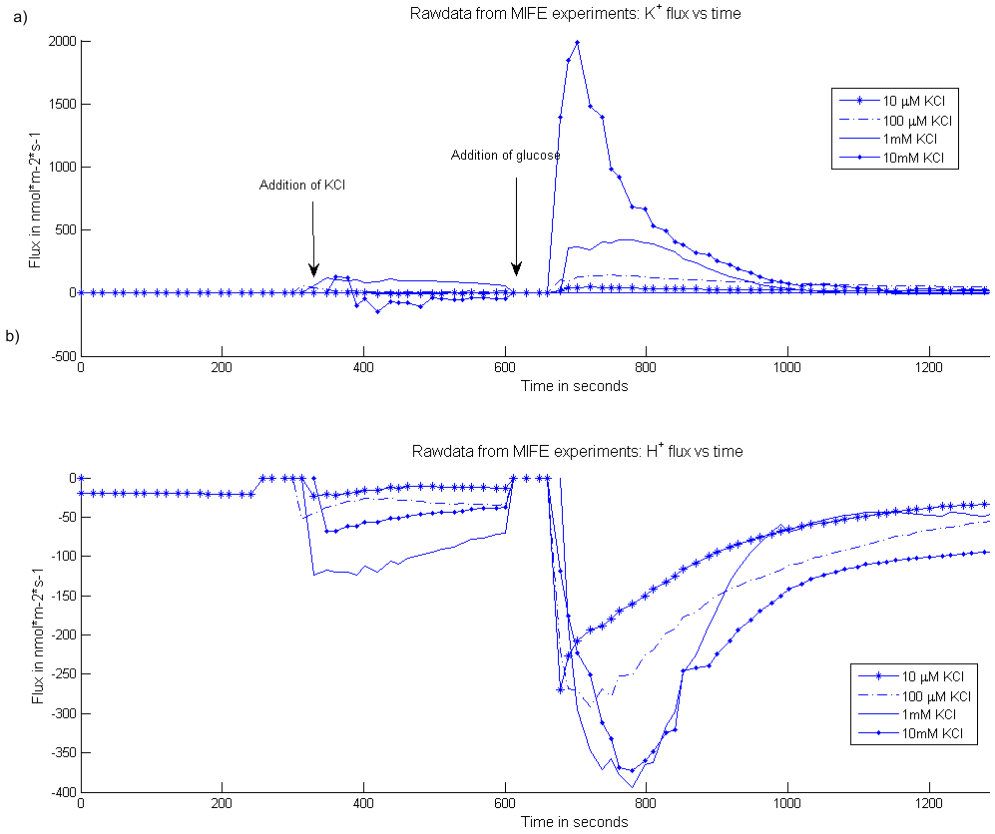

Figure 5.2: Data resulting from microelectrode ion flux measurements (**MIFE**) for **a)** potassium fluxes and **b)** proton fluxes in *S. cerevisiae* wild-type strains due to 4 different stimuli with KCl (0.01mM, 0.1mM, 1mM 10mM) followed by addition of glucose.

Global quantities and volumes	Value	Source
V_{in}	$1.8 \cdot 10^{-11}\ m^3$	Calculation
V_{out}	$2.85 \cdot 10^{-6}\ m^3$	Exp. condition
$L14_{init}$	0	Assumption
$L24_{init}$	0	Assumption
$L44_{init}$	0	Assumption
T	296 K	Exp. condition
d_m (membrane thickness)	$5 \cdot 10^{-09} m$	Gan et al. 2008 [GCJ08]
Surface (of all cells)	$2.29 \cdot 10^{-05}\ m^2$	Calculation
Proton buffer capacity (pbc)	$\frac{200mM}{pH}$	Experimental observation
conversion factor (cf)	1000 mmol/mol	

Table 5.1: Global quantities and volumes.

Species	Initial concentration (mM/L)	Reference
H_{in}	$2.4 \cdot 10^{-4}$	Exp. result (pH 6.62)
H_{out}	$3.162 \cdot 10^{-}3$	Exp. condition (pH 5.5)
K_{in}	230	Exp. result
K_{out}	0.053	Exp. condition
Cl_{in}	163	Exp. result
Cl_{out}	0.18	Exp. condition
ATP	0	assumption
$ATP_{stimulus}$	2.5	Özalp et al. [zPNO10].
$KCl_{Stimulus}$	0.01, 0.1, 1, 10	Exp. condition

Table 5.2: Initial concentrations of the model species.

standard deviation $1e^{-}6$, random number generator Mersenne Twister [MN98] and random seed. A Python script was used to run the algorithm with random initial parameter values as well as random upper and lower parameter bounds.
The best matching parameter set of the 1000 runs was finally taken; in case a parameter was located at a boundary, this boundary was extended by a factor of 100 and a subsequent parameter estimation was performed. The time course simulation was solved with the deterministic LSODA method [Pet83].

5.6 Results and Discussion

The phenomenological parameters were estimated with two different requirements: i) without any constraints ii) the straight coefficients (L_{11} and L_{22}) are constant and do not change after glucose addition. Both requirements resulted in close to identical flux-simulations (Figure 5.3), where Fit 1 resulted from requirement i) and Fit 2 from requirement ii) event though the parameters have slightly different values (given in Table 5.3).
As can be seen, the model is capable to reproduce the experimentally observed net flux rates of

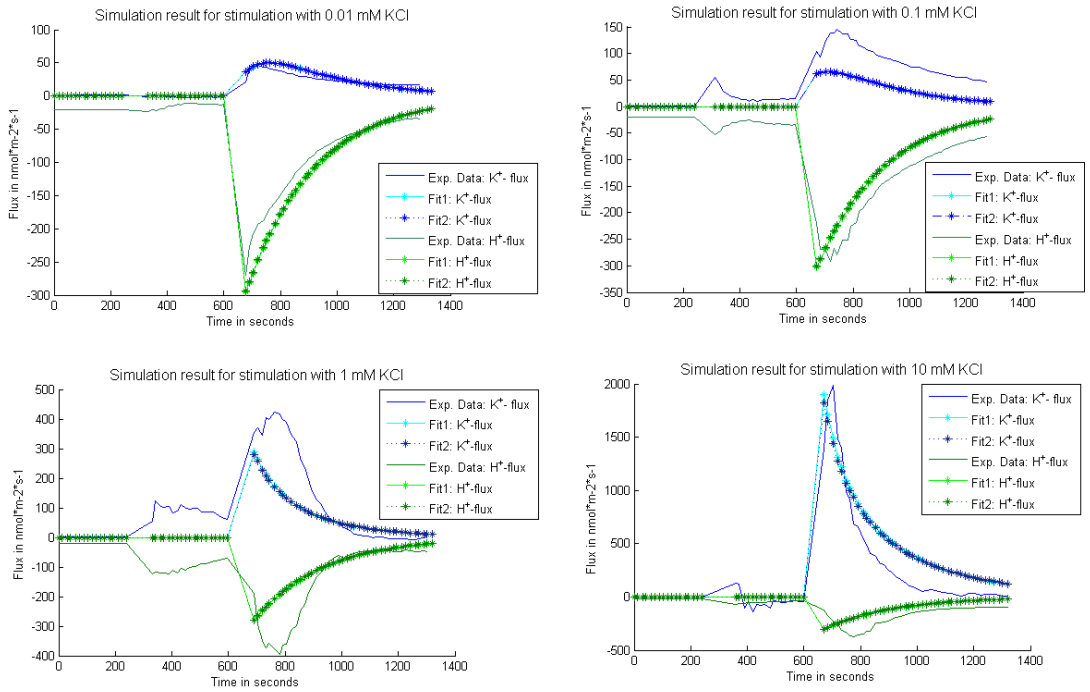

Figure 5.3: Simulation results for potassium and proton fluxes: Continuous lines (Exp. Data) are the experimental observations from Figure 5.2. Fit1 results in each case from parameter estimation without constraints whereas Fit2 has the constraint that the straight coefficients do not change during the simulation.

potassium and protons under the applied experimental conditions. The values of the estimated phenomenological coefficients given in Table 5.3 will be discussed on basis of the underlying biological interpretation in the following section:

Phenomenological Coefficients	Values Fit 1	Values Fit 2
$L11$ $[nmol^2/(J \cdot m \cdot s)]$	$1.07157 \cdot 10^{-15}$	$2.692 \cdot 10^{-15}$
$L22$ $[nmol^2/(J \cdot m \cdot s)]$	$2.285 \cdot 10^{-21}$	$9.666 \cdot 10^{-23}$
$L12$ $[nmol^2/(J \cdot m \cdot s)]$	$6.3778 \cdot 10^{-22}$	$6.222 \cdot 10^{-24}$
$L21$ $[nmol^2/(J \cdot m \cdot s)]$	$-2.525 \cdot 10^{-24}$	$-2.521 \cdot 10^{-24}$
$L11$ after glucose $[nmol^2/(J \cdot m \cdot s)]$	$1.298 \cdot 10^{-8}$	L_{11}
$L22$ after glucose $[nmol^2/(J \cdot m \cdot s)]$	$9.858 \cdot 10^{-5}$	L_{22}
$L12$ after glucose $[nmol^2/(J \cdot m \cdot s)]$	$9.86986 \cdot 10^{-7}$	$1.106 \cdot 10^{-6}$
$L21$ after glucose $[nmol^2/(J \cdot m \cdot s)]$	3.903	4.038
$L14$ after glucose $[nmol^2/(J \cdot m^2 \cdot s)]$	$1.929 \cdot 10^{6}$	$1.956 \cdot 10^{6}$
$L24$ after glucose $[nmol^2/(J \cdot m^2 \cdot s)]$	$-1.401 \cdot 10^{7}$	$-1.482 \cdot 10^{7}$
$L44$ after glucose $[nmol^2/(J \cdot s)]$	$6.259 \cdot 10^{10}$	$6.258 \cdot 10^{10}$

Table 5.3: Estimated model parameters for stress with 4 different concentrations of KCl. The second column (Values for Fit 1) gives the estimation results for fitting without previous constraints. The third column (Values for Fit 2) gives the results for the condition of L_{11} and L_{22} being constant before and after addition of glucose.

$\mathbf{L_{11}}$, that is the quantity relating the passive proton fluxes to the force of the proton gradient, obtained in both scenarios a tiny value. The underlying biological explanation - the strict suppression of passive proton fluxes in order to maintain a stable intracellular pH - is therefore confirmed by the simulation. Although the actual value - without constraints - seems to be dependent on an increasing X_1 after glucose addition L_{11} is still the most minor of all parameters and its influence on the proton flux will be insignificant.
This result, together with the observation that simulations with a constant L_{11} resulted in virtually identical fits give rise to the assumption that passive diffusion of protons can not be a critical parameter affecting the system. The maintenance of a stable internal pH is highly regulated and passive proton fluxes following a concentration gradient are more or less suppressed. The "straight coefficient" L_{11} can therefore assumed to be - in general - tiny and only leakage or intracellular buffering capacities may be seen as contributors.
Likewise $\mathbf{L_{22}}$, that is the quantity that determines directly the passive potassium flux rate has corresponding tiny dimension. This is - from the biological point of view - indeed reasonable since well operating regulation mechanisms are deployed.
Since the CaCl buffer in the external medium inactivates the function of the non-specific channel Nsc1, the amount of L_{22} can be contributed to the shared activity of Trk1,2 and Tok.
The dimension of L_{22} changes - similar to L_{11} - also after the addition of glucose but the total amount is still marginal. This observation leads to the same conclusion as above. Passive fluxes of potassium are more or less completely suppressed in order to avoid undesired disturbances of the intracellular concentrations.
$\mathbf{L_{44}}$, that is the straight coefficient that determines the reaction affinity and therefore the amount of ATP consumption was initially set to zero (due to the experimental condition of measuring with starved cells). Following the addition of glucose the value of L_{44} changes considerably into a positive direction which means that the more ATP is available the higher is the magnitude of chemical reaction affinity which leads to the consumption of ATP. This is also in good agreement

of what is expected and reasonable under biological consideration.
L_{12} and **L_{21}** are the coefficients that couple proton and potassium fluxes (*via* the activity of Nha1 and possibly Trk1,2. These coefficients were expected to fulfill the Onsager reciprocal relations $L_{1,2} = L_{2,1}$. Before the addition of Glucose, this is almost the case. Even though these values are obviously unequal in dimension and sign, they are both very tiny, but indeed close to zero and may thus have only negligible impact on their coupled fluxes.
This is consistent with the experimental observations: the fluxes displayed in the experimental data (Figure 5.2) show only minor fluctuation between addition of KCl and glucose. Even more, these observed fluctuations in the data between the two stimuli are thought to arise mainly by physical noise (removing and reinsertion of the electrodes and fluctuations caused by the addition of the fluids). (Reference: personal communication with the experimenters).
After glucose addition however, the coefficients differ enormous in the magnitude of their values. From the biological point of view this is reasonable: a high concentration (force) of K^+ does not automatically lead to proton fluxes. In contrast, the extremely high intracellular accumulation of potassium (up to thousandfold) appears unfeasible to be achieved if automatically accompanied by proton in- or efflux. This coupling (from the current point of understanding) only occurs when the internal K^+- concentration reaches a toxic level and K^+-cations are extruded in antiport with H^+ *via* Nha1. This secondary active transport system utilizes the inward gradient of protons as a driving force to eliminate sodium cations (and to some extend potassium when in excessive amount). Since the concentrations used here are far below a toxic level a coupling can be assumed to be out of the question.
The coupling coefficient L_{21} however, defined as impact of the force of the proton gradient on the flux of K^+ is after the glucose addition fairly high and positive. Direction and magnitude are consistent to what was expected: A high gradient of protons (generated via Pma1) drives K^+ in the cell, what in fact enables the cell to accumulate potassium in such a high amount in comparison to the environment. The significant difference in the coupling coefficients L_{12} and L_{21} is therefore remarkable from the physical (thermodynamic) understanding but is in good agreement with the biological observations.
L_{14}, which is the coupling coefficient of proton fluxes and ATP achieves a strong positive value as expected. As soon as ATP is available proton extrusion is fueled and driven. The active transport of protons *via* the ATPase Pma1 can be considered as a symport mechanisms: for each proton that is extruded, one ATP is consumed. In both cases, the intracellular concentration decreases.
In case of **L_{24}**, the coupling coefficient of potassium fluxes with ATP, the degree of coupling is determined - from the current understanding of the system - by the activity of the Ena1 detoxification system. As mentioned earlier, the concentrations used here are far below a toxic level and will therefore most likely not activate Pma1. This coupling coefficient should be therefore assumed to be marginal under the experimental conditions and - analogous to L_{14} - with a positive value. The estimated parameter, however has a negative sign and a high value which is surprising result and a strong indication for a - so far undetected - active inward transporter. On the other hand, an active transport mechanism could potentially be attributed to the Trk1,2 system whose properties have not been definitively established yet. This hypothesis should be investigated experimentally. L_{13}, L_{23} L_{32},L_{33} and L_{34} could not be estimated, due to missing experimental data. The estimation of these coefficients can be performed for further validation of the presented approach as soon as time-resolved measurements are available.

5.7 Conclusion

The presented approach concerned a systematic thermodynamic formulation of the major components contributing to the maintenance of stable intracellular cation concentrations in the yeast *S. cerevisiae*.
It could be demonstrated that the theory of nonequilibrium thermodynamics is well suited for the purpose of modeling such a complex systems of closely connected transport processes, particularly at an early stage of understanding. This entirely phenomenological approach does not depend on a detailed understanding and description of structure, function or kinetic parameters of individual constituent as parts of the system.
Consequently it can provide only limited insight into the underlying transport mechanisms. Nevertheless, by identifying the generalized forces being responsible for a given flux, the model may provide directions for further efforts aimed at defining transport processes at the molecular level. Thermodynamics can assist to reinterpret classical findings on ion flux propagation and may provide new viewpoints on processes that are seemingly in conflict with each other.
The presented model considers fluxes of the major cations K^+, Na^+ and H^+, the utilization of ATP as an active driving force and the calculation of the internal pH as well as the change in the membrane potential.
A reduced version of the model, excluding - due to missing data - sodium fluxes from the consideration was confronted with experimental data to show qualitative simulation results.
The results of this simulations are in good agreement with the experimental observations and the theoretical predictions achieved for the values of the phenomenological coefficients are reasonable from the biological point of view. However, the model is still amenable to development in view of a more comprehensive picture of cation homeostasis. Perspectives and weaknesses of the approach will be discussed as follows.

First of all, the restrictions set on the defined sub-volumes, as there are the temperature, the pressure and the concentrations are virtually constant, and that fluctuations are insignificant, imply certain limitations on the processes. If the gradients of the intensive parameters within the system are large it might be impossible to isolate a sub-volume that satisfies these requirements. The range of applicability of this theory cannot be specified on *a priori* grounds, and the justification of its use rests, in the final analysis, on the validity of the results obtained.

Another point that should be critically analyzed is the use of the Goldman equation for calculations of the membrane potential, $\Delta\varphi$. Under steady-state conditions, the $\Delta\varphi$ can be reliably approximated by this rather straightforward physiochemical formulation of the diffusive and electrogenic components [Gol43, BP93, HK49, Jac71, HFL89]. However, a description of the temporal behavior is more complex and should in general also incorporate the rates of changes of the cell volume due to effects on the intracellular osmolarity and changes of the permeabilities for the ions over time [Jak80, LRJ92, SSPW90, HC98]. These terms in turn would simultaneously affect the values of intracellular cation concentrations [Wil93, Jak80, TH60].
In the example presented above the volume was assumed to remain constant during the simulation. This is a reasonable assumption since the concentrations used in the experiments are far beyond the critical value (experiments studying the osmotic stress response *via* the activation of the Hog-pathway usually start with concentrations of several hundreds of mM NaCl [RRG$^+$99, VWRS$^+$00, RKTH00]) and already at 0.05M the Hog activation is down to a tenth of the maximum amplitude, (B. Nordlander; unpublished results)). Therefore, it is highly unlikely that salt concentrations lower than 0.01M have any significant osmotic or volume effects. On the other hand substantial progress has already been made in the field of modeling response to osmotic stress *via* volume and turgor regulation in the yeast *S. cerevisiae*

[KNK$^+$05, ZLK10, SAE$^+$10] and both models could highly benefit by getting joined. For further and extended versions of the here presented model, a combined observation of the regulation of the osmotic response as well as the homeostasis of the major cations Na^+, K^+ and intracellular pH should be envisaged for a broader understanding. As a second future perspective the model should also be validated with the support of proper deletion mutants. The impact of such mutant data would provide insights on the reliability of the model when it was confronted with actual measurements. Such data would be obtained under the same experimental conditions but not with the wild-type but with yeast strains lacking one of the major potassium transport systems.

6 Summary and global discussion

Some interesting issues concerning the research question of cation homeostasis in the yeast *S. cerevisiae* have been addressed within the previous chapters. In the following section, the different approaches presented in this thesis will be briefly summarized and discussed in the context of the TRANSLUCENT global project goal. In the first chapter within a short biological review the focus was set on the cellular ability of the unicellular organism *S. cerevisiae* to maintain a stable intracellular cation content. *S. cerevisiae* was presented as the project's and general model organism whose major components and plasma membrane transporters have been already characterized to obtain decisive roles within the homeostasis. In the second chapter, the systematic study and graphical analysis of the genomic promoter regions of two transport and two regulator systems was presented. In order to analyze the transcriptional regulation, a systematic query for already documented as well as potentially additional transcription factor binding sites on specific promoter regions was performed. Within this study, a *S. cerevisiae* specific tool was developed for an improved computational analysis and graphical representation of potential matches on genomic sequences. The predictions obtained by the developed tool were experimentally validated and results of this study were published as "*S. Gerber, G. Hasenbrink, W. Hendriksen, P. Van Heusden, J. Ludwig, E. Klipp, and H. Lichtenberg-Fraté;* Graphical analysis and experimental evaluation of *Saccharomyces cerevisiae* $P_{TRK1|2}$ and $P_{BMH1|2}$ promoter region. Genome Informatics 22, (11-20);(2010)*.*".

Heavy metal toxicity was addressed in the third chapter on the basis of DNA- microarray experiments. A detailed characterization of *S. cerevisiae* gene expression profiles upon unphysiologically high concentrations of $AgNO_3$, $AlCl_3$, $AsCl_3$, $CdCl_2$, $CoCl_2$, $HgCl_2$, $MnCl_2$, $NiSO_4$, VCl_3 and $ZnCl_3$, respectively was performed in order to identify common response mechanisms. For this purpose differentially expressed genes were filtered and identified from the experimental results, clustered and enriched with meta-information on (potential) transcription factors, affiliation to biochemical pathways and associated Gene Ontology terms. Even though several gene cluster appear to be co-regulated upon the different stresses the outcome of this study - that every single metal ion causes its own specific expression pattern - leads to the surprising conclusion that yeast is able to differentiate between the tested metal ions. However, the results presented within this thesis represent only a small part of the full experimental set. The detailed interpretation of all information that could be extracted from the bioinformatical analysis goes beyond the scope of this thesis and will involve expert-knowledge in molecular biology. This task is currently performed by Translucent project partners and it is planned to publish interesting results as *"D. Hosiner, S. Gerber, W. Glaser, E. Klipp and C. Schüller; STB5 plays an important role in heavy metal detoxification in the yeast Saccharomyces cerevisiae, manuscript in preparation"*

The spatio-temporal modeling environment "STSE", presented in chapter 4 describes a set of open source tools that can be used for the analysis and interpretation of time-resolved protein localization and accumulation data. Although STSE has not yet been fully exploited in the Translucent project it is anticipated that the software supports the application for the detection and quantification of proteins being involved in transport and/or detoxification processes. The tool was developed in the research group of Edda Klipp with Szymon Stoma being the main developer: *S. Stoma, M. Fröhlich, S. Gerber and E. Klipp: STSE: Spatio-Temporal Simulation*

Environment Dedicated to Biology, submitted to BMC Bioinformatics(2010).

In chapter 5 a systematic thermodynamic formulation of the major components contributing to the maintenance of stable intracellular cation concentrations in *S. cerevisiae* is provided. Even though significant efforts have been made during the last decade by experimental and theoretical analysis of the individual components of transport systems and individual transport-mechanisms such efforts did not result in an integration of the highly connected and complex system. The development of kinetic networks might well contribute to the understanding and visualization of cation homeostasis. Currently however, such kinetic systemic analysis would require more detailed biochemical information as is currently available. This problem was circumvented by using the entirely phenomenological approach of the theory of non-equilibrium thermodynamics. The method does not require the detailed understanding of structure, function or kinetic parameters of individual constituents of the system but produces some unique parameters related to thermodynamic couplings between different ion fluxes and ATP consumption. These estimated phenomenological constants combine the kinetic parameters and transport coefficients and control the coupling of fluxes. A model was developed on such NET basis. The model in principle considers fluxes of the major cations K^+, Na^+ and H^+, the utilization of ATP as an active driving force and the membrane potential. Due to the lack of detailed experimental data, a reduced version of the model, excluding sodium fluxes from the modeling was confronted with experimental data to test qualitative simulation results. The model is capable to reproduce the experimentally observed uptake rates of potassium, the proton fluxes and the change in the internal pH due to an external stimulus with KCL after starvation to a reasonable degree. Along the generalized formulation it can consequently, provide only limited knowledge into the underlying transport mechanisms. In any case , by describing the generalized forces that are responsible for a given flow the model provides information for further experiments and may support the reinterpretation of classical findings on ion flux propagation and on processes that are seemingly in conflict with each other. The work will be published as: *"S. Gerber, M. Fröhlich, H. Lichtenberg-Frate, J. Ludwig, S. Shabala and Edda Klipp; A basic thermodynamic model of cation homeostasis in the yeast Saccharomyces cerevisiae, manuscript in preparation"* By analyzing genomic sequences (chapter 2), or information arising from high-throughput technology, (3) and spatially resolved proteome information (chapter 4) substantial contributions to both the overarching Translucent aims and general interdisciplinary cooperation were performed. As a result of this data accumulation and increasing knowledge on kinetics and regulatory mechanisms of the individual components, it might become less important to treat the membrane as a black box and use an linearized model for predictions as done in chapter 5. But such data, instead of making the thermodynamic treatments obsolete, substantiate the choice between different modeling approaches for different purposes. As always in systems biology - at an early state of understanding of the system - the model is not the final goal but rather an instrument to increase the process of understanding the system. Biological questions and hypothesis are addressed by computational modeling and simulation and become verified or rejected in iterative cycles of validation in close collaboration with experimenters.

Supplementary Material A - Promotor Analysis

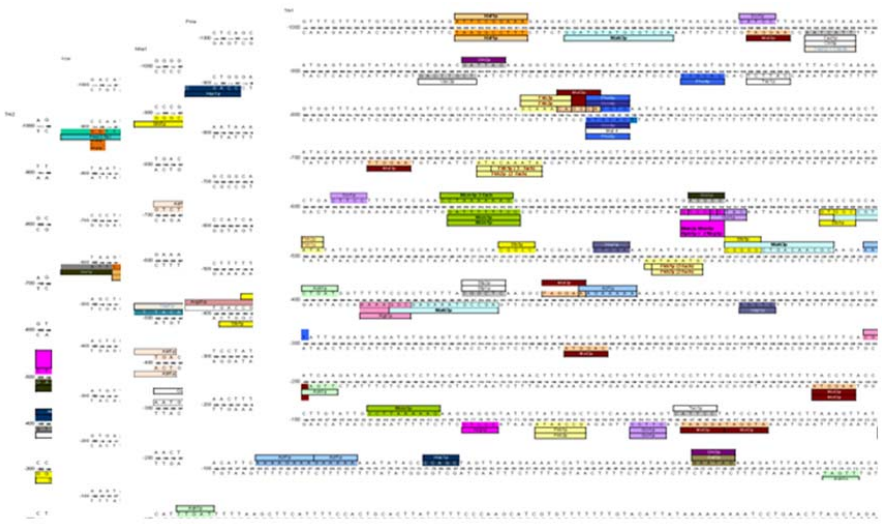

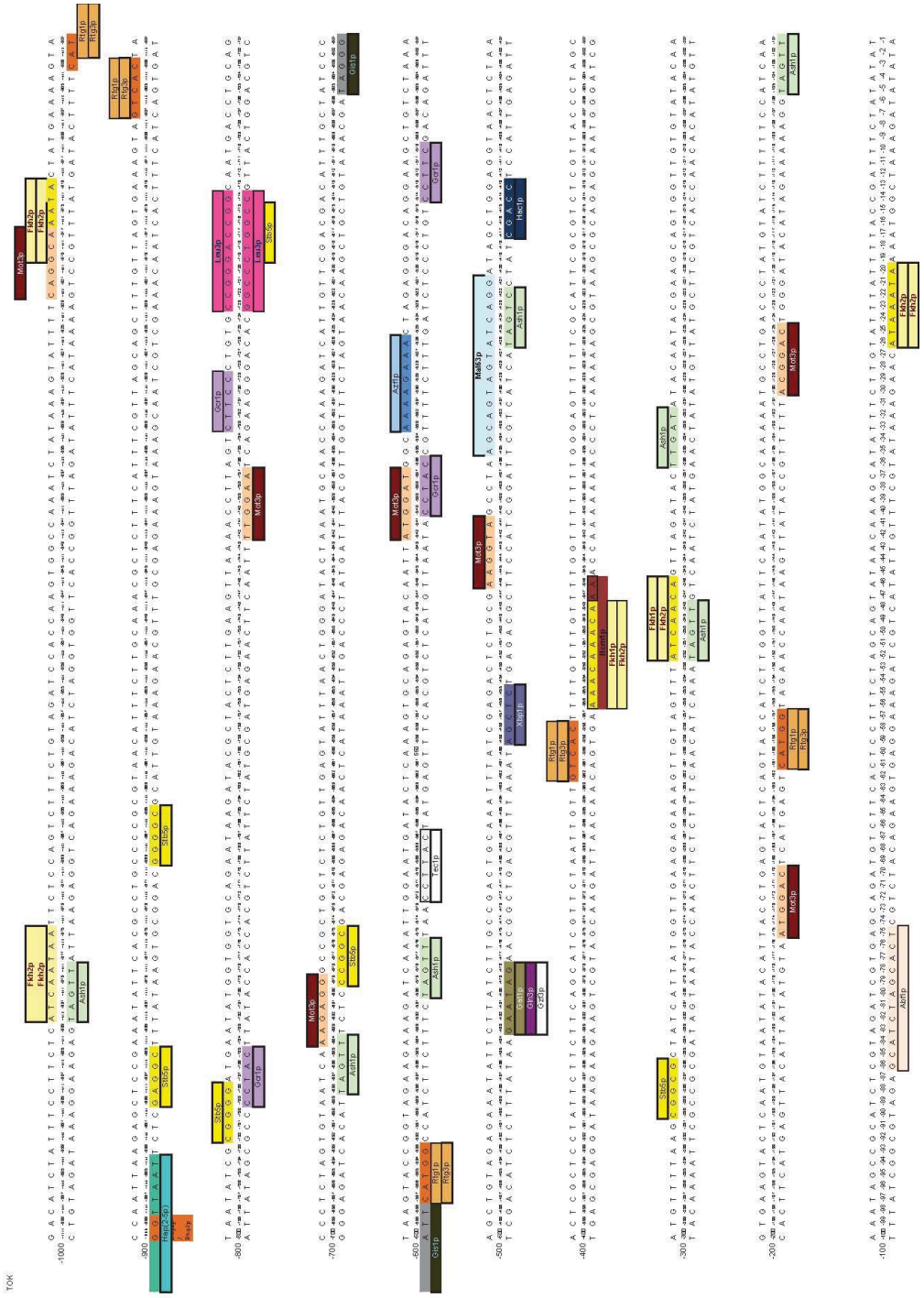

Figure 1: Graphical analysis of the TOK1 promotor region

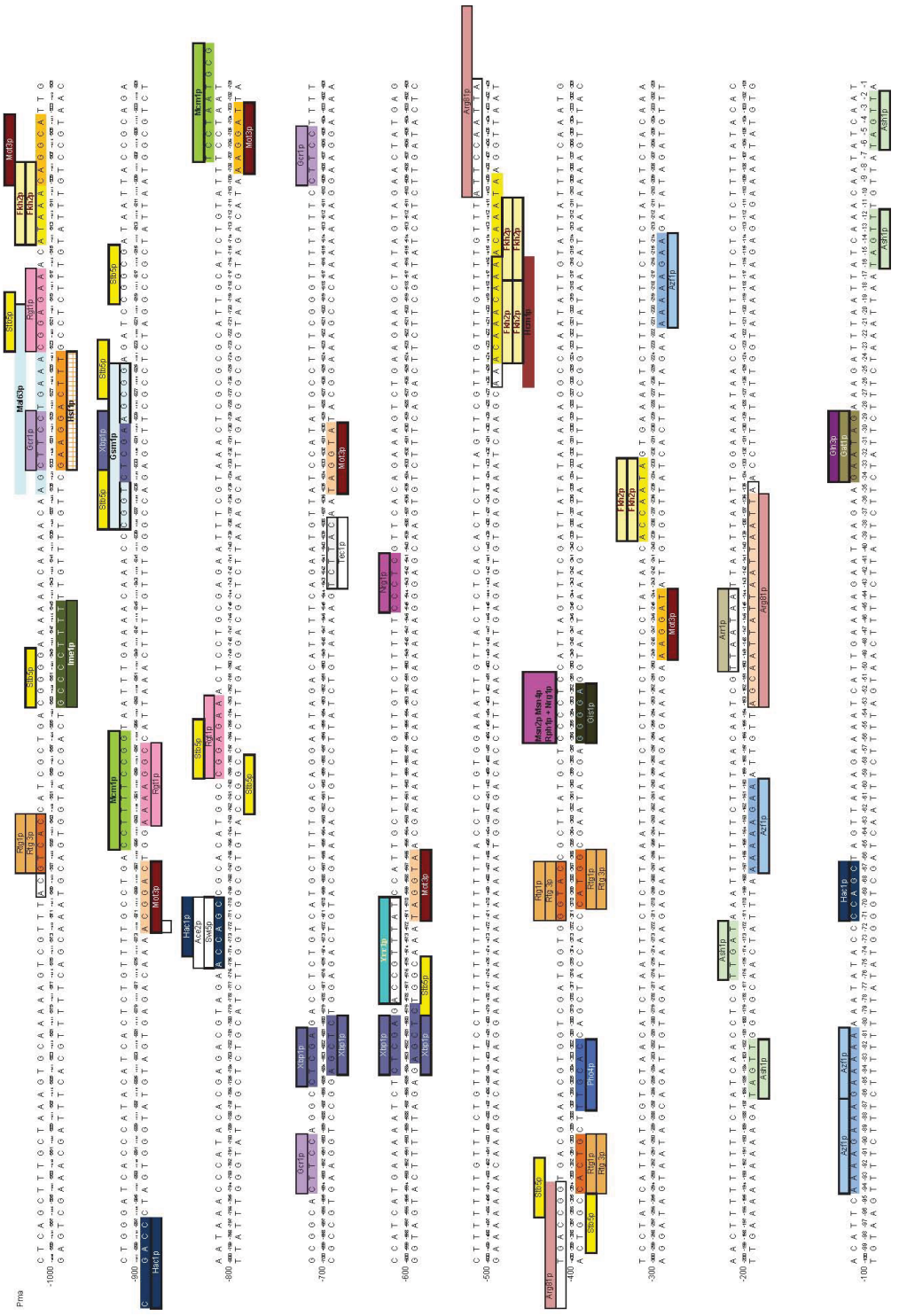

Figure 2: Graphical analysis of the PMA1 promotor region

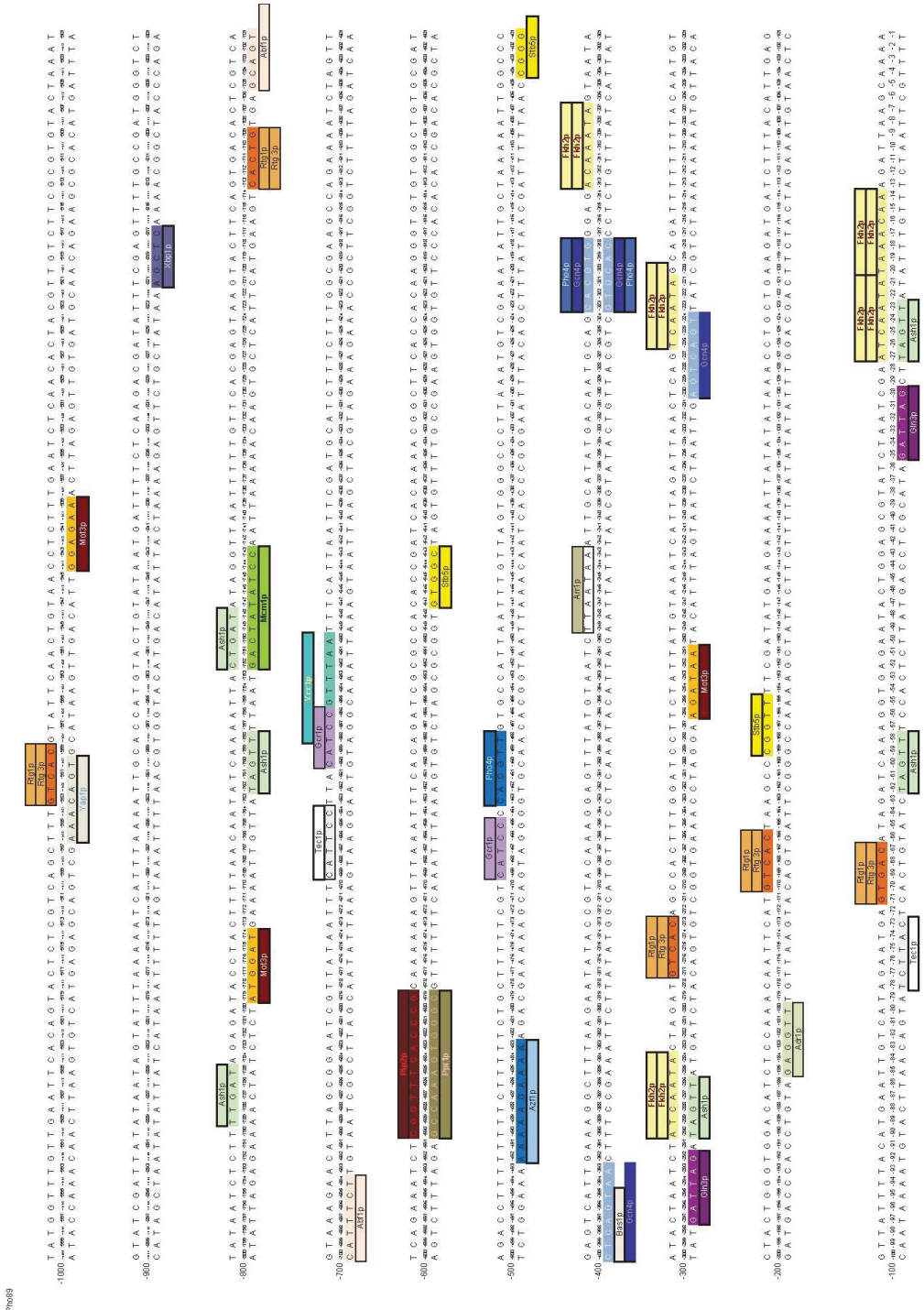

Figure 3: Graphical analysis of the PHO89 promotor region

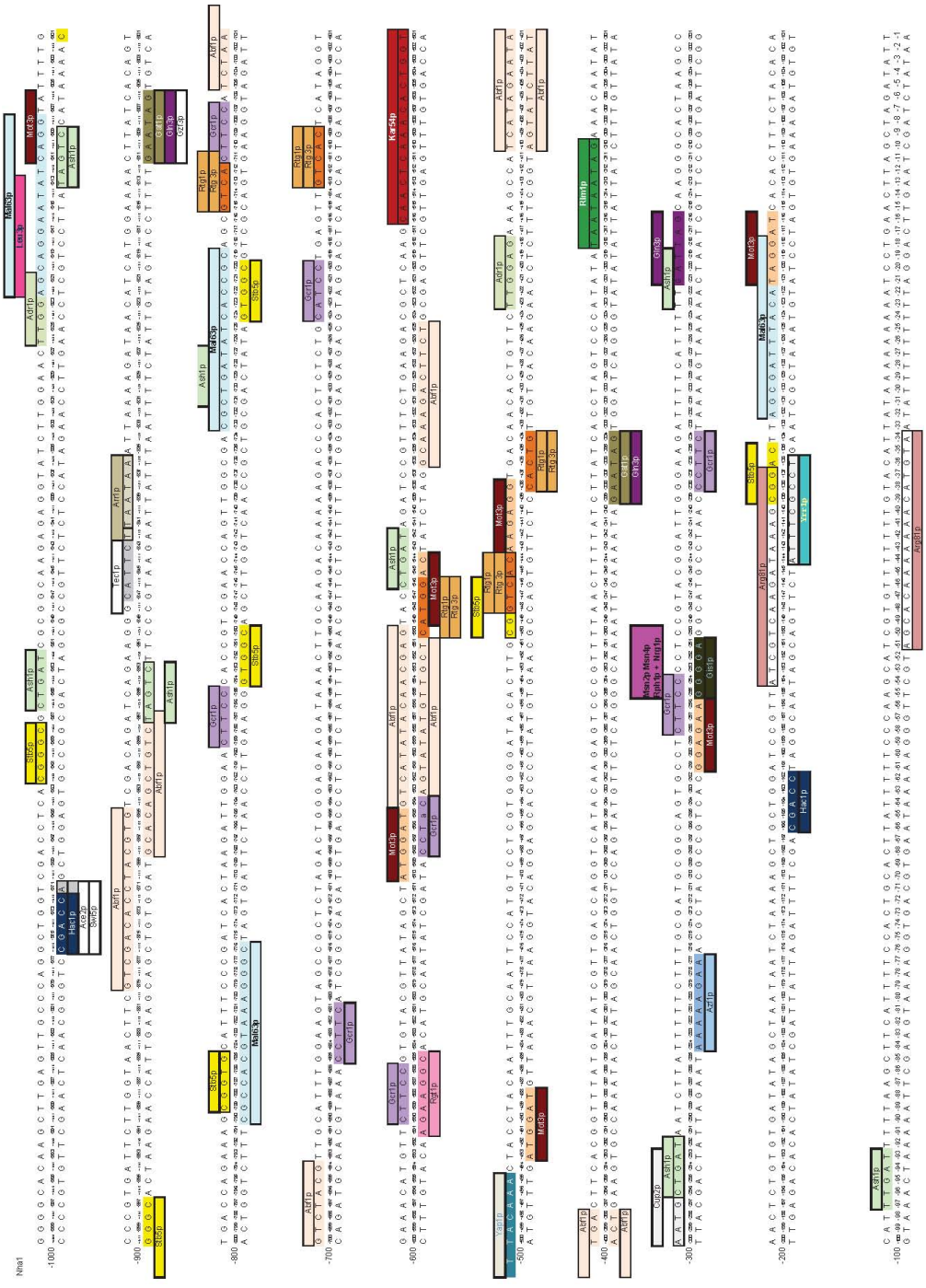

Figure 4: Graphical analysis of the NHA1 promotor region

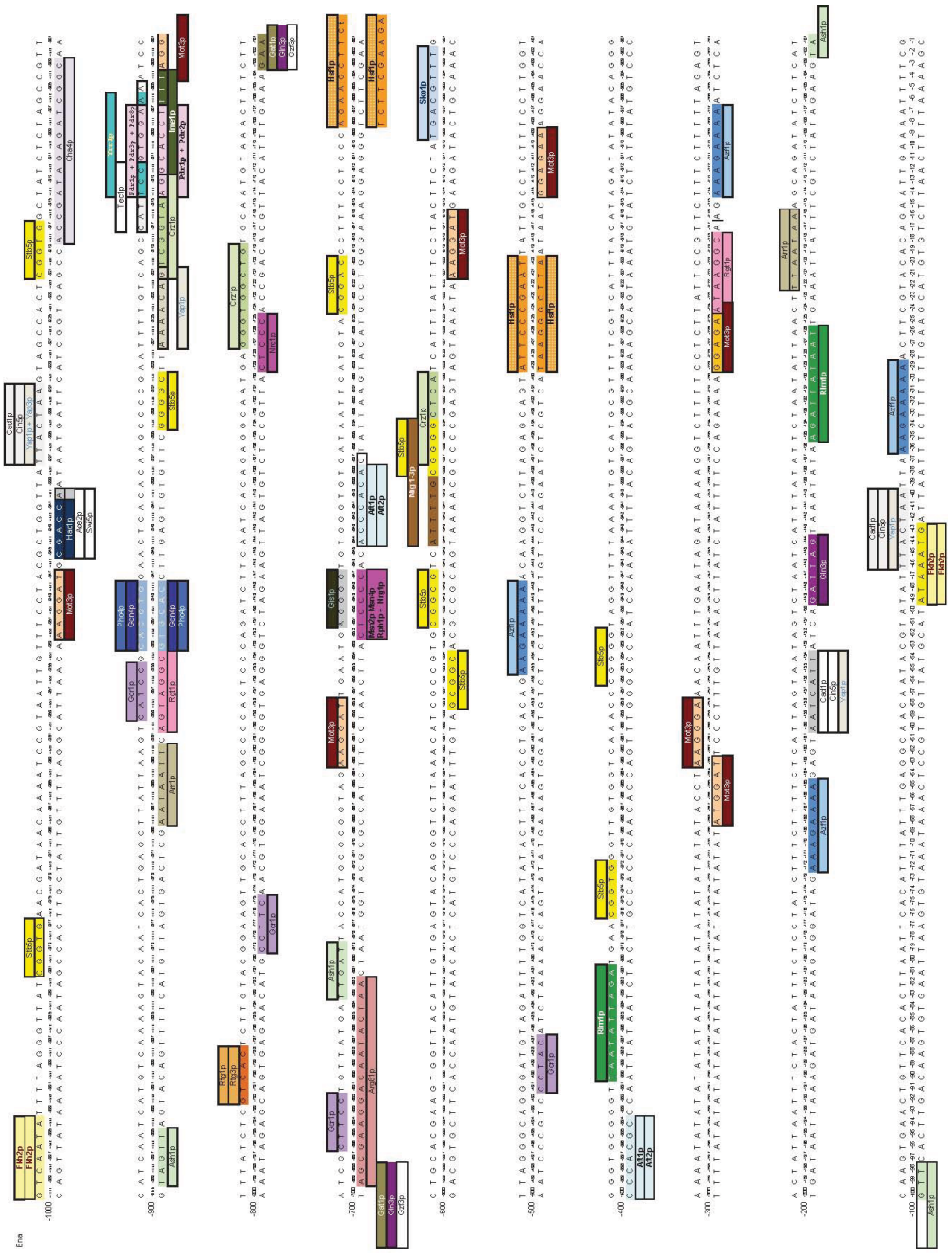

Figure 5: Graphical analysis of the ENA1 promotor region

Supplementary Material B - Microarray Analysis

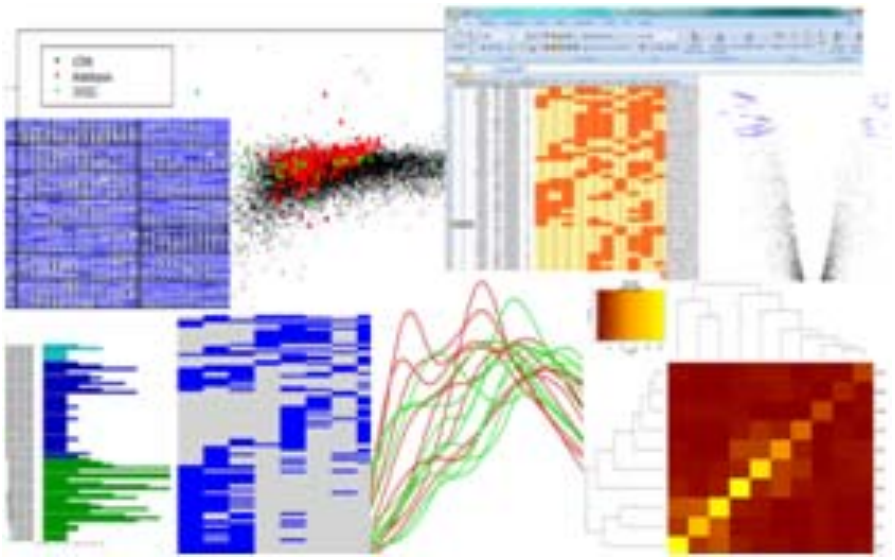

1 Manually enriched data after K-means clustering

Cluster	GO-Slim term	Genes annotated to the term
1	**response to oxidative stress**	CCP1, PRX1, TRR1, TSA1, YBL055C
	RNA metabolism: translation, splicing	AAR2, FMT1, NTC20
	vacuole organization and vesicle-mediated transport	ATG8, SEC17
	fungal-type cell wall organization	ECM13, ECM8
	chromosome organization	IOC3
	chromosome segregation	AME1
	cell cycle	TSA1
	biological process unknown	YAR066W, YBL059W, YBR141C
2	**nucleotide nucleoside nucleobase metabolism**	ADE17, ADE5,7, URA7, HPT1, HYP2, SAM1, NDE1, SHM2
	ribosome biogenesis and transcription	DBP2, ERB1, NOG1, NOG2, NOP7, NSR1, RRB1, UTP5
	transport	ATO3, FAA4, HSP78, NOG1, NOG2
	lipid, fatty acid and isoprenoid metabolism	ERG11, ERG3, URA7, SHM2, FAA4
	response to stress	HSP78, HSP42, PHO5
	generation of precursor metabolites and energy	NDE1
	biological process unknown	RTC2, YER156C, YNL022C
3	**sporulation**	
	chromosome organization	ACS1, SPC72
	conjugation/mating	FIG1
	ascospore wall assembly	GIP1
	generation of precursor metabolites and energy	ACS1
4	**DNA repair**	KRE29, RAD34, RAD5, SMC5
	ascospore formation	AQY1, YNL194C, YOR338W
	transcription	CAF130, TAD1, YOR338W
	mitotic cell cycle	DCR2, BIR1, YOR060C, CIS1
	histone demethylation/ transcriptional control	JHD2
	pseudohyphal growth/polysaccharid metabolism	PGU1
	water transport	AQY1
	biological process unknown	YFR006W, YJL218W, YLR445W, YML037C
5	**nitrogen compound metabolism**	CRF1, HAC1, HHT2, UTH1, ARO10, ARO9, ASN1, BAT2, ILV2, LYS9, STR2, TRP5, IRC7
	transcriptional control/mitotic cell cycle	CRF1, HAC1, HHT2, UTH1
	transport	ITR1, RTN1, SNG1
	biological process unknown	YIL169C
6	**response to stress**	HSC82, HSP26, HSP82, KAR2, SGT2, SSA1, SSA2, SSA4, SSE1, STI1

Cluster	GO-Slim term	Genes annotated to the term
	aldehyde metabolism	AAD10, AAD14, AAD15, AAD16, AAD3, AAD6
	transport	HSP60, HSP82, SSA1, SSC1, YDJ1 (mitochondrion) - FLR1, KAR2, PDR5, RSB1,SGT2, SSA2, SSA4, TRS31
	mitotic cell cycle/transcription	KAR2, YDJ1, CSE2, PCL9, VHS1, HAP3, STP1
	detoxification	FLR1, PDR5, GTT2
	generation of precursor metabolites and energy	PGK1, OYE2, OYE3
	metabolic process	ARA2, MET12, YGL039W
	ascospore formation/meiosis	SPS1
	fungal-type cell wall organization	TIP1
	lipid, fatty acid and isoprenoid metabolism	YML131W
7	**iron ion homeostasis**	FTR1, ARN1, ARN2, TIS11, FET3, ENB1
	siderophore transport	ARN1, ARN2, ENB1, FIT2
	glutamate biosynthesis	ACO1, GLT1
8	**chromosome organization**	BIM1, HEK2, HHF1, HHF2, HHT1, HIR1, HTA1, HTA2, HTB2, POL30
	chromatin organization	HTB2, HTA2, HIR1, HHF1, HHT1, HTA1, HHF2
	hexose transport	HXT7, HXT6, HXT3, HXT4, HXT1
	transport	BIM1, BRL1, FUI1, HXT1, HXT3, HXT4, HXT6, HXT7, PET9, QDR2, YIP3
	transcription / ribosome biogenesis	HHT1, HIR1, HTA1, POL30, RTT103, MAK 16
	protein modification	HHF1, HHF2, MNN2, PSA1
	(mitotic) cell cycle	BIM1, HHT1, POL30, RTT103, RNR2, YBL113C
	detoxification	QDR2, ERG5
	ascospore formation	CWP1
	respiration	PET9
	signaling process/conjugation	STE3
	fermentation	ALD6
	amino acid metabolism (glycine)	GLY1
	lipid metabolism	ELO1, ERG5
	protein degradation	CPS1
	vesicle-mediated transport	YIP3
9	**protein catabolism**	
	vesicle-mediated transport/endocytosis	VPS27 (ubiquit), ENT4, (YOL163W)
	protein degradation (upiquitination)	CDC4
	mitotic cell cycle	CDC4, STB1
	amino acid metabolism (sulfate)	MET8
	biological process unknown	RTR2
10	**protein catabolism (vacuolar)**	LAP4, PEP4, PRB1, RIM11, UBP10, YPS1, VPS68, ICY2 (mitoch)
	response to stress	HOR7, NCE103, PEP4, PRB1, RIM11, SED1, YBR016W
	cytokinesis/septum formation	CHS1

Cluster	GO-Slim term	Genes annotated to the term
	cell wall	YEF3, YJL171C
	phospate metabolism (cell wall)	PHO3
	plasma membrane	PUN1
	glutamate biosynthesis/TCA cycle	CIT2
	lactate fermentation	DLD3
	amino acid metabolism (sulfate)	MET10
	transcription	EDS1
	biological process unknown	RCN2, UIP3, YNL208W
11	**response to (oxidative) stress**	AHP1, DDR48, GRX2, TRX2, YDL124W, ZWF1, GRE2, YGP1
	ribosome biogenesis / transcription	CBF5, NOP4, RPS15, RRP5, RPL26A ESC1
	cysteine biosynthesis	CYS3, MET17
	transport	CTR1, FRE1, GLK1, RPS15, TRX2, PDI1
	carbohydrate metabolism / energy generation	GLK1, ZWF1, YDL124W, YNL134C
	nucleotide/nucleoside/nucleobase metabolism	GUA1, IMD4
	biological process unknown	YLR460C
12	**amino acid metabolism**	ARG1, ARG4, HIS3, HIS5, HIS7, IDP1, LYS1, LYS20, LYS21, ORT1, PRO2, SER1, SRY1, TRP2, TRP3, TRP4
	histidine metabolism	HIS3, HIS5, HIS7, PRO2, RIB3, SER1, SNZ1,
	glutamine family aa biosynthesis	IDP1, ARG4, ARG1, ORT1, PRO2
	tryptophan metabolism	TRP2, TRP3, TRP4
	lysine metabolism	LYS1, LYS20, LYS21
	transport/endocytosis	AKR1, ATG7, GNP1, MCH4, ORT1, PHO89, RCR1, SAC6, VHT1, YMC1
	protein modification/degradation	AKR1, ATG7, CMK2, GPI18, OTU1, YPI1, ALD5, GDH2, ICY1, HUA1
	transcription	BDP1, CDC6, ELP6, GCN4, HTB1, OTU1
	phospholipid metabolism	CHO1, GPI18, OLE1, OPI3
	cellular respiration/energy generation	COQ8 (resp), RIB3
	phosphate metabolism/energy generation	PFK2, YPI1, PMU1
	response to stress	YHB1, YJL055W, SNZ1
	translation (initiation)	ANB1, CLU1, DED1
	cell wall organization	RCR1, YLR194C
	pseudohyphal growth	DIA1
	biological process unknown	TMT1, YBR287W, YGL117W, YHR162W, YLR257W, YLR413W, YOR385W
13	**glutamine family amino acid metabolism**	GAP1, CAR1, GLN1
	transport	GAP1, OPT1, SSU1, YSC84
	endocytosis	YSC84
	vitamin metabolic process	NPT1
14	**sulfur amino acid metabolism**	MET1, MET14, MET16, MET2, MET3, MET6, MET5, SAM2, BNA3, SER33
	transport	ATG23, FCY2, MMP1, SEO1, SUL1, SUL2
	response to stress	APN2, ATG23, MNN4
	transcription	SEN34

Cluster	GO-Slim term	Genes annotated to the term
15	**transcription / chromosome organization**	ASF2, GAT1, HDA3, KSS1, MRE11, OAF1, PUF4, SGF29, SPT16, TRM3, UTP20
	response to stress	CCZ1, MRE11, NPP1, SAE2, SCC4, SPT16, RTA1
	transport	CCZ1, HXT8, PDR10, VTH2
	cellular membrane organization	CCZ1, FCJ1, YSW1
	vesicle-mediated transport	CCZ1, VTH2
	DNA repair/cell cycle	MRE11, SAE2, SCC4, SPT16
	translation	GCN20, PUF4, MTO1
	carbohydrate metabolism	OST1, PMT6, YPL088W, YNR071C
	signaling process/cell wall	KSS1, TUS1
	lipid metabolism	OAF1, SCS3, ARE2
	protein folding	ALF1
	biological process unknown	MTC3, NRP1, YCL047C, YER077C, YKL162C, YNL146W
16	**response to oxygen radical**	CUP1-1, CUP1-2
	glutathione catabolism	DUG2
	proton transport (H-ATPase)	PMA2
	RNA metabolism	RTC3
17	**protein catabolism**	ESP1, SWM1, DEF1, MDJ1, KAR4, DBF2, PBS2, RAD50
	mitotic/meiotic cell cycle	ESP1, KAR4, RAD50, SWM1
	response to stress	DEF1, MDJ1, PBS2, RAD50, MDR1
	protein modification	DBF2, PBS2, SWM1
18	**meiosis / sporulation**	
	transport	ADY2, AZR1, EMP46, LHS1, PEP3, PMA1
	transcription	ORC1, RKR1, SLM3, TEL2
	meiosis/sporulation	SPO7, ZIP1, SPS100, ADY2
	lipid metabolism	CSH1, SPO7
	cell growth	GPR1, MZM1
	vesicle-mediated transport	EMP46, PEP3
	protein degradation	RKR1
	biological process unknown	DRN1, YMR258C, YOL166C
19	**nitrogen compound metabolism**	ARO3, CPA1, CPA2, HIS1, HIS4, HOM2, HOM3, ILV6, LEU2, LEU4, LEU9, MET22, RIB5
	response to stress	GPX2, MET22, PCL5, YHI9
	transport	GGC1 (mitoch iron transp), SDA1, SVL3
	cell cycle/cytoskeleton organization	SDA1, SVL3, PCL5
20	**ribosome biogenesis / translation**	RPL12B, RPL15A, RPL16A, RPL1A, RPL21A, RPL24A, RPL24B, RPL28, RPL33B, RPS17A, RPS19B, RPS22A, RPS24B, PWP2
	response to stress	HSP104, CPR6
	carbohydrate metabolism/fermentation	ADH5, ADH6
	cytokinesis	PWP2
	gluconeogenesis	PYK2
	biological process unknown	YCL042W, YOR390W

Cluster	GO-Slim term	Genes annotated to the term

Table 1: Outcome of cluster enrichment for metal stress Ag, Al, As, Cd, Co, Hg, Mn, Ni; V, Zn

2 Results of mapping significant genes to biochemical pathways

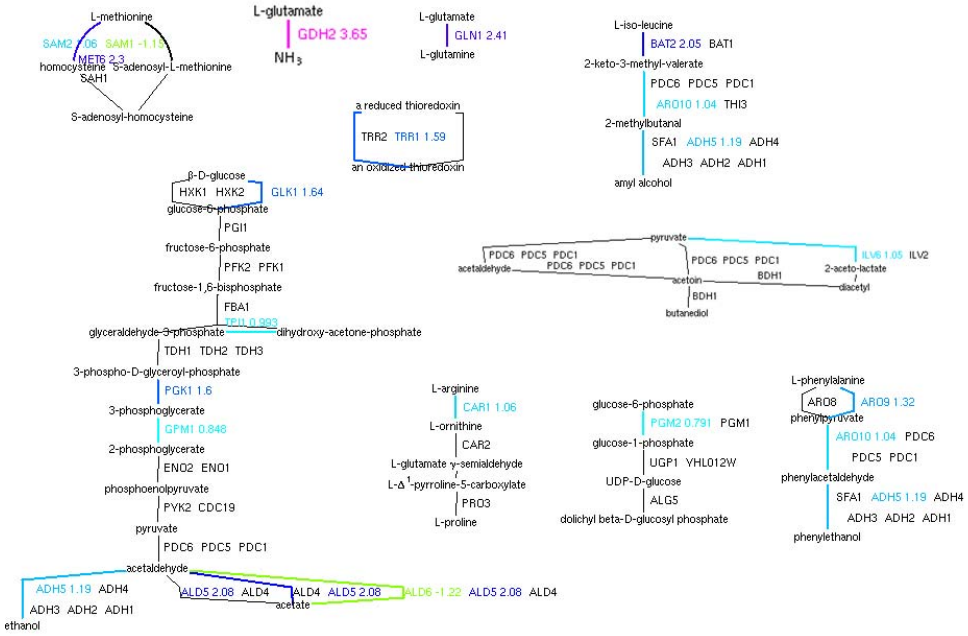

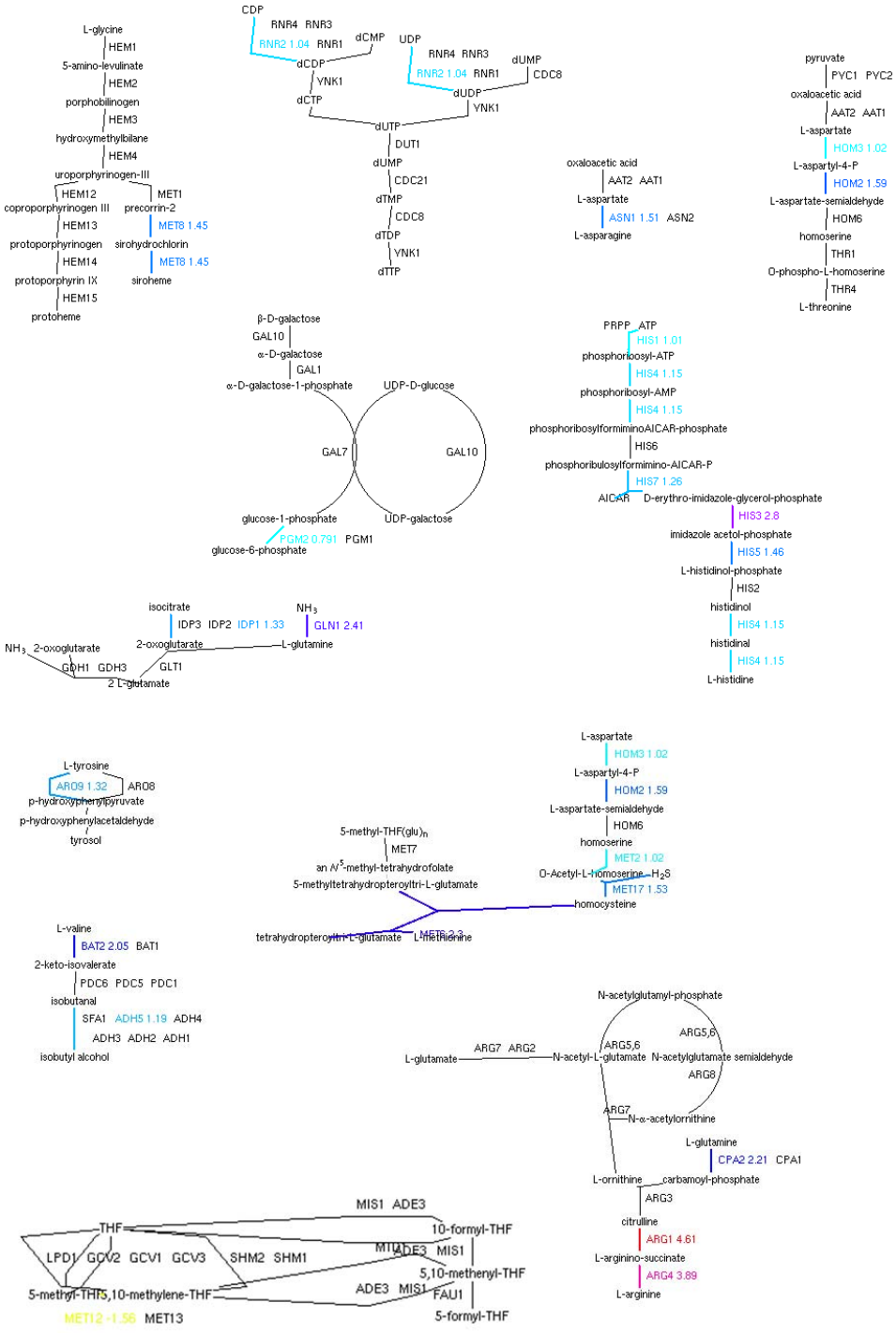
L-glycine
HEM1
5-amino-levulinate
HEM2
porphobilinogen
HEM3
hydroxymethylbilane
HEM4
uroporphyrinogen-III
HEM12
MET1
coproporphyrinogen III
precorrin-2
HEM13
MET8 1.45
protoporphyrinogen
sirohydrochlorin
HEM14
MET8 1.45
protoporphyrin IX
siroheme
HEM15
protoheme
CDP
RNR4 RNR3
RNR2 1.04 RNR1
dCMP
dCDP
YNK1
dCTP
UDP
RNR4 RNR3
RNR2 1.04 RNR1
dUMP
CDC8
dUDP
YNK1
dUTP
DUT1
dUMP
CDC21
dTMP
CDC8
dTDP
YNK1
dTTP
oxaloacetic acid
AAT2 AAT1
L-aspartate
ASN1 1.51 ASN2
L-asparagine
pyruvate
PYC1 PYC2
oxaloacetic acid
AAT2 AAT1
L-aspartate
HOM3 1.02
L-aspartyl-4-P
HOM2 1.59
L-aspartate-semialdehyde
HOM6
homoserine
THR1
O-phospho-L-homoserine
THR4
L-threonine
β-D-galactose
GAL10
α-D-galactose
GAL1
α-D-galactose-1-phosphate
UDP-D-glucose
GAL7
GAL10
glucose-1-phosphate
UDP-galactose
PGM2 0.791 PGM1
glucose-6-phosphate
PRPP ATP
HIS1 1.01
phosphoribosyl-ATP
HIS4 1.15
phosphoribosyl-AMP
HIS4 1.15
phosphoribosylformiminoAICAR-phosphate
HIS6
phosphoribulosylformimino-AICAR-P
HIS7 1.26
AICAR D-erythro-imidazole-glycerol-phosphate
HIS3 2.8
imidazole acetol-phosphate
HIS5 1.46
L-histidinol-phosphate
HIS2
histidinol
HIS4 1.15
histidinal
HIS4 1.15
L-histidine
isocitrate
IDP3 IDP2 IDP1 1.33
NH3
GLN1 2.41
NH3 2-oxoglutarate
2-oxoglutarate
L-glutamine
GDH1 GDH3
GLT1
2 L-glutamate
L-tyrosine
ARO9 1.32
ARO8
p-hydroxyphenylpyruvate
p-hydroxyphenylacetaldehyde
tyrosol
L-aspartate
HOM3 1.02
L-aspartyl-4-P
HOM2 1.59
L-aspartate-semialdehyde
HOM6
homoserine
MET2 1.02
O-Acetyl-L-homoserine
H2S
MET17 1.53
homocysteine
5-methyl-THF(glu)n
MET7
an N5-methyl-tetrahydrofolate
5-methyltetrahydropteroyltri-L-glutamate
tetrahydropteroyltri-L-glutamate
L-methionine
L-valine
BAT2 2.05 BAT1
2-keto-isovalerate
PDC6 PDC5 PDC1
isobutanal
SFA1 ADH5 1.19 ADH4
ADH3 ADH2 ADH1
isobutyl alcohol
N-acetylglutamyl-phosphate
ARG5,6
L-glutamate
ARG7 ARG2
N-acetyl-L-glutamate
N-acetylglutamate semialdehyde
ARG8
ARG7
N-α-acetylornithine
L-glutamine
CPA2 2.21 CPA1
L-ornithine
carbamoyl-phosphate
ARG3
citrulline
ARG1 4.61
L-arginino-succinate
ARG4 3.89
L-arginine
MIS1 ADE3
THF
10-formyl-THF
LPD1 GCV2 GCV1 GCV3
SHM2 SHM1
MTD1 ADE3 MIS1
5,10-methenyl-THF
5-methyl-THF
5,10-methylene-THF
ADE3 MIS1
FAU1
5-formyl-THF
MET12 1.56 MET13

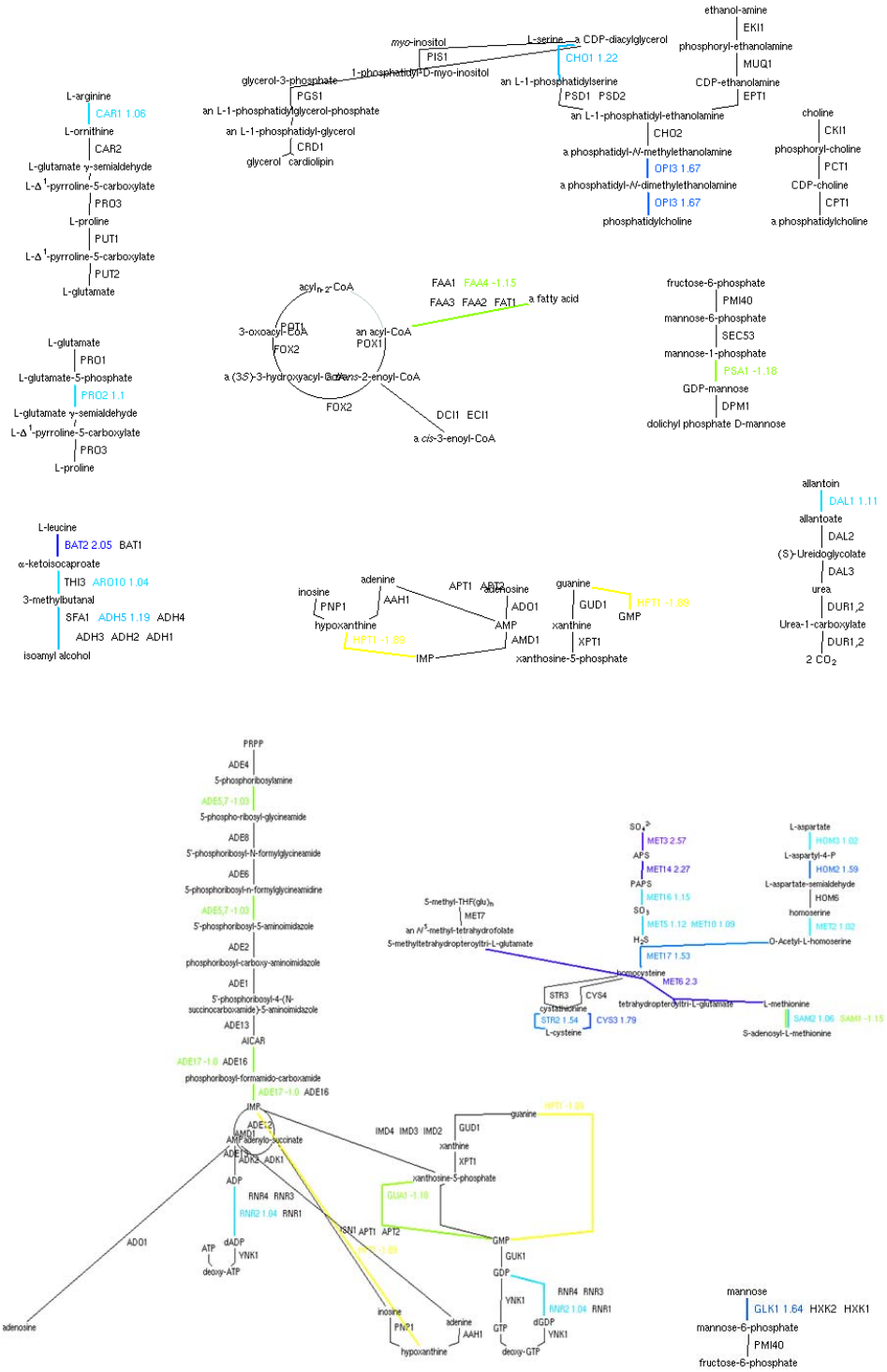
ethanol-amine
EKI1
phosphoryl-ethanolamine
MUQ1
CDP-ethanolamine
EPT1
myo-inositol
PIS1
L-serine
a CDP-diacylglycerol
CHO1 1.22
1-phosphatidyl-D-myo-inositol
an L-1-phosphatidylserine
PSD1 PSD2
an L-1-phosphatidyl-ethanolamine
CHO2
a phosphatidyl-N-methylethanolamine
OPI3 1.67
a phosphatidyl-N-dimethylethanolamine
OPI3 1.67
phosphatidylcholine
choline
CKI1
phosphoryl-choline
PCT1
CDP-choline
CPT1
a phosphatidylcholine
glycerol-3-phosphate
PGS1
an L-1-phosphatidylglycerol-phosphate
an L-1-phosphatidyl-glycerol
CRD1
glycerol
cardiolipin
L-arginine
CAR1 1.06
L-ornithine
CAR2
L-glutamate γ-semialdehyde
L-Δ1-pyrroline-5-carboxylate
PRO3
L-proline
PUT1
L-Δ1-pyrroline-5-carboxylate
PUT2
L-glutamate
acyln-2-CoA
3-oxoacyl-CoA
POT1
FOX2
an acyl-CoA
POX1
a (3S)-3-hydroxyacyl-CoA
a trans-2-enoyl-CoA
FOX2
DCI1 ECI1
a cis-3-enoyl-CoA
FAA1 FAA4 -1.15
FAA3 FAA2 FAT1
a fatty acid
fructose-6-phosphate
PMI40
mannose-6-phosphate
SEC53
mannose-1-phosphate
PSA1 -1.18
GDP-mannose
DPM1
dolichyl phosphate D-mannose
L-glutamate
PRO1
L-glutamate-5-phosphate
PRO2 1.1
L-glutamate γ-semialdehyde
L-Δ1-pyrroline-5-carboxylate
PRO3
L-proline
allantoin
DAL1 1.11
allantoate
DAL2
(S)-Ureidoglycolate
DAL3
urea
DUR1,2
Urea-1-carboxylate
DUR1,2
2 CO2
L-leucine
BAT2 2.05 BAT1
α-ketoisocaproate
THI3 ARO10 1.04
3-methylbutanal
SFA1 ADH5 1.19 ADH4
ADH3 ADH2 ADH1
isoamyl alcohol
inosine
PNP1
hypoxanthine
adenine
AAH1
APT1 APT2
adenosine
ADO1
AMP
HPT1 -1.89
IMP
AMD1
guanine
GUD1
HPT1 -1.89
GMP
xanthine
XPT1
xanthosine-5-phosphate
PRPP
ADE4
5-phosphoribosylamine
ADE5,7 -1.03
5-phospho-ribosyl-glycineamide
ADE8
5'-phosphoribosyl-N-formylglycineamide
ADE6
5-phosphoribosyl-n-formylglycineamidine
ADE5,7 -1.03
5'-phosphoribosyl-5-aminoimidazole
ADE2
phosphoribosyl-carboxy-aminoimidazole
ADE1
5'-phosphoribosyl-4-(N-succinocarboxamide)-5-aminoimidazole
ADE13
AICAR
ADE17 -1.0 ADE16
phosphoribosyl-formamido-carboxamide
ADE17 -1.0 ADE16
IMP
ADE12
AMD1
AMP adenylo-succinate
ADE13
ADK2 ADK1
ADP
RNR4 RNR3
RNR2 1.04 RNR1
ATP
dADP
YNK1
deoxy-ATP
ADO1
adenosine
IMD4 IMD3 IMD2
GUD1
xanthine
XPT1
xanthosine-5-phosphate
GUA1 -1.18
ISN1 APT1 APT2
GMP
GUK1
GDP
YNK1
RNR4 RNR3
RNR2 1.04 RNR1
dGDP
YNK1
GTP
deoxy-GTP
inosine
PNP1
hypoxanthine
adenine
AAH1
SO4 2-
MET3 2.57
APS
MET14 2.27
PAPS
MET16 1.15
SO3
MET5 1.12 MET10 1.09
H2S
MET17 1.53
L-aspartate
HOM3 1.02
L-aspartyl-4-P
HOM2 1.59
L-aspartate-semialdehyde
HOM6
homoserine
MET2 1.02
O-Acetyl-L-homoserine
5-methyl-THF(glu)n
MET7
an N5-methyl-tetrahydrofolate
5-methyltetrahydropteroyltri-L-glutamate
homocysteine
MET6 2.3
tetrahydropteroyltri-L-glutamate
L-methionine
STR3 CYS4
cystathionine
STR2 1.54
CYS3 1.79
L-cysteine
SAM2 1.06 SAM1 -1.15
S-adenosyl-L-methionine
mannose
GLK1 1.64 HXK2 HXK1
mannose-6-phosphate
PMI40
fructose-6-phosphate

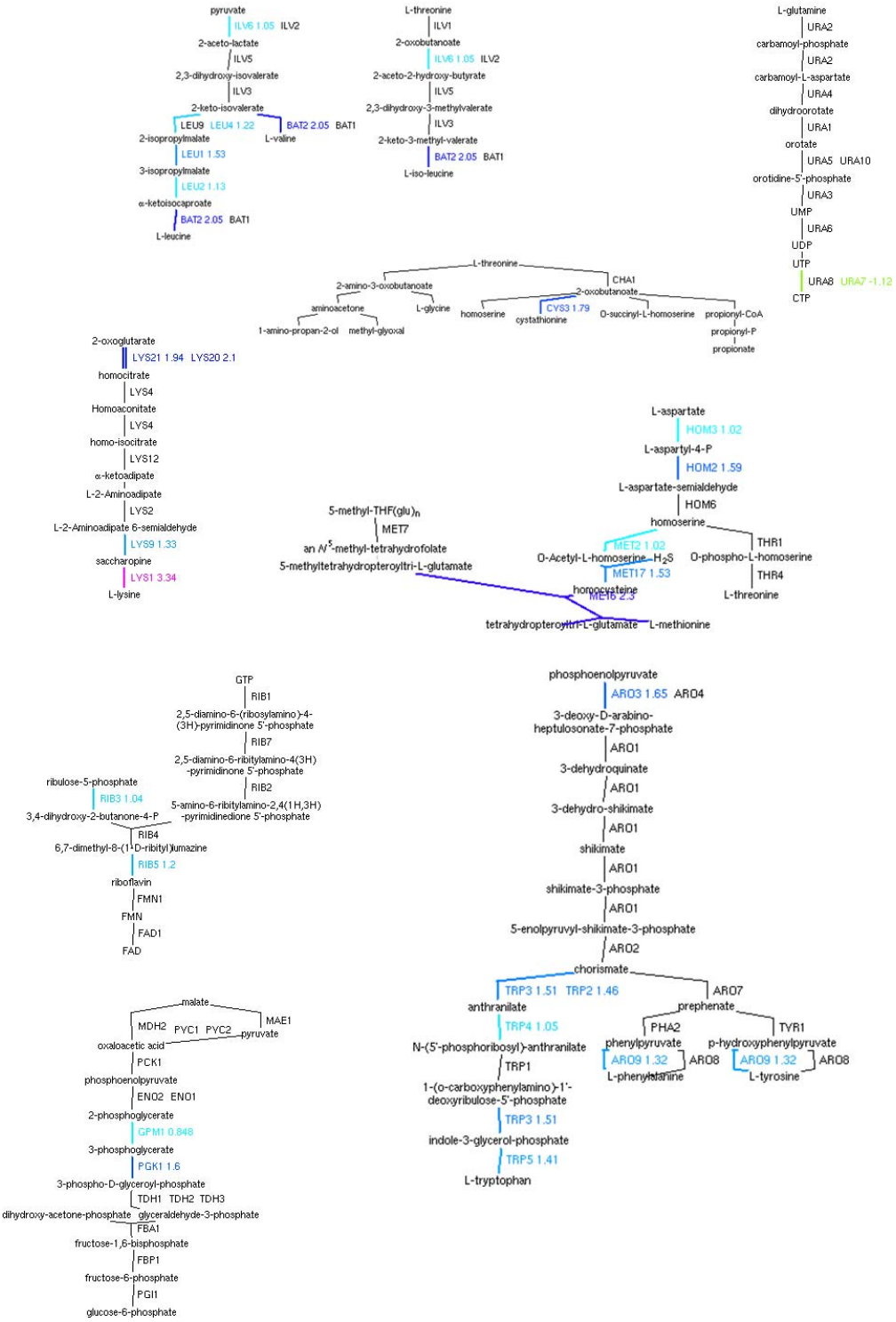
pyruvate
ILV6 1.05 ILV2
2-aceto-lactate
ILV5
2,3-dihydroxy-isovalerate
ILV3
2-keto-isovalerate
LEU9 LEU4 1.22
BAT2 2.05 BAT1
L-valine
2-isopropylmalate
LEU1 1.53
3-isopropylmalate
LEU2 1.13
α-ketoisocaproate
BAT2 2.05 BAT1
L-leucine
L-threonine
ILV1
2-oxobutanoate
ILV6 1.05 ILV2
2-aceto-2-hydroxy-butyrate
ILV5
2,3-dihydroxy-3-methylvalerate
ILV3
2-keto-3-methyl-valerate
BAT2 2.05 BAT1
L-iso-leucine
L-glutamine
URA2
carbamoyl-phosphate
URA2
carbamoyl-L-aspartate
URA4
dihydroorotate
URA1
orotate
URA5 URA10
orotidine-5'-phosphate
URA3
UMP
URA6
UDP
UTP
URA8 URA7 -1.12
CTP
L-threonine
2-amino-3-oxobutanoate
CHA1
2-oxobutanoate
aminoacetone
L-glycine
homoserine
CYS3 1.79
cystathionine
O-succinyl-L-homoserine
propionyl-CoA
1-amino-propan-2-ol
methyl-glyoxal
propionyl-P
propionate
2-oxoglutarate
LYS21 1.94 LYS20 2.1
homocitrate
LYS4
Homoaconitate
LYS4
homo-isocitrate
LYS12
α-ketoadipate
L-2-Aminoadipate
LYS2
L-2-Aminoadipate 6-semialdehyde
LYS9 1.33
saccharopine
LYS1 3.34
L-lysine
L-aspartate
HOM3 1.02
L-aspartyl-4-P
HOM2 1.59
L-aspartate-semialdehyde
HOM6
homoserine
THR1
O-phospho-L-homoserine
THR4
L-threonine
5-methyl-THF(glu)n
MET7
an N5-methyl-tetrahydrofolate
5-methyltetrahydropteroyltri-L-glutamate
MET2 1.02
O-Acetyl-L-homoserine
H2S
MET17 1.53
homocysteine
MET6 2.3
tetrahydropteroyltri-L-glutamate
L-methionine
GTP
RIB1
2,5-diamino-6-(ribosylamino)-4-(3H)-pyrimidinone 5'-phosphate
RIB7
2,5-diamino-6-ribitylamino-4(3H)-pyrimidinone 5'-phosphate
RIB2
5-amino-6-ribitylamino-2,4(1H,3H)-pyrimidinedione 5'-phosphate
ribulose-5-phosphate
RIB3 1.04
3,4-dihydroxy-2-butanone-4-P
RIB4
6,7-dimethyl-8-(1'D-ribityl)lumazine
RIB5 1.2
riboflavin
FMN1
FMN
FAD1
FAD
phosphoenolpyruvate
ARO3 1.65 ARO4
3-deoxy-D-arabino-heptulosonate-7-phosphate
ARO1
3-dehydroquinate
ARO1
3-dehydro-shikimate
ARO1
shikimate
ARO1
shikimate-3-phosphate
ARO1
5-enolpyruvyl-shikimate-3-phosphate
ARO2
chorismate
TRP3 1.51 TRP2 1.46
ARO7
anthranilate
prephenate
TRP4 1.05
PHA2
TYR1
N-(5'-phosphoribosyl)-anthranilate
phenylpyruvate
p-hydroxyphenylpyruvate
ARO9 1.32
ARO8
ARO9 1.32
ARO8
L-phenylalanine
L-tyrosine
TRP1
1-(o-carboxyphenylamino)-1'-deoxyribulose-5'-phosphate
TRP3 1.51
indole-3-glycerol-phosphate
TRP5 1.41
L-tryptophan
malate
MDH2
PYC1 PYC2
MAE1
oxaloacetic acid
pyruvate
PCK1
phosphoenolpyruvate
ENO2 ENO1
2-phosphoglycerate
GPM1 0.848
3-phosphoglycerate
PGK1 1.6
3-phospho-D-glyceroyl-phosphate
TDH1 TDH2 TDH3
dihydroxy-acetone-phosphate
glyceraldehyde-3-phosphate
FBA1
fructose-1,6-bisphosphate
FBP1
fructose-6-phosphate
PGI1
glucose-6-phosphate

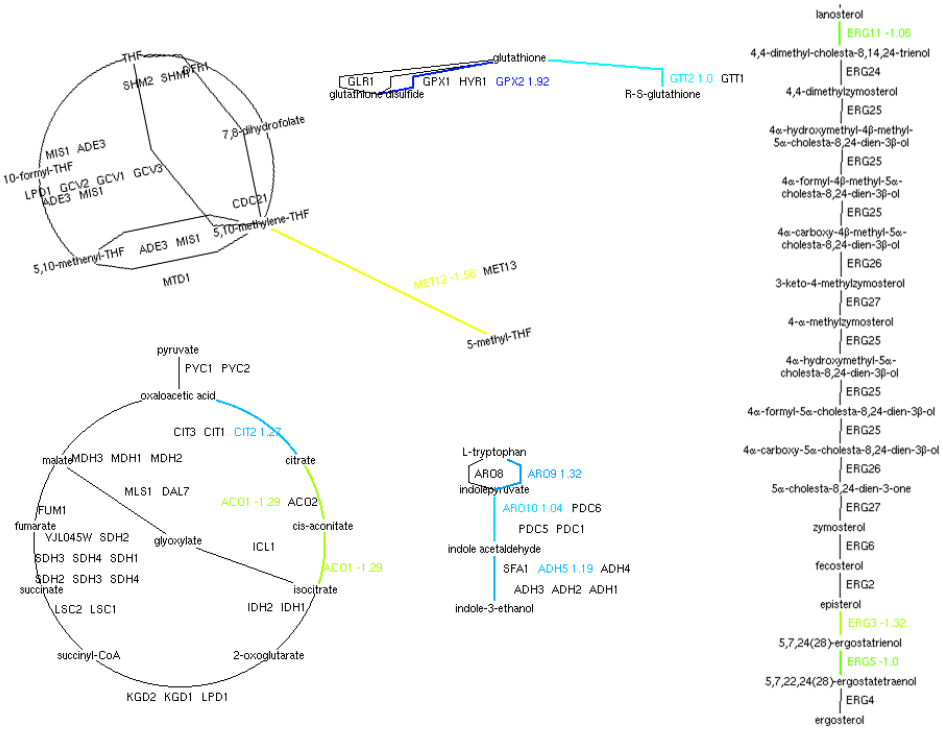
THF
SHM2 SHM1 GLY1
7,8-dihydrofolate
MIS1 ADE3
10-formyl-THF
LPD1 GCV2 GCV1 GCV3
ADE3 MIS1
CDC21
5,10-methylene-THF
5,10-methenyl-THF
ADE3 MIS1
MTD1
MET12 -1.56 MET13
5-methyl-THF
glutathione
GLR1
GPX1 HYR1 GPX2 1.92
glutathione disulfide
GTT2 1.0 GTT1
R-S-glutathione
pyruvate
PYC1 PYC2
oxaloacetic acid
CIT3 CIT1 CIT2 1.27
malate
MDH3 MDH1 MDH2
citrate
MLS1 DAL7
ACO1 -1.29 ACO2
FUM1
fumarate
cis-aconitate
YJL045W SDH2
glyoxylate
ICL1
SDH3 SDH4 SDH1
ACO1 -1.29
SDH2 SDH3 SDH4
succinate
isocitrate
LSC2 LSC1
IDH2 IDH1
succinyl-CoA
2-oxoglutarate
KGD2 KGD1 LPD1
L-tryptophan
ARO8
ARO9 1.32
indolepyruvate
ARO10 1.04 PDC6
PDC5 PDC1
indole acetaldehyde
SFA1 ADH5 1.19 ADH4
ADH3 ADH2 ADH1
indole-3-ethanol
lanosterol
ERG11 -1.06
4,4-dimethyl-cholesta-8,14,24-trienol
ERG24
4,4-dimethylzymosterol
ERG25
4α-hydroxymethyl-4β-methyl-5α-cholesta-8,24-dien-3β-ol
ERG25
4α-formyl-4β-methyl-5α-cholesta-8,24-dien-3β-ol
ERG25
4α-carboxy-4β-methyl-5α-cholesta-8,24-dien-3β-ol
ERG26
3-keto-4-methylzymosterol
ERG27
4-α-methylzymosterol
ERG25
4α-hydroxymethyl-5α-cholesta-8,24-dien-3β-ol
ERG25
4α-formyl-5α-cholesta-8,24-dien-3β-ol
ERG25
4α-carboxy-5α-cholesta-8,24-dien-3β-ol
ERG26
5α-cholesta-8,24-dien-3-one
ERG27
zymosterol
ERG6
fecosterol
ERG2
episterol
ERG3 -1.32
5,7,24(28)-ergostatrienol
ERG5 -1.0
5,7,22,24(28)-ergostatetraenol
ERG4
ergosterol

Supplementary Material C - Preparation of the cells

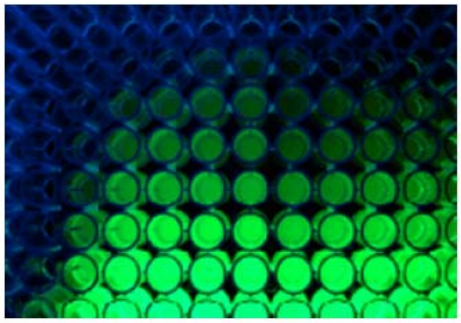

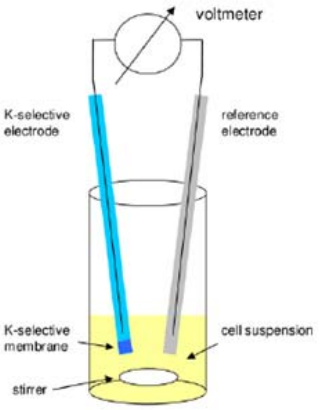

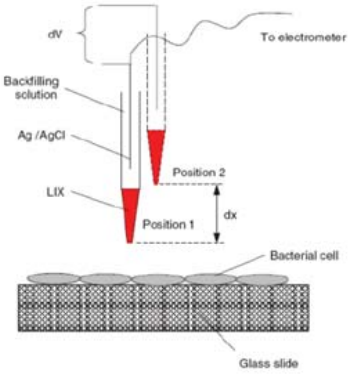

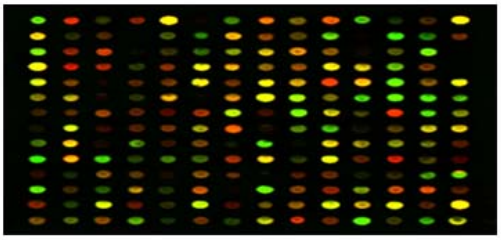

3 Yeast Strains, Media and Growth Tests for Promotor Analysis

Experiment 1

Haploid *S. cerevisiae* wild type, potassium transporter and TF mutant strains (BY4741; [BDC$^+$98]; Saccharomyces Genome Deletion Project) were used throughout this study as listed in Table 2.1. Strains were grown aerobically at 28 °C with rotational shaking at 250 rpm in liquid amino acid, ammonium sulfate and potassium free YNB-F media (CYN7505, Formedium). The medium was supplemented with a complete supplement mixture (DBSM225, Formedium), ammonium sulfate, 2% D-glucose and, for precultures 50 mM KCl. For test cultures KCl was added to concentrations as indicated. All medium components were dissolved in ultrapure MilliQ water and pH was adjusted to 5.8 with ammonium hydroxide. Stationary phase cells were washed three times in MilliQ water and diluted in fresh YNB-F medium to a start optical density OD600 of 0.4 (pathlength 1 cm, Pharmacia Ultrospec 2000 Spectrophotometer, corresponding to 6x106 cells per mL) with respective KCl concentration. Growth assessment was obtained by photometric determination of the turbidity at 600 nm in 15-min intervals in transparent 96-well microtiter plates using a microplate reader (Tecan, Infinite F200) with 28 °C incubation and constant agitation for 17 h. Growth calculation and statistical analysis was performed by integral determination (approx-imation of the area under the growth curves) obtained within 17h incubation according to [HSK$^+$05]. Subsequently values for growth were normalized to those of wild type strain values at 50 mM KCl.

Experiment 2

In a second experimental scenario the BY4743 wild type $MATa/\alpha$ $his3\Delta1/his3\Delta1$ $leu2\Delta0/leu2\Delta0$ $LYS2/lys2\Delta0$ $met15\Delta0/MET15$ $ura3\Delta0/ura3\Delta0$) and transcription factor mutant cells (*Saccharomyces* Genome Deletion Project [Gia02]) were grown exponentially in YPD broth to an OD_{620} of 0.6-0.8. The cells were harvested by immediately freezing with liquid nitrogen. Total RNA was isolated using the RiboPure^{TM}-Yeast Ambion RNA isolation kit (Ambion) according to the manual. This procedure included a DNase treatment to breakdown all chromosomal DNA. Subsequently, cDNA was produced using the Superscript III Reverse Transcriptase (Invitrogen), according to the manual. cDNA was diluted two times and 1 μl was used as a template for qPCR using the DyNAmo^{TM} Probe qPCR Kit (Finnzymes, Bioke). ACT1, BMH1, and BMH2 relative gene expression was measured on the Chromo4^{TM} Real-Time Detector (Biorad) using Opticon3 motion software (Biorad). The oligonucleotide primers used in this study are listed in table 2.2. BMH1 and BMH2 gene expression ratios were calculated using the $\Delta\Delta$C(t) method [LS01], and these ratios were normalized to ACT1 expression and normalized to wild type BMH1 and BMH2 expression. This procedure was performed for two biological duplicates and expression was measured in triplicate and in duplicate for every sample.

4 Preparation of Yeast RNA for Microarray Experiments

Over-night cultures were grown in fresh YPD and stressed with either the indicated concentrations of metal ions 3.1 or, as control were grown untreated. After 30 min incubation with AlC_l, $AgNO_3$, $AsCl_3$, $CdCl_2$, $CoCl_2$, $HgCl_2$, $MnCl_2$, $NiSO_4$, VCl_3 or $ZnCl_2$, respectively at 30°C, both untreated and treated cells were harvested, and cells were immediately washed in ice-cold DEPC-H2O, re-harvested and frozen at -80°C. Total RNA was prepared by extraction with hot acidic phenol according to [ABK$^+$97] with the only difference that three instead of one chloroform extractions were performed following phenol extraction. RNA was quantified by spectrophotometry at 260/280nm. The total mRNAs of both, the stressed cells and the control culture were prepared, labeled with fluorescence-dyes (cy3-CTP, cy5-CTP), and simultaneously hybridized to cDNA microarrays. The experiments were repeated three times for each condition, using independently grown yeast cultures. The microarrays were scanned using an Axon GenePix 4000B scanner (Molecular Devices, Sunnyvale,CA). The image data were quantified using the GenePix Pro4.1 software (Molecular Devices) that returns quantitative intensities for each spot.

5 MIFE (Proton and Potassium Fluxes)

The considered datasets for potassium and proton fluxes were prepared and provided from the laboratory of Prof. Sergey Shabala (University of Tasmania).
S. cerevisiae cells were grown in YNB-F supplemented with 50 mM KCl till late-log phase, harvested by centrifugation and washed twice with double-distilled water. With 30 μl aliquots of the cell suspension even monolayers were produced on poly-L-lysine covered glass coverslips and taken for each assay in a total of 3 ml sample buffer volume. Net fluxes of K^+ and H^+ were measured non-invasively using micro electrode ion flux measuring (the MIFE; University of Tasmania, Hobart, Australia) technique, essentially as described in publications from Sergey Shabala [SNJ97, Sha00, SDS$^+$06]. Briefly, micro electrodes were pulled and silanised with tributylchlorosilane. The electrode tips were filled with a commercially available ionophore cocktails (Fluke catalogue No. 95297 for H^+ and No. 60031 for K^+ (both from Fluka, Busch, Switzerland). Electrodes were calibrated in a set of known buffers covering the concentration range for each ion measured. Electrodes with a slope of less than 50 mV per decade and correlation less then 0.999 were discarded. The reference electrode was a flattened glass micro electrode with tip diameter of about 50 μm containing 1 M KCl in 2% agar. The electrodes were mounted on a three-dimensional micromanipulator (MX2; Narishige, Tokyo, Japan), and positioned 20 μm above the cell monolayer. During the measurements, a computer-controlled stepper motor moved the electrodes between two positions (20 and 70 μm, respectively) from the cell surface in a 6 s square-wave manner. The CHART software (see Shabala et al. 1997 and Newman 2001 [SNJ97, New01] for details) recorded the potential difference between the two positions and converted them into electrochemical

potential differences using the calibrated Nernst slope of the electrodes. Ion fluxes were then calculated by using the MIFEFLUX software for cylindrical diffusion geometry ([New01]).

Bibliography

[AA77] Al-Awqati, Q: Effect of aldosterone on the coupling between H+ transport and glucose oxidation. In: *J. Clin. Itivest.*, volume 60:pp. 1240–1247, 1977.

[AABA10] Andrews, Steven S.; Addy, Nathan J.; Brent, Roger; Arkin, Adam P.: Detailed simulations of cell biology with Smoldyn 2.1. In: *PLoS computational biology*, volume 6(3):pp. e1000705+, 2010.

[AAMS77] Al Awqati, Q; Mueller, A.; Steinmetz, P.: Transport of h+ against electrochemical gradients in the turtle bladder. In: *Am.J. Physiol.*, volume 233:pp. F502–F508, 1977.

[ABDV+04] Ander, M.; Beltrao, P.; Di Ventura, B.; Ferkinghoff-Borg, J.; Foglierini, M.; Kaplan, A.; Lemerle, C.; Tomás-Oliveira, I.; Serrano, L.: SmartCell, a framework to simulate cellular processes that combines stochastic approximation with diffusion and localisation: analysis of simple networks. In: *Systems biology*, volume 1(1):pp. 129–138, 2004.

[ABK+97] Ausubel, Frederick M.; Brent, Roger; Kingston, R.E.; Moore, David D.; Seidman, J. G.; Smith, JG; K.Struhl: *Current Protocols in Molecular Biology*. Wiley, John & Sons, 1997.

[AJ02] Alberts, B; Johnson, A.: *Molecular Biology of the cell*. Garland Science, 2002.

[Alo06] Alon, Uri: *An Introduction to Systems Biology - Design Principles of Biological Circuits*. Chapman & Hall/ CRC Mathematical & Computational Biology, 2006.

[AMR04] Abramoff, MD; Magalhaes, PJ; Ram, SJ.: Image processing with imagej. In: *Biophotonics International*, volume 11:pp. 36–42, 2004.

[AMS00] Ambesi, A M; Miranda, V, V.and Petrov; Slayman, C.W.: Biogenesis and function of the yeast plasma-membrane h(+)-atpase. In: *J Exp Biol.*, volume 203:pp. 155–160, 2000.

[AMT+11] Abdulrehman, Dario; Monteiro, Pedro Tiago; Teixeira, Miguel Cacho; Mira, Nuno Pereira; Lourenço, Artur Bastos; dos Santos, Sandra Costa; Cabrito, Tânia Rodrigues; Francisco, Alexandre Paulo; Madeira, Sara Cordeiro; Aires, Ricardo Santos; Oliveira, Arlindo Limede;

Sa Correia, Isabel; Freitas, Ana Teresa: YEASTRACT: providing a programmatic access to curated transcriptional regulatory associations in Saccharomyces cerevisiae through a web services interface. In: *Nucleic Acids Research*, volume 39(1):pp. D136–D140, 2011.

[ARS10] Ariño, J; Ramos, J; Sychrova, H: Alkali metal cation transport and homeostasis in yeasts. In: *Microbiol Mol Biol Rev*, volume 74(1):pp. 95–120, 2010.

[AW05] Alberghina, Lilia; Westerhoff, Hans: *Systems Biology: Definitions and Perspectives*. Springer, 2005.

[AYGM+00] Albert, A.; Yenush, L.; Gil-Mascarell, MR.; Rodriguez, PL.; Patel, S.; Martinez-Ripoll, M.; Blundell, T.L.; Serrano, R.: X-ray structure of yeast hal2p, a major target of lithium and sodium toxicity, and identification of framework interactions determining cation sensitivity. In: *J. Mol. Biol.*, volume 295:pp. 927–938, 2000.

[BAA76] Beauwens, R; Al-Awqati, Q: Active h+ transport in the turtle urinary bladdercoupling of transport to glucose oxidation. In: *J Gen Physiol*, volume 68(4):pp. 421–439, 1976.

[Bal02] Ballatori, Nazzareno: Transport of toxic metals by molecular mimicry. In: *Environ Health Perspect*, volume 110:pp. 689–694, 2002.

[BBR+98] Bertl, A; Bihler, H; Reid, JD; Kettner, C; CL, Slayman: Physiological characterization of the yeast plasma membrane outward rectifying k+ channel, duk1 (tok1), in situ. In: *J Membr Biol*, volume 162:pp. 67–80, 1998.

[BCC97] Botstein, David; Chervitz, Steven A.; Cherry, J. Michael: Genetics: Yeast as a model organism. In: *Science*, volume 277(5330):pp. 1259–1260, 1997.

[BDC+98] Brachmann, C.B.; Davies, A.; Cost, G.J.; Caputo, E.; Li, J.; Hieter, P.; Boeke, J.D.: Designer deletion strains derived from saccharomyces cerevisiae s288c: a useful set of strains and plasmids for pcr-gene disruption and other applications. In: *Yeast*, volume 14:pp. 115 – 32, 1998.

[BDS90] Barnes, G; Drubin, DG; Stearns, T.: The cytoskeleton of saccharomyces cerevisiae. In: *Curr Opin Cell Biol*, volume 1:pp. 109–115, 1990.

[BF88] Botstein, D; Fink, GR: Yeast: an experimental organism for modern biology. In: *Science*, volume 240:pp. 1439–1443, 1988.

[BFWW91] Basun, H; Forssell, LG; Wetterberg, L; Winbald, B: Metals and trace elements in plasma and cerebrospinal fluid in normal aging and alzheimer's disease. In: *J Neural Transm Park Dis Dement Sect*, volume 3(4):pp. 231–258, 1991.

[BGRN02] Benito, Begona; Garciadeblas, Blanca; Rodriguez-Navarro, Alonso: Potassium- or sodium-efflux atpase, a key enzyme in the evolution of fungi. In: *Microbiology*, volume 148:pp. 933–941, 2002.

[BGS01] Brown, CS; Goodwin, PC; Sorger, PK: Image metrics in the statistical analysis of dna microarray data. In: *Proc Natl Acad Sci U S A.*, volume 98(16):pp. 8944–9, 2001.

[BH95] Benjamini, Y.; Hochberg, Y.: Controlling the false discovery rate: a practical and powerful approach to multiple testing. In: *Journal of the Royal Statistical Society Series B,*, volume 57:pp. 289–300, 1995.

[BH08] Beyersmann, D; Hartwig, A: Carcinogenic metal compounds: recent insight into molecular and cellular mechanisms. In: *Arch Toxicol*, volume 82:pp. 493–512, 2008.

[BIB04] Bergmann, S; Ihmels, J; Barkai, N: Similarities and differences in genome-wide expression data of six organisms. In: *PLoS Biol.*, volume 2:pp. 85–93, 2004.

[BIsS03] Bolstad, B.M.; Irizarry, R.A; Åstrand, M.; Speed, T.P.: A comparison of normalization methods for high density oligonucleotide array data based on variance and bias. In: *Bioinformatics*, volume 19(2):pp. 185–193, 2003.

[BJ00] Brazma, A; J., Vilo: Gene expression data analysis. In: *FEBS Lett.*, volume 480(1):pp. 17–24, 2000.

[BMRT05] Belcastro, M; Marino, T; Russo, N; Toscano, M.: Interaction of cysteine with cu2+ and group iib (zn2+, cd2+, hg2+) metal cations: a theoretical study. In: *J Mass Spectrom*, volume 40(3):pp. 300–6, 2005.

[BP93] Borst-Pauwels, G.W.F.H.: Mutual interaction of ion uptake and membrane potential. In: *Biochimica et Biophysica Acta (BBA) - Biomembranes*, volume 1145(1):pp. 15 – 24, 1993.

[BR02] Bozinov, Daniel; Rahnenführer, Jörg: Unsupervised technique for robust target separation and analysis of DNA microarray spots through adaptive pixel clustering. In: *Bioinformatics*, volume 18(5):pp. 747–756, 2002.

[BRL+03] Bertl, A; Ramos, J; Ludwig, J; Lichtenberg-Frate, H; Reid, J; Bihler, Martinez P & Ljungdahl PO, H Calero F: Characterization of potassium transport in wild-type and isogenic yeast strains carrying all combinations of trk1, trk2 and tok1 nullmutations. In: *Mol Microbiol*, volume 47:pp. 767–780, 2003.

[BS88] Byrne, JH.; Schultz., SG: *An Introduction to Membrane Transport and Bioelectricity.* New York: Raven Press, 1988.

[BSB98] Bihler, H.; Slayman, C.L.; Bertl, A.: Nsc1: A novel high-current inward rectifier for cations in the plasma membrane of saccharomyces cerevisae. In: *Febs Letters*, volume 432:pp. 59–64, 1998.

[BSB02] Bihler, Hermann; Slayman, Clifford L.; Bertl, Adam: Low-affinity potassium uptake by saccharomyces cerevisiae is mediated by nsc1, a calcium-blocked non-specific cation channel. In: *Biochimica et Biophysica Acta*, volume 1558:pp. 109–118, 2002.

[BSBG+98] Banuelos, Maria; Sychrova, Hana; Bleykasten-Grosshans, Claudine; Souciet, Jean-Luc; Potier, Serge: The nha1 antiporter of saccharomyces cerevisiae mediates sodium and potassium efflux. In: *Microbiology*, volume 144:pp. 2749–2785, 1998.

[BSG93] Bertl, A; Slayman, CL; Gradmann, D: Gating and conductance in an outward-rectifying k+-channel from the plasma membrane of saccharomyces cerevisiae. In: *J Membr Biol*, volume 132(3):pp. 183–199, 1993.

[BTA98] Blackwell, KJ; Tobin, JM; Avery, SV: Manganese toxicity towards saccharomyces cerevisiae: dependence on intracellular and extracellular magnesium concentrations. In: *Appl Microbiol Biotech*, volume 49:pp. 751–757, 1998.

[CAB+98] Cherry, JM; Adler, C; Ball, C; Chervitz, SA; Dwight, SS; Hester, ET; Jia, Y; Juvik, G; Roe, T; Schroeder, M; Weng, S; Botstein, D: Sgd: Saccharomyces genome database. In: *Nucleic Acids Res*, volume 26:pp. 73–79, 1998.

[Cas45] Casimir, H. B. G.: On onsager's principle of microscopic reversibility. In: *Rev. Mod. Phys.*, volume 17(2-3):pp. 343–350, 1945.

[CBE01] Chiang, DY; Brown, PO; Eisen, MB: Visualizing associations between genome sequences and gene expression data using genome-mean profiles. In: *BCM Bioinformatics*, volume 17:pp. 49–55, 2001.

[CdKG97] Catty, P.; de Kerchove, A.; Goffeau, A.: The complete inventory of the yeast saccharomyces cerevisiae p-type transport atpases. In: *FEBS Lett*, volume 409:pp. 325–332, 1997.

[CE77] Caplan, S. R; Essig, A.: A thermodynamic treatment of active sodium transport. In: *Curr. Top. Membr. Transp.*, volume 9:pp. 145–175, 1977.

[CFG+05] Cartharius, K; Frech, K; Grote, K; Klocke, B; Haltmeier, M; Klingenhoff, A; Frisch, M; Bayerlein, M; Werner, T: Matinspector and beyond: promoter analysis based on transcription factor binding sites. In: *Bioinformatics*, volume 21(13):pp. 2933–42, 2005.

[CMA+99] Cheung, VG; Morley, M; Aguilar, F; Massimi, A; Kucherlapati, R; G, Childs: Making and reading microarrays. In: *Nat Genet.*, volume 21:pp. 15–9, 1999.

[CME98] Cornett, CR; Markesbery, WR; Ehmann, WD: Imbalances of trace elements related to oxidative damage in alzheimer's disease brain. In: *Neuro Toxicology*, volume 19(3):pp. 339–346, 1998.

[CO04] Castrillo, JI; Oliver, SG: Yeast as touchstone in post-genomic research: strategies for integrative analysis in functional genomics. In: *Biochem Mol Biol*, volume 37:pp. 93–106, 2004.

[Con00] Consortium, Gene Ontology: Gene ontology: tool for the unification of biology. In: *Nat. Genet*, volume 25:pp. 25–29, 2000.

[Cro81] Cronin, Jane: *Mathematics of Cell Electrophysiology - Lecture Notes in pure and applied mathematics -volume 63.* Marcel Dekker, 1981.

[CRRN81] Camacho, M.; Ramos, J.; Rodriguez-Navarro, A.: Potassium requirements of saccharomyces cerevisiae. In: *Curr. Microbiol*, volume 6:pp. 295–299, 1981.

[CS02] Chen, F; Shi, X: Intracellular signal transduction of cells in response to carcinogenic metals. In: *Crit Rev Oncol Hemat*, volume 42:pp. 105–121, 2002.

[CSM00] Crestensen, CA; Starke, DW; Mieyal, JJ: Acute cadmium exposure inactivates thioltransferase (glutaredoxin), inhibits intracellular reduction of protein-glutathionyl-mixed disulfides and initiates apoptosis. In: *JBC*, volume 275:pp. 26556–26565, 2000.

[Dem07] Demirel, Yasar: *Nonequilibrium Thermodynamics: Transport and Rate Processes in Physical and Biological Systems.* Elsevier, 2007.

[Dem08] Demirel, Yasar: Modeling of thermodynamically coupled reaction-transport systems. In: *Chemical Engineering Journal*, volume 139(1):pp. 106–117, 2008.

[DHD+02] Dwight, SS; Harris, MA; Dolinski, K; Ball, CA; Binkley, G; Christie, KR; Fisk, DG; Issel-Tarver, L; Schroeder, M; Sherlock, G; Sethuraman, A; Weng, S; Botstein, D; Cherry, JM: Saccharomyces genome database (sgd) provides secondary gene annotation using the gene ontology (go). In: *Nucleic Acids Res*, volume 30:pp. 69–72, 2002.

[dHINM04] de Hoon, ML.; Imoto, S.; Nolan, J; Miyano, S.: Open source clustering software. In: *Bioinformatics*, volume 20(9):pp. 1453–1454, 2004.

[Din88] Dinno, A: *Membrane Biophysics: Biological Transport (Progress in Clinical & Biological Research).* A.R.Liss,N.Y, 1988.

[DM62] DeGroot, SR; Mazur, P: *Non-Equilibrium Thermodynamics*. Interscience, New York, 1962.

[DM82] Dvorak, I.; Marsik, F.: Nonequilibrium thermodynamics of biological. In: *Cesk Fysiol*, volume 31:pp. 245–256, 1982.

[DS01] Demirel, Y; Sandler, S.I.: Linear non-equilibrium thermodynamics theory for coupled heat and mass transport. In: *International Journal of Heat and Mass Transfer*, volume 44:pp. 2439–2451, 2001.

[DS02] Demirel, Y.; Sandler, S.I.: Thermodynamics and bioenergetics. In: *Journal of Biophysical Chemistry*, volume 97:pp. 87–111, 2002.

[DTW05] Deonier, Richard C.; Tavare, Simon; Waterman, Michael S.: *Computational Genome Analysis*. Springer, 2005.

[DV74] Danisi, G.; Vieira, F. L.: Nonequilibrium thermodynamic analysis of the coupling between active sodium transport and oxygen consumption. In: *J. Gen. Physiot*, volume 64:pp. 372–391, 1974.

[EAW+98] Echeverria, D; Aposhian, HV; Woods, JS; Heyer, NJ; Aposhian, MM; Bittner, AC; Mahurn, RK; Cianciola, M: Neurobiological effects from exposure to dental amalgam hg: new distinctions between recent exposure and hg body burden. In: *FASEB Journal*, volume 12::pp. 971–980, 1998.

[EC68] Essig, A; Caplan, SR: Energetics of active transport processes. In: *Biophys J.*, volume 8(12):pp. 1434–1457, 1968.

[EC81] Essig, Alvin; Caplan, Roy: Active transport: Conditions for linearity and symmetry far from equilibrium (nonequilibrium thermodynamics/reciprocity relationships). In: *Proc. Natl Acad. Sci. USA - Biophysics*, volume 78(3):pp. 1647–1651, 1981.

[ECN+05] Eide, David J; Clark, Suzanne; Nair, T. Murlidharan; Gehl, Mathias; Gribskov, Michael; Guerinot, Mary Lou; Harper, Jeffrey F: Characterization of the yeast ionome: a genome-wide analysis of nutrient mineral and trace element homeostasis in saccharomyces cerevisiae. In: *Genome Biol*, volume 6(9):p. R77, 2005.

[EGOAB01] Ercal, N; Gurer-Orhan, H; Aykin-Burns, N: Toxic metals and oxidative stress part i: mechanisms involved in metal-induced oxidative damage. In: *Curr Top Med Chem*, volume 1:pp. 529–539, 2001.

[EHHM07] Endresen, LP.; Hall, K.; Hoye, JS.; Myrheim, J.: A theory for the membrane potential of living cells. In: *Biological Physics*, volume 1:pp. 1–22, 2007.

[Eid00] Eide, D. J.: Metal ion transport in eukaryotic microorganisms: insights from Saccharomyces cerevisiae. In: *Adv Microb Physiol*, volume 43:pp. 1–38, 2000.

[Eid01] Eide, David J: Functional genomics and metal metabolism. In: *Genome Biology*, volume 2(10):pp. 1028.1–1028.3, 2001. URL `http://genomebiology.com/2001/2/10/reviews/1028`.

[ESBB98] Eisen, MB; Spellman, PT; Brown, PO; Botstein, D: Cluster analysis and display of genome-wide expression patterns. In: *Proc Natl Acad Sci USA*, volume 95(25):pp. 14863–8, 1998.

[EW71] Evans, HJ; Wildes, RA: Potassium and it's role in enzyme activation. In: *Proceedings of the 8th Colloquium of the International Potash Institute*, volume 39. Berne. Switzerland: International Potash Institute, 1971.

[FKR+95] Ferrando, Alejandro; Kron, Stephen; Rios, Gabino; Fink, Gerald R.; Serrano, Ramon: Regulation of cation transport in saccharomyces cerevisiae by the salt tolerance gene hal3. In: *Mol Cell Biol*, volume 15(10):pp. 5470–548, 1995.

[FLA+02] Fauchon, M; Lagniel, G; Aude, JC; Lombardial, L; Soularue, P; Petat, C; Marguerie, G; Sentenac, A; Werner, M; Labarre, J.: Sulfur sparing in the yeast proteom in response to sulfur demand. In: *Mol. Cell*, volume 9:pp. 713–723, 2002.

[Fle91] Fleet, GH: *The yeasts*, volume 4, chapter Cell walls, pp. 199–226. Academic Press, London, 2nd edition, 1991.

[FMNM05] Farcasanu, IC; Mizunuma, M; Nishiyama, F; Miyakawa, T: Role of l-histidine in conferring tolerance to ni2+ in saccharomyces cerevisiae cells. In: *Biosci. Biotechnol. Biochem.*, volume 69:pp. 2343–2348, 2005.

[FPYC98] Figueiredo-Pereira, ME; Yakushin, S; Cohen, G: Disruption of the intracellular sulfhydryl homeostasis by cadmium-induced oxidative stress leads to protein thiolation and ubiquitination in neuronal cells. In: *JBC*, volume 273:pp. 12703–12709, 1998.

[Fra05] Fraga, CG: Relevance, essentiality and toxicity of trace elements in human health. In: *Mol. Aspects Med.*, volume 26(4-5):pp. 235–244, 2005.

[FSC03] Fernandes, R.; Sá-Correia, I.: Transcription patterns of pma1 and pma2 genes and activity of plasma membrane h+-atpase in saccharomyces cerevisiae during diauxic growth and stationary phase. In: *Yeast*, volume 20:pp. 207–219, 2003.

[FZBB96] Fortuniak, A; Zadzinski, R; Bilinski, T; Bartosz, G: Glutathione depletion in the yeast saccharomyces cerevisiae. In: *Biochem Mol Biol Int*, volume 38:pp. 901–910, 1996.

[FZK99] Fairman, C; Zhou, X; Kung, C: Potassium uptake through the tok1 k+ channel in the budding yeast. In: *J Membr Biol*, volume 168(2):pp. 149–57, 1999.

[Gab88] Gaber, RF: Trk1 encodes a plasma membrane protein required for high-affinity potassium transport in saccharomyces cerevisiae. In: *Mol Cell Biol*, volume 8(7):pp. 2848–59, 1988.

[Gad93] Gadd, GM: Interaction of fungi with toxic metals. In: *New Phytol*, volume 124:pp. 25–60, 1993.

[GBB+96] Goffeau, A.; Barrell, B. G.; Bussey, H.; Davis, R. W.; Dujon, B.; Feldmann, H.; Galibert, F.; Hoheisel, J. D.; Jacq, C.; Johnston, M.; Louis, E. J.; Mewes, H. W.; Murakami, Y.; Philippsen, P.; Tettelin, H.; Oliver, S. G.: Life with 6000 genes. In: *Science*, volume 274(5287):pp. 546–567, 1996.

[GCJ08] Gan, L; Chen, S; Jensen, GJ: Molecular organization of gram-negative peptidoglycan. In: *Proc Natl Acad Sci U S A.*, volume 105(48):pp. 18953–7, 2008.

[GCLC+07] Gordon, Andrew; Colman-Lerner, Alejandro; Chin, Tina E; Benjamin, Kirsten R; Yu, Richard C; Brent, Roger: Single-cell quantification of molecules and rates using open-source microscope-based cytometry. In: *Nat Methods*, volume 4(2):pp. 175–181, Feb 2007. doi:10.1038/nmeth1008. URL `http://dx.doi.org/10.1038/nmeth1008`.

[GdBDC03] Gardner, TS; di Bernardo, D; D, Lorenz; Collins, JJ: Inferring genetic networks and identifying compound mode of action via expression profiling. In: *Science*, volume 301:pp. 102–105, 2003.

[GdLVS92] Gaxiola, R; de Larrinoa, F; Villalba, JM; Serrano, R: A novel and conserved salt-induced protein is an important determinant of salt tolerance in yeast. In: *EMBO J*, volume 11(9):pp. 3157–3164, 1992.

[GFF+00] Goosens, Alain; Fuente, Natalia De La; Forment, Javier; Serrano, Ramon; Portillo, Francisco: Regulation of yeast h1-atpase by protein kinases belonging to a family dedicated to activation of plasma membrane transporters. In: *Molecular and Cellular Biology*, volume 20(20):pp. 7654–7661, 2000.

[GHH+10] Gerber, S; Hasenbrink, G; Hendriksen, W; Van Heusden, P; Ludwig, J; Klipp, E andLichtenberg-Frate: Graphical analysis and experimental evaluation of saccharomyces cerevisiae ptrk1|2 and pbmh1|2 promoter region. In: *Genome Inform*, volume 1:pp. 11–20, 2010.

[GHM+01] Gasch, AP; Huang, M; Metzner, S; Botstein, D; Elledge, SJ; Brown, PO: Genomic expression responses to dna-damaging agents and the regulatory

role of the yeast atr homolog mec1p. In: *Mol Biol Cell*, volume 12:pp. 2987–3003, 2001.

[Gia02] Giaever, G.: Functional profiling of the saccharomyces cerevisiae genome. In: *Nature*, volume 25(418(6896)):pp. 387–91, 2002.

[Gir10] Girke, Thomas: *R & Bioconductor Manual*. UC Riverside, 2010.

[Gol43] Goldman, DE: Potential, impedance and rectification in membranes. In: *J Gen Physiol*, volume 27:pp. 37–60, 1943.

[GRQ+93] Garciadeblas, Blanca; Rubio, Francisco; Quintero, Francisco J.; Bañuelos, María A.; Haro, Rosario; Rodríguez-Navarro, Alonso: Differential expression of two genes encoding isoforms of the atpase involved in sodium efflux in <i>saccharomyces cerevisiae</i>. In: *Molecular and General Genetics MGG*, volume 236:pp. 363–368, 1993.

[GS81] Goffeau, A.; Slayman, C.: The proton-translocating atpase of the fungal plasma membrane. In: *Biochim Biophys Acta*, volume 639(3-4s):pp. 197–223, 1981.

[GS89] Gancedo, C; Serrano, R: *The Yeast Vol. 3*, chapter Energy yielding metabolism in yeast, pp. 205–259. Academic Press, New York, 1989.

[GS00] Gasch, AP; Spellman, PT: Genomic expression programs in the response of yeast cells to environmental changes. In: *Mol Cell Biol*, volume 11(12):pp. 4241–4257, 2000.

[GSK+00] Gash, AP; Spellman, PT; Kao, CM; Cermel-Harel, O; Eisen, MB; Storz, G; Botstein, D; Brown, PO: Genomic expression programs in the response of yeast cells to environmental changes. In: *Mol. Cell. Biol.*, volume 11:pp. 4241–4267, 2000.

[GTG+93] Gläser, HU; Thomas, D; Gaxiola, R; Montrichard, F; Surdin-Kerjan, Y; Serrano, R: Salt tolerance and methionine biosynthesis in saccharomyces cerevisiae involve a putative phosphatase gene. In: *EMBO J*, volume 12(8):pp. 3105–10, 1993.

[Gug29] Guggenheim, EA: The conceptions of electrical potential difference between two phases and the individual activities of ions. In: *J.Phys. Chem*, volume 33:pp. 842–849, 1929.

[GWS93] Gassmann, W; Ward, JM; Schroeder, JI: Physiological roles of inward-rectifying k+ channels. In: *Plant Cell*, volume 11(5):pp. 1491–1493, 1993.

[GZMK88] Gustin, MC; Zhou, XL; Martinac, B; Kung, C: A mechanosensitive ion channel in the yeast plasma membrane. In: *Science*, volume 242(4879):pp. 762–765, 1988.

[Ham09] Hamilton, Nicholas: Quantification and its applications in fluorescent microscopy imaging. In: *Traffic*, volume 10(8):pp. 951–961, 2009.

[Har02] Hartwell, LH: Nobel lecture: Yeast and cancer. In: *Biosci Rep*, volume 22:pp. 373–94, 2002.

[HBM+00] Hollenhorst, PC.; Bose, ME.; Mielke, MR.; Müller, U.; Fox, CA.: Forkhead genes in transcriptional silencing, cell morphology and the cell cycle. overlapping and distinct functions for fkh1 and fkh2 in saccharomyces cerevisiae. In: *Genetics*, volume 154(4):pp. 1533–48, 2000.

[HC98] Hernandez, Julio; Cristina, Ernesto: Modeling cell volume regulation in nonexcitable cells: the roles of the na+ pump and of cotransport systems. In: *Am J Physiol Cell Physiol*, volume 275:pp. 1067–1080, 1998.

[HDR+97] Hudson, J.R.J.; Dawson, E.P.; Rushing, K.L.; Jackson, C.H.; Lockshon, D.; Conover, D.; Lanciault, C.; Harris, J.R.: The complete set of predicted genes from saccharomyces cerevisiae in a readily usable form. In: *Genome Res.*, volume 7:pp. 1169–73, 1997.

[Hei07] Heimburg, Thomas: *Thermal biophysics of membranes*. Wiley, 2007.

[Hel62] Helfferich, F: *Ion Exchange*. New York, McGraw-Hill Book Co Inc„ 1962.

[HETC00] Hughes, JD.; Estep, PW.; Tavazoie, S.; Church, GM.: Computational identification of cis-regulatory elements associated with groups of functionally related genes in saccharomyces cerevisiae. In: *J Mol Biol.*, volume 296(5):pp. 1205–14, 2000.

[HFE05] Hattne, Johan; Fange, David; Elf, Johan: Stochastic reaction-diffusion simulation with mesord. In: *Bioinformatics*, volume 21(12):pp. 2923–2924, 2005.

[HFL89] Hernandez, Julio; Fischbarg, Jorge; Liebovitch, Larry: Kinetic model of the effects of electrogenic enzymes on the membrane potential. In: *Journal of Theoretical Biology*, volume 137(1):pp. 113–125, 1989.

[HG84] Halliwell, B.; Gutteridge, J. M. C.: Oxygen toxicity, oxygen radicals, transition metals and disease. In: *Biochem. J.*, volume 219:pp. 1–14, 1984.

[HGRN91] Haro, Rosario; Garciadeblas, Blanca; Rodriguez-Navarro, Alonso: A novel p-type atpase from yeast involved in sodium transport. In: *FEBS Letters*, volume 291(2):pp. 189 – 191, 1991.

[Hil66] Hill, TL.: Studies in irreversible thermodynamics. iv. diagrammatic representation of steady state fluxes for unimolecular systems. In: *J Theor Biol.*, volume 10(3):pp. 442–459, 1966.

[HK49] Hodgkin, A. L.; Katz, B.: The effect of sodium ions on the electrical activity of the giant axon of the squid. In: *J Physiol*, volume 108(1):pp. 37–77, 1949.

[HKC+04] Haugen, AC; Kelly, R; Collins, JB; Tucker, CJ; C, Deng; Afshari, CA; Brown, JM; Ideker, T; Van Houten, B: Integrating phenotypic and expression profiles to map arsenic-response networks. In: *Genome Biol*, volume 5(12):p. R95, 2004.

[Hos05] Hosiner, Dagmar: *Heavy Metal Response in Saccharomyces Cerevisiae*. Master's thesis, Institut für Genetik und Mikrobiologie der Uni Wien; Abteilung für Genetik, 2005.

[HRN02] Haro, R.; Rodriguez-Navarro, A.: Molecular analysis of the mechanism of potassium uptake through the trk1 transporter of saccharomyces cerevisiae. In: *Biochim Biophys Acta*, volume 1564:pp. 114–122, 2002.

[HS99] Hertz, GZ.; Stormo, GD.: Identifying dna and protein patterns with statistically significant alignments of multiple sequences. In: *Bioinformatics*, volume 15((7-8)):pp. :563–7–7, 1999.

[HS03] Harris, GK; Shi, X: Signaling by carcinogenic metals and metal-induced reactive oxygen species. In: *Mutat Res*, volume 533:pp. 183–200, 2003.

[HSC87] Hussain, T; Shukla, GS; Chandra, SV: Effects of cadmium on superoxide dismutase and lipid peroxidation in liver and kidney of growing rats in vivo and in vitro studies. In: *Pharmacol Toxicol*, volume 60:pp. 355–358, 1987.

[HSG+06] Hoops, S; Sahle, S; Gauges, R; Lee, C; Pahle, J; Simus, N; Singhal, M; Xu, L; Mendes, P; Kummer, U: COPASI - a COmplex PAthway SImulator. In: *Bioinformatics*, volume 83:pp. 3067–3074, 2006.

[HSK+05] Hasenbrink, G.; Schwarzer, S.; Kolacna, L.; Ludwig, J.; Sychrova, H.; Lichtenberg-Fraté, H.: Analysis of the mkir2.1 channel activity in potassium influx defective strains determined as changes in growth characteristics. In: *FEBS Letters*, volume 579(7):pp. 1723–1731, 2005.

[Hug02] Hughes, Timothy R.: Yeast and drug discovery. In: *Funct Integr Genomics*, volume 2:pp. 199–211, 2002.

[Ive62] Iverson, Kenneth E.: *A Programming Language*. John Wiley & Sons, 1962.

[Jac12] Jaccard, P.: The distribution of ?ora in the alpine zone. In: *New Phytologist*, volume 11:pp. 37–50, 1912.

[Jac71] Jacquez, John A.: A generalization of the goldman equation, including the effect of electrogenic pumps. In: *Mathematical Biosciences*, volume 12(1-2):pp. 185–196, 1971.

[Jak80] Jakobsson, Eric: Interactions of cell volume, membrane potential and membrane transport parameters. In: *Am J Physiol.*, volume 238:pp. C196–C206, 1980.

[Jen95] Jennings, DH: *The physiology of fungal nutrition.* Cambridge University Press, 1995.

[JG06] J, Gollub; G., Sherlock: Clustering microarray data. In: *Methods Enzymol.*, volume 411:pp. 194–213, 2006.

[JHC06] Jeffery, Ian B; Higgins, Desmond G; Culhane, Aedin C: Comparison and evaluation of methods for generating differentially expressed gene lists from microarray data. In: *BMC Bioinformatics*, volume 7:p. 359, 2006.

[JLLF09] Jost Ludwig, Marcel Schmitt; Lichtenberg-Fraté, Hella: *Saccharomyces cerevisiae as biosensor for cyto- and genotoxic activity*, chapter Atmospheric and Biological Environmental Monitoring, pp. 253–261. Springer Science & Business media B.V., 2009.

[JNH04] Jonak, Claudia; Nakagami, Hirofumi; Hirt, Heribert: Heavy metal stress. activation of distinct mitogen-activated protein kinase pathways by copper and cadmium. In: *Plant Physiology*, volume 136(2):pp. 3276–3283, 2004. doi:10.1104/pp.104.045724.

[JOP01] Jones, Eric; Oliphant, Travis; Peterson, Pearu: Scipy: Open source scientific tools for python. In: *http://www.scipy.org/*, volume 1:p. 1, 2001.

[JP83] Jones, RG; Pollard, A: *Encyclopedia of Plant Physiology*, volume 15B. Springer-Verlag, Berlin, 1983.

[KAC+05] Kooperberg, Charles; Aragaki, Aaron; Carey, Charles C.; Rutherford, Suzannah; Hutchinson, Fred: Significance testing for small microarray experiments. In: *Stat. Med.*, volume 24:pp. 2281–2298, 2005.

[Kar02] Karp, P.D.: The pathway tools software. In: *Bioinformatics*, volume 18:pp. 225–32, 2002.

[Kat67] Katchalsky, A.: *The Neurosciences, A. Study Program.* Rockefeller University Pres,New York, 1967.

[Kat70] Katchalsky, A.: *Permeability and Function of Biological Membranes.* Elsevier, Amsterdam, 1970.

[KBG90] Ko, Christopher H.; Buckley, Ann M.; Gabe, Richard F.: Trk2 is required for low affinity k+ transport in saccharomyces cerevisiae. In: *Genetics*, volume 125:pp. 305–312, 1990.

[KC65] Katchalsky, A; Curran, PF: *Nonequilibrium Thermodynamics in Biophysics.* Books in Biophysics, 1. Harvard Univ. Press, 1965.

[KE95] Kennedy, J.; Eberhart, R.: Particle swarm optimization. In: *Proc. Conf. IEEE Int Neural Networks*, volume 4, pp. 1942–1948. 1995. doi:10.1109/ICNN.1995.488968.

[KG91] Ko, CH.; Gaber, RF.: Trk1 and trk2 encode structurally related k^+ transporters in saccharomyces cerevisiae. In: *Mol Cell Biol*, volume 11(8):pp. 4266–73, 1991.

[KG94] Kuo, MH; Grayhack, E: A library of yeast genomic mcm1 binding sites contains genes involved in cell cycle control, cell wall and membrane structure, and metabolism. In: *Mol Cell Biol.*, volume 14(1):pp. 348–59, 1994.

[KG00] Kanehisa, M.; Goto, S.: KEGG: Kyoto Encyclopedia of Genes and Genomes. In: *Nucleic Acids Res.*, volume 28:pp. 27–30, 2000.

[KGF+10] Kanehisa, M.; Goto, S.; Furumichi, M.; Tanabe, M.; Hirakawa, M.: Kegg for representation and analysis of molecular networks involving diseases and drugs. In: *Nucleic Acids Res.*, volume 38:pp. D355–D360, 2010.

[KJS+95] Ketchum, KA; Joiner, WJ; Sellers, AJ; Kaczmarek, LK; Goldstein, SA: A new family of outwardly rectifying potassium channel proteins with two pore domains in tandem. In: *Nature*, volume 376(6542):pp. 690–5, 1995.

[Kle89] Klein, Rolf: *Concrete and Abstract Voronoi Diagrams*, volume 200 of *Lecture Notes in Computer Science*. Springer-Verlag, 1989. ISBN 3540520554.

[KLG93] Ko, C.H.; Liang, H.; Gaber, R.: Roles of multiple glucose transporters in saccharomyces cerevisiae. In: *Mol. Cell. Biol.*, volume 13:pp. 638–648, 1993.

[Kli07] Klipp, Edda: Modelling dynamic processes in yeast. In: *Yeast*, volume 24:pp. 943–959, 2007.

[KLW+09] Klipp, E.; Liebermeister, W; Wierling, C.; Kowald, A.; Lehrach, H.; Herwig, R.: *Systems Biology: A Textbook*. Wiley Verlag, 2009.

[KNK+05] Klipp, Edda; Nordlander, B; Krüger, R; Gennemark, P; Hohmann, S: Integrative model of the response of yeast to osmotic shock. In: *Nat Biotechnol*, volume 23(8):pp. 975–82, 2005.

[Knu92] Knuth, Donald E.: Two notes on notation. In: *Am. Math. Monthly*, volume 99(5):pp. 403–422, 1992.

[Ko90] Ko, CH.: Trk2 is required for low affinity k^+ transport in saccharomyces cerevisiae. In: *Genetics*, volume 125(2):pp. 305–12, 1990.

[KO04] Kell, D.B.; Oliver, S.G.: Here is the evidence, now what is the hypothesis? the complementary roles of inductive and hypothesis-driven science in the post-genomic era. In: *Bioessays*, volume 26:pp. 99–1, 2004.

[KPS01] Kinclova, O; Potier, S; Sychrova, H: The candida albicans na+/h+ antiporter exports potassium and rubidium. In: *FEBS Lett*, volume 504:pp. 11–15, 2001.

[KRPS01] Kinclova, O; Ramos, J; Potier, S; Sychrova, H: Functional study of the saccharomyces cerevisiae nha1p c-terminus. In: *Mol Microbiol*, volume 40:pp. 656–668, 2001.

[KS68] Katchalsky, A; Spangler, R.: Dynamics of membrane processes. In: *Q Rev Biophys*, volume 1(2):pp. 127–175, 1968.

[KS98] Keener, James; Sneyd, James: *Mathematical Physiology*. Springer, 1998.

[KZGS06] Kinclova-Zimmermannova, O; Gaskova, D; Sychrova, H: The na+,k+/h+ -antiporter nha1 influences the plasma membrane potential of saccharomyces cerevisiae. In: *FEMS Yeast Res*, volume 6(5):pp. 792–800, 2006.

[Lak69] Lakshminarayanaiah, N: *Transport phenomena in membranes*. Academic Press, New York, 1969.

[Lak84] Lakshminarayanaiah, N: *Equations of Membrane Biophysics*. Academic Press, Orlando, 1984.

[LAP+05] Lecchi, Silvia; Allen, Kenneth E; Pardo, Juan Pablo; Mason, A Brett; Slayman, Carolyn W: Conformational changes of yeast plasma membrane h(+)-atpase during activation by glucose: role of threonine-912 in the carboxy-terminal tail. In: *Biochemistry Easton*, volume 44:pp. 16624–32, 2005.

[LC09] Ljosa, Vebjorn; Carpenter, Anne E.: Introduction to the quantitative analysis of two-dimensional fluorescence microscopy images for cell-based screening. In: *PLoS Comput Biol*, volume 5(12):p. e1000603, 12 2009. doi:10.1371/journal.pcbi.1000603.

[LCE77] Lang, MA; Caplan, SR; Essig, A.: Thermodynamic analysis of active sodium transport and oxidative metabolism in toad urinary bladder. In: *J Membr Biol.*, volume 24;31(1-2):pp. 19–2, 1977.

[LDM+97] Lashkari, DA; DeRisi, JL; McCusker, JH; Namath, AF; Gentile, C; Hwang, SY; Brown, PO; Davis, RW: Yeast microarrays for genome wide parallel genetic and gene expression analysis. In: *Proc Natl Acad Sci USA*, volume 94(24):pp. 13057–1306, 1997.

[LGR+98] Leonard, S; Gannett, PM; Rojanasakul, Y; Schwegler-Berry, D; Castranova, V; Vallyathan, V; Shi, X.: Cobalt mediated generation of reactive oxygen species and its possible mechanism. In: *J Inorg Biochem*, volume 70(3-4):pp. 239–44, 1998.

[LK98] Lapathitis, G; Kotyk, A: Univalent cation fluxes in yeast. In: *Biochem Mol Biol Int*, volume 44:pp. 371–380, 1998.

[LKB+04] Luo, F; Khan, L; Bastani, F; Yen, IL; Zhou, J.: A dynamically growing self-organizing tree (dgsot) for hierarchical clustering gene expression profiles. In: *Bioinformatics*, volume 20(16):pp. 2605–17, 2004.

[LNS07] Lecchi, Silvia; Nelson, Clark J; Slayman, Carolyn W: Tandem phosphorylation of ser-911 and thr-912 at the c terminus of yeast plasma membrane h+-atpase leads to glucose-dependent activation. In: *J Biol Chem*, volume 282:p. 35471, 2007.

[LRJ92] Lemieux, D.R.; Roberge, F.A.; Joly, D.: Modeling the dynamic features of the electrogenic na,k pump of cardiac cells. In: *Journal of Theoretical Biology*, volume 154(3):pp. 335 – 358, 1992.

[LS99] Loukin, S. H.; Saimi, Y.: K(+)-dependent composite gating of the yeast k(+) channel, tok1. In: *Biophys J*, volume 77(6):pp. 3060–3070, Dec 1999.

[LS01] Livak, K.J.; Schmittgen, T.D.: Analysis of relative gene expression data using real-time quantitative pcr and the 2(-delta delta c(t)) method. In: *Methods*, volume 2:pp. 402–408, 2001.

[LSC07] Lamprecht, MR; Sabatini, DM; Carpenter, AE: Cellprofiler: free, versatile software for automated biological image analysis. In: *Biotechniques*, volume 42(1):pp. 71–75, 2007.

[Mar87] Margineanu, DG: Equilibrium and non-equilibrium approaches in biomembrane thermodynamics. In: *Archives Of Physiology And Biochemistry*, volume 95(3):pp. 381–422, 1987.

[MBS95] Murguia, J.R.; Belles, J.M.; Serrano, R.: A salt-sensitive 3'(2'),5'-bisphosphate nucleotidase involved in sulfate activation. In: *Science*, volume 267:pp. 232–234, 1995.

[MDA05] McLachlan, Geoffrey J.; Do, Kim-Anh; Ambroise, Christophe: *Analyzing Microarray Gene Expression Data*. Wiley Series in Probability and Statistics, 2005.

[MDK95] Mager, WH; De Kruijff, AJJ: Stress-induced transcriptional activation. microbiol. rev. In: *59*, volume 3:pp. 506–531, 1995.

[MFG+00] Mewes, H. W.; Frishman, D.; Gruber, C.; Geier, B.; Haase, D.; Kaps, A.; Lemcke, K.; Mannhaupt, G.; Pfeiffer, F.; Schüller, C.; Stocker, S.; Weil, B.: Mips: a database for genomes and protein sequences. In: *Nucleic Acids Res.*, volume 28(1):pp. 37–40, 2000.

[MGRRN98] Madrid, R; Gómez, MJ; Ramos, J; Rodríguez-Navarro, A: Ectopic potassium uptake in trk1 trk2 mutants of saccharomyces cerevisiae correlates with a highly hyperpolarized membrane potential. In: *J Biol Chem*, volume 273(24):pp. 14838–14844, 1998.

[MHK+07] Maeder, C I; Hink, M A; Kinkhabwala, A; Mayr, R; Bastiaens, P I H; Knop, M: Spatial regulation of fus3 map kinase activity through a reaction-diffusion mechanism in yeast pheromone signalling. In: *Nature Cell Biology*, volume 9:pp. 1319–1326, 2007.

[MHL63] Moszynski, J.R; Hoshiko, T.; Lindley, B.D.: Note on the curie principle. In: *Biochim Biophys Acta*, volume 75:pp. 447–449, 1963.

[MI01] Momose, Y; Iwahashi, H: Bioassay of cadmium using a dna microarray: genome-wide expression patterns of saccharomyces cerevisiae response to cadmium. In: *Env Tox Chem*, volume 20:pp. 2353–2360, 2001.

[Mil60] Miller, Donald G.: Thermodynamics of irreversible processes. the experimental verification of the onsager reciprocal relations. In: *Chem. Rev.*, volume 60(1):pp. 15–37, 1960.

[Mil66] Miller, D.G.: Application of irreversible thermodynamics to electrolyte solutions. i. determination of ionic transport coefficients l_{ij} for isothermal vector transport processes in binary electrolyte systems. In: *J. Phys Chem*, volume 70:pp. 2639–2659, 1966.

[Mil67] Miller, D.G.: Application of irreversible thermodynamics to electrolyte solutions. ii. ionic coefficients l_{ij} for isothermal vector transport processes in ternary systems. In: *J. Phys Chem*, volume 71:pp. 616–632, 1967.

[Mil69] Miller, D.G.: *Transport Phenomena in Fluids*, chapter 11. Marcel Dekker, New York, 1969.

[Mil95] Miller: The origins of onsager's key role in the development of linear irreversible thermodynamics. In: *Journal of Statistical Physics*, volume 78(1/2):pp. 563–573, 1995.

[Mis98] Mishev, Ilya D.: Finite volume methods on Voronoi meshes. In: *Numer. Methods Partial Differential Eq.*, volume 14(2):pp. 193–212, 1998.

[Mit79] Mitchell, P: Compartmentation and communication in living systems. ligand conduction: a general catalytic principle in chemical, osmotic and chemiosmotic reaction systems. In: *Eur. J. Biochem.*, volume 95:pp. 1–20, 1979.

[MM74] Miller, D.G.; Mason, E.A.: *Foundations of Continuum Thermodynamics*, chapter 10+11. Macmillan, London, 1974.

[MMZ+09] Maresova, L; Muend, S; Zhang, YQ; Sychrova, H; Rao, R: Membrane hyperpolarization drives cation influx and fungicidal activity of amiodarone. In: *J Biol Chem.*, volume 284(5):pp. 2795–802, 2009.

[MN98] Matsumoto, M; Nishimura, T: Mersenne twister: A 623-dimensionally equidistributed uniform pseudorandom number generator. In: *ACM Transactions on Modeling and Computer Simulation*, volume 8:pp. 3–30, 1998.

[MP96] Martinez-Pastor, MT.: The saccharomyces cerevisiae zinc finger proteins msn2p and msn4p are required for transcriptional induction through the stress response element (stre),. In: *EMBO J*, volume 15(9):pp. 2227–35, 1996.

[MQ67] Mac Queen, JB: Some methods for classification and analysis of multivariate observations. In: *Proceedings of 5-th Berkeley Symposium on Mathematical Statistics and Probability*, volume 1, pp. 281–297. University of California Press, 1967.

[MRRNP94] Mendoza, I; Rubio, F; Rodriguez-Navarro, A; Pardo, JM: The protein phosphatase calcineurin is essential for nacl tolerance of saccharomyces cerevisiae. In: *J Biol Chem*, volume 269(12):pp. 8792–8796, 1994.

[MS96] Marquez, José; Serrano, Ramon: Multiple transduction pathways regulate the sodium-extrusion gene pmr2/ena1 during salt stress in yeast. In: *FEBS Letters*, volume 382(1-2):pp. 89–92, 1996.

[MS09] McCarthy, DJ; Smyth, GK: Testing significance relative to a fold-change threshold is a treat. In: *Bioinformatics*, volume 25(6):pp. 765–71, 2009.

[MSG00] Morsomme, P; Slayman, CW; Goffeau, A: Mutagenic study of the structure, function and biogenesis of the yeast plasma membrane h(+)-atpase. In: *Biochim Biophys Acta*, volume 1469(3):pp. 133–157, 2000.

[MUGS06] Maresova, L; Urbankova, E; Gaskova, D; Sychrova, H: Measurements of plasma membrane potential changes in saccharomyces cerevisiae cells reveal the importance of the tok1 channel in membrane potential maintenance. In: *FEMS Yeast Res*, volume 6(7):pp. 1039–46, 2006.

[MvC07] Meijering, E.; van Cappellen, G: *Quantitative biological image analysis.* Imaging Cellular and Molecular Biological Function. Springer Berlin, 2007.

[New01] Newman, I.A.: Ion transport in roots: measurement of fluxes using ion-selective microelectrodes to characterize transporter function. In: *Plant Cell and Environment*, volume 24:pp. 1–1, 2001.

[Nie99] Nies, DH: Microbial heavy-metal resistance. In: *Appl Microbiol Biotechnol*, volume 51(6):pp. 730–750, 1999.

[NS02] Nadon, R.; Shoemaker, J: Statistical issues with microarrays: processing and analysis. In: *Trends Genet*, volume 18:pp. 265–27, 2002.

[OC94] Oehlen, B.; Cross, FR.: Signal transduction in the budding yeast saccharomyces cerevisiae. In: *Curr. Opin. Cell Biol.*, volume 6:pp. 836–841, 1994.

[Ons31a] Onsager, Lars: Reciprocal relations in irreversible processes i. In: *Phys. Rev.*, volume 37(4):pp. 405–426, Feb 1931. doi:10.1103/PhysRev.37.405.

[Ons31b] Onsager, Lars: Reciprocal relations in irreversible processes ii. In: *Phys. Rev.*, volume 38(12):pp. 2265–2279, Dec 1931. doi:10.1103/PhysRev.38.2265.

[ORN85] Ortega, MD; Rodriguez-Navarro, A.: Potassium and rubidium effluxes in saccharomyces cerevisiae. In: *Z Naturforsch C*, volume 40:pp. 721–725, 1985.

[PCA93] Posas, F; Casamayor, A; Ariño, J.: The ppz protein phosphatases are involved in the maintenance of osmotic stability of yeast cells. In: *FEBS Lett*, volume 318(3):pp. 282–286, 1993.

[PCA95] Posas, F; Camps, M; Ariño, J: The ppz protein phosphatases are important determinants of salt tolerance in yeast cells. In: *J Biol Chem*, volume 270(22):pp. 13036–41, 1995.

[PCH+00] Posas, Francesc; Chambers, James R.; Heyman, John A.; de Nadal, James P. Hoeffler Eulalia; Arino, Joaquin: The transcriptional response of yeast to saline stress. In: *The Journal of Biological Chemistry*, volume 275(23):pp. 17249–17255, 2000.

[Pen08] Peng, Hanchuan: Bioimage informatics: a new area of engineering biology. In: *Bioinformatics*, volume 24(17):pp. 1827–1836, 2008.

[Pet83] Petzold, L: Automatic selection of methods for solving stiff and nonstiff systems of ordinary differential equations. In: *SIAM Journal on Scientific and Statistical Computing*, volume 4:pp. 136 – 148, 1983.

[Pev09] Pevsner, Jonathan: *Bioinformatics and Functional Genomics*, chapter Gene Expression: Microarray Data Analysis, pp. 279–370. Wiley-Blackwell, 2009.

[PEZ+98] Porwol, T; Ehleben, W.; Zierold, K.; Fandrey, J.; Acker, H.: The in?uence of nickel and cobalt on putative members of the oxygen-sensing pathway of erythropoietin-producing hepg2 cells. In: *Eur. J. Biochem.*, volume 256:pp. 16–23, 1998.

[PFS+10] Pau, Gregoire; Fuchs, Florian; Sklyar, Oleg; Boutros, Michael; Huber, Wolfgang: Ebimage - an r package for image processing with applications to cellular phenotypes. In: *Bioinformatics*, volume 26(7):pp. 979–981, 2010.

[PK83] Poolman, Bert; Konings, Wil N.: Secondary solute transport in bacteria. In: *Biochimica et Biophysica Acta*, volume 1993:pp. 5–39, 1183.

[PK06] Paley, S.M.; Karp, P.D.: The pathway tools cellular overview diagram and omics viewer,. In: *Nucleic Acids Research*, volume 34:pp. 3771–8, 2006.

[PLFS+06] Patterson, Tucker A; Lobenhofer, Edward K; Fulmer-Smentek, Stephanie B; Collins, Patrick J; Chu, Tzu-Ming; Bao, Wenjun; Fang, Hong; Kawasaki, Ernest S; Hager, Janet; Tikhonova, Irina R; Walker, Stephen J; Zhang, Liang; Hurban, Patrick; de Longueville, Francoise; Fuscoe, James C; Tong, Weida; Shi, Leming; Wolfinger, Russell D: Performance comparison of one-color and two-color platforms within the microarray quality control (maqc) project. In: *Nat. Biotechnol*, volume 24:pp. 1140–1150, 2006.

[PNB74] Prigogine, I.; Nicolis, G.; Babloyantz, A.: Nonequilibrium problems in biological phenomena. In: *Annals of the New York Academy of Sciences*, volume 231:pp. 99–100, 1974.

[POH48] Prigogine, I.; Outer, P.; Herbo, C.: Affinity and reaction rate close to equilibrium. In: *J Phys Colloid Chem*, volume 52(2):pp. 321–333, 1948.

[PPSS96] Prior, C; Potier, S; Souciet, JL; Sychrova, H: Characterization of the nha1 gene encoding a na+/h+-antiporter of the yeast saccharomyces cerevisiae. In: *FEBS Lett*, volume 387:pp. 89–93, 1996.

[PR06] Platara, M; Ruiz, A.: The transcriptional response of the yeast na(+)-atpase ena1 gene to alkaline stress involves three main signaling pathways. In: *J Biol Chem*, volume 281(48):pp. 36632–36642, 2006.

[Pri67] Prigogine, I.: *Introduction of thermodynamics of Irreversible Processes*. Interscience, New York, 1967.

[PS99] Pearce, DA; Sherman, F: Toxicity of copper, cobalt, and nickel salts is dependent on histidine metabolism in the yeast saccharomyces cerevisiae. In: *J. Bact.*, volume 181(16):pp. 4774–4779, 1999.

[PS00] Pevzner, PA.; Sze, SH.: Combinatorial approaches to finding subtle signals in dna sequences. In: *Proc Int Conf Intell Syst Mol Biol.*, volume 8:pp. 269–78, 2000.

[PSvL+05] Peart, Melissa J.; Smyth, Gordon K.; van Laar, Ryan K.; Bowtell, David D.; Richon, Victoria M.; Marks, Paul A.; Holloway, Andrew J.;

Johnstone, Ricky W.: Identification and functional significance of genes regulated by structurally different histone deacetylase inhibitors. In: *Proc. Natl Acad. Sci. USA*, volume 102:pp. 3697–3702, 2005.

[PVR82] Plat, G.; Vongvanich, T.; Rowley, R. L.: The diffusion thermoeffect in ternary nonelectrolyte liquid mixtures. In: *J. Chem. Phys.*, volume 77:pp. 2113–212, 1982.

[QB05] Qian, H.; Breard, DA: Thermodynamics of stoichiometric biochemical networks in living systems far from equilibrium. In: *Biophys Chem*, volume 114:pp. 213–220, 2005.

[QZSH06] Qiu, Shuo; Zhang, Min; Sun, Yan-dong; Huang, Su-zhen: Research advances in the mechanisms of cd (2+) uptake,transport,accumulation and tolerance in plants. In: *Acta Botanica Boreali-Occidentalia Sinica*, volume 1:p. 12, 2006.

[RA07] Ruiz, Amparo; Arino, Joaquin: Function and regulation of the saccharomyces cerevisiae ena sodium atpase system. In: *Eukaryot Cell.*, volume 6(12):pp. 2175–2183, 2007. 2007.

[RAHRN94] Ramos, Jose; Alijo, Rafael; Haro, Rosario; Rodriguez-Navarro, Alonso: Trk2 is not a low-affinity potassium transporter in saccharomyces cerevisiae. In: *Journal of Bacteriology*, volume 176(1):pp. 249–252, 1994.

[RB05] Rainbow, P.S.; Black, W.H.: Cadmium, zinc and the uptake of calcium by two crabs, carcinus maenas and eriocheir sinensis. In: *Aquatic Toxicol*, volume 72:pp. 45–65, 2005.

[RC00] Resnick, MA; Cox, BS: Yeast as an honorary mammal. In: *Mutat Res*, volume 451:pp. 1–11, 2000.

[RCRN85] Ramos, J; Contreras, P.; Rodriguez-Navarro, A.: A potassium transport mutant of saccharomyces cerevisiae. In: *Arch. Microbiol*, volume 143:pp. 88–93, 1985.

[RDN+06] Ritchie, Matthew E; Diyagama, Dileepa; Neilson, Jody; Laar, Ryan Van; Dobrovic, Alexander; Holloway, Andrew; Smyth, Gordon K: Empirical array quality weights in the analysis of microarray data. In: *BMC Bioinformatics*, volume 7:p. 261, 2006.

[REES80] Rothschild, K J; Ellias, S A; Essig, A; Stanley, H E: Nonequilibrium linear behavior of biological systems. existence of enzyme-mediated multidimensional inflection points. In: *Biophys J.*, volume 30(2):pp. 209–22, 1980.

[RH86] Rowley, R. L.; Hall, M. D.: Heat of transport from the diffusion thermoeffect in binary liquid mixtures of toluene, chlorobenzene and bromobenzene. In: *J. Chem. Phys.*, volume 85:pp. 3550–3555, 1986.

[RHRN90] Ramos, José; Haro, Rosario; Rodriguez-Navarro, Alonso: Regulation of potassium fluxes in saccharomyces cerevisiae. In: *Biochimica et Biophysica Acta (BBA) - Biomembranes*, volume 1029(2):pp. 211 – 217, 1990.

[RKTH00] Rep, Martijn; Krantz, Marcus; Thevelein, Johan M.; Hohmann, Stefan: The transcriptional response of saccharomyces cerevisiae to osmotic shock. In: *Journal of Biological Chemistry*, volume 275(12):pp. 8290–8300, 2000. doi:10.1074/jbc.275.12.8290. `http://www.jbc.org/content/275/12/8290.full.pdf+html`, URL `http://www.jbc.org/content/275/12/8290.abstract`.

[RMR+97] Rasio, D; Murakumo, Y; Robbins, D; Roth, T; Silve, A; Negrini, M; Schmidt, C; Burczak, J; Fishel, R; Croce, CM: Characterization of the human homologue of rad54: a gene located on chromosome 1p32 at a region of high loss of heterozygosity in breast tumors. In: *Cancer Res*, volume 57:pp. 2378–2383, 1997.

[RN00] Rodríguez-Navarro, A: Potassium transport in fungi and plants. In: *Biochim Biophys Acta*, volume 1469(1):pp. 1–30, 2000.

[RNBS86] Rodriguez-Navarro, A; Blatt, MR; Slayman, CL.: A potassium-proton symport in neurospora crassa. In: *J Gen Physiol*, volume 87(5):pp. 649–674, 1986.

[RNKB07] Rubi, J. Miguel; Naspreda, Manel; Kjelstrup, Signe; Bedeaux, Dick: Energy transduction in biological systems: A mesoscopic non-equilibrium thermodynamics perspective. In: *Journal of Non-Equilibrium Thermodynamics*, volume 32(4):pp. 351–378, 2007.

[RNQG94] Rodríguez-Navarro, A; Quintero, FJ; Garciadeblás, B: Na(+)-atpases and na+/h+ antiporters in fungi. In: *Biochim Biophys Acta*, volume 1187(2):pp. 203–205, 1994.

[RNR84] Rodriguez-Navarro, Alonso; Ramos, Rose: Dual system for potassium transport in saccharomyces cerevisiae. In: *Journal of Bacteriology*, volume 159(3):pp. 940–945, 1984.

[Ros02] Rosen, Barry P: Transport and detoxification systems for transition metals, heavy metals and metalloids in eukaryotic and prokaryotic microbes. In: *Comp Biochem Physiol A Mol Integr Physiol*, volume 133(3):pp. 689–693, Nov 2002.

[Rot64] Rothstein, A.: *The cellular functions of membrane transport*, chapter Membrane function and physiological activity of microorganisms, pp. 23–39. Prentice-Hall, Englewood Cliffs, N., 1964.

[Rot79] Rottenberg, H.: Non-equilibrium thermodynamics of energy conversion in bioenergetics. In: *Biochim Biophys Acta.*, volume 549(3-4):pp. 225–53, 1979.

[Row89] Rowley, R.I.: Measurements of heats of transport in ternary liquid mixtures via the diffusion thermoeffect. In: *Journal of Non-Equilibrium Thermodynamics*, volume 14:pp. 293–297, 1989.

[RRG+99] Rep, Martijn; Reiser, Vladimir; Gartner, Ulrike; Thevelein, Johan; Hohmann, Stefan; Ammerer, Gustav; Ruis, Helmut: Osmotic stress-induced gene expression in saccharomyces cerevisiae requires msn1p and the novel nuclear factor hot1. In: *Molecular and Cellular Biology*, volume 19(8):pp. 5474–548, 1999.

[RSO+07] Ritchie, Matthew; Silver, Jeremy; Oshlack, Alicia; Holmes, Melissa; Diyagama, Dileepa; Hollowa, Andrew; Smyth, Gordon: A comparison of background correction methods for two-colour microarrays. In: *Bioinformatics*, volume 23(20):pp. 2700–2707, 2007.

[RYA03] Ruiz, Amparo; Yenush, Lynne; Arino, Joaquin: Regulation of ena1 na+-atpase gene expression by the ppz1 protein phosphatase is mediated by the calcineurin pathways. In: *Eukaryot Cell*, volume 2(5):pp. 937–948, 2003.

[RZT+08] Raouf, A; Zhao, Y; To, K; Stingl, J; Delaney, A; Barbara, M; Iscove, N; Jones, S; McKinney, S; Emerman, J; Aparicio, S; Marra, M; Eaves, C: Transcriptome analysis of the normal human mammary cell commitment and differentiation process. In: *Cell Stem Cell.*, volume 3:pp. 109–118, 2008.

[SAE+10] Schaber, Jörg; Adrover, Miquel Angel; Eriksson, Emma; Pelet, Serge; Petelenz-Kurdziel, Elzbieta; Klein, Dagmara; Posas, Francesc; Goksör, Mattias; Peter, Mathias; Hohmann, Stefan; Klipp, Edda: Biophysical properties of saccharomyces cerevisiae and their relationship with hog pathway activation. In: *Eur Biophys J.*, volume 11:pp. 1547–1556, 2010.

[Sal04] Saldanha, Alok J.: Java treeview - extensible visualization of microarray data. In: *Bioinformatics*, volume 20(17):pp. 3246–3248, 2004.

[SB95] Stohs, SJ; Bagchi, D: Oxidative mechanisms in the toxicity of metal ions. In: *Free Radical Bio Med*, volume 18:pp. 321–336, 1995.

[SBM09] Suarez, Erick; Burguete, Ana; McLachlan, Geoffrey J.: Microarray data analysis for differential expression: a tutorial. In: *Puerto Rico Health Sciences Journal*, volume 28(2):pp. 5–18, 2009.

[SBS+01] Stiles, Joel R.; Bartol, Thomas M.; Salpeter, Miriam M.; Salpeter, Edwin E.; Sejnowski, Terrence J.: Synaptic Variability: New Insights from

Reconstructions and Monte Carlo Simulations with MCell. In: *Synapses*, volume 1:pp. 681–731, 2001.

[Sch62] Schrödinger, Erwin: *What is life?: the physical aspect of the living cell*. New York: The University Press, 1962.

[Sch71] Schwartz, TL: *Biophysics and Physiology of Excitable Membranes*, chapter The thermodynamic foundations of membrane physiology, pp. 47–95. New York, Van Nostrand Reinhold, 1971.

[Sch76] Schultz, SG.: Transport across epithelia: some basic principles. In: *Kidney Int.*, volume 9(2):pp. 65–75, 1976.

[Sch80] Schultz, Stanley: *Basic Principles of Membrane Transport*. Cambridge University Press, 1980.

[Sch99] Schermer, Mack J.: *DNA microarrays: a practical approac*, chapter Confocal scanning microscopy in microarray detection, pp. 17–42. Oxford University Press, 1999.

[SDS+06] Shabala, S; Demidchik, V; Shabala, L; Cuin, TA; Smith, SJ; Miller, AJ; Davies, JM; Newman, IA: Extracellular ca2+ ameliorates nacl-induced k+ loss from arabidopsis root and leaf cells by controlling plasma membrane k+-permeable channels. In: *Plant Physiology*, volume 141:pp. 1653–1665, 2006.

[Ser83] Serrano, R: In vivo glucose activation of the plasma membrane atpase. In: *FEBS Lett*, volume 156:pp. 11–14, 1983.

[Ser89] Serrano, R.: Structure and function of plasma membrane atpase. In: *Annu. Rev. Plant Physiol. Plant Mol. Biol*, volume 40:pp. 61–94, 1989.

[Ser91] Serrano, R.: *The molecular and cellular biology of the yeast Saccharomyces, vol. 1. Genome dynamics, protein synthesis and energetics.*, chapter Transport across yeast vacuolar and plasma membranes, pp. 523–585. Cold Spring Harbor Laboratory Press, Cold Spring Harbor, N.Y, 1991.

[Ser96] Serrano, Ramon: *International Review of Cytology: A Survey of Cell Biology*, chapter Salt Tolerance in Plants and Microorganisms: Toxicity Targets and Defense Response, pp. 1–40. Academic Press, 1996.

[SGC+05] Smyth, G. K; Gentleman, R.; Carey, V.; Dudoit, S.; Irizarry, R.; Huber, W.: *Limma: linear models for microarray data. In: Bioinformatics and Computational Biology Solutions using R and Bioconductor*. Springer, New York, 2005.

[SH10] Soh, Keng Cher; Hatzimanikatis, Vassily: Network thermodynamics in the post-genomic era. In: *Current opinion in microbiolog*, volume 13:pp. 350–357, 2010.

[Sha00] Shabala, S: Ionic and osmotic components of salt stress specifically modulate net ion fluxes from bean leaf mesophyll. In: *Plant Cell Environ*, volume 23:pp. 825–838, 2000.

[She02] Sherman, Fred: Getting started with yeast. In: *Methods Enzymol*, volume 350:pp. 3–41, 2002.

[SKBF86] Serrano, Ramon; Kielland-Brandt, Morten; Fink, Gerald: Yeast plasma membrane atpase is essential for growth and has homology with (na+ and k+), k+ and ca2+-atpases. In: *Nature*, volume 319:pp. 689–693, 1986.

[SKS90] Slayman, CL; Kaminski, P; Stetson, D.: *In Biochemistry of Cell Walls and Membranes in Fungi*, chapter Structure and function of fungal plasmamembrane ATPases, pp. 299–316. Springer Berlin, 1990.

[SLC+08] Stoma, Szymon; Lucas, Mikael; Chopard, Jérôme; Schaedel, Marianne; Traas, Jan; Godin, Christophe: Flux-based transport enhancement as a plausible unifying mechanism for auxin transport in meristem development. In: *PLoS Comput Biol*, volume 4(10):pp. e1000207+, October 2008. doi:10.1371/journal.pcbi.1000207.

[SLG74] Scherrer, R; Louden, RL; Gerhardt, P.: Prosity of the yeast cell wall and membrane. In: *J Bacteriol*, volume 118:pp. 534–540, 1974.

[SMS05] Smyth, G. K.; Michaud, J.; Scott, H.: The use of within-array replicate spots for assessing differential expression in microarray experiments. In: *Bioinformatics*, volume 21(9):pp. 2075–2067, 2005.

[Smu01] Smutzer, G: Yeast: an attractive, yet simple model. In: *Scientist*, volume 15:pp. 24–25, 2001.

[Smy04a] Smyth, G. K.: Linear models and empirical bayes methods for assessing differential expression in microarray experiments. In: *Statistical Applications in Genetics and Molecular Biology*, volume 3:pp. 1– 3, 2004.

[Smy04b] Smyth, GK: Statistical applications in genetics and molecular biology. In: *Statistical Applications in Genetics and Molecular Biology*, volume 3(1):p. 3, 2004.

[SNJ97] Shabala, S.N.; Newman, I.A.; J., Morris: Oscillations in h+ and ca2+ ion fluxes around the elongation region of corn roots and effects of external ph. In: *Plant Physiology*, volume 113:pp. 111–118, 1997.

[SO97] Schug, J.; Overton, GC.: Tess: Transcription element search software on the www. Technical Report Tech. Rep. CBIL-TR-1997-1001-v0.0, School of Medicine, University of Pennsylvania, Computational Biology and Informatics Laboratory, 1997.

[SOIS93] Shibasaki, T; Ohno, I; Ishimoto, F; Sakai, O: Characteristics of cadmium-induced nephrotoxicity in syrian hamsters. In: *Nippon Jinzo GakkaiShi*, volume 8:pp. 913–917, 1993.

[SRN01] Serrano, R; Rodriguez-Navarro, A.: Ion homeostasis during salt stress in plants. In: *Curr Opin Cell Biol*, volume 13(4):pp. 399–404, 2001.

[SRS09] Silver, J.; Ritchie, ME.; Smyth, GK.: Microarray background correction: maximum likelihood estimation for the normal-exponential convolution model. In: *Biostat*, volume 10(2):pp. 352–363, 2009. URL `http://biostatistics.oxfordjournals.org/cgi/content/abstract/kxn042`.

[SS03] Smyth, GK; Speed, TP: Normalization of cdna microarray data. In: *Methods*, volume 31:pp. 265–273, 2003.

[SSDB95] Schena, M; Shalon, D; Davis, RW; Brown, PO: Quantitative monitoring of gene expression patterns with a complementary dna microarray. In: *Science*, volume 270(5235):pp. 467–470, 1995.

[SSPW90] Strieter, J; Stephenson, JL; Palmer, LG; Weinstein, AM: Volume-activated chloride permeability can mediate cell volume regulation in a mathematical model of a tight epithelium. In: *J Gen Physiol*, volume 96(2):pp. 319–44, 1990.

[Ste86] Stein, Wilfred D: *Transport and Diffusion Across Cell Membranes.* Academic Press, 1986.

[Ste90a] Stein, WD: *Channels, carriers and pumps. An introduction to membrane transport.* Academic Press, New York, 1990.

[Ste90b] Stein, Wilfred D.: *Channels, Carriers, and Pumps: An Introduction to Membrane Transport.* Academic Press, 1990.

[STF+05] Shi, L; Tong, W; Fang, H; Scherf, U; Han, J; Puri, RK; Frueh, FW; Goodsaid, FM; Guo, L; Su, Z; Han, T; Fuscoe, JC; Xu, ZA; Patterson, TA; Hong, H; Xie, Q; Perkins, RG; Chen, JJ; Casciano, DA: Cross-platform comparability of microarray technology: intra-platform consistency and appropriate data analysis procedures are essential. In: *BMC Bioinformatics*, volume 15:p. S12, 2005.

[Syc04] Sychrova, H.: Yeast as a model organism to study transport and homeostasis of alkali metal cations. In: *Physiol Res.*, volume 53:pp. 91–98, 2004.

[SYP91] Seto-Young, D; Perlin, DS: Effect of membrane voltage on the plasma membrane h(+)-atpase of saccharomyces cerevisiae. In: *The Journal of Biological Chemistry*, volume 266:pp. 1383–1389, 1991.

[TH60] Tosteson, D. C.; Hoffman, J. F.: Regulation of cell volume by active cation transport in high and low potassium sheep red cells. In: *J Gen Physiol*, volume 44(1):pp. 169–194, 1960.

[THC+99] Tavazoie, S; Hughes, JD; Campbell, MJ; Cho, RJ; Church, GM: Systematic determination of genetic network architecture. In: *Nat Genet. 1999*, volume 3:pp. 281–5, 1999.

[TLN10] Tolle, Dominic P.; Le Novère, Nicolas: Meredys, a multi-compartment reaction-diffusion simulator using multistate realistic molecular complexes. In: *BMC systems biology*, volume 4:p. 24, 2010.

[TM05] Tamas, MJ; Martinoia, E: *Molecular Biology of Metal Homeostasis and Detoxification: from Microbes to Man.* Springer Verlag, Heidelberg, 2005.

[TMJ+06] Teixeira, M.C.; Monteiro, P.; Jain, P.; Tenreiro, S.; Fernandes, A.R.; Mira, N.P.; Alenquer, M.; Freitas, A.T.; Oliveira, A.L.: The yeastract database: a tool for the analysis of transcriptional relatory associations in saccharomyces cerevisiae. In: *Nucleic Acids Res*, volume 34 (Database Issue):pp. D446–D451, 2006.

[TO03] Thompson, KH; Orvig, C: Boon and bane of metal ions in medicine. In: *Science*, volume 300:pp. 936–939, 2003.

[Tom05] Tompa, M.: Assessing computational tools for the discovery of transcription factor binding sites. In: *Nature Biotechnology*, volume 23:pp. 137–144, 2005.

[Tos64] Tosteson, D. C.: *Regulation of cell volume by sodium and potassium transport*, chapter The cellular functions of membrane transport, pp. 3–22. Prentice-Hall, Englewood Cliffs, N., 1964.

[vdRKN+95] van der Rest, ME; Kamminga, AH; Nakano, A; Anraku, Y; Poolman, B; Konings, WN: The plasma membrane of saccharomyces cerevisiae: structure, function, and biogenesis. In: *Microbiol Rev.*, volume 59(2):pp. 304–322, 1995.

[vH03] van Helden, J.: Regulatory sequence analysis tools. In: *Nucleic Acids Res*, volume 31:pp. 3593 – 3596, 2003.

[vH09] van Heusden, GP: 14-3-3 proteins: Insights from genome-wide studies in yeast. In: *Genomics*, volume 94(5):pp. 287–93, 2009.

[vHS06] van Heusden, G. P.; Steensma, HY.: Yeast 14-3-3 proteins. In: *Yeast*, volume 23(3):pp. 159–71, 2006.

[VMC05] Valko, M.; Morris, H.; Cronin, M.T.D.: Metals, Toxicity and Oxidative Stress. In: *Current Medicinal Chemistry*, volume 12:pp. 1161–1208, 2005.

[VSL+01] Vido, K; Spector, D; Lagniel, G; Lopez, S; Toledano, MB; Labarre, J: A proteome analysis of the cadmium response in saccharomyces cerevisiae. In: *JBC*, volume 276:pp. 8469–8474, 2001.

[VWRS+00] Van Wuytswinkel, O; Reiser, V; Siderius, M; Kelders, MC; Ammerer, G; Ruis, H; Mager, WH.: Response of saccharomyces cerevisiae to severe osmotic stress: evidence for a novel activation mechanism of the hog map kinase pathway. In: *Mol Microbiol.*, volume 37(2):pp. 382–97, 2000.

[WCF+01] Wingender, E.; Chen, X.; Fricke, E.; Geffers, R.; Hehl, R.; Liebich, I.; Krull, M.; Matys, V.; Michael, H.: The transfac system on gene expression regulation. In: *Nucleic Acids Res*, volume 29:pp. 281–283, 2001.

[WDKK96] Wingender, E.; Dietze, P.; Karas.H.; Kniippel, R.: Transfac: a database on transcription factors and their dna binding sites. In: *Nucleic Acids Res.*, volume 24:pp. 238–241, 1996.

[WEM90] Wenstrup, D; Ehmann, WD; Markesbery, WR: Trace element imbalances in isolated subcellular fractions of alzheimer's disease brains. In: *Brain Research*, volume 533:pp. 125–131, 1990.

[WHA+81] Westerhoff, HV; Hellingwerf, K J; Arents, J C; Scholte, B J; Dam, K Van: Mosaic nonequilibrium thermodynamics describes biological energy transduction. In: *Proc Natl Acad Sci U S A.*, volume 78(6):pp. 3554–3558, 1981.

[Wil93] Wilders, R: *From single channel kinetics to regular beating: a model study of cardiac pacemaker activity.* Ph.D. thesis, University of Amsterdam, 1993.

[WJSK98] Westerhoff, H. V.; Jensenc, P. R.; Snoepa, J. L.; Kholodenkod, B. N.: Thermodynamics of complexity. the live cell. In: *Thermochimica Acta*, volume 309:pp. 111–120, 1998.

[WMDJ02] Westwater, John; McLaren, Niall F.; Dormer, Ulla H.; Jamieson, Derek J.: The adaptive response of saccharomyces cerevisiae to mercury exposure. In: *Yeast*, volume 19(3):pp. 233–239, 2002. ISSN 1097-0061. doi:10.1002/yea.835. URL `http://dx.doi.org/10.1002/yea.835`.

[WNS+95] Wieland, J; Nitsche, AM; Strayle, J; Steiner, H; Rudolph, HK: The pmr2 gene cluster encodes functionally distinct isoforms of a putative na+ pump in the yeast plasma membrane. In: *EMBO J.*, volume 14:pp. 3870–3882, 1995.

[WRFR09] Waldron, KJ; Rutherford, JC; Ford, D; Robinson, NJ: Metalloproteins and metal sensing. In: *Nature*, volume 460:pp. 823–830, 2009.

[WRG+97] Wright, M.B.; Ramos, J.; Gómez, M.J.; Moulder, K.; Scherrer, M.; Munson, G.; Gaber, R.: Potassium transport by amino acid permeases in saccharomyces cerevisiae. In: *J Biol. Chem.*, volume 272:pp. 13647–13652, 1997.

[WS07] Wollman, Roy; Stuurman, Nico: High throughput microscopy: from raw images to discoveries. In: *J Cell Sci*, volume 120(Pt 21):pp. 3715–3722, 2007.

[WSA+99] Winzeler, Elizabeth A.; Shoemaker, Daniel D.; Astromoff, Anna; Liang, Hong; Anderson, Keith; Andre, Bruno; Bangham, Rhonda; Benito, Rocio; Boeke, Jef D.; Bussey, Howard; Chu, Angela M.; Connelly, Carla; Davis, Karen; Dietrich, Fred; Dow, Sally Whelen; El Bakkoury, Mohamed; Foury, Françoise; Friend, Stephen H.; Gentalen, Erik; Giaever, Guri; Hegemann, Johannes H.; Jones, Ted; Laub, Michael; Liao, Hong; Liebundguth, Nicole; Lockhart, David J.; Lucau-Danila, Anca; Lussier, Marc; M'Rabet, Nasiha; Menard, Patrice; Mittmann, Michael; Pai, Chai; Rebischung, Corinne; Revuelta, Jose L.; Riles, Linda; Roberts, Christopher J.; Ross-MacDonald, Petra; Scherens, Bart; Snyder, Michael; Sookhai-Mahadeo, Sharon; Storms, Reginald K.; Véronneau, Steeve; Voet, Marleen; Volckaert, Guido; Ward, Teresa R.; Wysocki, Robert; Yen, Grace S.; Yu, Kexin; Zimmermann, Katja; Philippsen, Peter; Johnston, Mark; Davis, Ronald W.: Functional Characterization of the S. cerevisiae Genome by Gene Deletion and Parallel Analysis. In: *Science*, volume 285(5429):pp. 901–906, 1999.

[WT10] Wysocki, Robert; Tamas, Markus J.: How saccharomyces cerevisiae copes with toxic metals and metalloids. In: *FEMS Microbiology Reviews*, volume 34(6):pp. 925–951, 2010.

[WTDG03] Wheeler, GL; Trotter, EW; Dawes, IW; Grant, CM: Coupling of the transcriptional regulation of glutathione biosynthesis to the availability of glutathione and methionine via the met4 and yap1 transcription factors. In: *JBC*, volume 278(50):pp. 49920–49928., 2003.

[XJP+04] Xie, Yang; Jeong, Kyeong S.; Pan, Wei; Khodursky, Arkady; Carlin, Bradley P.: A case study on choosing normalization methods and test statistics for two-channel microarray data. In: *Comp.Funct. Genomics*, volume 5:pp. 432–444, 2004.

[YLA+08] Yu, L; Lopez, A.; Anaflous, A; El Bali, B; Hamal, A; Ericson, E: Chemical-genetic profiling of imidazo[1,2-a]pyridines and pyrimidines reveals target pathways conserved between yeast and human cells. In: *PLoS Genet*, volume 4:p. e1000284., 2008.

[YMHS05] Yenush, Lynne; Merchan, Stephanie; Holmes, James; Serrano, Ramon: ph-responsive, posttranslational regulation of the trk1 potassium transporter by the type 1-related ppz1 phosphatase. In: *Molecular and Cellular Biology*, volume 25(19):pp. 8683–8692, 2005.

[YR89] Yi, S. C.; Rowley, R. L.: Measurement of heats of transport in ternary liquid mixtures via the diffusion thermoeffect. In: *J. NonEquilib. Thermodyn.*, volume 14:pp. 293–297, 1989.

[YT03] Yang, Y. H.; Thorne, N. P.: Normalization for two-color cdna microarray data. In: Goldstein, D. R., editor, *Science and Statistics: A Festschrift for Terry Speed, IMS Lecture Notes*, volume 40, pp. 403–418. 2003.

[ZCR06] Zimkus, A.; Chaustova, L.; Razumas, V.: Effect of lithium and sodium cations on the permeability of yeast saccharomyces cerevisiae cells to tetraphenylphosphonium ions. In: *Biologija*, volume 2:pp. 47–49, 2006.

[ZLK10] Zi, Z; Liebermeister, W; Klipp, E.: A quantitative study of the hog1 mapk response to fluctuating osmotic stress in saccharomyces cerevisiae. In: *PLoS One*, volume 5(3):p. e9522., 2010.

[zPNO10] Özalp, VC; Pedersen, TR; Nielsen, LJ; Olsen, LF: Time-resolved measurements of intracellular atp in the yeast saccharomyces cerevisiae using a new type of nanobiosensor. In: *J Biol Chem*, volume 26(285(48)):pp. 37579–88, 2010.

List of Figures

List of Tables

Selbständigkeitserklärung

Ich erkläre, dass ich die vorliegende Arbeit selbständig und nur unter Verwendung der angegebenen Literatur und Hilfsmittel angefertigt habe.

Berlin, den 24.03.2011 Susanne Gerber